Order Number 9325046

Thermodynamic analysis of an OC-OTEC system in the direct-contact condenser configuration incorporating predeaeration and reinjection

Oney, Stephen Keith, Ph.D.

University of Hawaii, 1993

U·M·I
300 N. Zeeb Rd.
Ann Arbor, MI 48106

THERMODYNAMIC ANALYSIS OF AN OC-OTEC SYSTEM IN THE DIRECT-CONTACT CONDENSER CONFIGURATION INCORPORATING PREDEAERATION AND REINJECTION

A DISSERTATION SUBMITTED TO THE GRADUATE DIVISION OF THE UNIVERSITY OF HAWAII IN PARTIAL FULFILLMENT OF THE REQUIREMENTS FOR THE DEGREE OF

DOCTOR OF PHILOSOPHY
IN OCEAN ENGINEERING
MAY 1993

by
Stephen Keith Oney

Dissertation Committee:

Hans-Jurgen Krock, Chairman
Frans Gerritsen
Harold G. Loomis
Francis J. Sansone
Patrick Takahashi

ACKNOWLEDGEMENTS

The author wishes to express his deepest appreciation to all committee members for their continued support and assistance. Special thanks and warmest appreciation are extended to Dr. Hans Krock, committee chairman, without whom this dissertation could never have been completed. His continued encouragement and support have proven irreplacable and will never be forgotten. Likewise, I would like to express my deepest gratitude to each of the participating committee members; Dr. Frans Gerritsen, Dr. Hal Loomis, Dr. Frank Sansone and Dr. Patrick Takahashi for their individual contributions towards my education and professional development.

The help and support of the staff of the Ocean Engineering Department and the J.K.K. Look Laboratory has been extraordinary and is tremendously appreciated as well. Specifically, the technical assistance and frienship offered by the senior mechanical technician at the Laboratory, Roland Kanno has proven invaluable in this endeavor. Likewise, the support and encouragement offered by Ms. Edith Katada, Ms. Linda Benevides and Mr. John Pfizenmaier can never be replaced.

The author would also like to express his deep appreciation to the following organizations and individuals without whom the successful completion of this study would have been impossible: Dr. Stuart Ridgway; Hal Link, SERI; Travis Tarumoto, PICHTR; Ernest Galt, NELH; Arnie Haas, NELH; Dr. Federica Zangrando, SERI; and especially the Pacific International Center for High Technology Research (PICHTR), the Solar Energy Research

Institute (SERI), and the Natural Energy Laboratories of Hawaii (NELH) for permitting the use of the Heat- and Mass- Transfer Scoping Test Apparatus (HMTSTA) for these experiments.

The financial support by the Pacific International Center for High Technology Research, under the direction of Andrew Trenka, is greatly appreciated. Special thanks to OTEC project manager Dr. Luis Vega for his interest and support in this work. Also, the financial assistance of the Hawaii Natural Energy Institute under the direction of Dr. Patrick Takahashi is appreciated.

Special thanks to my fellow students; Dr. Manfred Zapka, Dr. Dayananda Vithanage, Dr. Joong Woo Lee, Dr. Francis Benevides, Dr. Srinivasamurthy Chitrapu and Dr. Warren Bucher who provided advice and encouragement throughout my educational career at the University of Hawaii.

I would also like the extend my sincere appreciation to Mr. Michael Strojnowski, my high school Chemistry teacher, for his excellence in teaching which originally fostered my interest in the sciences and who has faithfully followed my educational career and professional development.

Also, the friendly staff of I Love Country Cafe should be thanked for their continued support and encouragement over the development of this dissertation.

My sincere appreciation must also be extended to my brother, Matthew Oney, my sister, Tricia Oney, and my close friend, Robert Miller for their continued support and encouragement in finishing this project in a timely manner. Their positive attitudes and confidence in me will never be forgotten!

Last, but certainly not least, I would like to express my deepest appreciation to the two most wonderful parents any person could ever be blessed by God with, Carl and Beth Oney. Without their never ceasing enthusiasm and confidence in me, this dissertation could never have been completed. I am truly indebted to them for their love and many sacrifices made so that I could accomplish this goal.

To the many other, unnamed individuals who contributed to the present study goes the author's most sincere gratitude. Without all of the friendly assistance and support so warmly extended to the author, this research could have never been realized. The author will never forget everyone's kindness. Mahalo!

ABSTRACT

The present study addresses the pertinent Open-Cycle Ocean Thermal Energy Conversion (OC-OTEC) noncondensable gas desorption rates and the subsequent effects this evolution of gases has on typical OC-OTEC system component thermodynamic performances. This study has determined that the OC-OTEC warm seawater resource can be expected to desorb approximately 70 - 80% of the available dissolved noncondensables under typical vertical spout evaporator temperatures and pressures. The cold seawater resource, under a coaxial direct-contact condenser configuration, can be expected to desorb approximately 90 - 100% of the dissolved noncondensables. These values were determined experimentally on a prototype scale 1.0+ MW OC-OTEC system (excluding the turbine system) under typical OC-OTEC seawater resource flow rates, temperatures and system pressures.

With this experimentally determined knowledge and the overall mass transfer rates for these noncondensables as determined by previous researchers, a thermodynamic evaluation and design was performed to determine the relative thermodynamic benefits associated with a 10 MW_{gross} predeaerated and reinjected OC-OTEC system. A comparative approach was employed in the present study in which a 10 MW_{gross} OC-OTEC system was initially designed without warm or cold seawater predeaeration or reinjection of the noncondensables. A second thermodynamic analysis was then performed implementing predeaeration and reinjection as a means of handling the desorbed noncondensable gases. It was determined that a gross power

recovery of nearly 4% could be realized through the implementation of a predeaeration and reinjection approach to noncondensable handling.

Two hydraulic compressor configurations were investigated; a standard discharge pipe design and a tapering pipe design. It was found that a nominal savings of approximately 0.1% of the total gross power production could be recovered through the use of the tapering pipe design over the standard discharge pipe design.

TABLE OF CONTENTS

LIST OF TABLES

LIST OF FIGURES

Figure page

Figure page

CHAPTER 1
INTRODUCTION

1.1 BACKGROUND

The largest collection and storage medium for solar energy incident upon the earth is the tropical ocean mixed surface layer. The vast potential of this energy source can be brought into perspective by noting that a quantity of electric power equal to the entire projected U.S. demand for the year 2000 A.D. (approximately 700,000 MW) could be obtained by tapping 0.004% of the solar energy contained within the $\pm 10^{\circ}$ latitude band flanking the equator [9]. Put another way, on an average day the 60 million km^2 of tropical oceans absorb an amount of solar radiation equivalent in heat content to approximately 245 billion barrels of oil [43]. If less than 0.1% of this stored solar energy could be converted into electric power, it could supply over 20 times the amount of current U.S. electricity consumption [43]. It is this vast potential which has led to renewed interest within the last two decades in the technology aimed at exploiting this tremendous energy resource, namely ocean thermal energy conversion (OTEC).

Ocean thermal energy conversion systems exploit the temperature difference between the warm surface seawater and the cold deep seawater in generating electrical power via a simple Rankine cycle. The OTEC concept consists of two principal variations, the "closed-cycle" and "open-cycle" concepts. In a closed-cycle OTEC (CC-OTEC) system (see Figure 1.1), the warm surface seawater at 25 - 30 $^{\circ}$C is introduced into a heat exchanger and

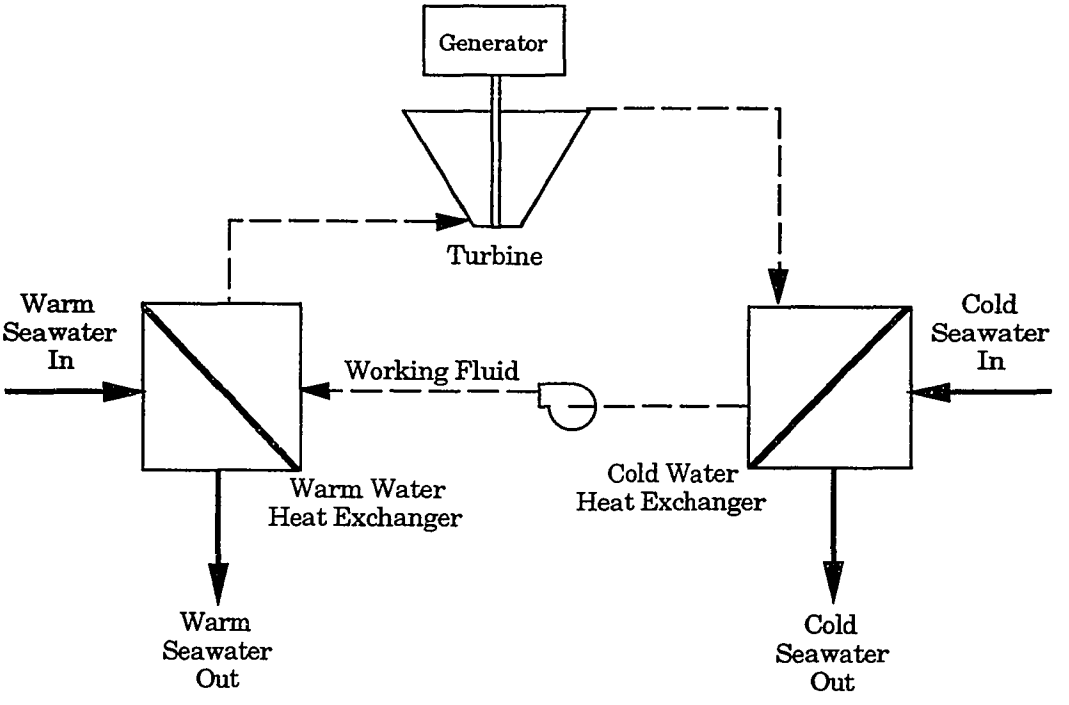

Figure 1.1: Block Diagram of CC-OTEC Concept

evaporates an auxillary working fluid such as ammonia or Freon®. The vaporized working fluid passes through an appropriate turbine connected to an electrical generator which produces net power after all parasitic power requirements are accounted. After expansion through the turbine system, the working fluid is subsequently condensed by the cold, deep ocean water in another heat exchanger and is pumped back to the evaporator to be revaporized, thus "closing" the cycle.

In the open-cycle OTEC (OC-OTEC) concept, the seawater itself is the working fluid (see Figure 1.2). The warm surface water is introduced into an evaporator section of a vacuum chamber where the pressure is maintained sufficiently below the vapor pressure at the incoming surface water

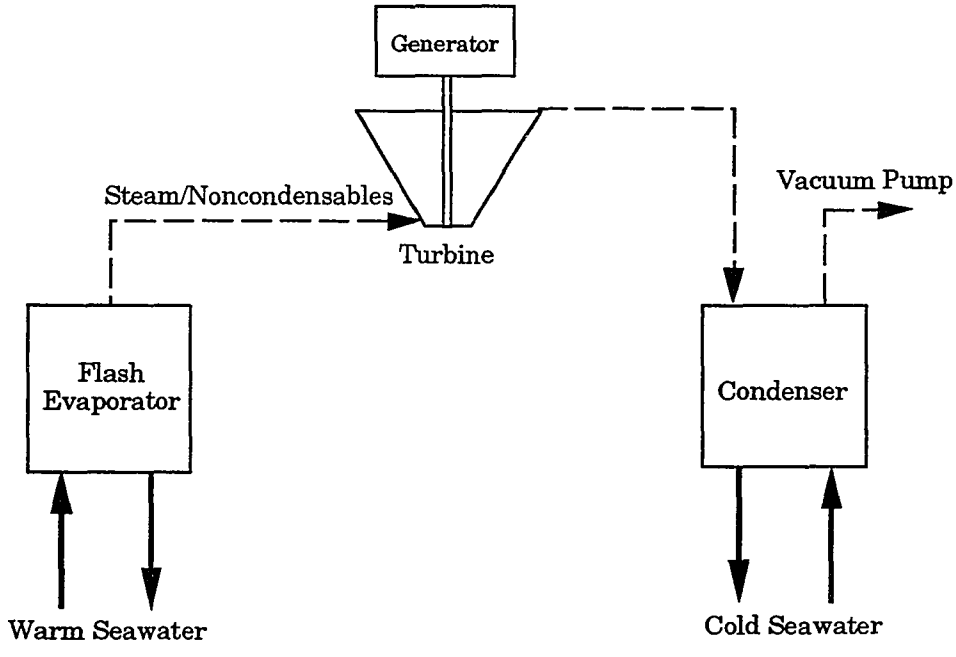

Figure 1.2: Block Diagram of OC-OTEC Concept

temperature (generally 25 - 30°C) so that flash evaporation occurs and steam is produced. Water droplets carried by the wet steam are removed in a mist eliminator. Cold deep seawater at about 5 - 8 °C from a depth of about 600 - 1000 meters is introduced into either a surface condenser (if fresh water production is desired) or a direct-contact condenser (if fresh water production is not desired) to condense the generated steam after expansion through a low pressure turbine. The turbine is mechanically linked to a generator, which yields net power after all power requirements are accounted for (pumping warm and cold seawater, vacuum pumps for noncondensables, etc.).

A third OTEC configuration, essentially an attempt to combine the attractive features of both the closed- and open-cycle concepts while avoiding the drawbacks, is called the "hybrid" cycle (see Figure 1.3). In this concept the

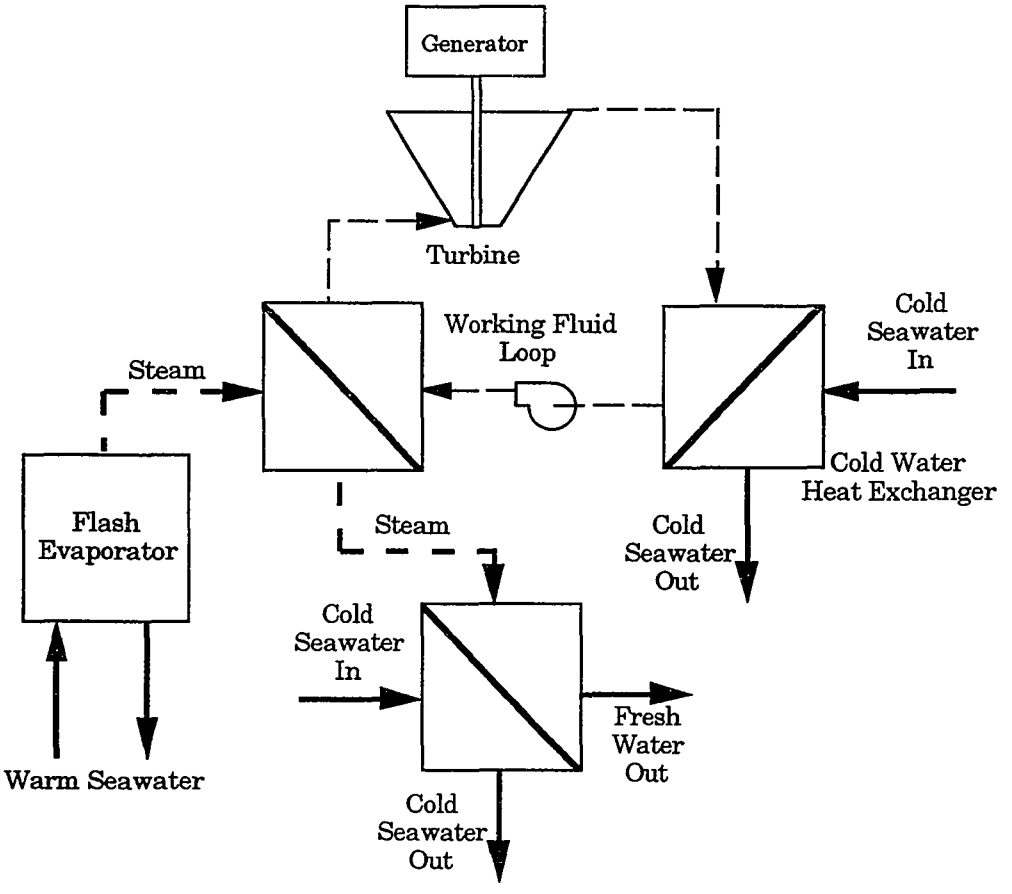

Figure 1.3: Block Diagram of "Hybrid" OTEC Concept

warm seawater is flash evaporated as in the OC-OTEC design. The generated steam is subsequently used to vaporize a working fluid (ammonia or Freon®) in a heat exchanger and is then condensed in a surface condenser to provide desalinated water. The vaporized working fluid then follows a similar scheme as that described for the closed-cycle concept previously. The major problem associated with this OTEC concept is the implementation of an extra heat exchange step which further reduces an already low Carnot efficiency.

The concept of harnessing the power stored in the tropical oceans was originally recognized by a French physicist, Jacques Arsene d'Arsonval, in 1881 [1]. D'Arsonval envisioned a closed-cycle concept in which ammonia was utilized as the working fluid. However, d'Arsonval never pursued the idea beyond conceptual design. The concept was further developed by a student of d'Arsonval's, George Claude, who conceived and constructed a working open-cycle OTEC facility in Matanzas, Cuba, in 1930 [7]. This facility produced 22 kW of electricity; however, due to poor site location (a storm destroyed the cold water pipe shortly after installation) and a seawater thermal differential of only 14°C, the project never produced net power (the pumping requirements exceeded the gross power produced). Claude continued his attempts at proving that the OC-OTEC concept could produce net energy, but never overcame the inherent difficulties associated with the cold water pipe deployment [28].

The high capital cost associated with an OTEC facility construction, especially with the uncertainties assocated with the cold water pipe, delayed OTEC development for many years. With only one exemption, a small OC-OTEC project carried on by the French government on the west coast of Africa in 1956 [28], the concept of OTEC lied dormant until the temporary world-wide energy shortages of the early 1970's revived the interest in alternative energy sources which could significantly reduce the world's dependance on dwindling and politically unstable fossil fuel resources. This increased attention on the OTEC concept (primarily the closed-cycle concept due to it's ability to be readily designed utilizing technologically available components and materials) led several countries to pursue laboratory scale experiments (France and the

Netherlands) [43] and the United States and Japan to build small-scale, proof-of-concept facilities [31] [44].

With the relatively low cost of fossil fuels enjoyed throughout the 1980's and thus far into the 1990's, the interest in all forms of alternative energy sources has waned on the political agenda and this complacency has been reflected in the funding appropriated to the development of such technologies. In more recent years the development of OTEC has begun to focus more on improving the open-cycle concept because of its attractive fresh water production potential, higher thermal efficiencies and lower environmental risks associated with avoiding the potentially dangerous working fluids necessary in the closed-cycle concepts. However, with the cutback of the U.S. Department of Energy (DOE) funding in recent administrations, the research efforts have been of laboratory scale designed at improving specific component performance with very little attention paid to the total integrated system analysis.

One exception to this trend has been the Sea Coast Test Facility (SCTF) located at the Natural Energy Laboratory of Hawaii (NELH) at Keahole Point on the Big Island of Hawaii. Over the past few years, the facility has been utilized to design and operate a Heat- and Mass- Transfer Scoping Test Apparatus (HMTSTA) which functions as a means of validating the seawater performance of spout evaporators, surface condensers and direct-contact condensers for the OC-OTEC system design. It also demonstrated for the first time that surface condensers utilized in an OC-OTEC system can produce desalinated water [43]. It is here that the experimental portion of this investigation was performed. Presently, the construction of a Net Power

Producing Experiment (NPPE) is under construction at Keahole Point and is aimed at providing net power utilizing an OC-OTEC configuration [40] [26].

1.2 NONCONDENSABLE GASES

Seawater contains dissolved gases consisting primarily of oxygen and nitrogen with relatively small amounts of free carbon dioxide and argon. Surface seawater also contains bubbles that are formed by biological activities. In addition, seawater contains suspended particles that are formed mainly by sedimentation of surface particles and can be produced in situ via biological activities. These dissolved gases will desorb at high rates when exposed to the low pressures of the OC-OTEC systems. The desorption of these gases is enhanced by the existence of entrained bubbles and suspended particles containing microbubbles, which provide gas-liquid interfaces for mass transfer and act as nucleation sites for newly formed bubbles.

One of the major technical issues facing the designer of an OC-OTEC power plant is to quantify the amount of gas that comes out of solution and to then determine its impact on the design of plant components. Desorption of gases in the evaporator and direct-contact condenser (if fresh water production is not desired) can significantly degrade the condenser performance, increase the size of condenser required, and increase the demand for cold water.

Specifically, the primary concern about the evolution of the noncondensables derives from their negative impact on the condensation process. As the noncondensables which desorbed in the evaporator during the evaporation process accompany the steam through the turbine, these gases

join those desorbed within the direct-contact condenser from the incoming cold water stream and those leaking into the system from the atmosphere, and accumulate at the condensing surfaces. The presence of these gases at the condensing surface work to lower the partial pressure of the steam, in turn lowering the steam saturation temperature. This lower temperature leads to a lower thermal differential between the steam and the cooling water, thus lowering the efficiency of the condensation process and increasing the cold water requirements. Simultaneously, the noncondensables raise the system pressure of the condenser and this requires more parasitic vent compression power to maintain the necessary system pressures for optimum evaporator and condenser performance. In order to address these problems associated with the evolution and leakage of the noncondensables within an OC-OTEC system, several varying approaches have been proposed.

The first method, and most widely accepted for present OC-OTEC designs, is to simply remove the accumulating noncondensables directly from the condenser itself via mechanical compression and vent the resulting gases directly to the atmosphere. One of the benefits of this method, which have led to its widespread acceptance for previous OC-OTEC designs, is that this approach does not require the introduction of any new components which would increase capital costs or possibly additional hydraulic head losses within the seawater flow system. Also, the concept of mechanical compression of gases is well established and requires no further development for implementation in an OC-OTEC facility. The principal drawback of this method of noncondensable removal is that it requires the extraction of the accumulated noncondensable gases at the lowest system pressure (approximately 1.2 KPa

for a direct-contact condenser configuration) and this requires a significant portion of the gross power production to compress the gases for atmospheric venting (approximately 10 - 15% of gross power production is lost to this function depending upon the fraction of noncondensables desorbed [6]).

Another method proposed for the handling of the noncondensable gases is predeaeration of the incoming water resource. Predeaeration implies the removal of the noncondensables prior to their introduction into the vacuum chambers of the evaporator (for the warm water flow) and the direct-contact condenser (for the cold water flow). The principal benefits of predeaeration consist of being able to remove the gases at higher system pressures (therefore less compression power requirements) and therefore minimizing the accumulation of the gases within the condenser, which would improve its efficiency and lower the cold water requirements. The principal drawbacks of the predeaeration concept are that this method requires the introduction of additional components within the OC-OTEC design which would increase initial capital costs and potentially increase hydraulic losses within the seawater flow system.

The predeaeration concept itself consists of two seperate approaches for vacuum deaeration, active and passive predeaeration. Active predeaeration consists of introducing the incoming seawater into a packed-column device which, through the use of the chemically inert packing material, provides a means to increase the available gas-liquid surface area which in turn enhances the gas desorption process. Various studies on this form of predeaeration have been performed [11] [12] [22] [51] and will be discussed further shortly. Krock and Zapka's [22] [51] investigations concluded that seawater predeaeration in

an active predeaerator can be significant, but the additional capital costs and significant hydraulic head losses through the predeaerator component make this form of predeaeration impractical.

Passive predeaeration, on the other hand, does not necessarily require the addition of new components to the OC-OTEC design. It does require the modification of present evaporator and direct-contact condenser configurations (see Figure 5.2 and Figure 5.4), but does not introduce any significant hydraulic head losses. Passive predeaeration is a concept which permits the natural desorption of gases to occur within the system's upcomers (intake pipes) as the pressure progressively decreases within the seawater flow and the seawater becomes increasingly supersaturated with the noncondensables. The presence of the microbubbles mentioned previously (or artifically added bubbles, regarded as bubble "seeding" by Zapka [51] and utilized in the following analysis) within the seawater provides the necessary gas-liquid interface to enhance the desorption of the gases. At some point along the seawater flow prior to introduction into the system's vacuum chambers, a free surface is provided for collecting the desorbed noncondensables and the gases are removed either via mechanical or hydraulic compression.

With the noncondensables removed from the OC-OTEC system, there are several alternatives available for the disposal of these gases. As mentioned previously, the principal means chosen for disposal of the evolved noncondensables is to simply vent them directly to the atmosphere following mechanical compression. This approach promotes the emission of carbon dioxide directly to the atmosphere and the discharge of large volumes of deoxygenated effluent water back into the ambient ocean.

A second alternative, which has yet to receive much attention from OC-OTEC design engineers, is the concept of utilizing the already existing downcomers as hydraulic compressors for the reinjected noncondensables. Reinjection of the noncondensables either removed from the condenser or predeaerators back into the system's existing downcomer (with some minor alterations) provides potential benefits in two ways:

1.) The reinjection of the evolved and leaked noncondensables back into the effluent water stream avoids the discharge of deoxygenated seawater back into the ambient ocean and avoids any discharge of environmentally damaging greenhouse gases such as carbon dioxide assuming no bubbles or CO_2 enriched discharge water make it to the surface.

2.) The usage of the existing downcomer as an hydraulic compressor harnesses some of the otherwise wasted kinetic energy of the effluent streams and could possibly significantly reduce the necessary mechanical compression requirements (and subsequent parasitic power losses) presently associated with the handling and discharge of the evolved and leaked noncondensables.

1.3 PREVIOUS EXPERIMENTAL WORK

The key technical questions regarding the handling of noncondensables within an OC-OTEC system which need to be addressed are:

(1) How much outgassing takes place in the upcomers of an OTEC plant under normal operating pressures?

(2) What are the differences between warm and cold seawater outgassing?

(3) Should the cold and warm streams be deaerated prior to introduction into the evaporator and condenser?

(4) Should the evolved and leaked noncondensables be reinjected into the systems downcomers, and what is the potential thermodynamic savings, if any?

(5) What are the thermodynamic benefits or losses attributable to the various noncondensable handling techniques mentioned previously?

In order to answer these questions, the Department of Energy in conjunction with the Solar Energy Research Institute (SERI), Argonne National Laboratories (ANL), the University of Hawaii, the Pacific International Center for High Technology Research (PICHTR), the Natural Energy Laboratory of Hawaii, the Research Corporation of Hawaii (RCUH) and the Hawaii Natural Energy Institute (HNEI) have funded several research projects over the last few years.

Several of the studies [11] [12] [22] [25] [51] have attempted to predict the desorption rate of noncondensables in OC-OTEC system upcomers. Lindenmuth et al. [25] designed and constructed a test loop and carried out tests to investigate outgassing in an upcomer using fresh water. The test parameters included flow velocity, deaeration pressure and nucleation site content. Golshani and Chen [11] [12] investigated deaeration in a packed column and in a barometric intake using fresh water. The parameters investigated included deaeration pressure, flow velocity and number of nuclei in

the water. Krock and Zapka [22] measured deaeration levels in upcomers and in a debubbler using warm and cold seawater and fresh water. They showed that seawater outgassing can be substantial.

Zapka [51] also researched the effects of bubble seeding on seawater in an effort to design efficient predeaeration systems. Once again, significant levels of outgassing of noncondensables was observed (approaching 90 - 95%).

Oney [30] performed molecular diffusion experiments using seawater and obtained molecular diffusion coefficients for oxygen and nitrogen which support the findings of Krock and Zapka [22] that seawater outgassing should be more substantial than that of fresh water, which was utilized in the previously mentioned experiments.

Thermodynamic investigations have been performed by several authors investigating the thermodynamic performances of varying OC-OTEC configurations [49] [6] [32] [45] [50]. Westinghouse [49] developed a thermoeconomic analysis of a 100-MW_e OC-OTEC power plant. They determined that the uncertainties associated with the cold water pipe designs and the lack of a suitable technologically available turbine for this size plant made OC-OTEC technologically too costly for further development within the private sector. Block and Valenzuela [6] performed a thermoeconomic study on an OC-OTEC facility comparing the thermodynamic and economic parameters of an OC-OTEC plant configured for energy production versus one configured for freshwater production.

Parsons et al. [32] developed a thermodynamic model and computer program for the determination of the thermodynamic performances of the integrated OC-OTEC system using direct-contact condensation with input

parameters of plant gross power capacity, inlet and outlet turbine steam temperatures and warm and cold seawater resource temperatures. Test parameters included plant sizes, the effects of predeaeration on system performance (utilizing equilibrium approximations to estimate predeaeration percentages) and varying turbine inlet and outlet steam temperatures.

Valenzuela et al. [45] presented a thermoeconomic study which included analyses of the effect of seasonal variations of seawater resource temperatures on OC-OTEC system components' performance and evaluated the various alternative strategies proposed for handling the system noncondensable gases in OC-OTEC plants. Their analysis concluded that barometric riser predeaeration and hydraulic compression have the potential for significantly decreasing plant cost.

Zangrando et al. [50] performed thermodynamic analyses on all major components for an OC-OTEC system, excluding the turbine, used in the HMTSTA at Keahole Point, Hawaii. Their analyses provided great insight into the expected performances of spout flash evaporators, surface condensers, direct-contact condensers and warm water predeaerators. They suggest that warm water predeaeration can save up to 25% of noncondensable pumping power, which translates into an overall plant savings of approximately 3% [50].

Golshani and Chen [13] investigated hydraulic air compression for open-cycle OTEC applications. Their studies were performed utilizing fresh water as the working fluid, and therefore reabsorption of the noncondensables in their investigation was limited. They concluded that in spite of negligible reabsorption, hydraulic compression within existing system downcomers was a

potentially cost-effective mechanism for OC-OTEC consideration and that further investigations into the extent of the potential benefits should be performed.

The noncondensable gas experiment tests reported in this text are a natural progression from the small scale, flow path dependent experiments mentioned previously. These noncondensable gas measurements on actual OC-OTEC components using tropical seawater should greatly enhance confidence in noncondensable outgassing predictions and improve system designs with more accurate noncondensable loading information. Also, information on the composition of the noncondensables should provide greater insight into the environmental impact of venting evolved noncondensables directly into the atmosphere or discharging significant volumes of degassed seawater back into the ambient ocean.

Likewise, the thermodynamic evaluation of the OC-OTEC system incorporating the new desorption and reabsorption rates predicted by Zapka [51] and reported here in this report should provide a better understanding of the potential thermodynamic, and eventual economic, savings associated with implementing predeaeration and reinjection of noncondensables within future OC-OTEC system designs.

1.4 OBJECTIVES OF PRESENT STUDY

The lack of reliable experimental data on the extent of noncondensable outgassing occurring under normal operating conditions of a prototype OC-OTEC system has created the need for the research to be addressed in this

dissertation. One of the primary objectives of this research is to quantify the levels of outgassing occurring in the various components of the OC-OTEC system. Prior to this research, very little was known as to the extent of outgassing which occurred in the system with seawater as the working fluid. At best, only very rough estimates have been used to predict the extent of the noncondensable outgassing. With this more accurate account of the gases being desorbed, design engineers can better determine methods of handling the noncondensable problem presently hindering OC-OTEC condenser performance.

A second objective of these tests is to determine the differences between warm and cold seawater outgassing in a functional D.C.C. OC-OTEC configuration. This information should provide greater insight into the predeaeration requirements of the respective warm and cold water streams. This, in turn, should lead to greater OC-OTEC efficiencies and, hopefully, lower operational costs for future OC-OTEC designs.

A third objective of these tests is to determine the noncondensable gas composition. With this knowledge, a greater understanding of the desorption process could be inferred through analysis of the extent of specific gas outgassing. Also, a better estimate of the levels of CO_2 outgassing occurring in the cold water stream would greatly enhance predictions as to the environmental effects of venting noncondensables desorbed directly to the atmosphere.

Upon completion of the experimental work described in the first three objectives of this dissertation, which should provide a great deal of insight into the outgassing rates of the noncondensable gases in a direct-contact configured

OC-OTEC system, the potential benefits of predeaeration and reinjection of the evolved noncondensables will be determined. In order to determine the potential thermodynamic gains associated with such procedures for handling the noncondensables, it is necessary to compare a conventional design which ignores the noncondensables and utilizes a standard vent compressor system, versus a plant incorporating predeaeration and reinjection as an alternative approach for handling the noncondensables. Since several designs for plants using conventional mechanical compression are available [6] [32] [49], it would be extremely useful to develop a preliminary design incorporating predeaeration and reinjection components into the OC-OTEC plant infrastructure. Such a design would require careful integration of the deaeration data discussed above and the small-scale predeaeration/reinjection efficiencies obtained by Zapka [51] for designing the necessary components for an optimal OC-OTEC configuration. This is the main objective of this dissertation.

In order for a proper comparison of overall efficiencies and potential savings for an OC-OTEC facility incorporating predeaeration/reinjection versus conventional vent compression, a complete thermodynamic evaluation of the OC-OTEC system utilizing direct-contact condensation must be performed. This thermodynamic evaluation must account for the gas exchange processes occurring in both the predeaerators and reinjectors, the additional losses associated with these components, as well as the overall energy requirements associated with a typical direct-contact condensed OC-OTEC system. From the results of this thermodynamic analysis, a simple comparison of efficiencies can be performed utilizing the results obtained when

using another reported OC-OTEC plant design model incorporating typical vent compressors.

Similarly, this type of analysis needs to determine and quantify the potential environmental advantages/disadvantages afforded an OC-OTEC facility incorporating a reinjection mechanism. Specifically, the differences in the environmental effects which occur between a conventional OC-OTEC plant, which discharges oxygen-deficient seawater back into the ambient ocean and vents the removed noncondensables to the atmosphere, and a plant designed with predeaeration/reinjection, must be evaluated as well.

In order to develop a reasonable preliminary design of this nature incorporating predeaeration and reinjection, the results obtained from the experimental portion of this research, in conjunction with the results of previously reported small-scale experiments, will be utilized to predict the gas exchange efficiencies and rates within designed system components. From this data, specifically those obtained by the author on the HMTSTA and by Zapka [51], the optimum design of the predeaeration device as well as the reinjection mechanism will be developed. The design of the specific components will combine present existing industrial gas exchange technology with specific requirements of the OTEC process realized through previous research. These designs must also include an analysis determining the optimal locations for these devices to minimize parasitic energy losses associated with these components. This will require the determination of optimal locations for gas venting, the extent of predeaeration to be performed, and the optimal location for gas reinjection to take advantage of naturally occurring system pressures, all of which should lead to minimizing parasitic losses.

An extensive thermodynamic analysis of the entire designed system, including the gas desorption and reabsorption processes, will be included as well. This, in turn, will be useful when incorporated with an overall energy balance of the entire system.

CHAPTER 2
EXPERIMENTAL METHODOLOGY

The following chapter outlines the methodology utilized in this investigation to arrive at the noncondensable outgassing rates presented in Section 3.0 of this report. As previously discussed, the outgassing rates were measured on the 1.0+ MW prototype (excluding the turbine system) HMTSTA test facility located at NELH at Keahole Point, Kailua-Kona, Hawaii. All data has been acquired under typical OC-OTEC system pressures and temperatures utilizing a direct-contact condenser configuration with no predeaeration or reinjection of the evolved and leaked noncondensables. The methodology utilized to arrive at these outgassing rates is presented here to provide a means for future investigations to reproduce the experimental conditions and results reported in this text.

2.1 THE MASS SPECTROMETER

A Quadrex 100 Residual Gas Analyzer (RGA or mass spectrometer) was used to measure the raw noncondensable composition in the working HMTSTA system. This mass spectrometer allows for the direct measurement of specific gas partial pressures from a vacuum system (see Appendix E for the schematic and description of the mass spectrometer system). This proved to be an ideal method by which the various noncondensable gases being deaerated within the OC-OTEC system could be measured in the vacuum spaces above the liquid. In order to utilize the mass spectrometer, it was

initially necessary to set the calibration factors for each specific gas prior to actual data acquisition. Therefore, a detailed description of the calibration techniques utilized in this experiment is appended (Appendix A).

2.2 ARGON TRACER METHOD

As previously stated, one of the primary objectives of this investigation was to determine the extent of outgassing of the various noncondensable gases present in seawater. To obtain a rate of outgassing for each gas, a means of measuring the flow of vapor through the HMTSTA was necessary. With this information and the volume- percent composition data obtained from the Quadrex, an accurate account of the noncondensables flowing through the HMTSTA could be determined. The argon tracer method, or "mixture" method [35], was developed and implemented to provide this information.

Basically, the argon tracer method consists of injecting a known amount of pure argon through a Dwyer visi-float flowmeter (model # VFB) at a measured inlet pressure (generally 2 atm. gage) into the top of the evaporator and comparing the change in argon partial pressure read by the Quadrex to the partial pressures of each specific gas. From this comparison and the knowledge of the flow rate of the argon injection, the amount of each noncondensable flowing through the HMTSTA could be determined (the actual formulas and data conversion techniques are discussed in more detail later in the text). Argon was chosen as the tracer gas due to its chemical inertness and its non-interfering nature of its the mass spectrum (argon has essentially one distinct peak at mass 40).

In order to ensure that the outgassing data acquired throughout these tests using this technique are representative of actual noncondensable outgassing, it was necessary to check the validity of the argon tracer method. To check this method, air was leaked into the system at the top of the evaporator through a Dwyer Rate Master Flowmeter (model #RMC-104) at various flow rates and under various common HMTSTA conditions (previously measured warm and cold water flow rates).

The flow of noncondensables through the HMTSTA (including the contribution from the atmospheric air injection originally measured in cubic feet per hour (cfh) and then converted to metric units) was then measured using the argon tracer method. The values obtained for nitrogen and argon (chosen for their relatively inert behavior and conservative characteristics) were compared to the expected values for each gas under the control flow condition and known air injection rate. The expected gas values were obtained as follows:

$$M_{je} = M_{j,ave} + y_{air,j} Q_{air} \qquad (2\text{-}1)$$

where M_{je} = expected molar flow rate of gas j through HMTSTA under air injection mode.

$M_{j,ave}$ = average molar flow rate of gas j through HMTSTA without air injection under same experimental flow conditions using outgassing figures presented in Section 3.0 of this report

$y_{air,j}$ = average volumetric composition of gas j in atmospheric air in Kona taken from data presented in Appendix A. ($y_{air,N2} = 0.762$, $y_{air,Ar} = 0.0090$)

Q_{air} = molar air injection rate into HMTSTA

Table 2.1 and 2.2 present the data comparison for nitrogen and argon, respectively, and show the accuracy of the argon tracer method.

2.3 SAMPLING PROCEDURE

Imperative to any scientific investigation is a clear and accurate account of sampling procedures and techniques to ensure the reproducibility of the data. The following sections contain detailed descriptions of the sample locations, sampling techniques and methods used to convert the raw data into pertinent information.

2.3.1 SAMPLE LOCATIONS

The Quadrex RGA system originally purchased from Leybold-Inficon was designed and configured to handle up to four (4) remote sample locations. Therefore, four sample sites were chosen on the HMTSTA (see Figure 2.1) and were connected to the RGA system using either 1/16" or 1/4" stainless steel sample capillaries depending on system vacuum at the sample location (1/16" capillaries were used when system pressures approached atmospheric--

Table 2.1: Argon Tracer Method Validity Test Using Quadrex N_2 Values

WW/CW Flow (liter/sec)	Air Injection Flow (cfh)	Expected N_2 Flow* (mmol/sec)	Actual N_2 Flow† (mmol/sec)	% Deviation (%)
10/10	100	47.24	41.40	7.2
10/10	120	52.59	50.92	1.8
10/10	300	100.72	99.44	0.8
10/25	100	54.99	54.06	1.0
73/50	100	94.89	93.87	0.6

* Expected value = Average value without injection (Figures 3.2 and 3.3) + Contribution expected from air injection

† Average value (3 data sets) measured by Quadrex for specific flow

Table 2.2: Argon Tracer Method Validity Test using Quadrex Ar Values

WW/CW Flow (liter/sec)	Air Injection Flow (cfh)	Expected Ar Flow* (mmol/sec)	Actual Ar Flow† (mmol/sec)	% Deviation (%)
10/10	100	0.66	0.59	6.1
10/10	120	0.72	0.62	8.0
10/10	300	1.30	1.14	7.1
10/25	100	0.91	0.90	0.6
73/50	100	1.82	1.85	0.9

* Expected value = Average value without injection (Figures 3.6 and 3.7) + Contribution expected from air injection

† Average value (3 data sets) measured by Quadrex for specific flow

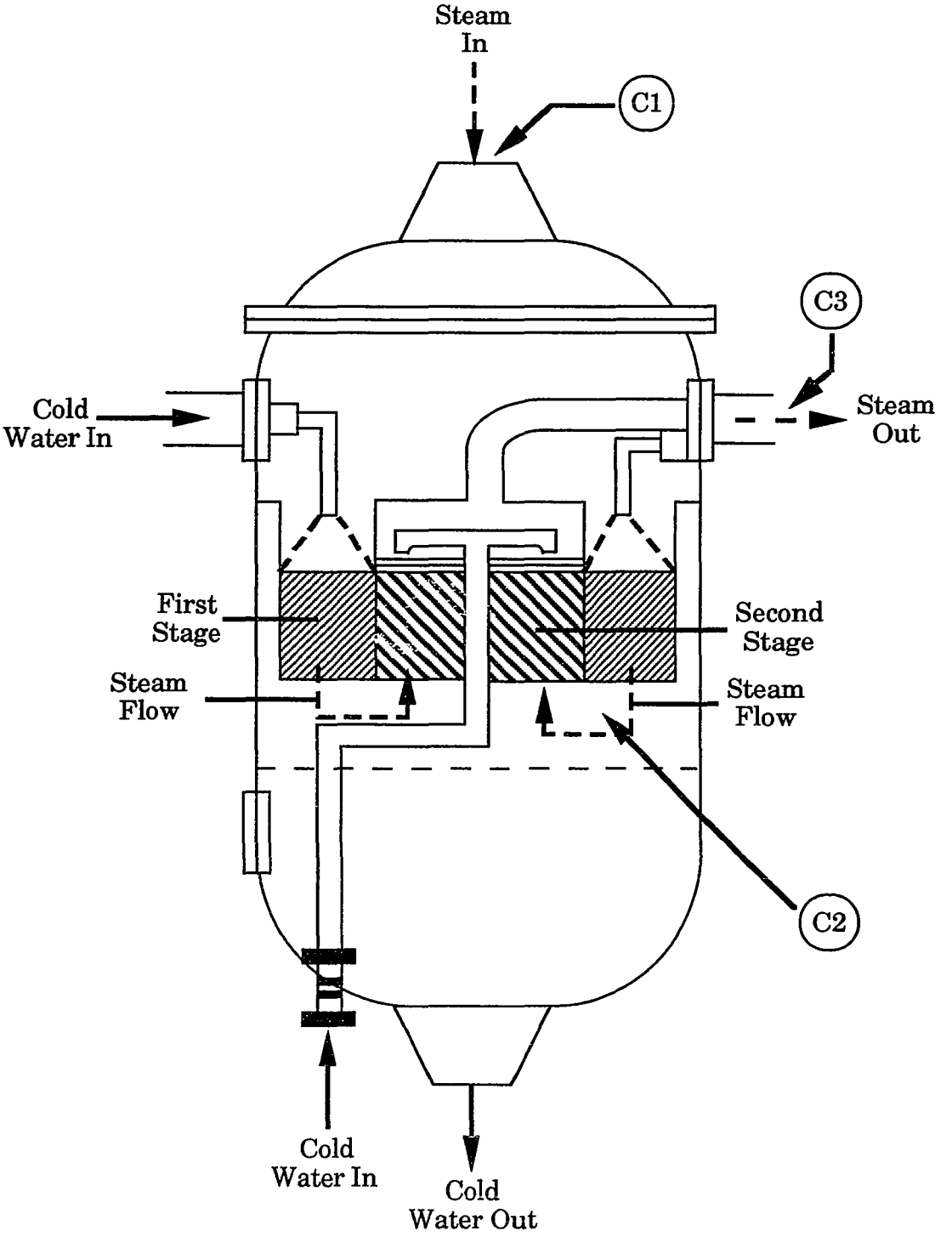

Figure 2.1: Direct-Contact Condenser Sample Port Locations (Sample Port CM = Outlet of Compressor - Not Shown)

compressor outlet, and 1/4" capillaries were used when system vacuum fell in the 10 - 20 torr range -- remaining sample ports).

The first sample port (C1 on Figure 2.1) was located at the entrance to the condenser. This site was chosen so that direct measurements of the noncondensable outgassing of the warm water stream in the evaporator could be obtained prior to addition of the noncondensables from the cold water stream. The second sample port (C2) was located at the interstage of the direct-contact condenser (DCC) between the co-current and counter-current cold water condensing stages. The third sample port (C3) was located in the exhaust pipe from the condenser to the compressor, and sampled the noncondensable contributions from both the warm water and cold water streams (evaporator and condenser) as well as the uncondensed water vapor (steam) remaining after being exposed to the DCC. The fourth and final sample location (CM) used during these experiments was located at the exhaust of the liquid-ring compressor.

Unfortunately, the data presented in the report was only taken from one of the four original sample locations, the exhaust of the DCC (C3). This is due to the fact that the data obtained at the other three locations during periods of steam generation proved very suspect for various reasons.

The first two sample ports, the entrance and interstage of the DCC (C1 and C2, respectively) were not able to be used due to the extremely high concentrations of water vapor (steam) at these two locations. The presence of such high quantities of steam saturated the electron multiplier (EM) sensor and interfered with accurate measurement of noncondensable partial

pressures. Therefore, the values obtained at these locations under steam generation were not used in this investigation.

The data from the fourth sample port, the exhaust of the liquid-ring compressor (CM) is not reported for two reasons. The first being that much of the data acquired at this sample port was taken before sufficient care was employed in preventing atmospheric air back-diffusion into the sample port, which caused many of the early values obtained to be very high. The second reason the data was not used is due to the result of compressing the air in a liquid-ring compressor, the relative composition of the oxygen and carbon dioxide in the stream were drastically altered during the compression process. The data obtained from the unreactive gases such as nitrogen and argon remained unaffected through the compressor (by comparison to the compressor entrance composition measured at sample port C3). Therefore, the data obtained at sample port CM are not presented in this report.

Fortunately, the data obtained at sample port C3 proved low enough in steam (the condensation process had been performed previously in the DCC) that data could be reliably taken. By varying flow conditions and rates of the warm and cold water feed streams, a great deal of information pertaining to relative outgassing of noncondensables in both the evaporator and DCC was obtained using the one sample port.

2.3.2 SAMPLING TECHNIQUES

In order to minimize human error in the data acquisition phase of the experiment and thereby enhance the reproducibility of the data acquired, a

structured sampling procedure was developed. This procedure, developed through experience and trial and error means, was utilized throughout the experimental tests.

Prior to taking actual, usable samples from the HMTSTA, the sampling capillaries interfacing the RGA system to the HMTSTA required "roughing down". This was accomplished two ways. Initially, upon reaching typical system vacuum, all of the sample capillaries were opened up to the HMTSTA while still being closed off to the RGA system. This permitted the HMTSTA system to do most of the work on purging the capillaries which in turn minimized the stress on the RGA vacuum pumps. After the capillaries had been open to the HMTSTA for a minimum of 5 minutes, the capillaries were opened up to a Leybold-Heraeus Trivac roughing pump which drew the sample gas from the HMTSTA through the capillaries. This brought the fore vacuum pressure of the Quadrex sensing chamber down to approximately 10^{-2} mbar which ensured sufficient flow of the desired sample gas as well as minimizing the stress encountered by the sensor's turbovacuum pump used to reach a sensing vacuum of approximately 10^{-6} - 10^{-5} torr. Next, the capillaries were opened up to the sensing chamber and the Leybold-Heraeus Turbovac 50 turbovacuum pump. After several minutes of drawing sample gas through the sensing chamber, the partial pressures of the sample gas were read and recorded by the Quadrex/IBM-PC computers using a PC-QPAK software program provided by Inficon with the mass spectrometer system. While the data was being recorded by the computer, the data was hand recorded on data sheets for immediate analysis. The sensing chamber was then closed off to the

capillary and a new sample location was opened up to the roughing pump and the procedure was repeated.

After all measurements had been taken at the four remote sampling locations under normal operating conditions, the above procedure had to be repeated for all locations during argon injection. Prior to repeating this procedure, the argon flow through the HMTSTA had to be initiated and allowed to arrive at steady state to ensure accurate outgassing results.

To inject the argon into the top of the evaporator, initially the injection pressure (generally 30 psig) was set by adjusting the argon tank regulator and observing a pressure gauge placed inline between the argon tank and the Dwyer visi-float flowmeter used to measure the flow rate of the argon injection. After setting the injection pressure, the flow rate was adjusted on the flowmeter to the desired setting (generally 8 scfh). Now, the argon flow was allowed to reach steady state throughout the HMTSTA system (generally 5 minutes during steam generation and over 15 minutes when steam was not being generated). While the argon was flowing through the HMTSTA, the concentration of argon at the sample port C3 was being monitored by the Quadrex/IBM-PC computer system in the ion chromatogram mode which permitted direct observation of argon concentrations during the initial injection period. After the argon flow reached steady state, the previously discussed sampling techniques were repeated.

Following data acquisition during argon injection, HMTSTA system flow conditions were changed and the entire procedure, with and without argon, was repeated. The data recorded was then analyzed as outlined in the following

sections during the period required to reach new HMTSTA steady state conditions under the new flow rates.

2.3.3 RAW DATA CONVERSION

At the beginning of the data acquisition period, measurements of the respective background partial pressures for each gas were taken, and are shown in the following table (Table 2.3). From time to time visual observations of the backgrounds were made to monitor the extent of hydrocarbon contamination occurring and to ensure no major emergence of other trace gases. The values of the backgrounds in Table 2.3 are insignificant when compared to the data presented in Appendix D (less than 3%) for each gas except CO_2 (the significance of this background will be dealt with later in this report). Therefore, in the handling of the raw data as described subsequently in this section, the residual backgrounds inherent in the data are ignored but will be treated later in the report and combined in the total background analysis.

A single peak conversion approach to analyzing the mass spectrum provided by the RGA was the principal means for determining the relative contribution of each significant noncondensable gas. This means that the measured relative abundance at (m/e) (mass equivalence) of 28 is interpreted as all coming from N_2. However, it is possible that trace elements and ions are present within the sample chamber with the same (m/e) as the significant gases. For example, CO^+ occurring from the fragmentation and ionization of hydrocarbons (such as roughing pump oils, cleaning solutions, etc.) would also contribute to the relative measurement at (m/e) 28.

TABLE 2.3: RGA Gas Backgrounds (x 10^8 torr)

	N_2	O_2	CO_2	Ar
	0.046	0.032	0.007	0.000
	0.047	0.030	0.007	0.000
	0.058	0.032	0.004	0.000
	0.055	0.029	0.003	0.000
	0.049	0.030	0.005	0.000
	0.050	0.030	0.003	0.000
	0.049	0.030	0.003	0.000
	0.060	0.036	0.006	0.000
	0.060	0.034	0.005	0.000
	0.060	0.051	0.011	0.000
	0.058	0.039	0.006	0.000
Mean, μ	0.054	0.034	0.005	0.000
σ	0.005	0.006	0.002	0.000

In order to determine the significance of this contribution, continual visual observations of the trace spectrum were performed throughout the data acquisition period. It was clear through these observations that the only significant peaks occurred at (m/e) representative of the gases analyzed in this report. The magnitude of these peaks was far greater than any other peaks occurring at (m/e) indicative of possible sample contaminating traces (such as m/e = 24, 25, 41, 42, etc.) [24]. Therefore, any contribution to these major peaks from these traces would easily be consumed by the natural backgrounds and errors to be reported in subsequent sections of this report (the only gas which could be significantly affected by such traces is CO_2 and is further addressed later in this report).

As previously stated, the Quadrex/IBM-PC computer system read the relative system noncondensable partial pressures directly. From these

relative partial pressures the rate of noncondensable outgassing was desired. Therefore, a means of converting the relative partial pressures into molar flow rates was developed.

All outgassing measurements taken in this investigation are based, essentially, on a comparison of the change in vapor composition in the HMTSTA system caused by changes in a controlled argon injection rate. Therefore, it was necessary to measure the partial pressures of the gases under conditions of no argon injection and with argon injection. From these two data sets, the background argon flow (actual amount of argon flowing throughout the HMTSTA without argon injection) could be obtained as follows (the value obtained without argon injection can not necessarily be taken directly as the argon background to be used in the calculations because the magnitude of the argon injection rate was occasionally significant enough to shift the relative partial pressures of the other noncondensables; however the shift was generally minor and the argon background was generally very close to that measured without argon injection):

$$PP_{Ar,BACK} = PP_{Ar,1} * PP_{N2,2} / PP_{N2,1} \qquad (2\text{-}2)$$

and from this

$$PP_{Ar,INJ} = PP_{Ar,2} - PP_{Ar,BACK} \qquad (2\text{-}3)$$

where

$PP_{Ar,BACK}$ = partial pressure of argon flowing in the second data set (argon injection) if the argon injection was absent (torr)

$PP_{N2,2}$ = partial pressure of nitrogen in the second data set

$PP_{N2,1}$ = partial pressure of nitrogen in the first data set

$PP_{Ar,1}$ = partial pressure of argon in the first data set (no argon injection)

$PP_{Ar,INJ}$ = partial pressure of argon due to argon injection into HMTSTA

$PP_{Ar,2}$ = partial pressure of argon in the second data set (includes argon injection)

The volume rate of argon injection was determined as follows:

$$Q_{Ar,INJ} = Q_{FM} * [(MW_{air} / MW_{Ar}) * (P_{INJ})]^{1/2} \quad (2\text{-}4)$$

where

$Q_{Ar,INJ}$ = argon injection rate (scfh)

Q_{FM} = flow meter reading (scfh)

MW_{air} = molecular weight of air

MW_{Ar} = molecular weight of argon

P_{INJ} = injection pressure into flowmeter (atm)

Equation (2-4) is essentially used to correct the air calibrated flowmeter value to account for argon injection rather than air at higher than atmospheric pressures. This was necessary since the difference in injection pressure and molecular weight of the gases would introduce significant error into the calculations if not corrected.

With values for the rate of argon injection ($Q_{Ar,INJ}$) and the partial pressure in the second data set due to the argon injection ($PP_{Ar,INJ}$), the extent of noncondensable outgassing for each specific gas, j, could be calculated as follows:

$$Q_j = Q_{Ar,INJ} * (PP_{j,2} / PP_{Ar,INJ}) \quad (2\text{-}5)$$

where

Q_j = rate of noncondensable outgassing for gas j (mmol/sec)

$PP_{j,2}$ = partial pressure for specific gas j in second data set (torr)

From these values total noncondensable outgassing (Q_{TOT}) for each HMTSTA flow condition can be determined.

$$Q_{TOT} = \Sigma Q_j \quad (2\text{-}6)$$

A Basic computer program was used on site in Kona to perform these calculations. A copy of the program is presented in Appendix C.

2.4 HMTSTA COMPONENT SPECIFICATIONS

2.4.1 EVAPORATOR

The evaporator vessel utilized in this experiment is 1.07 m (3.5 ft) in diameter by 6.9 m (22.5 ft) high (Table 2.4). The vessel was originally used for closed-cycle heat-exchanger tests at Argonne National Laboratories (ANL). It was modified for use in the HMTSTA by

- Removing internal tubes
- Providing a 76-cm (30 in) diameter steam outlet port
- Adding a port for seawater drainage
- Adding mounting fixtures for the evaporator spout plate assembly and the mist eliminator assembly

- Modifying and adding ports for viewing evaporation, deaeration, and mist removal processes.

Table 2.4: Specifications for the HMTSTA Evaporator Vessel

(Taken from [33])

Parameter	Value or Description
Water supply and discharge fittings	30.5 cm (12 in.) pipe flanges
Steam outlet pipe	76 cm (30 in.) diameter pipe
Spout mounting plate	1.07 m (42 in.) diameter, 38 mm (1.5 in.) thick, located 3.1 m (10 ft.) below the bottom of the steam outlet pipe
Spout size	25.4 cm (10 in.) diameter
Mist eliminator mounting tabs	8 each, 5 cm x 5 cm (2 in. x 2 in.), with a 1.4 cm (9/16 in.) diameter hole located 2 m (6.6 ft.) above the spout mounting plate
Lighting and view ports	2 each, 30 cm (12 in.) diameter ports, 76 cm (2.5 ft.) above the spout mounting plate 2 each, 30 cm (12 in.) diameter ports, just below the spout mounting plate 1 each, 30 cm (12 in.) diameter port, at the top of the evaporator vessel

2.4.2 DIRECT-CONTACT CONDENSER (DCC)

The DCC utilized in this experiment was shown in Figure 2.1 previously in the text. The co-current section is a hollow cylinder with an outside diameter of 1.45 m and an inside diameter of 0.68 m [33]. The countercurrent section fits in the hollow interior of the coaxial section with an 8.9 cm diameter central water supply pipe running up the center. Maximum packing height for the coaxial configuration is also 0.91 m.

Water distribution for the co-current section is provided by twelve 7.6 cm Munters dek-SPRAY nozzles. These nozzles are equally spaced, centered over the packing, nominally 5 cm above the packing. The central water supply pipe feeds a perforated plate with 756 - 5 mm water drain holes in a square pattern 1.8 cm apart. Ten 3.8 cm diameter risers along with approximately 2 cm gaps between the outside of the plate and the column edge and between the inside of the plate and the water supply pipe allow uncondensed steam and noncondensable gases to escape upward to the vacuum compressor line [33].

CHAPTER 3
EXPERIMENTAL RESULTS

The following sections break down the results of the noncondensable outgassing research and investigate the extent of outgassing for each individual gas. From this knowledge the total noncondensable outgassing can easily be derived as well as a more thorough understanding of the mechanisms governing the gas evolution process and the relative contribution to the overall noncondensable problem in OC-OTEC for each specific gas.

3.1 NITROGEN

Nitrogen is perhaps the most important gas for OC-OTEC considerations due to the quantity of this gas dissolved in seawater. One would expect nitrogen to be the principal gas found in the noncondensables which build up in the DCC since both the warm and cold water streams contain relatively large amounts of the gas (discussed in greater detail in the following section).

Its relative abundance and low chemical reactivity, as well as its fairly stable concentration characteristics on a day-to-day basis in seawater, make nitrogen a very attractive gas for observing warm water and cold water outgassing characteristics. Also, these same traits make nitrogen an obvious choice as the gas to use when attempting to quantify the air background (leak) into the HMTSTA and RGA systems (this is described in greater detail in Section 3.1.3).

Nitrogen is generally a very difficult gas to measure on-line since there are no probes or chemical tests which can simply be performed to give values of nitrogen content. Only through a mass spectrometric or chromatographic means is it possible to directly measure nitrogen content in a vapor or liquid stream. Thus, the results of this investigation, especially the results pertaining to nitrogen outgassing, are very important to OC-OTEC design engineers because they are the first of their nature that measure the most reliable indicator of noncondensable outgassing, nitrogen.

3.1.1 COMPOSITION IN SEAWATER

Nitrogen is found to be essentially at equilibrium in seawater with respect to the atmosphere at the given water temperature [21] (see Figure 3.1). This is fortunate since data pertaining to dissolved nitrogen content in warm and cold seawater suitable for OC-OTEC plants is very scarce. The only known source of such information which would be suitable for predicting initial nitrogen concentrations of the warm and cold water used in the HMTSTA in Kona (necessary for making predictions as to the extent of outgassing of the warm and cold water streams, since actual measurement of the nitrogen level prior to introduction into the system is impossible without the use of a gas chromatograph) was presented by Krock [21]. Krock measured dissolved nitrogen, oxygen and carbon dioxide in both the surface and deep water off the coast of Oahu in the spring and summer of 1981. One would expect very little

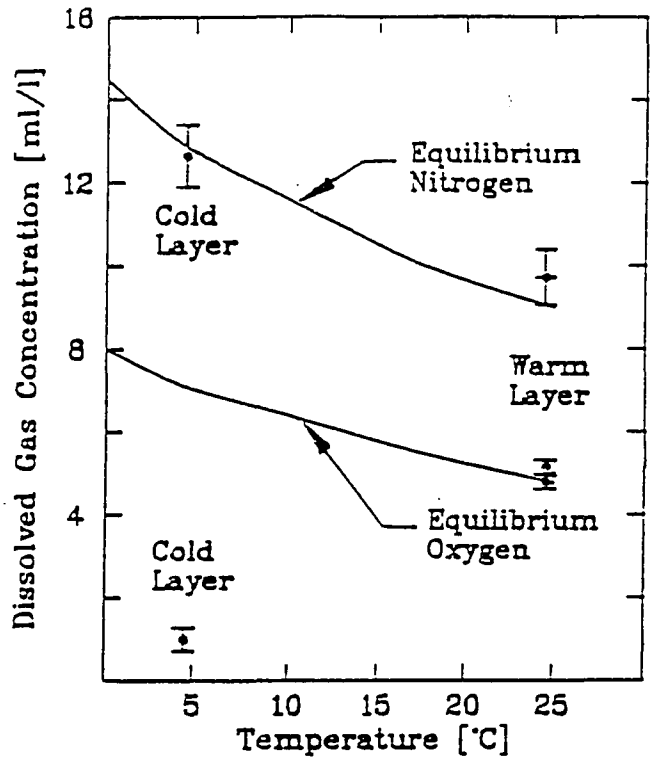

Figure 3.1: Comparison of Measured and Equilibrium Dissolved Gas Concentration
(Taken from [21], data points represent measured data)

deviation in the concentrations presented by Krock due to the relatively small spatial difference between Oahu and Kona. The majority of the data for this report was taken in the late spring and early summer of this year (similar to Krock's data), so small seasonal fluctuations should not present a problem either (especially in nitrogen's case). Therefore, the composition of nitrogen (oxygen and carbon dioxide as well) in the warm and cold water streams used in the HMTSTA in Kona are predicted using Krock's reported values.

Krock [21] reports the cold water dissolved nitrogen composition as 12.67 ml/l (0.566 mmol/l) at depths between 700-1000 meters (4 - 6°C) (Figure 3.1). The mean warm water dissolved nitrogen composition is 9.70 ml/l (0.433

mmol/l) at depths of 10 - 70 meters (23.5 - 25.5 °C). The depths and temperatures of these measurements correspond very well to those used in Kona for the warm and cold water streams for this study (warm water temperatures used in the HMTSTA generally fell in the 24.5 - 25.5 °C range and the cold water stream was generally in the 5.0 - 6.5 °C range). Therefore, Krock's data should provide very good estimates of ambient feed stream compositions to the HMTSTA.

3.1.2 TOTAL NITROGEN FLOW

Figures 3.2 and 3.3 represent the vapor flow of nitrogen through the HMTSTA during steam generation under various warm water and cold water flow conditions. From the slopes of these plots, it is easy to see the relative contribution the warm water and cold water streams have on the total nitrogen outgassing. It should be noted that these plots represent the total flow of nitrogen through the HMTSTA, which includes the nitrogen outgassed from the warm and cold water streams, the leak of nitrogen into the HMTSTA from the atmosphere as well as any leaks into the mass spectrometer sampling system. In order to make proper conclusions as to the extent of outgassing of nitrogen and the other gases from the OC-OTEC process, it is first necessary to quantify the contribution of each of the aforementioned components of the total noncondensable flow rates. The following section addresses the relative contribution of leaks in the data presented in Figure 3.2 and 3.3.

3.1.3 LEAK (BACKGROUND) ESTIMATION

In order to quantify the leak (or background) of nitrogen present in the data shown in Figures 3.2 and 3.3, it was necessary to determine, from these data, the amount of nitrogen gas which would be present in the HMTSTA with zero warm and cold water flow rates. Since it was not feasible to take data directly using the argon tracer method with zero warm or cold water flow rates under steam generation, it was necessary to extrapolate the data presented to obtain zero warm and cold water nitrogen outgassing levels. First the zero warm water nitrogen outgassing rate occurring under known cold water flow rate extrapolated from Figure 3.2 was plotted and then the zero cold water nitrogen outgassing flow rate occurring under known warm water flow rate extrapolated from Figure 3.3 was plotted (see Figure 3.4). Theoretically, with zero warm and zero cold water flows, the two lines should intercept the y-axis at the same point (zero flow rate) and the result would be the nitrogen leak (or background) of the system. This procedure is only feasible if the gas being observed is relatively inert and chemically inactive like nitrogen.

Figure 3.4 shows a nitrogen background of approximately 11.5 mmol/sec with excellent precision between the zero cold water and zero warm water flow extrapolations (y-intercepts). Unfortunately, with the data obtained in this investigation, it is very difficult to separate the contribution to the nitrogen background of the atmospheric leak into the HMTSTA and the leak into the mass spectrometer sample lines. This poses a problem for design engineers who wish to use this data to estimate realistic OC-OTEC system leak rates

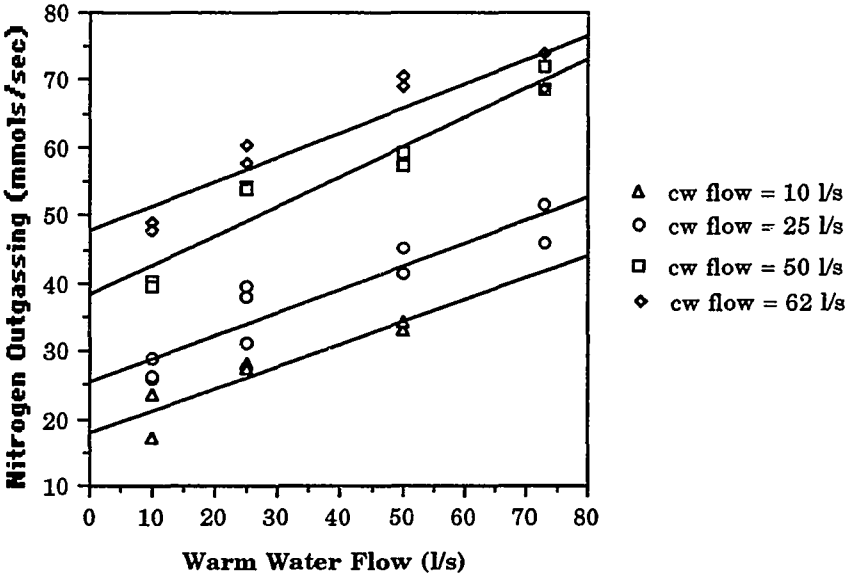

Figure 3.2: Nitrogen Outgassing vs. Warm Water Flow with Steam Generation

along with the extent of noncondensable outgassing. For the purpose of this investigation, the simple determination of the extent of feed stream outgassing, it is sufficient to have a good, precise estimate of the nitrogen background.

However, in order to provide OC-OTEC design engineers with a working estimate as to the contribution to the total leak of 11.5 mmol/sec of nitrogen from the HMTSTA system and the mass spectrometer sampling system, the following procedure was developed. Initially, the mass spectrometer sensor chamber was closed off to the remainder of the sampling system to obtain an estimate of the pressures at the ultimate vacuum capable of the turbovacuum pump. The highest nominal ionic (not true pressure, since the sensor pressure gauge reads only ionic pressures) vacuum reached under these conditions was

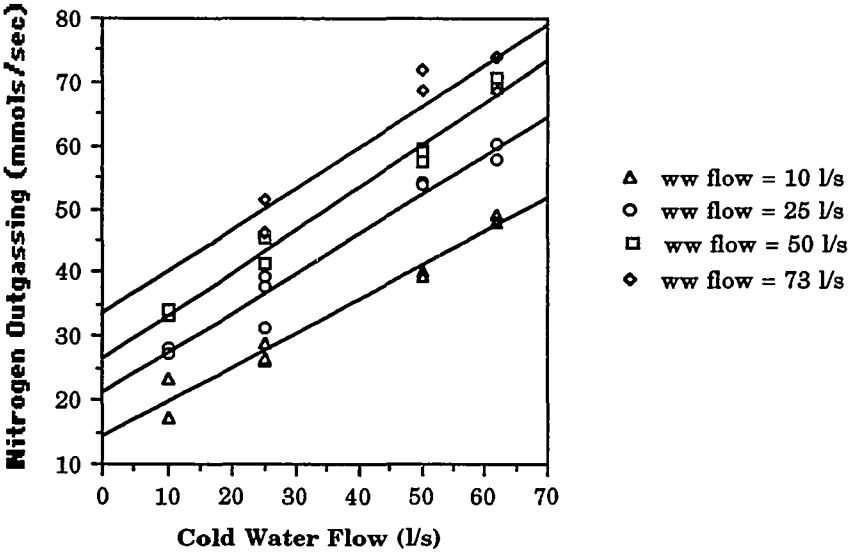

Figure 3.3: Nitrogen Outgassing vs. Cold Water Flow with Steam Generation

approximately 8.0 x 10^{-7} torr (which was even slightly below the nominal working pressures expected by the manufacturers for a new turbovacuum pump). Now, the sensor chamber was exposed to the sample line (closed off to the HMTSTA system) used to collect all of the data utilized in this investigation, and the nominal vacuum achieved by the turbovacuum pump was read under this configuration, conservatively speaking, as approximately 3.0 x 10^{-6} torr. The discrepancy between these two pressures can be considered an estimate of the atmospheric leak into the mass spectrometer sampling system.

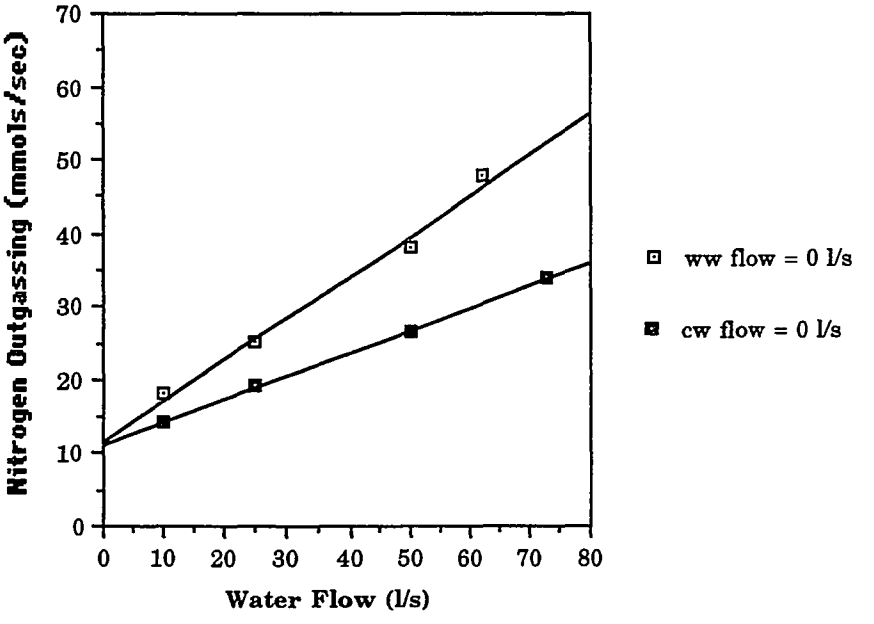

Figure 3.4: Zero Warm and Cold Water Flows vs. Nitrogen Outgassing with Steam Generation (Leak Estimate)

In order to determine an estimate of the relative contribution this leak in the mass spec system has on a total sample, the estimated pressure above must be compared to that of a common sampling pressure for the HMTSTA (approximately 1 x 10^{-5} torr) as read by the RGA. From these pressures and the volumetric flow of the respective pumps (turbovac and roughing) as suggested by the manufacturer, a simple mass balance assuming ideal behavior was performed on the mass spec sampling system (see Appendix E). The results of this mass balance indicate that a normal sample from the HMTSTA is contaminated with as much as 22% of the sample attributable to atmospheric leaks into the mass spec sampling system and degassing or evaporating water from the sample line walls. With these rough means of leak

analysis, it would be nearly impossible to make a direct conjecture as to the definitive contribution of leaks to the determined nitrogen background; therefore, the leak estimates obtained by SERI and PICHTR investigators for the HMTSTA should be considered best estimates (approximately 90 mg/sec or 3.1 mmols/sec of air), with the remainder of the relative gas backgrounds attributable primarily to leaks in the RGA sampling system.

This contamination of the analyzed sample does not lead to excessive errors in the data (as will be seen later in the relative errors calculated in Appendix B and presented in the following sections). This is due largely to the fact that the total pressure at which the RGA operated throughout the experimental period (especially during the later periods of the investigations when most of the pertinent data was accumulated) remained very consistent (since operating pressures within the HMTSTA were relatively stable at the same sample point, C3). Therefore, a variable leakage into the mass spec system would not be expected since the turbovac worked under almost identical conditions throughout the experiment. The precision of the nitrogen background estimate and the relatively small errors attained in the nitrogen data reflect this.

3.1.4 EXTENT OF OUTGASSING

With the determination of the available nitrogen in the feed streams estimated from [21], the total nitrogen flow through the HMTSTA can be separated into contributions from air leakage and seawater outgassing. Table 3.1 shows the total available nitrogen based on Krock's measured values of

12.67 ml/l (0.566 mmol/l) and 9.70 ml/l (0.433 mmol/l) of nitrogen in the cold water and warm water feed streams, respectively.

Table 3.2 represents the data taken directly from Figures 3.2 and 3.3 and corrected for an estimated 11.5 mmol/sec nitrogen background at various experimental feed stream flow rates. Table 3.3 shows the percentage of total nitrogen (for both warm water and cold water streams) outgassed during various experimental flow configurations.

With the overall outgassing rates determined, it is desirable to find the relative contribution and level of outgassing for the cold water and warm water feed streams. To accomplish this, Figure 3.5 has been developed which shows 100% outgassing (dotted line) for both the cold water (upper line) and warm water (lower line) feed streams as well as the measured outgassing levels (with leak present) for zero warm (cold water flow - upper line) and zero cold (warm water flow - lower line) water flows in the HMTSTA taken from Figure 3.4 (solid lines). From this graph we can compare the slopes of the 100% warm water outgassing and 100% cold water outgassing to their respective zero flow curve (zero cold water flow and zero warm water flow curves, respectively).

Theoretically, for 100% outgassing of the respective streams, one would expect the slopes of these curves to be identical assuming linearity of outgassing rates, which appears to be a reasonable assumption when observing available data. The linear equations for the respective lines are as follows:

$Y = 0.43X$	100% warm water outgassing
$Y = 0.57X$	100% cold water outgassing

Table 3.1: Total Available Nitrogen with Respect to Warm and Cold Water Flow Rates (100% Outgassing of Both Streams) (mmols/sec)

Warm Water Flow (liters/sec)	Cold Water Flow (liters/sec)			
	10	25	50	62
10	9.99*	18.47	32.61	39.40
25	16.49	24.97	39.11	45.90
50	27.31	35.79	49.93	56.72
73	37.27	45.75	59.89	66.68

* Values based on Krock Data [21].

Table 3.2: Nitrogen Outgassing Corrected for Nitrogen Leak Rate (Background) (mmols/sec)

Warm Water Flow (liters/sec)	Cold Water Flow (liters/sec)			
	10	25	50	62
10	9.1†	16.9	30.6	38.6
25	14.5	23.8	39.1	46.9
50	22.2	31.2	48.6	56.0
73	29.5	39.1	57.0	62.5

† Values represent the mean of data taken from Figures 3.2 and 3.3 and then corrected for an estimated leak rate of 11.5 mmols/sec N_2.

Table 3.3: Percentage of Total Available Nitrogen Outgassed

(% Outgassed)

Warm Water Flow (liters/sec)	Cold Water Flow (liters/sec)			
	10	25	50	62
10	91.1	91.5	93.8	98.0
25	87.9	95.3	100.0	102.2
50	81.3	87.2	97.3	98.7
73	79.2	85.5	95.2	93.7

and

$Y = 0.31X + 11.3$ warm water outgassing (zero cold flow)

$Y = 0.56X + 11.7$ cold water outgassing (zero warm flow)

Therefore, the estimated level of outgassing for the warm water stream is 72 ± 7% and the estimated level of cold water outgassing is 98 ± 9%.

This trend of the cold water stream outgassing at a higher level than the warm water stream is consistent with logic for several reasons. First, the cold water stream is exposed to a significantly higher vacuum in the DCC (approximately 10 torr in DCC versus approximately 18 torr in the evaporator under steam generation). With bubble nucleation sites or microbubbles available (possibly present due to small leaks in the cold water feed pipes, heterogeneous nucleation sites along pipe walls, or created by cavitation at the feed pumps) coupled with the high available exchange surface area created in

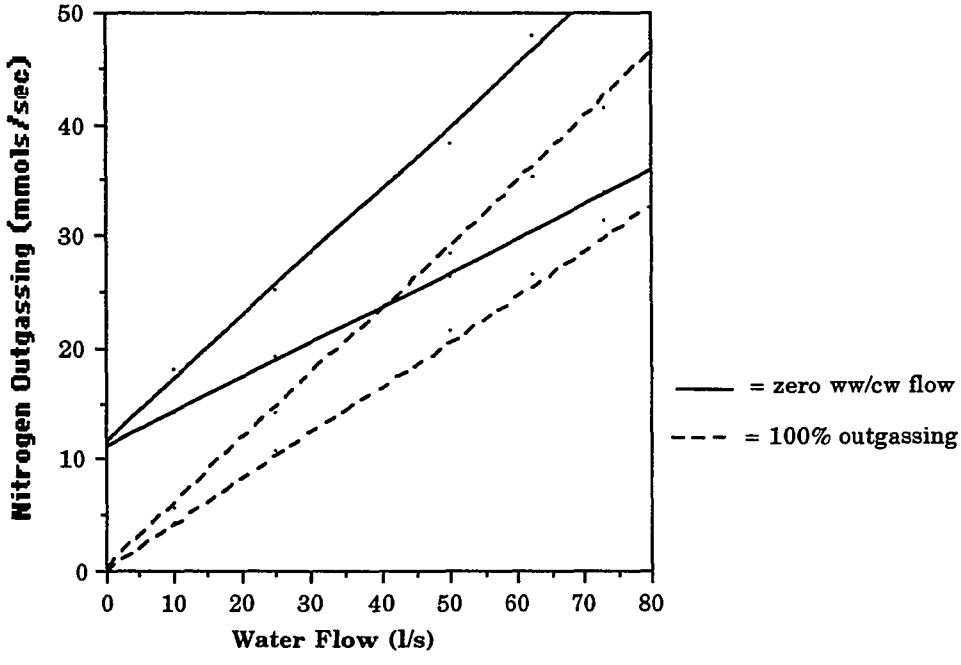

Figure 3.5: Comparison of Zero Flow Slopes to 100% Outgassing Slopes (Nitrogen)

the DCC, the higher vacuum would suggest a higher outgassing rate for the cold water stream.

Second, the existence of microorganisms and other surfactants in the surface water might have a contributing effect to this observation. These microorganisms will be subjected to pressures in the evaporator which would indicate a high level of lysing which in turn raises the surfactant concentration in the warm water stream.

The presence of surfactants in surface seawater hinders the exchange of gases. Surfactants possess a unique quality in which one side is hydrophilic (has an affinity for water) and one side is hydrophobic (incapable of dissolving in water). Thus, the surfactants tend to congregate around the gas/liquid

interfaces necessary for the gas exchange process, significantly decreasing the available exchange surface area and creating another boundary layer in which the process of molecular diffusion of the gases must occur. Therefore, since the deep ocean water is very low in microorganism and surfactant concentration, one would expect the cold ocean water to desorb gases at a higher rate than the warm water side, which is consistent with the results obtained in this investigation.

Third, the equilibrium shifts due to temperature in both the cold and warm water streams are also consistent with the trends observed. Specifically, the cold water used in the DCC generally warmed approximately 4 ^{o}C during the condensation process which would shift the nitrogen equilibrium so as to promote a lower gas concentration dissolved in the water, thus enhancing the evolution of nitrogen from the cold water stream. Likewise, the warm water stream cools approximately 3 ^{o}C during the evaporation process which shifts the nitrogen equilibrium towards a higher dissolved concentration. This shift would work in deterring nitrogen evolution (and other noncondensables as well) as observed by the lower outgassing level of the warm water stream.

The coupling of these effects have lead to the level of nitrogen outgassing experienced in this investigation. The most significant contributor to the difference in feed stream outgassing levels for nitrogen is most likely due to the significant difference in vacuum each stream is exposed to, with a slightly smaller contribution due to the temperature driven equilibrium shifts and the lysing of microorganisms in the evaporator.

3.2 ARGON

For open-cycle OTEC noncondensable considerations, argon is a relatively insignificant gas. Argon is found in seawater at equilibrium with the atmosphere at the temperature present during the last seawater exposure to the surface. Thus, with atmospheric compositions of argon less than 1% by volume, the quantity of argon present in OC-OTEC feed waters would be essentially negligible as compared to nitrogen and oxygen.

However, like nitrogen, argon is chemically inert and thereby possesses stable concentration characteristics in the cold and warm water streams as long as feed stream temperatures remain fairly consistent. This characteristic makes argon an attractive gas for checking the validity of the leak check method described previously for nitrogen in Section 3.1.3. This is the main purpose for emphasizing the extent of argon outgassing in this investigation.

As in nitrogen's case, the low chemical reactivity and inert behavior of the gas means that no simple probes or chemical tests have been developed which can be simply performed to analyze argon compositions in seawater. Argon can only be measured in situ via a mass spectrometer or by chromatographic means. Therefore, very little data is available pertaining to the level of outgassing of argon in an OC-OTEC system.

3.2.1 COMPOSITION IN SEAWATER

Argon in seawater is found to be essentially at equilibrium with the atmosphere at the given water temperature [16]. Kester [19] calculates the

argon concentration in seawater at 5 °C and 35 ‰ as 0.01501 mmol/kg_{sw} (0.015 mmol/l) and 25 °C and 35 ‰ as 0.01011 mmol/kg_{sw} (0.010 mmol/l) using the following equation developed by Weiss [48]:

$$\ln(C_{Ar}) = A_1 + A_2(100/T) + A_3\ln(T/100) + A_4(T/100) + S\,‰[B_1 + B_2(T/100) + B_3(T/100)^2] \quad (3\text{-}1)$$

where

C_{Ar} = Concentration of Argon (μmol/kg)

A_n = Solubility constant

S = Salinity (taken as 35 ‰)

B_n = Salinity solubility constant

T = Water temperature (°K)

The values reported by Kester [19] calculated using the above equation are the values used in this investigation for calculating argon outgassing rates. The temperatures and salinities used by Kester are very close to those reported by Krock [21] for the waters off Oahu and are assumed to be similar to those around Keahole Point, Kona.

3.2.2 TOTAL ARGON FLOW

Figures 3.6 and 3.7 represent the vapor flow of argon through the HMTSTA during steam generation under various warm water and cold water flow conditions. From the slopes of these plots it is easy to see the relative contribution the warm water and cold water streams have on the total argon

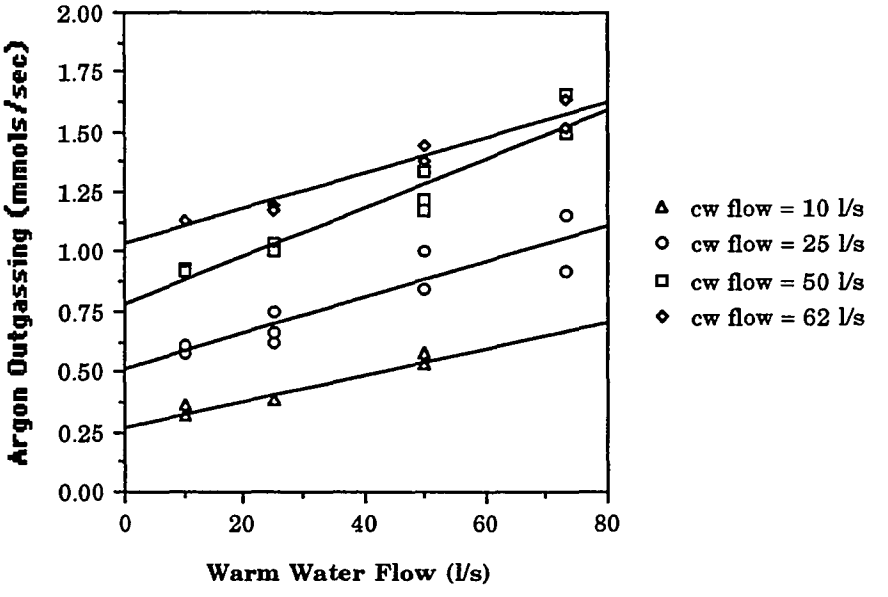

Figure 3.6: Argon Outgassing vs. Warm Water Flow with Steam Generation

outgassing. Once again, these plots represent the total flow of argon through the HMTSTA system. This includes the argon outgassing from the warm and cold water streams in the evaporator and condenser, respectively, as well as any leaks of argon into the HMTSTA or RGA sampling system from the atmosphere. As previously stated in the nitrogen analysis, it is necessary to quantify the contribution of each of the aforementioned components to the total noncondensable flow rates. The following section addresses the relative contribution of leaks in the data presented in Figures 3.6 and 3.7, as well as how this contribution can be used as a validity check of the leak estimate analysis.

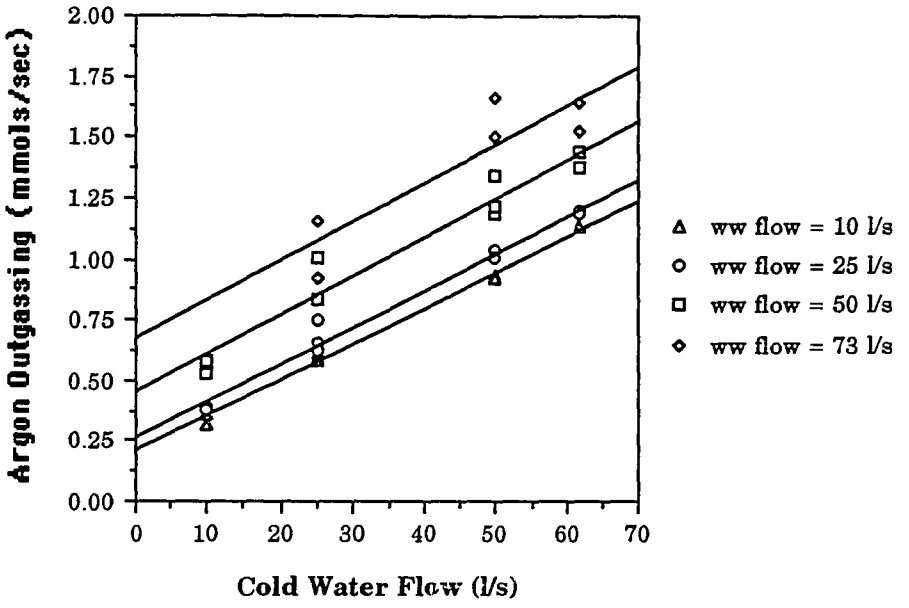

Figure 3.7: Argon Outgassing vs. Cold Water Flow with Steam Generation

3.2.3 LEAK (BACKGROUND) ESTIMATION ANALYSIS

With the same low chemical reactivity and inert behavior characteristics that nitrogen possesses, the leak estimation procedure followed for nitrogen should be appropriate for argon as well. Figures 3.6 and 3.7 were used to obtain the zero flow data necessary to develop Figure 3.8.

Figure 3.8 shows an argon background of approximately 0.14 mmol/sec with excellent precision between the zero cold water and zero warm water flow extrapolations (y-intercepts). This is the value used for the argon background (leak) in this investigation.

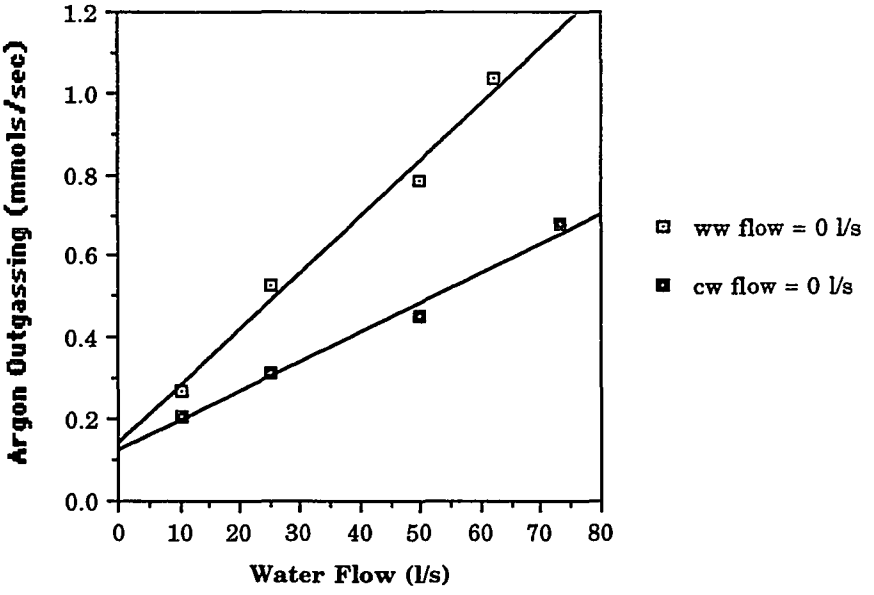

Figure 3.8: Zero Warm and Cold Water Flows vs. Argon Outgassing with Steam Generation (Leak Estimate)

As stated previously, this value for the argon leak can be used as a check to ensure the validity of the method described to estimate the leak rate. Theoretically, with the HMTSTA system and RGA sampling system both exposed exclusively to air at atmospheric conditions, then the leak estimates of argon (0.14 mmol/sec) and nitrogen (11.5 mmol/sec) from the data should be in the same ratio by volume as those found in the atmosphere (0.93 for argon and 76.3 for nitrogen using the average composition of air in Kona determined using standard air compositions and a psychrometric sling to calculate water vapor content). The ratio of argon/nitrogen in the data is 0.0122 while the ratio of argon/nitrogen in atmospheric Kona air is 0.0122. With the data agreeing

precisely with the ratio of atmospheric compositions, it is safe to assume the leak estimation method is a valid account of the argon and nitrogen background occurring in the data sets. The precision of the data sets also suggests that the nitrogen and argon backgrounds (leaks) were very consistent throughout the entire data acquisition period.

3.2.4 EXTENT OF OUTGASSING

With the determination of the available argon in the feed streams estimated using equation 3-1 developed by Weiss [48], the total argon flow through the HMTSTA, the contribution of argon in the data due to leaks in the systems as well as the extent of outgassing for the feed streams can be determined. Table 3.4 shows the total available argon based on Weiss' equation which yields 0.0154 mmol/l and 0.0104 mmol/l for the cold and warm water feed streams, respectively.

Table 3.5 represents the data taken directly from Figures 3.6 and 3.7 and corrected for an estimated 0.14 mmols/sec argon background at various experimental feed stream flow rates. Table 3.6 shows the percentage of total argon (for both the warm water and cold water streams) outgassed during various experimental flow configurations.

With the overall argon outgassing rates determined, it is necessary to find the relative contribution and level of outgassing for the cold and warm water feed streams. Figure 3.9 shows the 100% outgassing (dotted lines) for argon in both the cold (upper line) and warm (lower line) water feed streams as well as the measured argon outgassing levels (with leak present--solid lines) for

Table 3.4: Total Available Argon with Respect to Warm and Cold Water Flow Rates (100% Outgassing of Both Streams) (mmols/sec)

Warm Water Flow (liters/sec)	Cold Water Flow (liters/sec)			
	10	25	50	62
10	0.26*	0.49	0.87	1.06
25	0.41	0.65	1.03	1.21
50	0.67	0.91	1.29	1.47
73	0.91	1.14	1.53	1.71

* Values based on Weiss' equation [48].

Table 3.5: Argon Outgassing Corrected for Argon Leak Rate (Background) (mmols/sec)

Warm Water Flow (liters/sec)	Cold Water Flow (liters/sec)			
	10	25	50	62
10	0.21†	0.45	0.77	0.98
25	0.30	0.56	0.91	1.08
50	0.44	0.73	1.14	1.28
73	0.62	0.93	1.37	1.47

† Values represent the mean of data taken from Figures 3.6 and 3.7 and then corrected for an estimated leak rate of 0.14 mmols/sec Ar.

Table 3.6: Percentage of Total Available Argon Outgassed

(% Outgassed)

Warm Water Flow (liters/sec)	Cold Water Flow (liters/sec)			
	10	25	50	62
10	80.8	91.8	88.5	92.5
25	73.2	86.2	88.3	89.3
50	65.7	80.2	88.4	87.1
73	68.1	81.6	89.5	86.0

zero warm (cold water flow-upper line) and zero cold (warm water flow-lower line) water flows in the HMTSTA taken from Figure 3.8. From this graph we can compare the slopes of the 100% warm water ougassing and 100% cold water outgassing to their respective zero flow curve (zero cold water flow and zero warm water flow curves, respectively).

As in nitrogen's case, one would expect the slopes of these curves to be identical for 100% argon outgassing, assuming linearity of outgassing rates. The linear equations for the respective lines are as follows:

$Y = 0.0104X$ 100% warm water outgassing

$Y = 0.0154X$ 100% cold water outgassing

and

$Y = 0.0073X + 0.12$ warm water outgassing (zero cold flow)

$Y = 0.0139X + 0.15$ cold water outgassing (zero warm flow)

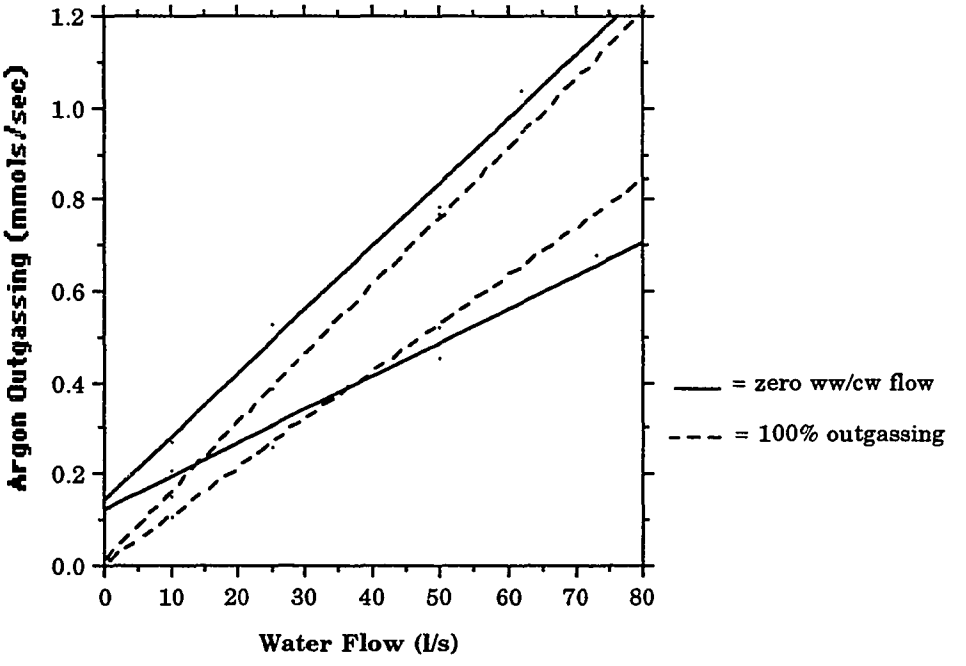

Figure 3.9: Comparison of Zero Flow Slopes to 100% Outgassing Slopes (Argon)

Therefore, the estimated level of argon outgassing for the warm water stream is 70 ± 13% and the estimated level of cold water argon outgassing is 90 ± 19%.

The difference experienced between the cold water argon outgassing rate is consistent with the nitrogen data.

3.3 CARBON DIOXIDE

Carbon dioxide is a very important gas for OC-OTEC considerations. It is neither a large contributor to the total noncondensable flow through the system like nitrogen, nor does it possess the chemically inert characteristics

useful for leak estimates such as argon; however, it is extremely important in environmental impact considerations for the OC-OTEC design engineers. It is the potential contribution to environmental problems caused by significant release of carbon dioxide from the seawater in the OC-OTEC system which makes the analysis of CO_2 outgassing so important to the design engineers.

The largest concern facing the designers of the OC-OTEC system in regards to CO_2 outgassing is its potential contribution to the already existing "greenhouse effect" if vented directly to the atmosphere from the DCC. In order to discern the magnitude of this problem, it is necessary to quantify the extent of CO_2 outgassing in the HMTSTA, and to then scale it up to projected OC-OTEC plants (this will be addressed in subsequent sections).

Another significant concern deals with the potential local chemical shift in the seawater carbonate system (discussed in the following section) created by the cold water discharge in the open ocean. It is necessary to determine the extent of CO_2 outgassing so that estimates of the shift in the seawater carbonate system (the shift in discharge water pH, alkalinity, etc.) can be made so that these factors may be included in the choice process for the discharge depth of the effluent waters.

These environmental concerns are the primary reasons for investigating the extent of carbon dioxide outgassing in this investigation. The significance of the CO_2 outgassing levels reported in the following sections will be addressed in more detail later in this report.

3.3.1 CO_2 SEAWATER CHEMISTRY

As stated previously, carbon dioxide is a very chemically reactive gas in the seawater environment. This is due primarily to the manner in which the inorganic carbon is chemically stored in the natural ocean environment as well as the biological processes by which dissolved carbon dioxide is consumed/produced during photosynthesis/respiration, and the equilibrium which is reached between these two forms of carbon storage in the presence of an aqueous solution.

First, carbon dioxide dissolves in water to give a hydrated molecule, $CO_2(aq)$, which then forms an equilibrium mixture containing bicarbonate (HCO_3^-) and carbonate (CO_3^{-2}) ions. At pH values lower than those found in seawater, carbonic acid (H_2CO_3) will also be present [29].

$$CO_2(gas) \xleftrightarrow{\text{water}} CO_2(aq) \quad (3\text{-}2)$$

$$H_2O + CO_2(aq) \longleftrightarrow H_2CO_3 \quad (3\text{-}3)$$

$$H_2CO_3 \longleftrightarrow H^+ + HCO_3^- \quad (3\text{-}4)$$

$$HCO_3^- \longleftrightarrow H^+ + CO_3^{-2} \quad (3\text{-}5)$$

Most oceanic waters have a pH in the range 8 to 8.3 [29], as they contain more hydroxide ions than hydrogen ions due to reactions 3-6 and 3-7, and the carbonate-bicarbonate mixture contains about 13% carbonate [29].

$$HCO_3^- \longleftrightarrow CO_2(aq) + OH^- \quad (3\text{-}6)$$

$$CO_3^{-2} + H_2O \longleftrightarrow HCO_3^- + OH^- \quad (3\text{-}7)$$

When carbon dioxide dissolves in seawater the overall reaction can be summarized by the following equation.

$$CO_2(aq) + H_2O + CO_3^{-2} \quad <------> \quad 2HCO_3^- \qquad (3\text{-}8)$$

The concentration of the various components varies with depth. In the surface layers where photosynthesis is active and CO_2 is being consumed, the reaction above (3-8) moves to the left. With an equilibrium condition existing as suggested by the above relationships, if there is removal of the dissolved carbon dioxide, $[CO_2(aq)]$, then the concentration of bicarbonate ion, $[HCO_3^-]$, must also be reduced.

In deep water there is a net production of carbon dioxide due to respiration and decay processes which oxidize the organic compounds settling through these deeper layers with little or no photosynthesis occurring. Under these conditions reaction 3-8 moves to the right as the extra carbon dioxide is partially converted to bicarbonate and equilibrium is again attained [29].

The presence of the various inorganic carbon species plays a particularly important part in controlling the pH of natural ocean waters. Essentially, the ocean waters are "buffered" (relatively large amounts of acid or base may be added to it without significantly altering the pH). However, the magnitudes of projected effluent discharges could prove significant enough (if in fact substantial amounts of carbon dioxide are degassed from the cold and warm water streams) to alter the local pH in the vicinity of the OC-OTEC discharge plume. Therefore, it is necessary to carefully choose a discharge depth in which this possible detrimental effect can be minimized in accordance with other discharge concerns (temperature, dissolved oxygen content, etc.).

3.3.2 COMPOSITION IN SEAWATER

When considering the total available inorganic carbon present in seawater in the various forms discussed in the previous section, carbon dioxide is by far the most abundant atmospheric gas present in the natural ocean environment. However, as just discussed, much of it is unavailable for degassing due to chemical "storage" which can only be reversed through chemical equilibrium shifts which require sufficient time for the chemical transformations to occur. These reaction rates are well documented [41] and suggest relatively slow reaction rates for the reaction 3-6 (the rate determining step in the equilibrium shift sequence most important to CO_2 outgassing considerations) in systems free from catalytic material. However, little is known about the hydration and dehydration reaction in natural seawater under the influence of the high ionic strength and organic content inherent in its composition [41]. Therefore, it is extremely difficult to determine the actual available CO_2 which may be outgassed during exposure to OC-OTEC working conditions and components. Any estimate will incorporate a large amount of potential error inherent in the nature of assuming a constant carbon dioxide composition. Thus, carbon dioxide will be observed in two different ways, one comparing the outgassing rate to the estimated "free" carbon dioxide taken from Krock [21] and an outgassing rate compared to the total carbon dioxide also taken from Krock's data.

Krock [21] reports the cold water "free" dissolved carbon dioxide content as 0.054 mmol/l and a total carbon dioxide content of 2.325 mmol/l (essentially 95% of this value represents the bicarbonate form) at depths between 700-

1000 meters (4-6 °C). The mean daytime warm water "free" dissolved carbon dioxide composition was 0.008 mmol/l while the total daytime carbon dioxide composition was approximately 1.933 mmol/l (essentially 85% of this value in the bicarbonate form). These are the values used to project effective carbon dioxide outgassing rates in the subsequent sections.

3.3.3 TOTAL CARBON DIOXIDE FLOW

Figures 3.10 and 3.11 represent the vapor flow of carbon dioxide through the HMTSTA during steam generation under various warm water and cold water flow conditions. From the slopes of these plots, it is easy to see the relative contribution the warm water and cold water streams have on the total flow of carbon dioxide through the HMTSTA, which includes the carbon dioxide outgassed from the warm and cold water streams, the leak of carbon dioxide into the HMTSTA from the atmosphere and any leaks into the mass spectrometer due to its sampling system. In order to make proper conclusions as to the extent of outgassing of carbon dioxide from the OC-OTEC process, it is first necessary to quantify the contribution of each of the aforementioned components of the total noncondensable flow rates. The following section addresses the relative contribution of leaks in the data presented in Figures 3.10 and 3.11.

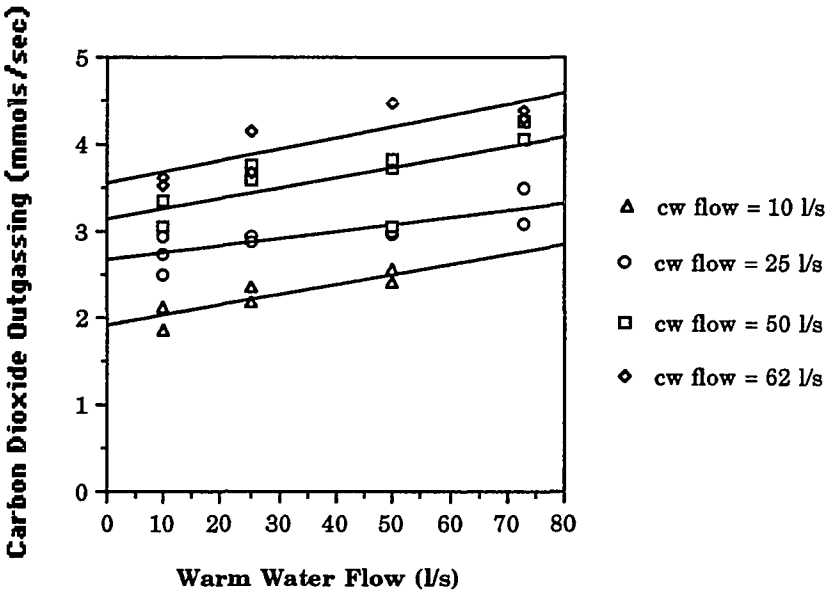

Figure 3.10: Carbon Dioxide Outgassing vs. Warm Water Flow with Steam Generation

3.3.4 LEAK (BACKGROUND) ESTIMATION ANALYSIS

Due to the chemical reactivity of the carbon dioxide gas in seawater, as discussed in previous sections, a similar leak check procedure as devised for nitrogen and argon will not indicate the leak of CO_2, but should provide a good "background" for the CO_2 data. Therefore, the carbon dioxide background obtained in Figure 3.12 (1.73 mmols/sec) should not be attributed to an atmospheric leak (its value is much too high to correspond with the atmospheric leak predicted by nitrogen and argon in the previous sections). It can be explained, however, by the probable presence of hydrocarbon oils (pump oils) or solvents (possibly used to clean the pre-cleaned stainless steel

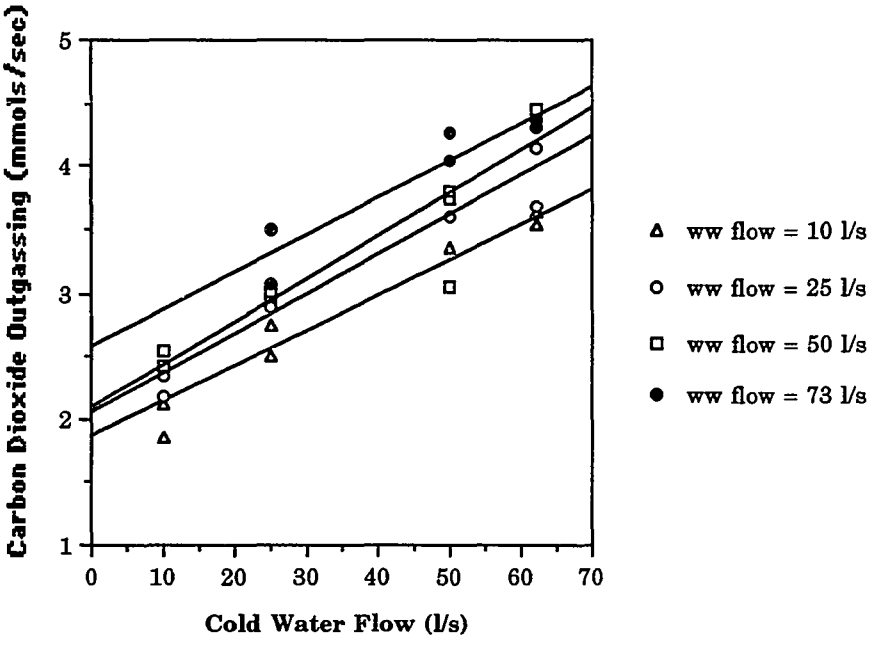

Figure 3.11: Carbon Dioxide Outgassing vs. Cold Water Flow with Steam Generation

sampling lines used to extract samples) which fragment under typical ionization voltages used by an EM sensor to indicate masses similar to that of carbon dioxide [24].

Also, the presence of oxygen and carbon (possibly from the sensor filament or trace hydrocarbons such as backstreaming pump oils) can artificially produce carbon dioxide during the ionization process created by the EM working voltages and lead to artificially high readings [24]. However, these readings should be consistently high and the background relatively stable since operating procedures for the RGA system were consistent throughout this investigation.

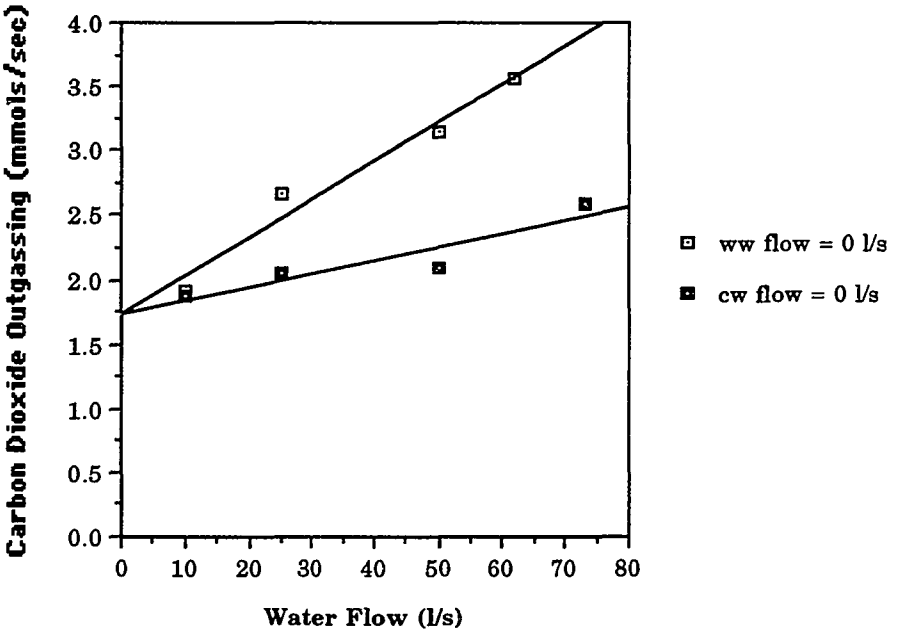

Figure 3.12: Zero Warm and Cold Water Flows vs. Carbon Dioxide Outgassing with Steam Generation (Background)

Since the composition ratios of argon to nitrogen in the data previously discussed were so closely related to those of atmospheric air, it was deemed reasonable that the carbon dioxide leak would similarly be found to be of atmospheric composition as well. Thus, the following equation was utilized to determine the relative contribution an atmospheric air leak of the magnitude suggested by the nitrogen and argon values would have on the presented carbon dioxide flow rates:

$$Q_{lkCO2} = [(Q_{lk,N2} / y_{air,N2} + Q_{lk,Ar} / y_{air,Ar}) / 2] * y_{air,CO2} \qquad (3\text{-}9)$$

where

$Q_{lk,CO2}$ = flow of carbon dioxide leak in data (mmol/sec)

$Q_{lk,N2}$ = flow of nitrogen leak in data (11.5 mmol/sec)

$Q_{lk,Ar}$ = flow of argon leak in data (0.14 mmol/sec)

$y_{air,N2}$ = molar composition of nitrogen in air (0.762)

$y_{air,Ar}$ = molar composition of argon in air (0.0093)

$y_{air,CO2}$ = molar composition of carbon dioxide in air (0.0003)

This equation yields a projected leak rate of carbon dioxide in the data of approximately 0.0045 mmol/sec. This leak rate is incorporated in the estimated carbon dioxide background of 1.73 mmols/sec for the data shown in Figures 3.10 and 3.11. Therefore, this value (1.73 mmols/sec) represents the carbon dioxide background for this set of data.

3.3.5 EXTENT OF CO_2 OUTGASSING

With the "free" carbon dioxide and total carbon dioxide in the feed streams estimated from Krock [21] and the carbon dioxide background, the total carbon dioxide flow through the HMTSTA due to feed stream outgassing, as well as the extent of outgassing for each feed stream, may now be determined. Table 3.7 shows the available "free" carbon dioxide based on Krock's values of 0.054 mmol/l and 0.008 mmol/l for the cold and warm water feed streams, respectively. Table 3.8 shows the total available carbon dioxide based on Krock's values of 2.325 mmol/l and 1.933 mmol/l for the cold and warm water feed streams, respectively.

With the overall outgassing rates determined, it is desirable to find the relative contribution and level of outgassing for the cold water and warm water

feed streams. To accomplish this, a similar method to that described for nitrogen and argon will be followed.

Table 3.9 represents the data taken directly from Figures 3.10 and 3.11 and corrected for a carbon dioxide background of 1.73 mmols/sec. Table 3.10 shows the percentage of "free" carbon dioxide outgassed during the various experimental flow configurations, while Table 3.11 shows the percentage of total carbon dioxide outgassed during the same conditions (in both cases the percentages represent the combined contributions from both the warm and cold water feed streams).

Figure 3.13 displays the curves for 100% outgassing of the "free" carbon dioxide (dotted lines) for both the cold water (upper line) and the warm water (lower line) feed streams. The slopes of these curves are then compared to the slopes of the curves developed for zero warm (cold water flow - upper line) and zero cold water (warm water flow - lower line) flow, just as was done with the nitrogen and argon data to determine the extent of outgassing for each stream.

The linear equations for the "free" carbon dioxide curves are:

$Y = 0.008X$ 100% warm water outgassing

$Y = 0.054X$ 100% cold water outgassing

and the linear equations for the total carbon dioxide curves are:

$Y = 1.933X$ 100% warm water outgassing

$Y = 2.325X$ 100% cold water outgassing

and for the actual carbon dioxide outgassing:

$Y = 0.011X + 1.73$ warm water outgassing (zero cold flow)

$Y = 0.030X + 1.73$ cold water outgassing (zero warm flow)

Table 3.7: Available "Free" CO_2 with Respect to Warm and Cold Water Flow Rates (100% "Free" CO_2 Outgassing of Both Streams) (mmols/sec)

Warm Water Flow (liters/sec)	Cold Water Flow (liters/sec)			
	10	25	50	62
10	0.62*	1.43	2.78	3.43
25	0.74	1.55	2.90	3.55
50	0.94	1.75	3.10	3.75
73	1.12	1.93	3.28	3.93

* Values based on Krock data [21].

Table 3.8: Total CO_2 Available with Respect to Warm and Cold Water Flow Rates (100% Outgassing of Total CO_2 from Both Streams) (mmols/sec)

Warm Water Flow (liters/sec)	Cold Water Flow (liters/sec)			
	10	25	50	62
10	42.58†	77.46	135.58	189.06
25	71.58	106.46	164.58	218.06
50	119.90	154.78	212.90	266.38
73	164.36	199.24	257.36	310.84

† Values based on Krock data [21].

Table 3.9: Carbon Dioxide Outgassing

(mmols/sec)

Warm Water Flow (liters/sec)	Cold Water Flow (liters/sec)			
	10	25	50	62
10	0.36*	0.93	1.53	1.92
25	0.56	1.13	1.80	2.22
50	0.73	1.27	2.04	2.47
73	1.09	1.56	2.31	2.75

* Values represent the mean of data taken from Figures 3.10 and 3.11 and corrected for a CO_2 background of 1.73 mmols/sec.

Table 3.10: Percentage of "Free" CO_2 Outgassed

(% Outgassed)

Warm Water Flow (liters/sec)	Cold Water Flow (liters/sec)			
	10	25	50	62
10	58.1	65.0	55.0	56.0
25	75.7	72.9	62.1	62.5
50	77.7	72.6	65.8	65.9
73	97.3	80.8	70.4	70.0

Table 3.11: Percentage of Total CO_2 Outgassed

(% Outgassed)

Warm Water Flow (liters/sec)	Cold Water Flow (liters/sec)			
	10	25	50	62
10	0.85	1.20	1.13	1.02
25	0.78	1.06	1.09	1.02
50	0.61	0.82	0.96	0.93
73	0.66	0.78	0.90	0.80

These results give estimated levels of "free" carbon dioxide outgassing from the warm water as 138 ± 10% and an estimated level of"free" carbon dioxide outgassing from the cold water as 56 ± 4%. They also give an estimated level of total carbon dioxide outgassing of 0.6 ± 0.1% for the warm water and 1.3 ± 0.1% for the cold.

The warm water stream indicates that over 100% of the "free" carbon dioxide available in the feed stream is being desorbed. This suggests that the carbonate system equilibrium is shifted in the warm water during the evaporative process (including exposure in the barometric upcomer) leading to a reduction of bicarbonate (HCO_3^-) to form more "free" CO_2. In contrast, the cold water stream does not release all of its available "free" carbon dioxide (only 56%).

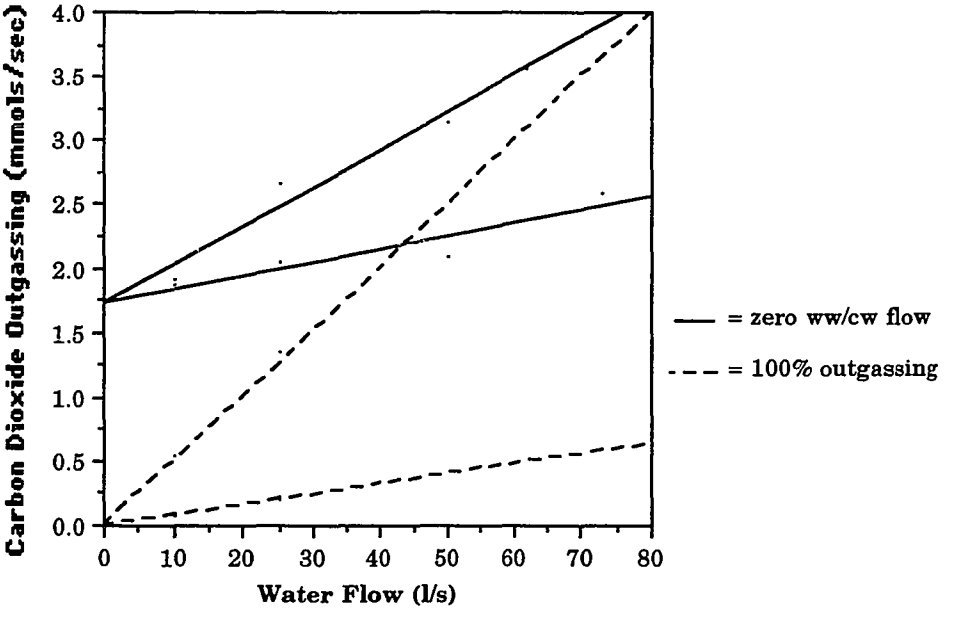

Figure 3.13: Comparison of Zero Flow Slopes to 100% Outgassing Slopes (Carbon Dioxide)

This result is consistent with logic. First, the cold water stream contains a significantly greater amount of "free" carbon dioxide than does the warm water stream (on the order of seven times more). One would expect that with similar desorption rates for "free" carbon dioxide, the warm water stream would run out of available "free" carbon dioxide far sooner than the cold water stream. Thus, the extent of outgassing for the warm water stream would be limited by the reaction rate of converting bicarbonate into available dissolved carbon dioxide.

Secondly, the reaction rate governing the warm water bicarbonate equilibrium shift would be significantly increased by the warmer temperature experienced in the warm water stream as compared to the cooler temperatures experienced in the cold water stream [15]. This would suggest

that the warm water stream could in fact more readily shift its carbonate equilibrium than the cold water stream.

Thirdly, the availability of microbubbles and microparticles inherent in the warm water stream also may help provide the necessary time required for this reaction to occur by providing a free surface in the bulk liquid under vacuum conditions in which the desorption of carbon dioxide may occur.

All of these factors have probably contributed to the shift in carbonate equilibrium experienced in the warm water stream. It should be noted, however, that as one would expect, the cold water stream did in fact degas more of its total carbon dioxide (approximately 1.3% versus 0.6% for the warm water). This shows that even though the reaction rate for the equilibrium conversion of bicarbonate into "free" carbon dioxide in the warm water stream has been enhanced by the previously mentioned conditions, it cannot release CO_2 at the same rate as the cold water stream can release its "free" CO_2. This enforces the universal assumption that the reaction rate of the bicarbonate equilibrium shift is the limiting reaction (occurs slower than does the actual desorption of the gas molecule) involved in carbon dioxide release in OC-OTEC waters.

3.3.6 SIGNIFICANCE OF CARBON DIOXIDE RELEASE

With estimates of carbon dioxide outgassing rates determined under common OC-OTEC flow conditions, it is now possible to make rough estimations of CO_2 emissions of specifically sized plants. A system model developed by SERI gives initial seawater requirements of approximately 5710

kg/s (5576 l/s) of warm water and 2580 kg/s (2520 l/s) of cold seawater for a 1 MW, land-based OC-OTEC plant. Using the previously reported values for warm and cold seawater outgassing of carbon dioxide (0.011 mmol/l and 0.030 mmol/l, respectively), expected CO_2 emission levels would approach 21.7 g CO_2/KWh (136.9 mmol/MWs).

EPRI [10] gives estimates of CO_2 emission rates for present typical power plants using nominal heat rates for natural gas, fuel oil, and coal burning plants as 530 g CO_2/KWh, 730 g CO_2/KWh, and 935 g CO_2/KWh, respectively. Obviously, the expected CO_2 emission from a similar sized OC-OTEC plant is significantly less than any of the present fossil fueled plants now in existence. Specifically, the expected CO_2 emission of the most conservative fossil fueled power plant (natural gas) has an average CO_2 emission nearly 25 times that of an OC-OTEC plant of similar power capacity.

3.4 OXYGEN

Oxygen is a very important gas for OC-OTEC considerations. Not only is it a substantial contributor to the overall noncondensable flow through the OC-OTEC system, it also has a very big role in environmental concerns of the OC-OTEC process.

Its importance as a significant gas in the total noncondensable flow in the OC-OTEC system will be addressed in the following sections. The environmental concerns of oxygen outgassing in the OC-OTEC process lie in the tremendous role that oxygen plays in the biological activity which occurs in natural seawater. Specifically, oxygen is the primary gas consumed in the

respiration process in the ocean environment. Likewise, it is the primary product of photosynthesis occurring in the upper (warm water) layers of the oceans. Therefore, a great deal of the biological activity occurring in natural ocean waters depends on and effects the dissolved oxygen content.

The concern about the extent of oxygen outgassing, for OC-OTEC considerations, arises from the possible discharge of significant quantities of oxygen-deficient seawater into an ocean environment which cannot handle such a shock without drastic shifts in the biological activities in the local area. Therefore, to avoid such a problem, it is necessary to quantify the extent of oxygen outgassing so that proper techniques for dealing with the reaeration (reinjection) of the effluent stream can be determined if, in fact, oxygen outgassing is significant enough to create such a concern.

Unfortunately, the biological activity which is so important to protect through accurate accounts of oxygen outgassing is the same mechanism which makes it nearly impossible to obtain precise data. This activity (photosynthesis/respiration) is constantly altering the oxygen composition of the seawater, which makes the extent of outgassing very difficult to determine because there is no stable background upon which an oxygen flow comparison can be based (like there was for nitrogen and argon). Even more important, principally for the cold water background, is the fact that the cold water stream is subject to even further variation due to the vertical excursion of the density profile (primarily related to tidal changes). The excursion of the density profile, which could permit oxygen saturated water to venture into the normally undersaturated oxygen bottom water, is expected to be even more obvious in cold waters taken near the bottom (like the waters experienced in

the HMTSTA where the cold water pipe follows the contour of the continental slope and the inlet is probably no more than 10 meters from the ocean bottom). Therefore, the values presented in the following sections should be considered rough estimates of oxygen outgassing levels, and the relative errors associated with these measurements will reflect this fact.

3.4.1 COMPOSITION IN SEAWATER

Oxygen compositions are very dependant on time of day, available sunlight, season, etc. so that any attempt at providing an accurate account of feed stream oxygen content without actually measuring the streams oxygen content during each run will be rough estimations at best. It will suffice for this report to make rough estimates of the oxygen outgassing rates using mean values reported by Krock [21] of oxygen content of surface and deep ocean waters in the Hawaiian region.

Krock gives daytime oxygen levels for the warm water of 5.05 ml/l (0.225 mmol/l) and 1.06 ml/l (0.047 mmol/l) for the cold water (all data collected in this investigation were obtained between the hours of 0800 and 1700 during the late spring and mid-summer months). He found that the warm water was essentially at saturation for oxygen, while the deep ocean waters were well below oxygen saturation (see Figure 3.1). This can be attributed to the existence of respiration in the deep water in the absence of photosynthesis. These are the values used in this investigation to estimate the available oxygen for each feed stream in the outgassing analysis calculations.

3.4.2 TOTAL OXYGEN FLOW

Figures 3.14 and 3.15 represent the vapor flow of oxygen through the HMTSTA during steam generation under various warm water and cold water flow conditions. The erratic behavior of the curves in these diagrams graphically displays the problems associated with trying to quantify the extent of oxygen outgassing in the OC-OTEC system assuming a stable warm and cold water feed stream composition.

3.4.3 LEAK (BACKGROUND) ESTIMATION ANALYSIS

The extreme variability of the oxygen background is attributed primarily to the inherent variability in the oxygen background within natural ocean waters. The chemical and biological reactivity of the oxygen in the ocean environment makes it impossible to accurately predict initial feed stream oxygen contents without actually measuring them before every run. As mentioned previously in section 3.4.1, in Krock's data [21], which was used to estimate the oxygen composition of the warm and cold waters, oxygen was by far the most variable of the noncondensable gases investigated in this report. In fact the standard deviation of Krock's data was approximately ± 20% of the measured value. This inherent problem in the naturally occurring ocean water is the reason the oxygen data is so scattered and the background is not as precise as that of the other gases.

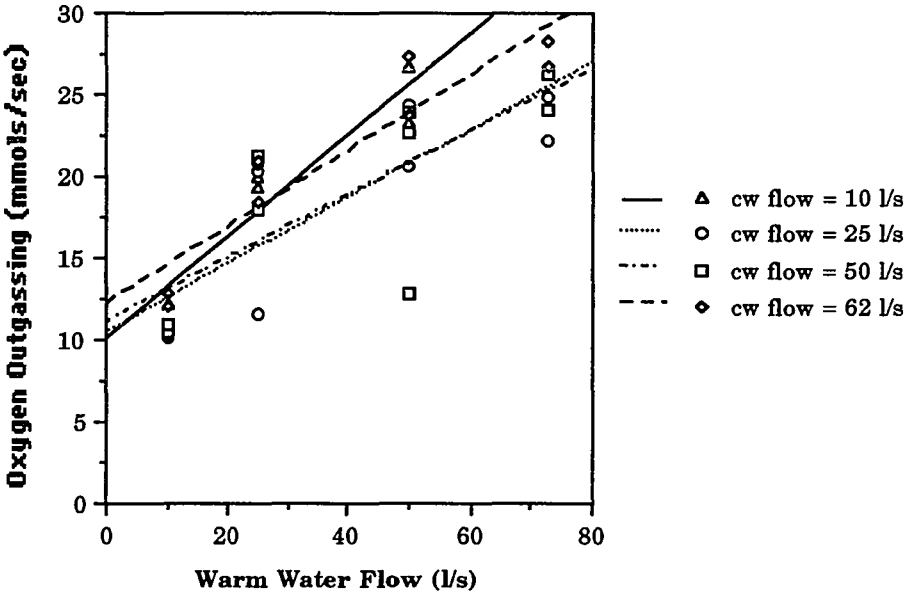

Figure 3.14: Oxygen Outgassing vs. Warm Water Flow with Steam Generation

Due to the instability inherent in the background composition of the warm and cold water feed streams and the reactivity of water vapor in the presence of the EM sensor head (oxygen can be artificially detected by an EM sensor due to the ionization and fragmentation of water vapor, much like carbon dioxide), the value obtained from the zero flow curves (9.03 mmols/sec) in Figure 3.16 should be considered an oxygen "background" with an atmospheric leak contribution calculated as follows.

An oxygen leak estimate (as described for carbon dioxide in a previous section) was performed using the estimated nitrogen and argon leak rates and the relative atmospheric composition of oxygen ($x_{air,O2}$ = 0.204). This

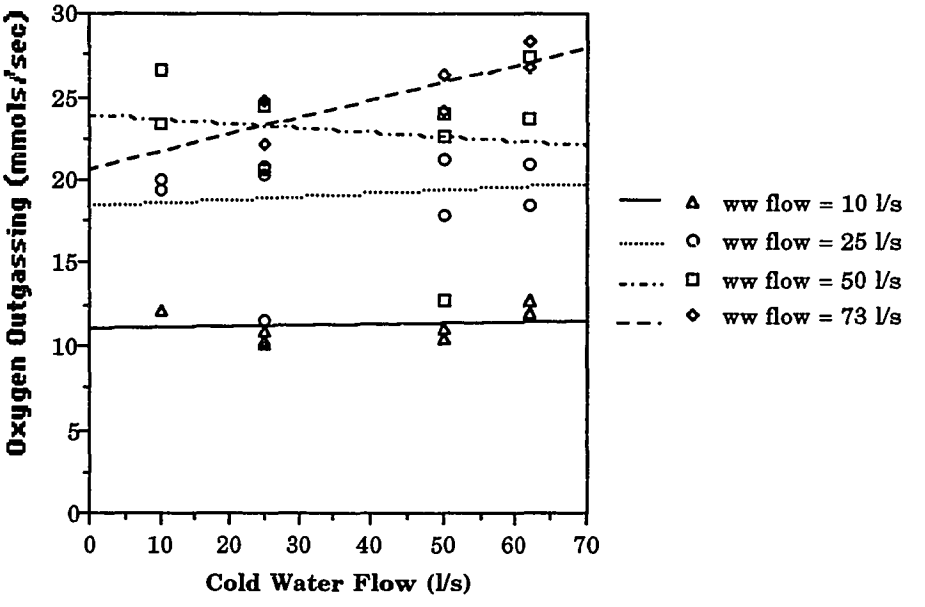

Figure 3.15: Oxygen Outgassing vs. Cold Water Flow with Steam Generation

procedure yielded a value of 3.07 mmol/sec as the estimated oxygen leak in the reported oxygen background.

3.4.4 EXTENT OF OUTGASSING

Table 3.12 shows the total available oxygen using Krock's values discussed in Section 3.4.1 under various warm and cold water flow configurations. Table 3.13 represents the data taken directly from Figures 3.14 and 3.15 and corrected for an estimated 9.03 mmols/sec oxygen background. Table 3.14 shows the percentage of total oxygen (for both the

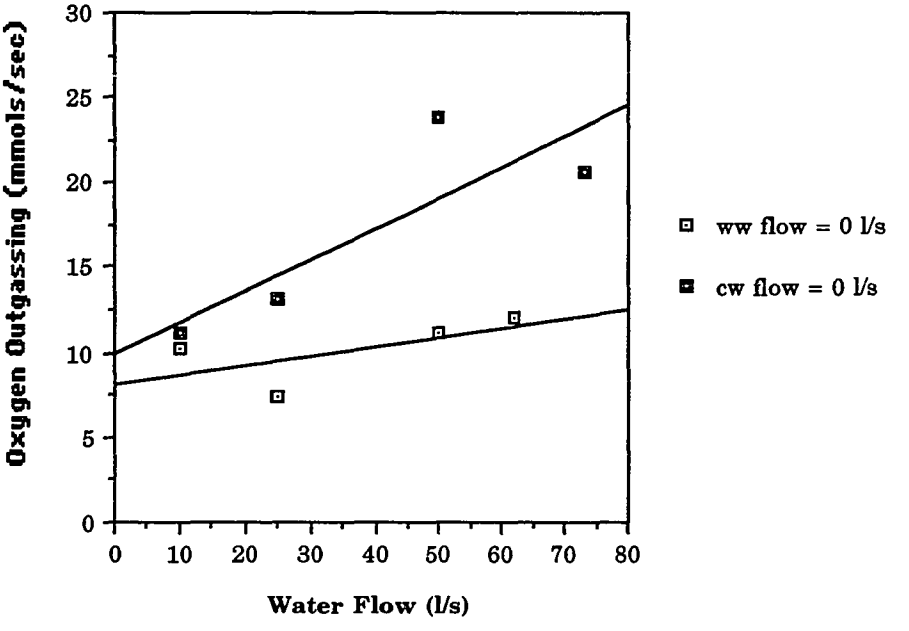

Figure 3.16: Zero Warm and Cold Water Flows vs. Oxygen Outgassing with Steam Generation (Background)

warm and cold water streams) outgassed during various experimental flow conditions.

With the overall outgassing rates determined, it is necessary to determine the extent of outgassing for each individual feed stream (warm and cold water). Figure 3.17 has been developed in the same manner as described for nitrogen in order to determine the outgassing contributions from each of the warm and cold water feed streams. It contains the zero cold water flow and zero warm water flow outgassing rates (solid lines) and the 100% outgassing curves developed from Krock's data (dotted lines). Assuming linearity of

Table 3.12: Total Available Oxygen with Respect to Warm and Cold Water Flow Rates (100% Outgassing of Both Streams) (mmols/sec)

Warm Water Flow (liters/sec)	Cold Water Flow (liters/sec)			
	10	25	50	62
10	2.72*	3.43	4.62	5.18
25	6.11	6.82	8.01	8.57
50	11.74	12.45	13.64	14.20
73	16.92	17.63	18.82	19.38

* Values based on Krock data [21].

Table 3.13: Oxygen Outgassing Corrected for Oxygen Background (mmols/sec)

Warm Water Flow (liters/sec)	Cold Water Flow (liters/sec)			
	10	25	50	62
10	3.2†	1.6	3.3	4.1
25	7.0	5.4	8.0	9.4
50	15.6	12.4	12.8	14.2
73	13.8	15.1	16.7	19.5

† Values represent the mean of data taken from Figures 3.14 and 3.15 and then corrected for an estimated background of 9.03 mmols/sec O_2.

Table 3.14: Percentage of Total Oxygen Outgassed

(% Outgassed)

Warm Water Flow (liters/sec)	Cold Water Flow (liters/sec)			
	10	25	50	62
10	117.6	46.6	71.4	79.2
25	114.6	79.2	99.9	109.7
50	132.9	99.6	93.8	100.0
73	81.6	85.6	88.7	100.6

outgassing rates at these feed stream flow rates, the linear equations for the respective lines are as follows:

$Y = 0.225X$ 100% warm water outgassing

$Y = 0.047X$ 100% cold water outgassing

and

$Y = 0.184X + 9.88$ warm water outgassing (zero cold flow)

$Y = 0.055X + 8.17$ cold water outgassing (zero warm flow)

Therefore, the estimated level of outgassing of oxygen for the warm water stream is 81 ± 16% and the estimated level of cold water outgassing is 117 ± 17%.

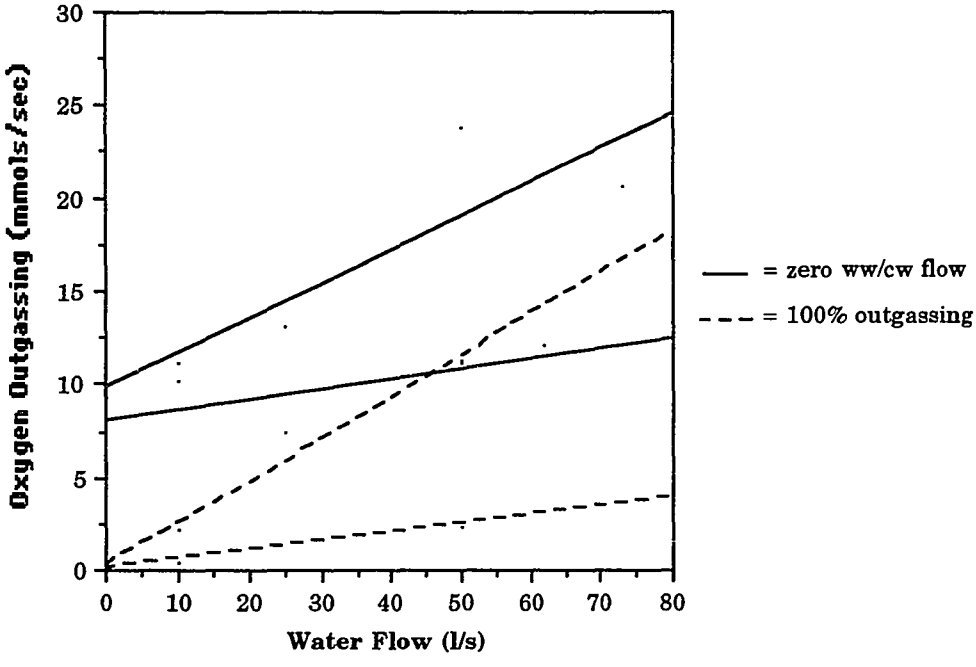

Figure 3.17: Comparison of Zero Flow Slopes to 100% Outgassing Slopes (Oxygen)

It would be safe to assume that there is nearly 100% outgassing of oxygen from the cold water stream, which is consistent with the findings for nitrogen. Also, one would expect a slightly higher outgassing rate for oxygen in the warm water stream as well due to the higher diffusion coefficient of oxygen in seawater [30]. Therefore, the trends observed are consistent with the nitrogen results obtained in this investigation. However, the results are still considered tentative for oxygen considering the relatively high fluctuation in the feed stream background compositions used as the basis of comparison in these outgassing rate calculations.

CHAPTER 4

COMPONENT SELECTION AND MODELING APPROACH NO PREDEAERATION

4.1 INTRODUCTION

The following section describes the general procedure utilized in this investigation for determining the component requirements and thermodynamic performances for a non-predeaerated 10 MW_{gross} OC-OTEC system with noncondensable venting directly to the atmosphere, as is present OC-OTEC design practice. Since the various components incorporated within this design are at various stages of technological development, every effort has been made to design a system which incorporates only realistic component designs within present technological restraints. In most cases the design has been developed to utilize only existing technologies even though more efficient components could theoretically be designed. It was deemed more appropriate to be realistic in component development. Therefore, in some cases such as the turbines, pumps and vent compressors, it was necessary to incorporate multiple systems in parallel to stay within the limits of modern technology.

Upon selecting appropriate system components, a general outline of the thermodynamic model utilized in the component design is discussed. These models have been chosen from various sources specifically aimed at adequately defining the thermodynamic performance of the particular component. In most cases the modeling approach is well developed and

utilized within OC-OTEC research [32] while other approaches (particularly in the predeaerated and reinjected system) were developed by the author utilizing the most recent information and data pertaining to the particular component performance. In either case the general intent of the thermodynamic modeling approach is to define system properties (temperature, pressure etc.), fluid flow rates, parasitic power losses, pressure drops and component sizes. The following is the thermodynamic evaluation and design procedures for the non-predeaerated OC-OTEC system.

Figure 4.1 represents the OC-OTEC configuration without predeaeration and reinjection designed in the following analysis. All numerical subscripts utilized in the following variables and figures correspond to the flow paths defined by this figure. Solid lines represent system paths composed primarily of liquids (seawater) while the dotted lines represent system paths primarily composed of vapors (steam and noncondensable gases).

4.2 TURBINE

4.2.1 SELECTION

For OC-OTEC operating conditions incorporporated in this design, it was determined that an axial flow turbine would be utilized as the turbine of choice. The axial flow configuration was chosen because it possesses the maximum efficiency potential at the typical OC-OTEC conditions experienced

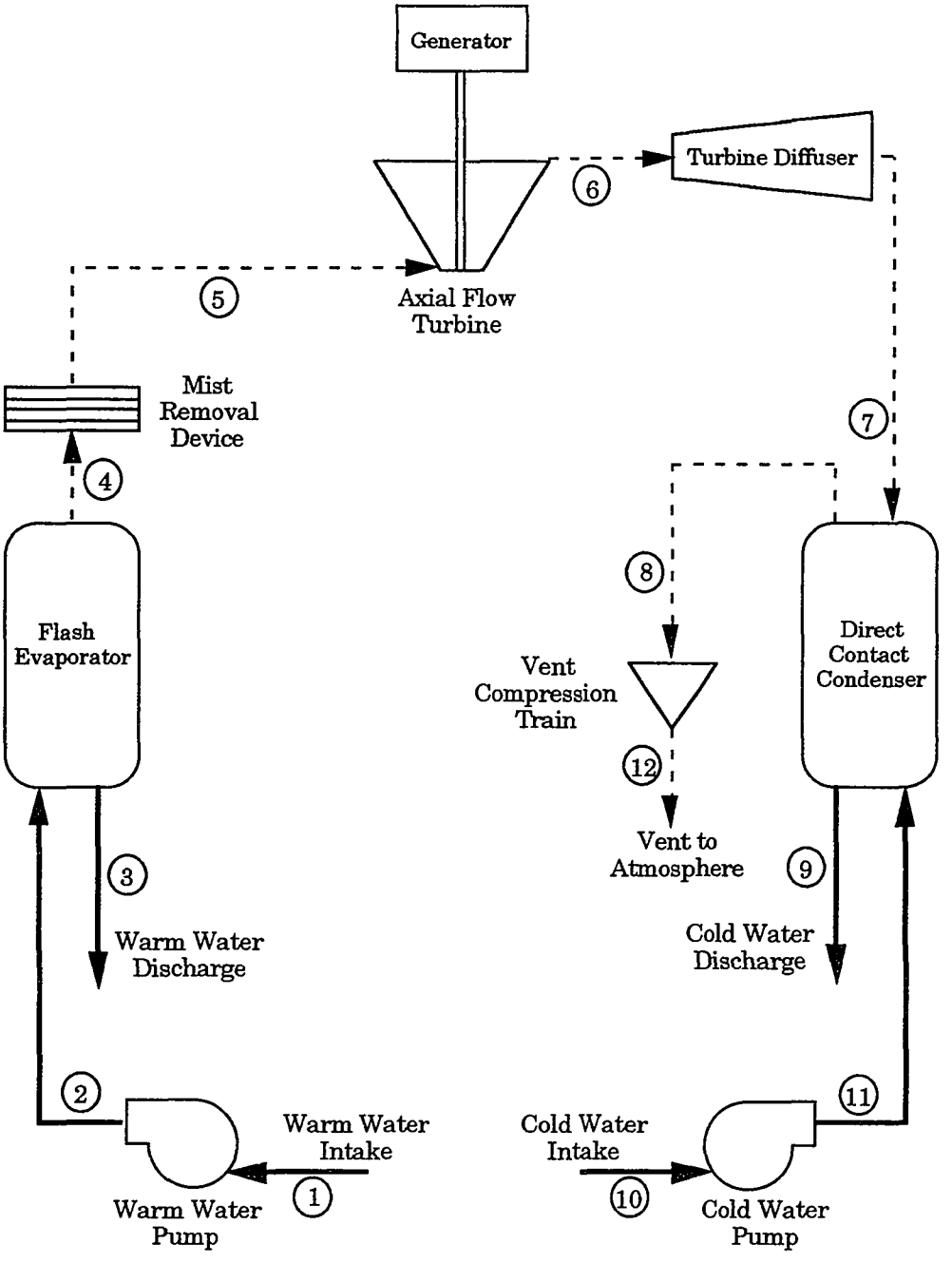

Figure 4.1: OC-OTEC System Without Predearation

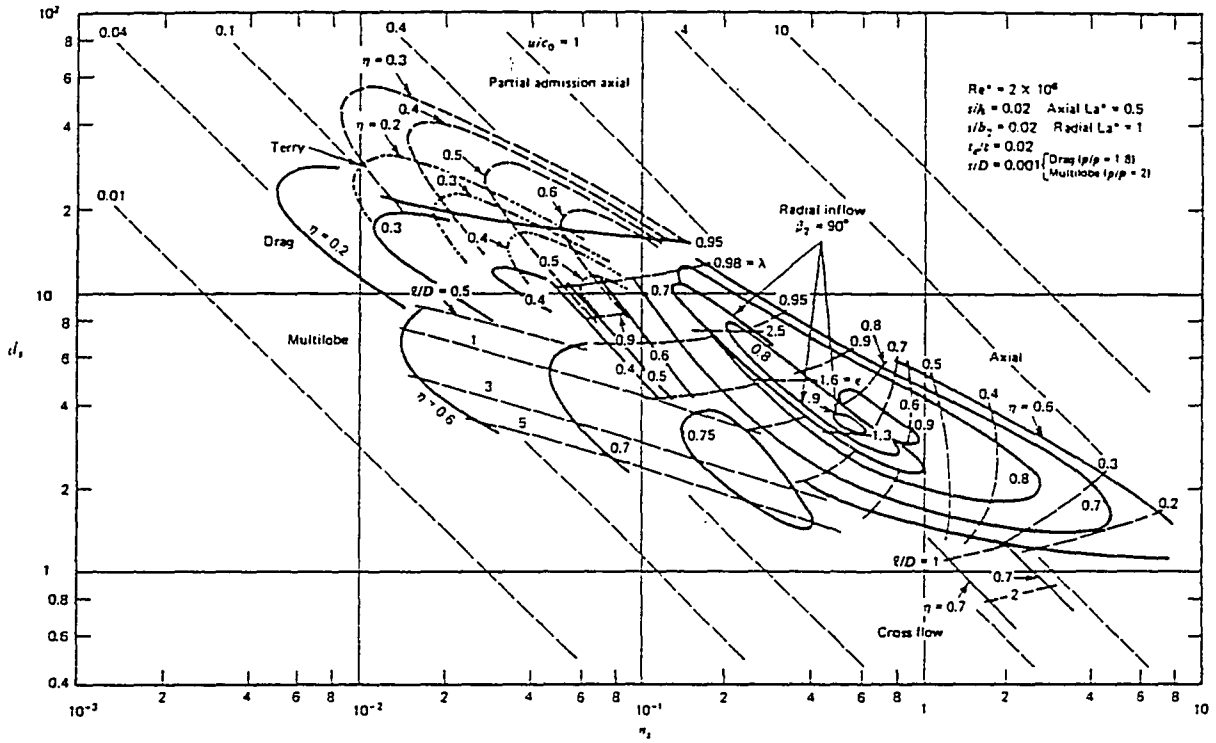

Figure 4.2: $n_s d_s$ Diagram for Single-Stage Turbines and Expanders Operating with Compressible Fluids.
(Taken from [2])

in this design. This conclusion was drawn after carefully analyzing Figure 4.2 (reproduced from [2]) from which the typical contours of total-to-static efficiency potential for various turbine types dealing with compressible fluids are shown. In this diagram the ordinate is a dimensionless specific diameter d_s and the abscissa is a dimensionless specific speed n_s, defined as

$$n_s = \omega_\tau V_6^{1/2} / \Delta h_{is,t}^{3/4} \qquad (4\text{-}1)$$

and

$$d_s = D_t (\Delta h_{is,t})^{1/4} / V_6^{1/2}, \qquad (4\text{-}2)$$

where

ω_τ = the rotational speed (rad/s)

D_t = the tip diameter (m)

V_6 = the exit volumetric flow of the working fluid (m^3/s)

$\Delta h_{is,t}$ = the isentropic enthalpy drop between inlet and outlet stagnation conditions.

Balje [2] defines the rotor tip speed (U_t) related to the $n_s d_s$ product as

$$U_t / C_o = n_s d_s / \sqrt{8} \qquad (4\text{-}3)$$

and a spouting velocity C_o (m/s) as a maximum potential speed:

$$C_o = (2\Delta h_{is,t})^{1/2} \qquad (4\text{-}4)$$

The maximum allowable tip speed for axial machines as defined by Dixon [8] is 450 m/s.

Parsons et al. [32] show that spouting velocities range from 370 to 400 m/s for OC-OTEC turbines operating with nearly saturated steam at approximately 21°C inlet temperatures experiencing a typical 8-10°C temperature drop through the rotor and stator sections. Those criteria limit the selection of a turbine to the diagonal line of $U_t/C_o \approx 1$ in Figure 4.2.

From the figure it is noted that both axial and radial turbines can yield total-to-static efficiencies greater than 80% along the criteria line of $U_t/C_o \approx 1$. However, since a higher specific speed (n_s) yields a lower specific (and actual) turbine diameter [32] an axial turbine is chosen because its range of specific speeds with efficiencies greater than 80% (about 0.15 - 3) is much larger than for radial turbines (approximately 0.2 - 1). It should be noted that cross flow turbines operate within a specific speed range of 1 to 4 but possess lower total-to-static efficiencies of approximately 70% [32].

Therefore, for the present study, axial flow turbines have been chosen as the turbine of choice beause of its high efficiency (80%) over a large specific speed range (0.15 - 3). Also, Bharathan and Penney [4] have identified the possibilities of utilizing existing rotors from low pressure power plant turbines already available with appropriately designed stator sections for shaft outputs of up to 5 MW. This implies that the technology already exists for utilizing this type of turbine for OC-OTEC design, which was one of the most important criteria for this investigation.

4.2.2 MODELING APPROACH

The procedure utilized in the turbine design has been developed primarily to define the turbine diameter and rotational speed given the assumed operating conditions of turbine and generator efficiencies (0.80 and 0.95, respectively), inlet and outlet steam temperatures (22.50°C and 12.00°C, respectively suggested by [27]) and the design shaft power (10 MW_{gross}). A detailed analysis of the rotor and stator losses, leakage losses, moisture corrections and blade profiles are beyond the scope of this investigation since both the non-predeaerated and predeaerated turbine designs will be nearly identical.

The detailed description of the model utilized for the turbine design is included in Appendix F.1. The following model description outlines the general procedure utilized in the design, and refers directly to the enthalpy vs. entropy diagram (Figure 4.3) taken from Dixon [8] which visually describes the expansion process through the turbine. The symbols utilized in

this description C, x, P, h, S denote absolute steam velocity, steam quality, pressure, enthalpy, and entropy, respectively. It is assumed for this analysis that the inlet steam quality is 1.00 (100% steam) and that the entire expansion process occurs within the wet steam region [32].

Since this design is aimed at determining a proper turbine size, it is initially necessary to assume an initial absolute steam velocity (C_5) from which an iterative procedure will eventually determine the actual design value. Parsons et al. [32] suggest an initial assumption of 60 m/s since this should be very close to typical OC-OTEC values. From this value an inlet stagnation enthalpy can be determined

$$h_{05} = h_5 + C_5^2 / 2 \tag{4-5}$$

Because we know that isentropic expansion occurs through the turbine component ($S_5 = S_{6ss}$), and the turbine outlet temperature is set at 12.00°C, the conditions at point 6ss from Figure 4.3 can be determined

$$C_{6ss} = C_5 \rho_5 x_{6ss} / \rho_{6ss} \tag{4-6}$$

$$h_{06ss} = h_{6ss} + C_{6ss}^2 / 2 \tag{4-7}$$

where ρ is the steam density determined from the mass of the steam and the specific volume of the steam at the specified temperature and pressure (see Appendix F.1 for more detail). With a total-to-static efficiency ($\eta_{t\text{-}s}$) assumed to be 0.8 (taken from Figure 4.2) for axial turbines and the definition of $\eta_{t\text{-}s}$

$$\eta_{t\text{-}s} = (h_{05} - h_{06}) / (h_{05} - h_{6ss}) \tag{4-8}$$

we find h_{06}. With this knowledge the remaining state variables at point 6 can be determined initially assuming $C_6 = C_{6ss}$ for the first iteration

$$h_6 = h_{06} - C_6^2 / 2. \tag{4-9}$$

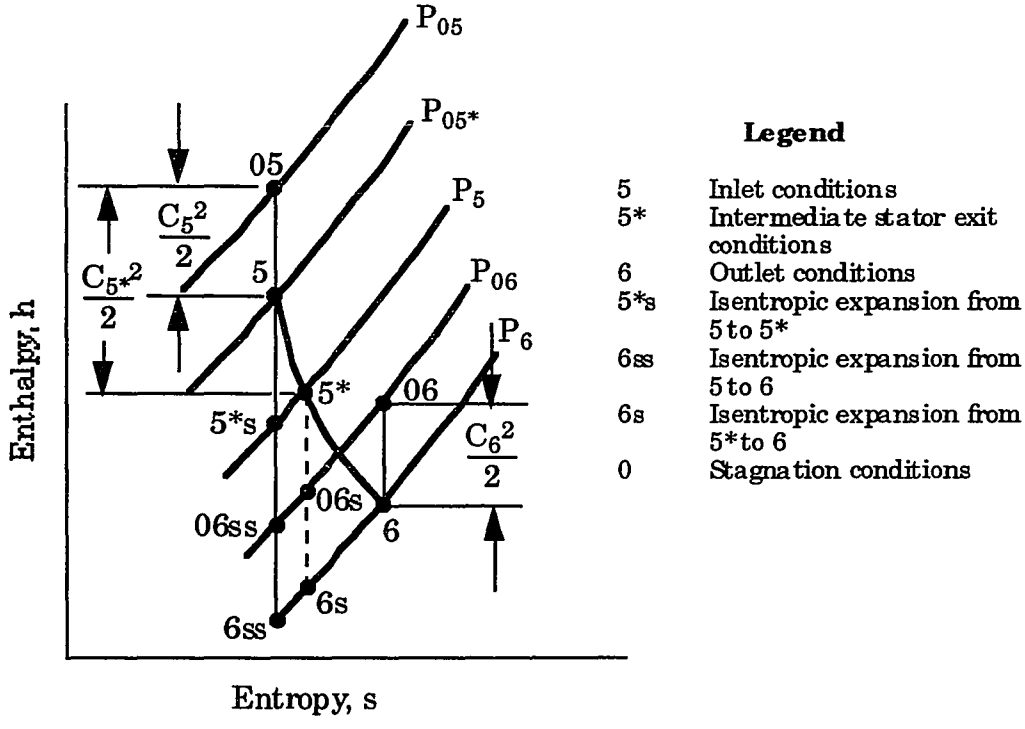

Figure 4.3: Enthalpy vs. Entropy Diagram of Turbine Expansion Process
(taken from [8])

The mass steam flow rate (m_s) is thus determined:

$$m_s = Po_{gross} / [\eta_g (h_{05} - h_{06})] \quad (4\text{-}10)$$

where η_g = generator efficiency = 0.95

Po_{gross} = gross power of plant = 10 MW

The spouting velocity C_o is

$$C_o = [2 (h_{05} - h_{06ss})]^{1/2} \quad (4\text{-}11)$$

From these values a mass balance is performed at the turbine outlet condition (6) using equation (4-3) and an assumed hub-to-tip ratio (λ) of 0.44 [32] which gives

$$d_s = (\sqrt{8}\, C_o)^{1/2} / [\pi C_6 (1 - \lambda^2)]^{1/2} \quad (4\text{-}12)$$

Also, with a given maximum tip speed $U_{t,max}$ = 450 m/s [8] and equation (4-3) we find a maximum specific speed n_s as

$$(n_s d_s)_{max} = \sqrt{8}\, U_{t,max} / C_o \qquad (4\text{-}13)$$

and a steam specific volume as

$$V_6 = (m_s x_6) / \rho_6 \qquad (4\text{-}14)$$

From the definition of specific speed we find a maximum turbine rotational speed ($\omega_{t,max}$)

$$\omega_{t,max} = n_s (C_o^2 / 2)^{3/4} / \sqrt{V_6} \qquad (4\text{-}15)$$

$$RPM_{t,max} = (\omega_{t,max})\, 60 / (2\pi) \qquad (4\text{-}16)$$

with the turbine rpm chosen to be less than the maximum speed and a multiple of 60 for power generation from synchronous machines of 60 Hz [32].

Now, with values of steam flow, turbine exit steam quality and turbine diameter determined, estimates for C_5 and C_6 are recomputed and the preceding procedure is repeated until the outlet turbine velocity (C_6) does not significantly change from one iteration to the next (± 0.1%).

4.3 TURBINE DIFFUSER

4.3.1 SELECTION

The major function of a turbine diffuser aparatus is to recover a portion of the kinetic energy from the turbine exhaust prior to entrance into the condenser which would otherwise be lost. It was deemed necessary to include a turbine diffuser within this OC-OTEC design since improvement of overall efficiencies is the primary objective of this investigation.

Parsons et al. [32] suggest either radial or axial diffusers for axial turbine OC-OTEC applications and chose a conical axial diffuser configuration for their design because much more data and information was available for that configuration versus the radial design. Therefore, the design described by Parsons et al. [32], as well as the procedure followed in designing the turbine diffuser apparatus, has been implemented in this investigation as well.

4.3.2 MODELING APPROACH

Utilizing data published in [2], this model estimates the diffuser dimensions and semi-vertex angle. Initially the modeling procedure determines the diffuser exit condition and provides reasonable estimates as to the diffuser dimensions utilizing known diffuser inlet conditions (turbine exit conditions) and an assumed turbine diffuser efficiency. Once again, a more detailed analysis of the modeling procedure is presented in Appendix F.2 and a general description of the diffusion process is outlined and shown in the enthalpy-entropy diagram in Figure 4.4 taken from [2].

The inlet conditions of the diffuser (same as the exit conditions of the turbine) are denoted by 6 and the diffuser outlet conditions by 7 (see Figure 4.1). State 7s is the endpoint of an isentropic diffusion process from state 6 to pressure 7 [32]. The following outlines the calculation procedures.

The design diffuser exit velocity C_7 is taken as one half the diffuser entrance velocity (turbine exit velocity) $C_6/2$, which for OC-OTEC applications is typically around 60 m/s [32].

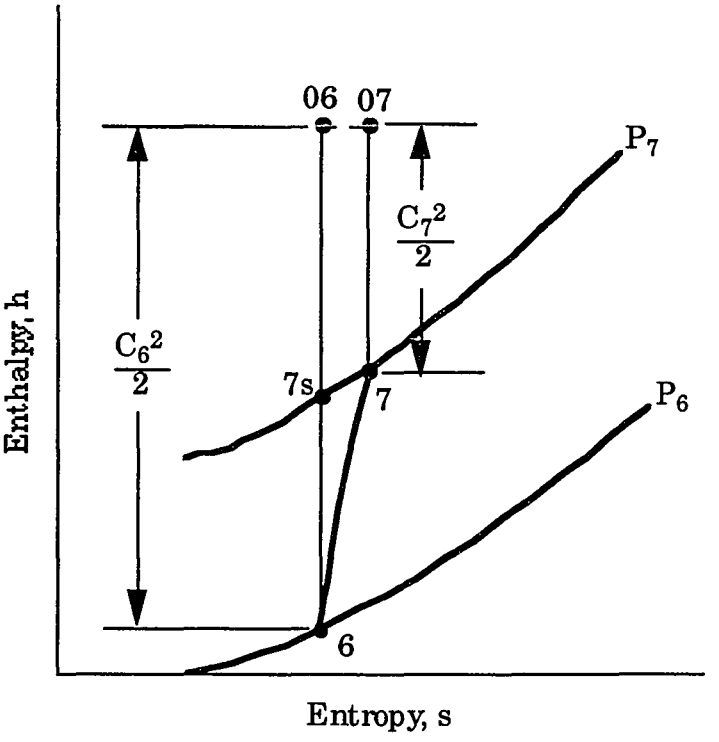

Figure 4.4: Enthalpy vs. Entropy Diagram of Diffusion Process
(taken from [8])

The definition of diffuser efficiency is

$$\eta_D = (h_{7s} - h_6) / (h_7 - h_6) = (C_6^2 - C_{7s}^2) / (C_6^2 - C_7^2) \qquad (4\text{-}17)$$

from which C_{7s} can be determined knowing the diffuser inlet conditions and the assumed diffuser efficiency (η_D) of 0.8 [2].

The pressure loss assocated with the steam passing through the diffuser can be estimated by initially assuming that the steam density at the outlet of the diffuser (ρ_7) is equal to the entrance density (ρ_6) [32], thus:

$$\Delta P = P_{06} - P_{07} = 1/2 \, [\, \rho_7 (C_7^2 - C_{7ss}^2) \,]. \qquad (4\text{-}18)$$

Since we know that $P_7 = P_6 - \Delta P$, h_{7s} and h_7 can now be assessed with the corresponding diffuser exit state variables along with the exit steam quality x_7 (see Appendix F.2 for more detailed calculations). However, since it is possible for the exit quality (x_7) to be greater than unity, indicating superheated steam, we assume there is sufficient cooling liquid available to limit the exit quality to saturation ($x_7 \leq 1.0$) [32]. Now that the exit steam conditions at the diffuser exit are fully defined, the exit steam density (ρ_7) can be recomputed and the calculations repeated until ρ_7 converges satisfactorily (± 0.1%).

Parsons et al. [32] suggest the following equation for defining the diffuser pressure recovery (C_p):

$$C_p = [C_6^2 - C_7^2 - (2\,\Delta P)/\rho_6] / C_6^2. \qquad (4\text{-}19)$$

Using this value of pressure recovery (C_p), and the turbine diameter D_t we can determine the diffuser length L_D, exit diameter $D_{e,D}$ and the semi-vertex angle θ_D for the minimum diffuser length using published data from [2] shown in Figure 4.5. Parsons et al. [32] suggest that these data may not be applicable for some OC-OTEC plant layouts and diffuser designs since minimum sizes are chosen and the data apply to a specific diffuser type. However, Parsons et al. [32] also suggest that even though more work is required before an actual appropriate diffuser design incorporating the complex velocity profiles and similar effects occurring in OC-OTEC designs can be accomplished accurately, this procedure should provide an order of magnitude approximation of size and performance. This is more than adequate for the intentions of this investigation pertaining to turbine diffuser analysis.

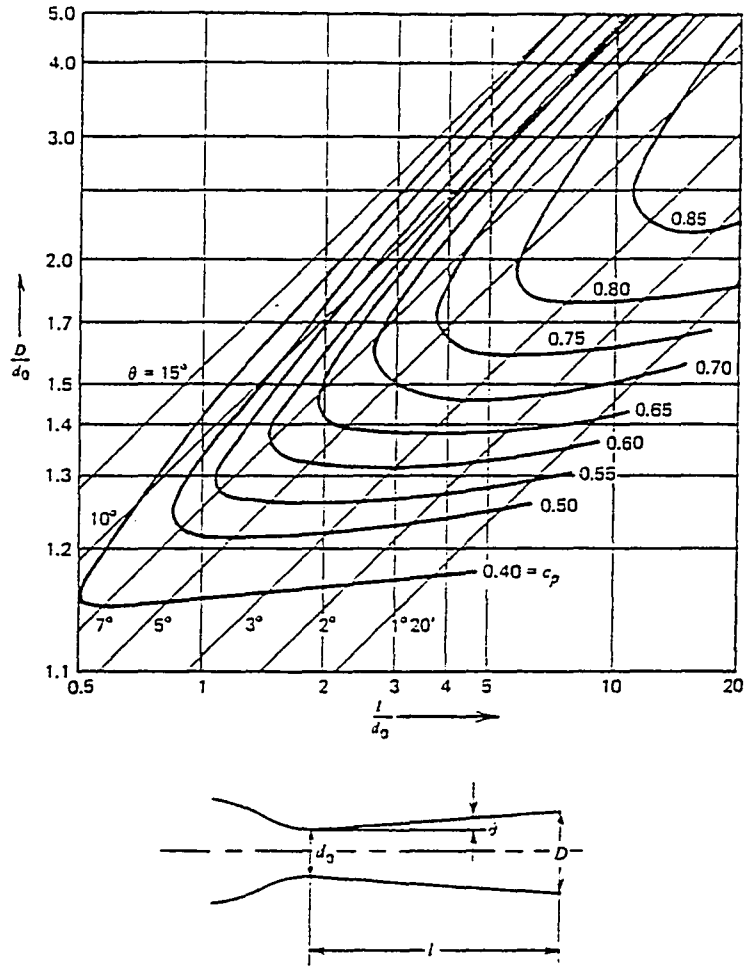

Figure 4.5: Test Data for Conical Diffusers
(Taken from [2])

4.4 EVAPORATOR AND MIST REMOVAL DEVICE

4.4.1 SELECTION

The main function of the mist removal device in an OC-OTEC system is to remove seawater droplets carried by the generated steam prior to

entrance into the system turbine components. If not removed, salt build-up and corrosion of turbine blades can seriously reduce efficiencies and the expected lifespan of the turbine systems [32].

For the purpose of this investigation a specific design for the mist removal device is not necessary and is not included. There are several configurations for mist removal devices suggested in the literature [32] including centrifugal separators, gravitational separators and impaction devices. Bharathan and Penney [5] investigated several various configurations of impaction separators currently available and suggested this form of separation device for OC-OTEC mist removal. Therefore, this type of device is analyzed in this investigation by defining the allowable maximum steam velocity, mist removal efficiency and the pressure loss through the device. Bharathan and Penney [5] concluded that parallel-channel devices can accommodate vapor velocities of up to 35 m/s with sufficient mist removal efficiencies and minimal pressure losses of approximately 40 Pa, which translates to a pressure loss coefficient for the mist removal device of K_{mr} = 10 [32].

The evaporator in the OC-OTEC system is the vacuum containment vessel in which steam is generated by flash evaporation by lowering the pressure within the vessel below the vapor pressure of the warm seawater. Important requirements necessary to consider when choosing an evaporation configuration include minimal liquid- and vapor-side pressure losses as well as maximum thermodynamic effectiveness [32].

Bharathan et al. [4] suggest four differing geometries (open-channel flow, falling films, falling jets, and spout evaporators) as the potential options

for OC-OTEC evaporators. Penney et al. [34] provide a detailed description of the relative merits of each configuration.

For the purposes of this investigation the vertical spout evaporator configuration was chosen, and the modeling procedures reflect this choice. The vertical spout configuration has been chosen for the following reasons:

1.) The noncondensable gas research described in earlier sections of this report, and used in this analysis for noncondensable emission rates, was performed under vertical spout evaporator conditions.
2.) The spout evaporator exhibits high effectiveness (close to the thermodynamic limit with minimal vapor and liquid pressure losses) [32].
3.) A significant amount of data exist for fresh water and seawater evaporation using a spout evaporator configuration under OC-OTEC conditions [4] [50].
4.) The design of the spout evaporator allows for a modular approach. Incrementing the number of spouts simplifies the determination of the design water and steam flow rates [32].

4.4.2 MODELING APPROACH

The streams focused on in the mist removal and evaporator analysis from Figure 4.1 are path 2 (warm water inlet), path 3 (warm water discharge), path 4 (generated steam, noncondensables and seawater droplets), and path 5 (mist removal steam and noncondensables).

Once again, no specific mist removal device was identified for this investigation so it has been treated as a pressure reducing restriction in the flow path [32] with an assumed steam velocity of 30 m/s and a pressure loss coefficient (K_{mr}) of 10 [32]. A more detailed description of the modeling procedure is included in Appendix F.3.

With a flow path 2 defined essentially by the warm water resource temperature (T_2 = 27.00°C, typical for most warm water sources suitable for OC-OTEC applications), a given mass steam flow rate determined by the turbine diffuser analysis (Appendix F.1), and the evaporator steam temperature T_4 defined in the mist removal analysis (Appendix F.3), the temperature of the warm water discharge T_3 can be determined as

$$\varepsilon_E = (T_2 - T_3) / (T_2 - T_4). \tag{4-20}$$

The evaporator effectiveness (ε_E) is estimated as 0.91 from data presented in Bharathan and Penney [4] for inlet cylindrical spout velocities ($x_{sp,E}$) of 2.00 m/s with one screen enhancement for droplet surface area renewal.

The required warm seawater mass flow rate ($m_{ww,2}$) is determined from the previously calculated steam generation rate ($m_{s,4}$), the seawater latent heat of vaporization ($h_{fg,2}$) and the seawater specific heat ($C_{p,2}$) (both determined from an empirical formula [32] as a function of seawater temperature as shown in Appendix F) as

$$m_{ww,2} = m_{s,4}\, h_{fg,2} / [C_{p,2}\, (T_2 - T_3)]. \tag{4-21}$$

Since only approximately 0.5% of the warm water introduced into the evaporator is utilized and lost as steam, it is assumed that $m_{ww,2} = m_{ww,3}$ without introducing any significant errors. From these values we can determine the number of spouts required (and thus required evaporator area with a set known area per spout) to handle the necessary seawater loading by dividing the total design warm water flow rate by the design flow rate per spout ($m_{sp,E}$) [32].

With the seawater flow rates defined and the data presented earlier in this report regarding noncondensable outgassing rates for the evaporator, the specific noncondensable mass release accompanying the steam generation can be determined for further use in estimating condenser noncondensable loading. The desorbed noncondensable flow now defined, the total noncondensable flow is developed by adding the desorbed mass flow ($m_{NC,E}$) to the evaporator leakage ($m_{air,lk,E}$) defined by [32] as

$$m_{air,lk,E} = 0.005\ Po_{gross} / 1000 \qquad (4\text{-}22)$$

where

Po_{gross} = gross power (kW).

Since the total determined noncondensable flow (both evolved and a result of atmospheric leakage) accounted for less than 0.3% of the total mass flow of the vapor through the turbine system, the potential contribution of these gases to increased power output from the previously designed turbine system was included but did not justify recalculation of turbine dimensions. A more detailed explanation and outline of the modeling procedures is presented in Appendix F.3.

4.5 DIRECT-CONTACT CONDENSER

4.5.1 SELECTION

The condenser portion of an OC-OTEC system performs two basic functions, the first being the condensation of a majority of the steam from the turbine diffuser exhaust, and the second being the accumulation and concentration of the evolved noncondensables.

For this investigation a direct-contact condenser configuration was chosen as the condensation mechanism of choice. The primary reasons for this choice were:

1.) The direct-contact condensation configuration (D.C.C.) possesses higher potential thermodynamic efficiencies over the competing surface condenser configuration [3].

2.) The lower capital cost of the D.C.C. components versus the capital-intensive surface condenser option.

3.) The ease with which the major objectives of a condenser can be met (condensation of steam and concentration of noncondensables), as well as the ease with which the condensation components can be designed [32].

4.) The noncondensable gas outgassing experiments presented earlier in this investigation were performed on a direct-contact condensation configuration and thus the results of these experiments can be more easily adapted to this configuration for this thermodynamic evaluation.

For this investigation the direct-contact condenser modeled in the following section is very similar to that displayed in Figure 2.1. This condenser system, because of its barometric placement and system integration constraints (specifically, downward flow of steam from turbine diffuser exhaust), consists of two stages necessary to keep plant volume and seawater pumping power low [3]. In the first section the co-current region, up to 90 - 95% of the exhausted steam can be condensed with a downward flow of steam and cooling seawater [32]. The second region, the counter-current section, further condenses the remaining steam and concentrates the accumulation of noncondensable gases with the steam and noncondensables flowing upward through a downward flow of cooling seawater. Parsons et al. [32] suggest that the gas-to-steam ratio in the counter-current region can be increased from 10% to 50% in the exhaust vapors, thus reducing the parasitic power requirements of the condenser vent compression system by up to 80%. Therefore, this configuration has been chosen for this investigation.

4.5.2 MODELING APPROACH

For the puposes of simplifying the direct-contact condenser analysis, the modeling procedure for the D.C.C. has been divided into two essentially separate regions defined as the co-current region and the counter-current region. The following analysis deals primarily with vapor streams 7 and 8 and liquid streams 9 and 11 in Figure 4.1, with the symbol A denoting the region between the co-current and counter-current regions of the D.C.C. not clearly identified in Figure 4.1.

4.5.2.1 CO-CURRENT REGION

The block diagram in Figure 4.6 represents a simplified account of the direct contact condenser shown in detail in Figure 2.1 and more clearly defines the flow paths modeled in the following analyses. For the following models the subscripts s and cw represent steam and cold seawater, respectively.

The inlet conditions of the steam entering the co-current condenser region are determined originally by finding the steam pressure drop in the diffuser-condenser passage and translating the saturation steam pressure at the diffuser exit, less this pressure drop, into a steam temperature (condenser inlet temperature T_{7*}) (see Appendix F.4 for further details). From these known values the cold water and steam outlet conditions as well as the required design cold water flow can be estimated. Since the cold water utilized in a direct-contact condensing mode releases noncondensable gases, the following calculation procedure necessitates an iterative procedure. This procedure also necessitates the appropriate assumption that condensation within the co-current region occurs at a constant condenser pressure with minimal vapor pressure losses [32].

As previously mentioned, the presence of noncondensable gases within the contacting region of the D.C.C. dramatically hinders the condensation process and the D.C.C. efficiencies. Therefore, an accurate account of noncondensables within these condensing regions is imperative to proper D.C.C. design.

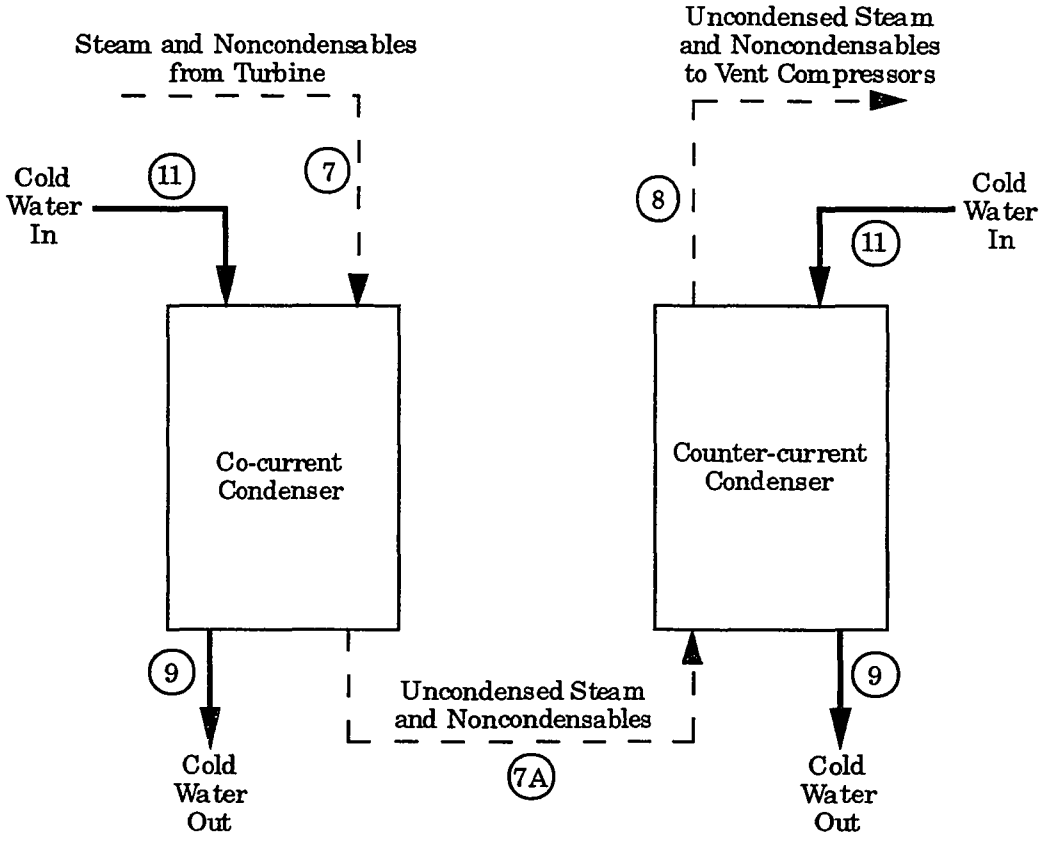

Figure 4.6: Block Diagram of Direct-Contact Condenser
(Taken from [32])

The noncondensable flow from the evaporator is used as an initial approximation as to the noncondensable mass fraction ($x_{nc,7}$) in the inlet steam for the co-current region. The corrresponding mole fraction ($y_{nc,7}$) thus permits the co-current condenser pressure (P_{co}) approximation assuming that the inlet steam is saturated at the condenser inlet temperature T_{7*}:

$$P_{co} = P_{7*} / (1 - y_{nc,7}) \qquad (4\text{-}23)$$

In the co-current region of the condenser this pressure is assumed constant since the seawater and steam are flowing in the same direction and the frictional vapor pressure drop is negligible [32].

For determining the design cold water flow and outlet steam condition for the co-current condenser region, a variation of heat load vs. outlet steam temperature diagram is generated (see Figure 4.7). In this figure the heat load is plotted as a function of the steam outlet temperature ($T_{s,7A}$). The slope of the curve itself is dependant upon the steam inlet temperature ($T_{s,7*}$), the condenser pressure (P_{co}) and the steam and noncondensable (nitrogen, oxygen, argon and carbon dioxide) mass flow rates [32]. The outlet steam temperature ($T_{s,7A}$) is varied from the inlet steam temperature ($T_{s,7*}$) to the cold water inlet temperature ($T_{cw,11}$) in gradual steps to develop the heat load diagram (see Appendix F.4.1 for more detailed calculations and equations). For each of the incremented outlet steam temperatures ($T_{s,7A}$), the outlet steam mass fraction is determined as

$$x_{s,7A} = P_{sat}(T_{s,7A}) / P_{co}. \tag{4-24}$$

From this value the outlet steam mass flow rate ($m_{s,7A}$) can be determined as

$$m_{s,7A} = [(m_{N2,7} / 28) + (m_{O2,7} / 32) + (m_{Ar,7} / 40) + (m_{CO2,7} / 44)]^* \\ 18\, x_{s,7A} / (1 - x_{s,7A}) \tag{4-25}$$

The co-current condenser heat load (HL_{CO}) is then determined according to

$$HL_{CO}(T_{s,7A}) = m_{s,7*}\, h_{s,7*} - m_{s,7A}\, h_{s,7A} + \text{sensible cooling of gases} \tag{4-26}$$

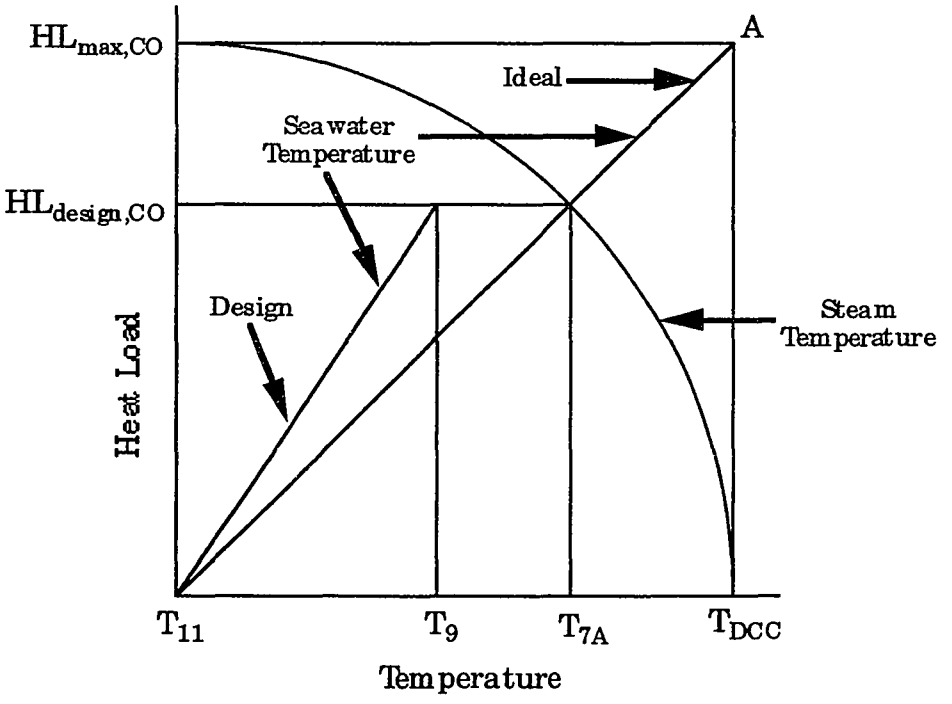

Figure 4.7: Condenser Heat Load Versus Steam Exit Temperature for the Co-Current Condenser Section
(Taken from [32])

where $h_{s,7*}$ and $h_{s,7A}$ are the enthalpies of the co-current steam at the inlet (7*) and outlet (7A), respectively [32].

The minimum cold water flow ($m_{cw\text{-}CO,\ 11,min}$) required to provide the necessary heat sink for this heat load is determined iteratively as

$$m_{cw\text{-}co,11,min}\ C_{p,cw,11}(T_{cw,9} - T_{cw,11}) = HL_{co}\ (T_{s,7A}) \qquad (4\text{-}27)$$

where $T_{s,7A} = T_{cw,9}$

since neither $m_{cw\text{-}co,11,min}$ nor the condenser outlet steam temperature ($T_{cw,9}$) are known.

This procedure assumes that the co-current region acts as an ideal contactor (ie. thermal equilibrium at the outlet). However, since achieving

thermal equilibrium between the outlet steam and cooling water streams would theoretically require an infinite contact length, the design seawater flow rate is increased above its minimum ideal flow rate by a conservative value of 1.2 typically utilized in gas-liquid contacting columns [20]. The design outlet steam temperature is then set to $T_{s,7A}$ and another heat balance is performed to determine the outlet seawater temperature ($T_{cw\text{-}co,9}$):

$$1.2\, m_{cw\text{-}co,11,min}\, C_{pcw,11}\, (T_{cw\text{-}co,9} - T_{cw,11}) = HL_{co}\, (T_{s,7A}). \qquad (4\text{-}28)$$

With an approximate design flow rate now determined, the noncondensable gas desorption occurring in the co-current section of the D.C.C. can now be estimated using the desorption rates determined earlier in the experimental portion of this investigation. These values are then used to revise the initial noncondensable flow estimates utilized at the outset of the co-current calculations. This entire procedure is then repeated until calculated values of P_{co} converge from one iteration to the next ($\pm$ 0.1%).

The cross-sectional area of the co-current condenser is determined in two ways, one based on the maximum allowable liquid loading and another based on maximum allowable inlet vapor velocity (see Appendix F.4.1 for more details) according to Parsons et al. [32].

Parsons et al. [32] suggest that the effectiveness of the co-current condenser is determined as

$$\varepsilon_{CO} = (T_{cw,9} - T_{cw,11}) / (T_{s,7A} - T_{cw,11}) \qquad (4\text{-}29)$$

knowing steam and seawater outlet temperatures. From this effectiveness the number of transfer units (NTU_{CO}) is found as

$$NTU_{CO} = - \ln (1 - \varepsilon_{CO}). \qquad (4\text{-}30)$$

The height of a transfer unit (HTU) is generally an experimentally determined value which is typically a function of pressure, gas content etc. Therefore, the value of 0.3 m is used in this investigation as suggested by [42] as a typical value for OC-OTEC direct-contact condenser applications nearly independant of noncondensable gas concentrations. The height of the contactor is attained by multiplying the NTU_{CO} by the HTU.

4.5.2.2 COUNTER-CURRENT REGION

The calculations for the counter-current region follow a very similar procedure as those previously discussed for the co-current condenser section. Once again the assumption of constant pressure within the condensing section is used even though this is a less accurate assumption for the counter-current section of the condenser due to the flow of vapor and water in opposite directions. However, this assumption does not introduce any significant error due to the relatively small vapor and water flows experienced in this portion of the condenser vs. the previous co-current section. The condenser pressure P_{CO} calculated in the previous section is utilized here as the working pressure of the counter-current section as well.

Once again, a variation of the heat load (HL_{CC}) as a function of outlet steam temperature ($T_{s,8}$) is performed as previously described (see Figure 4.8). From the heat load value a minimum cold water flow is determined

$$m_{cw\text{-}CC,min} = HL_{CC}(T_{s,8}) / C_{pcw,11}\,(T_{cw,9} - T_{cw,11}). \qquad (4\text{-}31)$$

The actual design counter-current cold water flow requirement is determined:

$$m_{cw\text{-}CC} = 1.2\ m_{cw\text{-}CC,min} \qquad (4\text{-}32)$$

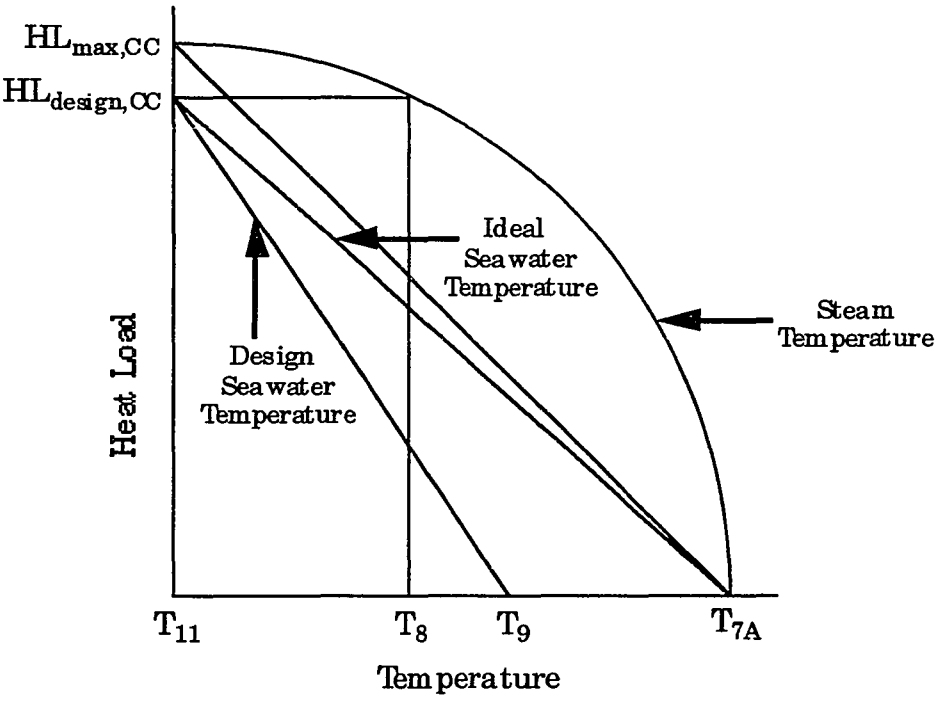

Figure 4.8: Condenser Heat Load Versus Steam Exit Temperature for the Counter-Current Condenser Section
(Taken from [32])

from which the water outlet temperature $T_{cw\text{-}cc,9}$ is found as

$$m_{cw\text{-}CC}\, C_{pcw,11}\, (T_{cw\text{-}cc,9} - T_{cw,11}) = HL_{CC}\, (T_{s,8}) \qquad (4\text{-}33)$$

In order to perform these operations the outlet steam and inlet water difference ($T_{s,8} - T_{cw,11}$) is set at 1.0°C [32]. As in the co-current section previously, the calculations are then revised to account for the new noncondensable flows encountered due to the desorbed gases from the newly determined design counter-current cold water flow.

The cross-sectional area of the counter-current condenser is calculated in the same manner as the co-current section according to maximum liquid loading and maximum allowable vapor velocity.

Parsons et al.[32] define a counter-current NTU_{CC} as

$$NTU_{CC} = \int_{T_{s,7A}}^{T_{s,8}} dT_s / (T_s - T_{cw}) \qquad (4\text{-}34)$$

which is numerically integrated and multiplied by an HTU value of 0.3 m to determine the contactor height. Appendix F.4.2 provides a more detailed analysis of the procedures and calculations described generally in this section.

4.6 CONDENSER EXHAUST COMPRESSORS

4.6.1 SELECTION

The primary function of the condenser exhaust compressors is to remove the noncondensable gases and residual water vapor (steam) remaining in the condenser following the condensation process in order to maintain the system pressure. For OC-OTEC applications without predeaeration and reinjection, in which typical condenser pressures range from 1.2 - 1.7 KPa [32] and exhaust the compressed vapor at atmospheric pressure (101.325 KPa), a staged compression train, as shown in Figure 4.9, is necessary. Designing the compression mechanism in stages permits compression ratios and compressor designs of reasonable values for each stage, thus reducing power requirements and initial capital outlay.

Interstage vent condensers (rectangular items shown in Figure 4.9) have been included within this design as suggested by [32] in order to further condense the residual water vapor accompanying the noncondensables through the vent compression train, thereby reducing the vapor flow and subsequently the power requirements. Also, since the compression process increases the gas temperature, these intercoolers reduce the vapor temperatures, thus minimizing parasitic power requirements associated with the compression process.

For the purposes of this investigation it was not necessary to specify the type of compression system used in this design but to only define the parasitic power losses associated with the vent compression system chosen. Mixed-flow and axial compressors both work at efficiencies of 0.8 - 0.85 under typical OC-OTEC conditions and could prove suitable choices as vent compressors [32].

4.6.2 MODELING APPROACH

The primary concerns of vent compressor calculations are the power required to run the compressors, the compression ratio per stage (assumed constant in this analysis), and the volumetric flow of vapor through each stage. The pressure drop through each intercooler (0.28 KPa) is assumed constant for each stage as suggested by [32]. The number of stages is determined through trial-and-error in an attempt to maintain reasonable, equal compression ratios for each compression stage. Assuming equal compression ratios for each stage implies that the vapor flow rate and

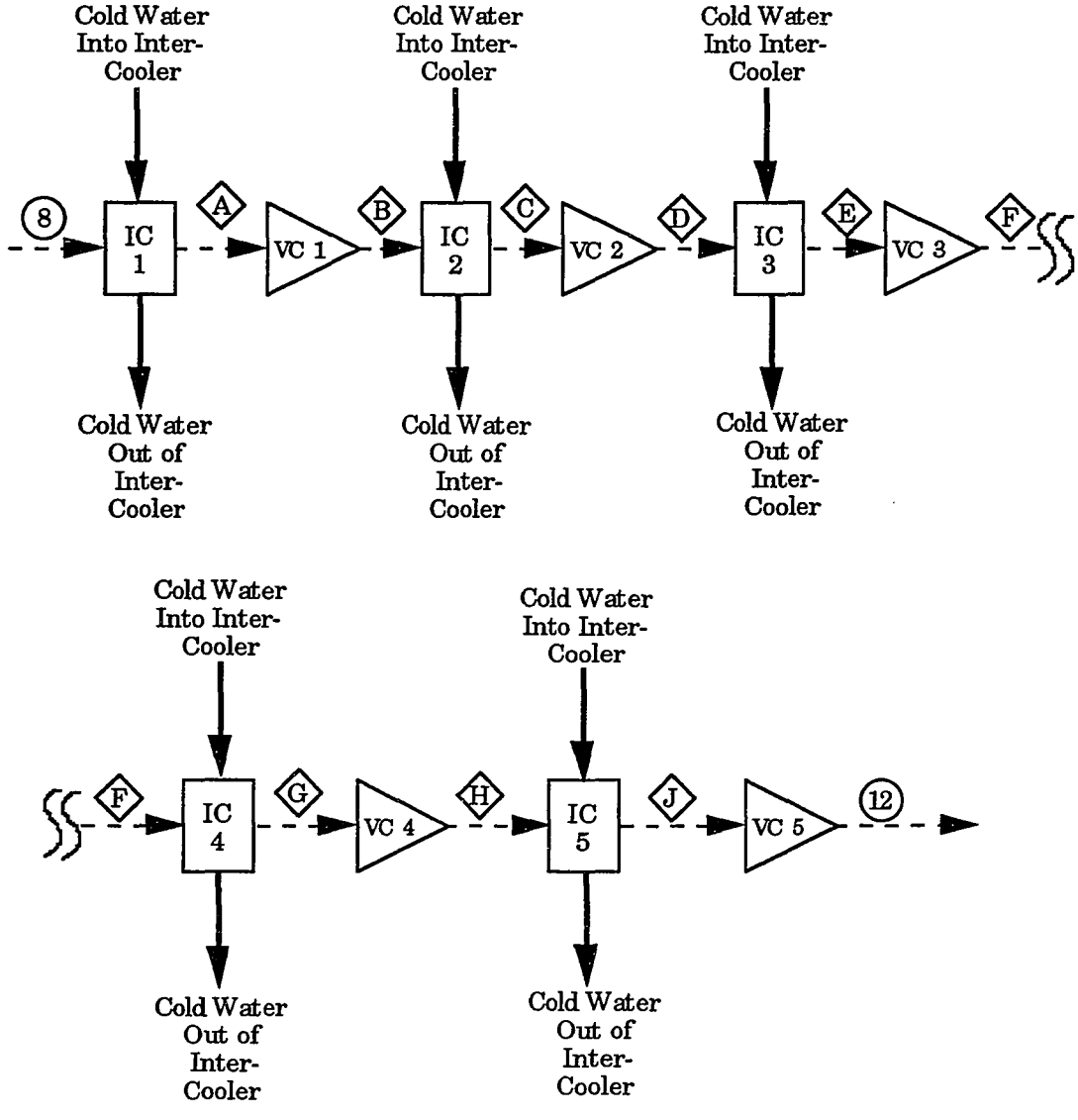

Figure 4.9: Vent Compression Train for OC-OTEC Direct Contact Condenser Without Predeaeration

compressor inlet temperatures remain constant, which in this analysis would lead to a minimum parasitic power requirement for exhausting these gases to the atmosphere [32]. However, the vapor flow varies from stage to stage due to the progressive condensation of water vapor in the intercoolers as the gas pressure increases through each compression stage. Therefore, the parasitic power predicted in this analysis is somewhat conservative compared to an optimized compression system accounting for this water vapor condensation [32].

The intercooler size and seawater requirements have been ignored in this analysis since its performance is easily defined by an assumed vapor pressure drop (0.28 KPa) and outlet gas temperature (+ 2°C above inlet water temperature, $T_{cw,11}$) [32]. The seawater flow requirements accompanying noncondensable desorption and atmospheric leakage associated with the intercoolers is insignificant compared to the direct-contact condenser seawater requirements [32] and is therefore ignored in this analysis.

Upon determining the compression ratio, the compressor inlet total pressure is determined as well as the individual partial pressures for each gas present (nitrogen, oxygen, argon, carbon dioxide and water vapor). From these partial pressures the gas mass flow rate through each compressor is computed. See Appendix F.5 for a more detailed description of the modeling approach.

4.7 SEAWATER FLOW SYSTEM

4.7.1 SELECTION

The seawater flow system for OC-OTEC applications consists primarily of a series of pipes designed to provide the necessary seawater resource (warm water and cold water intake) as well as a means to return the used seawater back to the ocean (warm water and cold water discharge). Theoretically, the design of the flow system is quite simple and well documented; however, practical limitations as to the diameter and length complicate the design. Due to the size of this designed facility, it may be necessary to incorporate a multiple pipe design in order to stay within present manufacturing limitations of approximately 2 - 4 m diameter pipes [32].

4.7.2 MODELING APPROACH

The procedure utilized in defining the seawater flow system has been designed to determine the overall head loss (pressure loss) through the entire system from seawater intake to discharge for both the warm and cold seawater systems. Several of the characteristics of the seawater flow system such as pipe length and seawater flow rate either have been assumed or determined in previous sections of this report. Pressure losses attributable to entrances, exits, pipe bends, friction and hydrostatic head are determined according to standard engineering practice and loss coefficients suggested by

[32]. An estimate as to the loss attributable to seawater density differences at pipe intake and discharge is also included. For both the warm and cold seawater flow system analyses, the seawater flow velocity is set at 2.0 m/s from which the necessary pipe diameters can be determined. The detailed calculations are presented more thoroughly in Appendix F.6.

4.8 SEAWATER PUMPS

4.8.1 SELECTION

The selection of the appropriate type of pump for a particular application requires knowledge of the design flow capacity (flow rate) and the design head (pressure loss through the flow system). With both of these values available from the previous analyses, it is only necessary to determine the optimum efficiency available for the pumping system. The maximum efficiency for various types of pumps is shown in Figure 4.10 taken from Parsons et al. [32]. The abscissa is a commonly used form of the specific speed (n_s) defined as

$$n_s = \omega Q^{1/2} / H^{3/4} \qquad (4\text{-}35)$$

where

Q = flow rate (gpm)

H = head loss (feet).

Open-cycle OTEC systems are generally characterized by a high water resource flow rate with low head loss corresponding to an n_s value of around 12,000 [32]. This value indicates that an axial flow choice of seawater pump

is most appropriate for maximizing the pump efficiency (Figure 4.10). Axial flow pumps are commercially available with efficiency ranges from 80 - 90%. However, for a 10 MW facility such as is designed in this investigation, it is necessary to use multiple pumps to handle the necessary flows with technologically available pumps.

4.8.2 MODELING APPROACH

With specific pump designs well established commercially, it was determined that this pump design would only determine the required pump power, efficiency, impeller diameter and rotational speed.

Generally, pump performance is defined using three basic dimensionless quantities: the capacity coefficient C_q, the head coefficient C_h and the power coefficient C_p [32]. These coefficients are defined as

$$C_q = Q / \omega D^3 \tag{4-36}$$

$$C_h = gH / \omega^2 D^2 \tag{4-37}$$

$$C_p = P / \rho \omega^3 D^5, \tag{4-38}$$

where

ω = rotational speed (rad/sec)

ρ = fluid density (kg/m^3)

P = power (W)

Pump efficiency is defined as

$$\eta_p = C_h C_q / C_p. \tag{4-39}$$

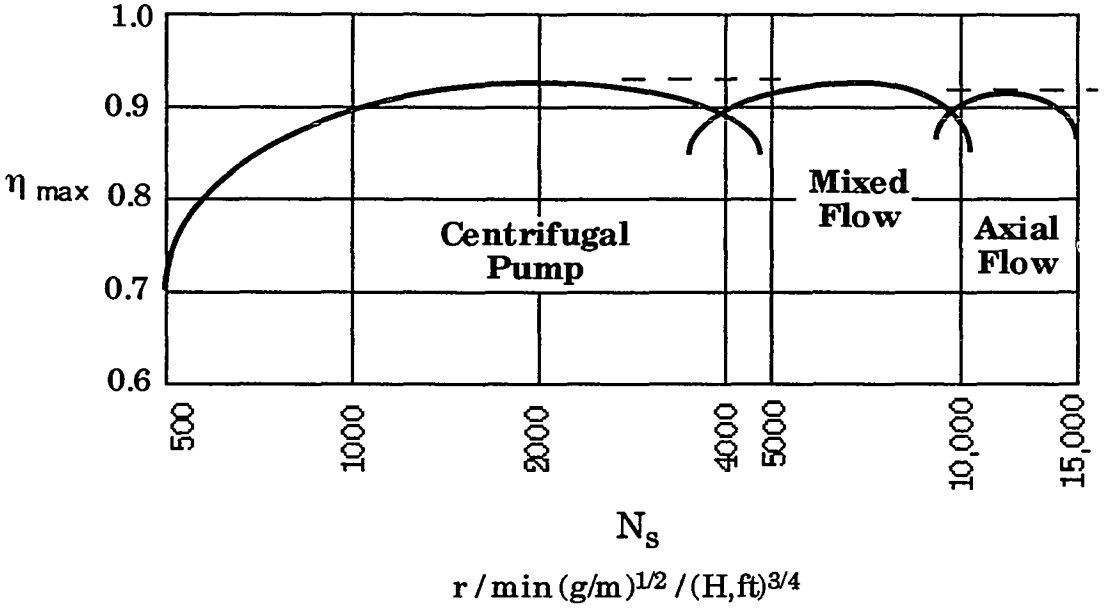

Figure 4.10: Maximum Efficiency Potential of Various Liquid Pump Designs
(Taken from [32])

For axial flow pumps, assuming that the Reynolds number and the roughness ratio have a constant effect, C_h and C_p are functions of C_q only [32]. Figure 4.11, derived from the Johnston Pump Company and developed by Parsons et al. [32], shows typical values of C_h, C_p and η_p as a function of C_q for axial flow pumps. From this figure we see that if C_q is set at 0.067, the efficiency is maximized and C_h and C_p are then defined. From the above definitions, the pump size, speed and power are determined. A more detailed analysis is presented in Appendix F.7.

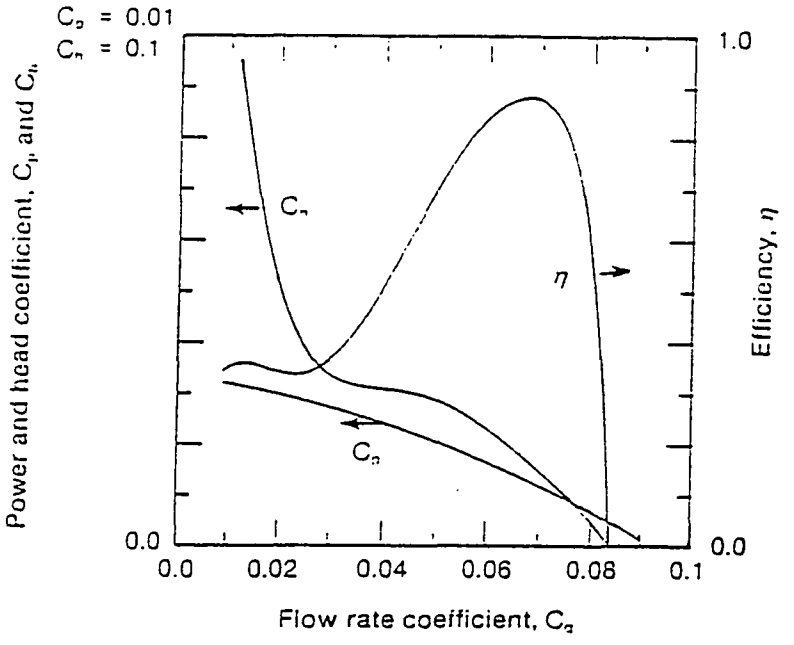

Figure 4.11: Relations Between Dimensionless Quantities for Axial Pumps
(Taken from [32]

4.9 SYSTEM SUMMARY

The following system summary has been developed to present the important design parameters determined in Appendix F for the non-predeaerated/reinjected 10 MW_{gross} OC-OTEC system. The sections are broken down into the specific system components described previously in this section. The complete procedural analyses utilized in this investigation to arrive at these values is presented and described in detail in Appendix F.

Turbine System:

Total power produced

(including noncondensable flow) = 10.027 MW

Turbine steam inlet temperature = 22.50 °C

Turbine steam outlet temperature = 12.00 °C

Number of turbines necessary for power requirements = 5

Turbine diameter = 6.16 M

Mass of steam flow entering turbine = 150.3 KG/S

Mass of steam flow exiting turbine = 146.9 KG/S

Turbine power density = 67.2 KW/M^2

Turbine Diffuser:

Turbine diffuser steam inlet temperature = 12.00 °C

Turbine diffuser steam outlet temperature = 12.47 °C

Pressure at diffuser exit = 1.44 KPa

Number of diffusers (corresponds to number of turbines) = 5

Inlet diffuser diameter = 6.17 M

Outlet diffuser diameter = 10.37 M

Diffuser length = 24.06 M

Evaporator and Mist Eliminator:

Seawater temperature entering evaporator = 27.00 °C

Seawater temperature exiting evaporator = 23.46 °C

Steam temperature from evaporator = 23.11 °C

Working pressure of evaporator = 2.83 KPa

Mole fraction of steam in evaporator = 0.9984

Number of vertical spouts necessary = 1003

Total evaporator area = 425.6 M^2

Total warm water flow necessary = 25 953 KG/S

Total noncondensable flow from evaporator = 0.40 KG/S

Direct-Contact Condenser:

Seawater temperature entering DCC = 5.00 °C

Seawater temperature exiting DCC = 10.60 °C

Working pressure of DCC = 1.43 KPa

Exit pressure of counter-current section (to vent) = 1.23 KPa

Inlet steam mass flow rate = 146.9 KG/S

Number of contactors necessary = 623

Total DCC area = 264.3 M^2

Total cold water flow necessary = 16 159 KG/S

Total noncondensable flow from DCC = 0.75 KG/S

Condenser Vent Compression Train:

Number of compressors = 5

Design compression ratio = 2.59

Design exhaust pressure = 124.0 KPa

Total parasitic power for vent compression = 878 KW

Seawater Flow System:

Warm Water Side:

Intake pipe diameter = 4.02 M

Number of design intake pipes = 1

Length of intake pipe = 500 M

Discharge pipe diameter = 4.02 M

Number of design discharge pipes = 1

Length of discharge pipe = 650 M

Total pressure loss through system = 23.43 KPa

Corresponding seawater head loss = 2.34 M

Cold Water Side:

Intake pipe diameter = 3.17 M

Number of design intake pipes = 1

Length of intake pipe = 2750 M

Discharge pipe diameter = 3.17 M

Number of discharge pipes = 1

Length of discharge pipe = 650 M

Total pressure loss through system = 43.07 KPa

Corresponding seawater head loss = 4.28 M

Seawater Pumps:

Warm Water Side:

Number of pumps = 3

Pump diameter = 1.85 M

Volumetric seawater flow per pump = 8.46 M^3/S

Total parasitic power for warm water pumps = 672 KW

Cold Water Side:

Number of pumps = 2

Pump diameter = 1.53 M

Volumetric seawater flow per pump = 7.88 M^3/S

Total parasitic power for cold water pumps = 767 KW

Total Parasitic Power to Run Plant = 2317 KW

CHAPTER 5
COMPONENT SELECTION AND MODELING APPROACH
PREDEAERATION/REINJECTION

5.1 INTRODUCTION

The following section describes the procedure utilized in this investigation for determining the component requirements and thermodynamic performances for a predeaerated 10 MW_{gross} OC-OTEC system with the noncondensables reinjected into the system's downcomer (two downcomer configurations are investigated in subsequent sections). As stated in the preceding chapter on non-predeaerated systems (Section 4.0), every effort has been made to design a system which incorporates only realistic component designs within present technological restraints.

Several of the components utilized within this predeaerated OC-OTEC design incorporating reinjection are identical to those developed for the non-predeaerated design. Those components, specifically the turbine and turbine diffuser, are designed according to design plant capacity (10 MW_{gross}) and assumed inlet and outlet steam temperatures which are the same for both designs. Those components that are not identical, in most cases, were designed using very similar procedures yet possess differing thermodynamic parameters because of the reduced noncondensable gas flows through the OC-OTEC system. Because of this similarity in design and modeling approach, several of the component sections in the following predeaerated and reinjected design are rather brief and refer to the corresponding section of the

previous chapter to prevent redundant procedural explanations. In either case, Appendices F and G provide in-depth models and calculations describing the design procedures for both the non-predeaerated and predeaerated/reinjected systems, respectively.

Figure 5.1 represents the OC-OTEC system incorporating predeaeration and reinjection designed in the following analysis. All numerical subscripts utilized in the following variables and figures correspond to the flow paths defined by the figure. Solid lines represent system paths composed primarily of liquids (seawater) while the dotted lines represent system paths composed primarily of gases (steam and noncondensables).

The following is the thermodynamic evaluation and design procedures for the predeaerated OC-OTEC system with reinjection of the desorbed noncondensable gases.

5.2 TURBINE / TURBINE DIFFUSER

5.2.1 SELECTION AND MODELING APPROACH

The thermodynamic evaluation and selection of the turbines and turbine diffusers for both the predeaerated/reinjected OC-OTEC system and the non-predeaerated OC-OTEC system produced the same turbine and turbine diffuser size and operating conditions. This is correct because the selection of an appropriate turbine system for a particular application depends on the maximum efficiency potential for the turbine type and

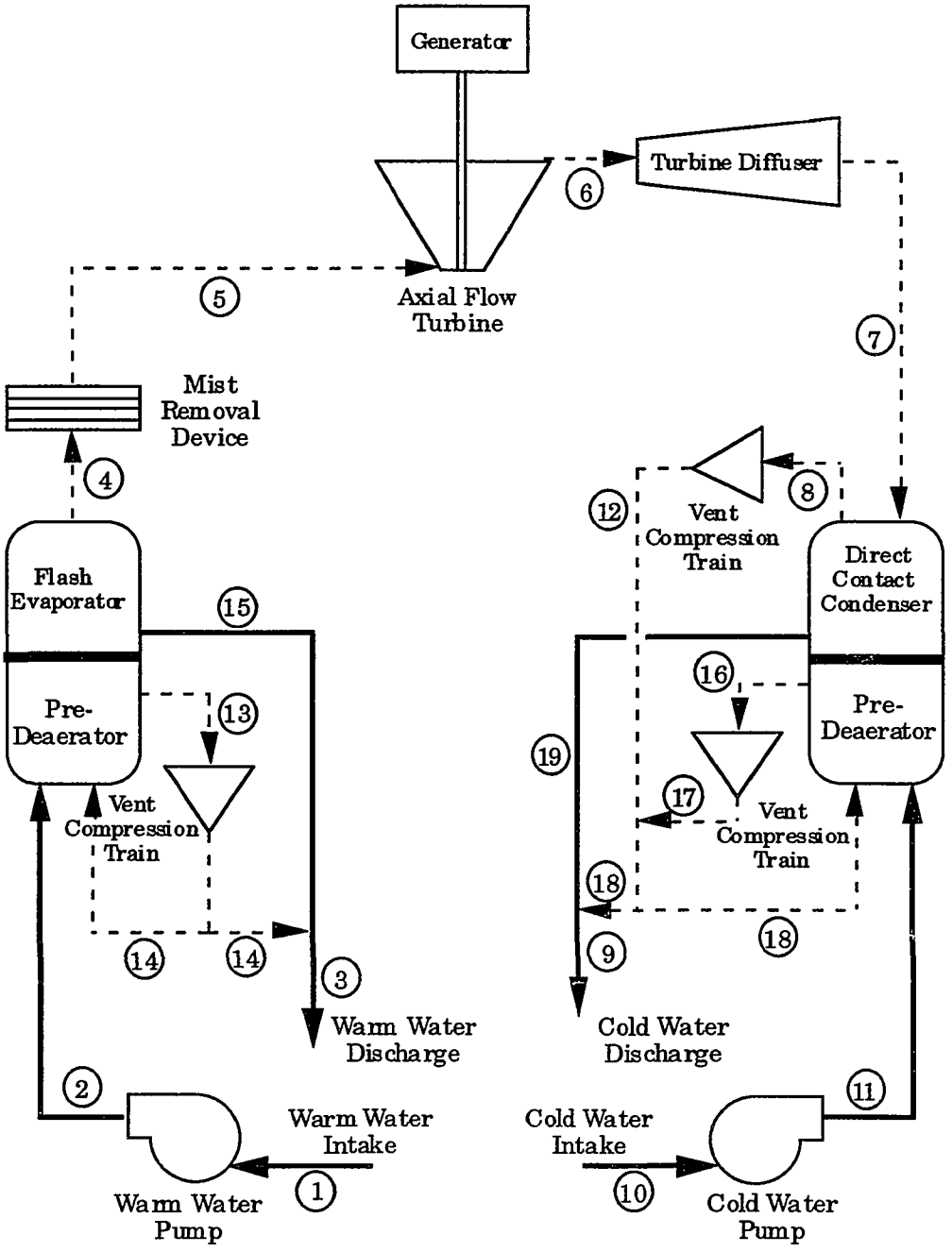

Figure 5.1: OC-OTEC System With Predearation and Reinjection

operating conditions. And, since these conditions are nearly identical for both systems (excluding a small error introduced into the non-predeaerated OC-OTEC system due to neglecting the noncondensable gases accompanying the steam through the turbine (< 0.3% error), it is correct to assume the same turbine and diffuser system is appropriate for both applications. Therefore, the turbine analysis described in Section 4.2 and the turbine diffuser analysis outlined in Section 4.3 also applies for the predeaerated/reinjected turbine system.

5.3 EVAPORATOR WITH PREDEARATION

5.3.1 SELECTION

The mist removal device and the spout evaporator selection and design procedures outlined in Section 4.4 of this report for the non-predeaerated system apply to the predeaerated design as well with some minor alterations. The specific evaporator design for the predearated warm water system utilized in this investigations was originally developed by Zapka and Krock [52]. Their evaporator/predeaerator concept has been adapted to this design and is shown in Figure 5.2. This evaporator/predeaerator concept was chosen for application in this investigation for the following reasons:

1.) Zapka [51] provides data for a predearation system utilizing bubble seeding of the inlet warm and cold water under applicable OC-

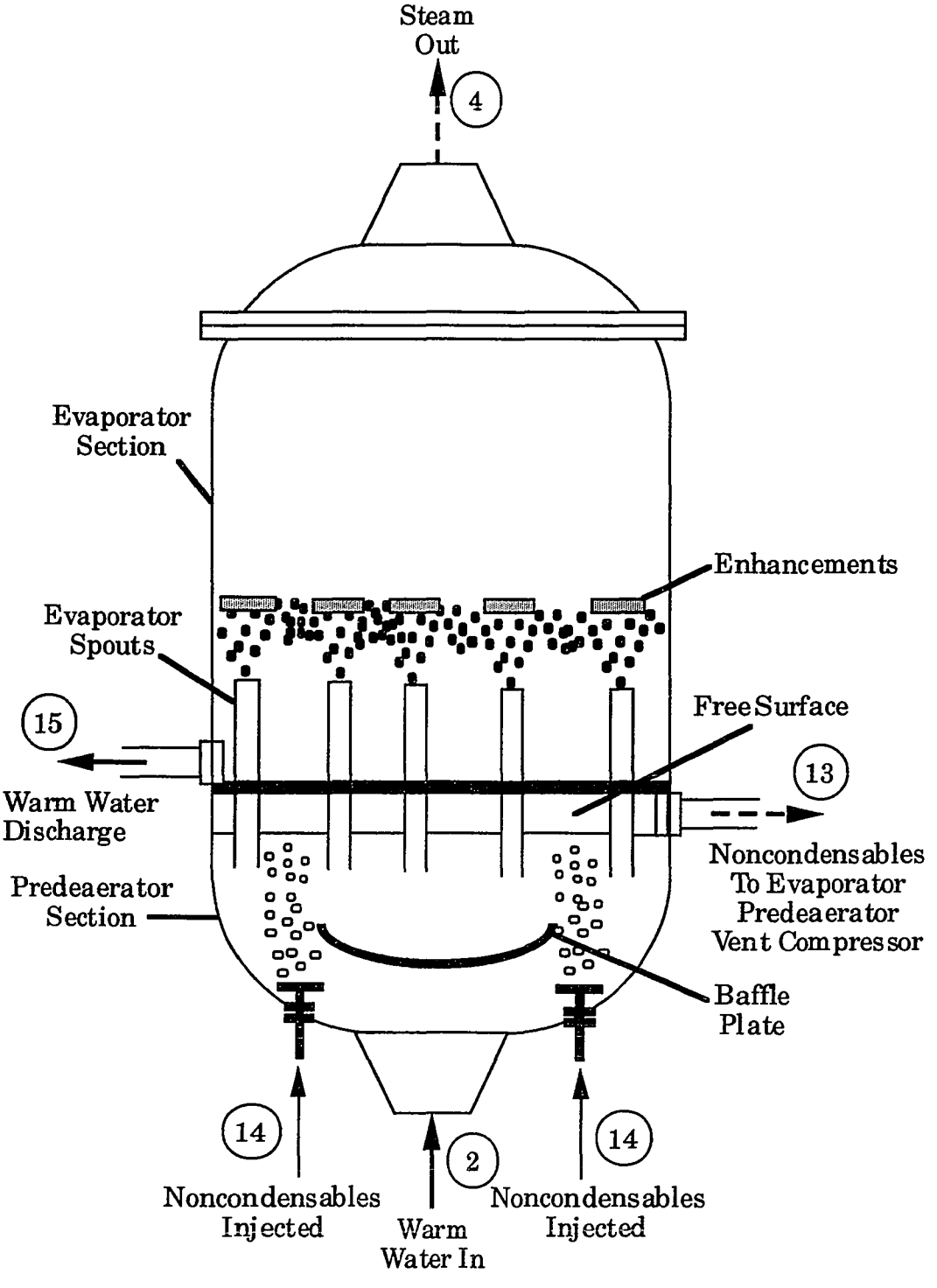

Figure 5.2: Evaporator with Predeaerator

OTEC system pressures which can be easily scaled to the desired OC-OTEC design parameters and flow rates.

2.) The spout evaporator section of the combined evaporator/ predeaerator configuration can be designed in the same manner as the spout evaporator previously designed in Section 4.4.

3.) With a spout evaporator very similar to those utilized in the desorption experiments presented earlier in this investigation and Zapka [51], desorption rates of the noncondensables within the predeaerator system and the evaporator itself should be directly applicable to this design configuration.

4.) Combining the predeaerator vacuum vessel and the evaporation vacuum vessel into one component should reduce initial capital costs which is one of the major complaints with the predeaeration concept by most OC-OTEC design engineers.

5.3.2 MODELING APPROACH

As stated earlier, the mist removal device and evaporator portion of this component were designed utilizing the same modeling procedures described previously in Section 4.4.2 of this report.

With the warm seawater flow defined from the evaporator analysis, the design of the predeaerator portion of this component can commence. Initially the predeaeration pressure ($P_{P,E}$) is set at the value utilized in Zapka [51] experiments ($P_{P,E}$ = 6.67 KPa) so that his conclusion that 85% noncondensable desorption with bubble seeding at this predeaeration

pressure could be directly applied to this analysis. From the seawater flow rate determined from this evaporator analysis ($m_{ww,2}$), the resource noncondensable composition measured by Krock [21] (values presented earlier in the experimental portion of this investigation, Section 3.0), and the predicted predeaeration noncondensable desorption percentage with bubble seeding (85%) from Zapka [51]; the total noncondensable desorption rates within the predeaerator could be determined as

$$m_{NC,P,E} = 0.85\,(M_{ww,N2}/24 + M_{ww,O2}/32 + M_{ww,Ar}/40 + M_{ww,CO2}/44\,)\; m_{ww,2} \qquad (5\text{-}1)$$

where

$M_{ww,j}$ = Mole fraction of gas j in warm water (kg-mol/kg).

The necessary noncondensable injection rate for bubble seeding within the predeaerator is then determined from Zapka's [51] data of air injection rate vs. warm seawater volume. With this noncondensable injection rate adjusted to account for the difference in pressure from atmospheric (utilized in Zapka's experiments [51]) and the injection pressure of 26.06 KPa (used in this design as an exit pressure from the evaporator predeaerator vent compression system discussed in the following section) and the composition of the injected gas identical to that being desorbed (since the design recycles the desorbed noncondensables and utilizes a portion of those as the injection gases), the total flow of noncondensables, both desorbed from the incoming seawater and injected for bubble seeding could be determined. This flow of noncondensables, joined with the water vapor determined assuming saturation at predeaeration pressures and temperatures, will be utilized in

the subsequent design of the evaporator predeaeration vent compressor analysis.

Since the desorption rate with bubble seeding in a predeaerator of 85% predicted by Zapka [51] is higher than the desorption rate found in the experimental section of this investigation for a spout evaporator with no bubble seeding (72% of nitrogen, 70% of argon, 0.6% of "total" carbon dioxide and 81% of oxygen), no further desorption of noncondensables within the evaporator would be expected. In fact, absorption of some of the leaked atmospheric gases could possibly occur. However, to maintain a conservative estimate as to the noncondensable flows within the predeaerated system, no reabsorption was calculated and the entire leaked atmospheric gases (determined in the same manner as described in Section 4.4.2) are carried over as the initial input noncondensable flow from the evaporator to the condenser analysis.

The area of the evaporator is determined in the same manner as discussed in the non-predeaerated analysis, by determining the necessary number of spouts to handle the warm water flow and an assumed area per spout suggested by Parsons et al. [32]. The determined design area of the evaporator (A_E) is then assumed to be the same as the accompanying predeaerator ($A_{P,E}$) (to simplify the design as one OC-OTEC component). The design depth of the predeaerator reservoir ($d_{P,E}$) is then determined according to Zapka's [51] suggested predeaerator seawater residence time ($RT_{P,E}$) of 25 seconds as

$$RT_{P,E} = A_{P,E}\ d_{P,E} / Q_{ww,E} \qquad (5\text{-}2)$$

where

$Q_{ww,E}$ = volume flow of warm water to evaporator.

A more detailed calculation procedure is developed and presented in Appendix G.3.

5.4 EVAPORATOR PREDEAERATION VENT COMPRESSOR

The evaporator predeaeration vent compression train (shown in Figure 5.3) is developed utilizing the same design procedures outlined in Section 4.6 for the non-predeaerated condenser vent compression train with a few minor alterations. The analysis is identical except that the design final pressure (26.06 KPa) is significantly lower than atmospheric (101.33 KPa) and therefore only two compression stages are necessary with a correspondingly low parasitic power requirement. This final pressure was decided upon by determining the minimal injection pressure required for the predeaerator bubble seeding which required an injection pressure greater than the sum of the predearator working pressure (set at 6.67 KPa by Zapka's experiments [51]) and the design predeaerator reservoir water head (approximately 1.50 meters). Otherwise, apart from the design vent pressure, the evaporator predearation vent compression train analysis is identical to the previously described procedure, and a detailed account of the calculations and values is presented in Appendix G.3.2.

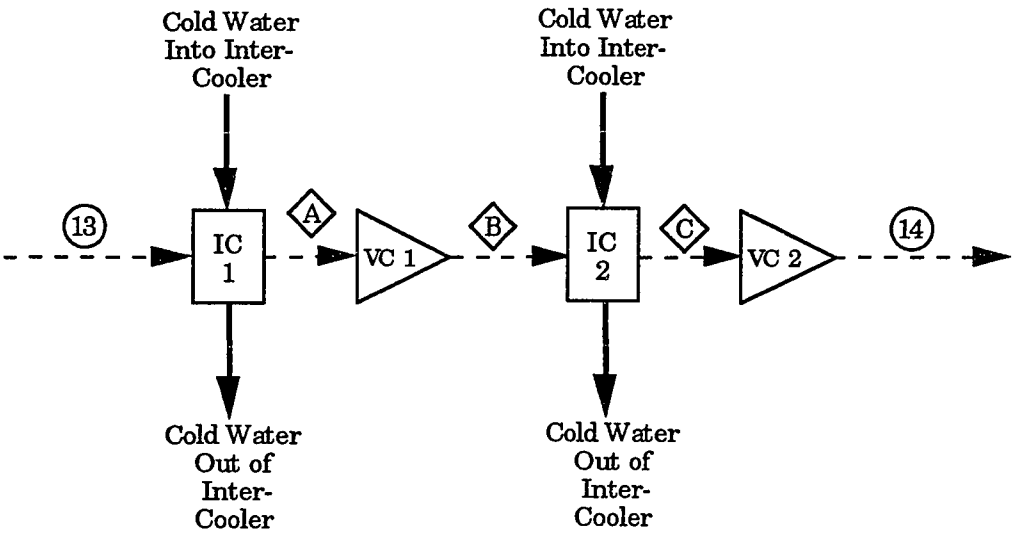

Figure 5.3: Evaporator Predeaerator Vent Compression Train for OC-OTEC With Predeaeration and Reinjection

5.5 DIRECT-CONTACT CONDENSER WITH PREDEAERATION

5.5.1 SELECTION

As in the Evaporator with Predeaeration section (Section 5.3) preceding this analysis, the direct-contact condenser is nearly the same as that developed for the non-predeaerated design, only with a cold water predeaerator section configured prior to seawater entrance into the condenser portions of the single component (see Figure 5.4). The selection of this predeaerator configuration possesses the same analytical reasons for its development as was outlined in the preceding Evaporator with Predeaeration section.

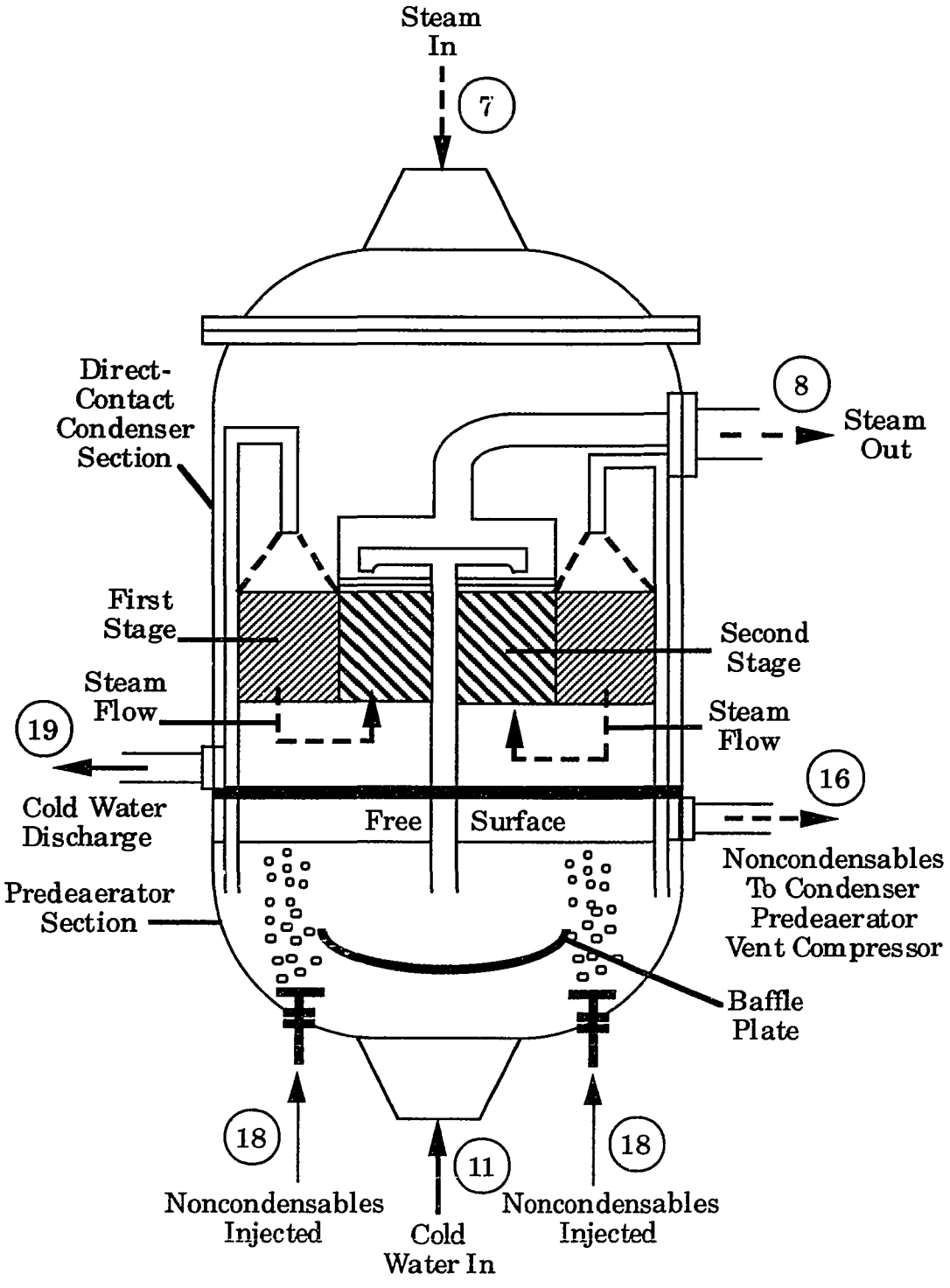

Figure 5.4: Direct-Contact Condenser with Predeaerator

5.5.2 MODELING APPROACH

The design procedures utilized for the development of the thermodynamic and design parameters necessary for the direct-contact co-current and counter-current sections of the condenser are similar to those procedures discussed in Section 4.5 for the non-predeaerated system.

Likewise, the design of the predeaeration section follows the same procedure as that outlined in Section 5.3.2 for the evaporator predeaerator system. The only significant difference between those two analyses and the modeling approach used to design the condenser/predeaerator system is that the noncondensable desorption predicted by Zapka [51] of 85% is less than the desorption values experienced in the cold water experiments reported earlier in this report (specifically, 98% for nitrogen, 90% for argon, 1.3% of the "total" carbon dioxide and 100% of the oxygen). Therefore, further noncondensable desorption was expected and accounted for (according to the procedures described for the non-predeaerated D.C.C. analysis) in the co-current and counter-current portions of the direct-contact condenser. This 5-15% (depending on the gas) extra noncondensable gas evolution was combined with the noncondensable flow from the evaporator (air leakage) and the predicted air leakage into the condenser portion, and used to develop the heat load analysis and necessary vent compression trains accordingly. The detailed analysis is presented in Appendix G.4.

5.6 CONDENSER PREDEAERATOR VENT COMPRESSOR

A schematic of the condenser predeaerator vent compression train is shown in Figure 5.5. The procedure utilized to develop the design is identical to that utilized to develop the evaporator predeaerator vent compression train as discussed in Section 5.4 preceding this analysis.

It should be noted that the first stage of the condenser predeaerator vent compression system does not possess an intercooler which would prove ineffective since the inlet vapor is already at the intercooler cooling water temperature, $T_{cw,11}$. This is the only difference in design approach with this design and those presented earlier.

A detailed description of the design procedure and calculations is presented in Appendix G.4.4.

5.7 CONDENSER VENT COMPRESSOR

The condenser vent compression train (shown in Figure 5.6) has been developed in the same manner as the evaporator predeaerator vent compression train described previously in Section 5.4. Due to the presence of uncondensed steam in the counter-current portion of the direct-contact condenser and the low system pressure (1.23 KPa), four stages for vent compression were required to bring the vapor stream pressure to a sufficient level for reinjection into the hydraulic compression region (to be discussed in the following section) of the cold water downcomer. The detailed

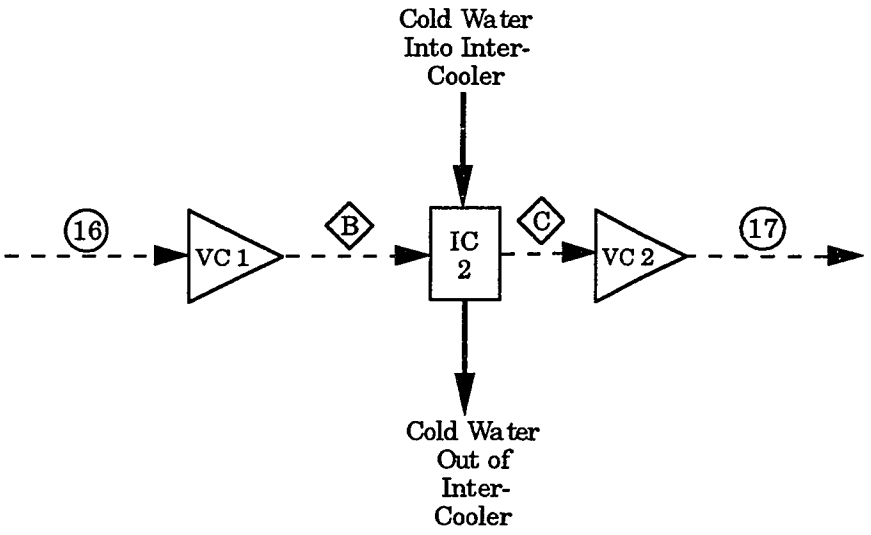

Figure 5.5: Condenser Predeaerator Vent Compression Train for OC-OTEC With Predeaeration and Reinjection

calculations performed in order to arrive at this design are presented in Appendix G.4.5.

5.8 HYDRAULIC COMPRESSORS

5.8.1 SELECTION

A hydraulic air compressor is essentially a gas compression mechanism which is driven by a vertical downward flow of water with an applied hydraulic head [13]. Downward water flow with injected gas entrains this gas as bubbles. Because of their buoyancy force in water, the bubbles tend to rise against the flow of water, but are carried downward when the viscous drag forces acting on them overcome their buoyancy. Thus, the gas

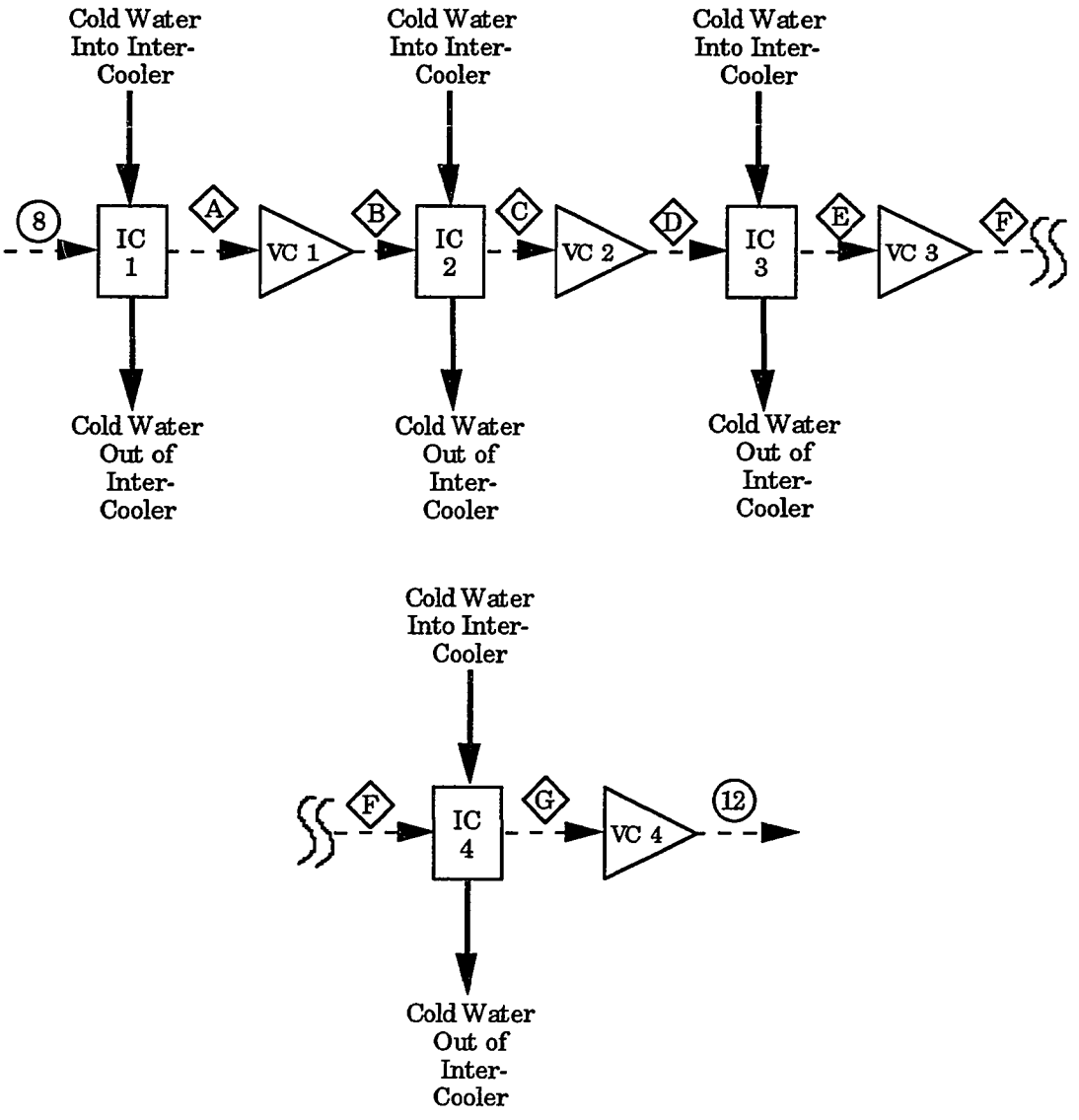

Figure 5.6: Vent Compression Train for OC-OTEC Direct Contact Condenser With Predeaeration and Reinjection

compression is achieved as the bubbles are carried downward by the water flow because the gas pressure of the bubbles is less than or equal to the hydrostatic pressure of the water at depth [13].

The need arises for an hydraulic compression system in this design because further compression of the noncondensables and uncondensed steam evolved in this predeaerated design is required. The concept of utilizing reinjection of the desorbed noncondensables into a variation of an hydraulic compressor has arisen due to the availability of a rather large water flow of low hydraulic head together with a noncondensable gas flow to be disposed of inherent in an OC-OTEC power system of this nature. The concept of hydraulic compression being utilized in an OC-OTEC system to reduce the compressor power requirements becomes even more attractive in a predeaerated system because the hydraulic compression is going to be accompanied by noncondensable reabsorption due to the concentration gradients between the bubbles and degassed seawater. This fact should even further reduce compression power requirements.

The principal reasons for choosing an hydraulic compression configuration for this OC-OTEC design are outlined by Golshani and Chen [13] as:

1.) An hydraulic air compressor is a simple machine and cost savings will be realized if a mechanical compressor is replaced by an hydraulic air compressor.
2.) An hydraulic air compressor is environmentally more acceptable for OTEC applications because it may improve the effluent water

quality by redissolving the noncondensable gases into the water during the compression process.

3.) The conversion of part of the kinetic energy contained in the warm and cold seawater effluent flow (which is otherwise wasted in previous designs) into air compression and the capability of direct-contact condensing of steam in the noncondensable gas stream make the hydraulic air compressor a promising device for OC-OTEC applications.

For the purposes of this investigation, two varying hydraulic compression designs for the warm and cold water applications are investigated. One option utilizes the existing downcomer pipe as the compression mechanism (with varying seawater velocity due to the changing noncondensable void fraction in the liquid stream) (Figure 5.7) and the other uses a tapering pipe system (Figure 5.8) (in order to maintain a constant seawater flow).

5.8.2 MODELING APPROACH

The following procedures outlined for the design of the hydraulic compressors utilized in this investigation apply to both the warm water compressor as well as the cold water compressor. Of course, the values obtained will be different for each compressor system; however, the precedure and equations will be the same.

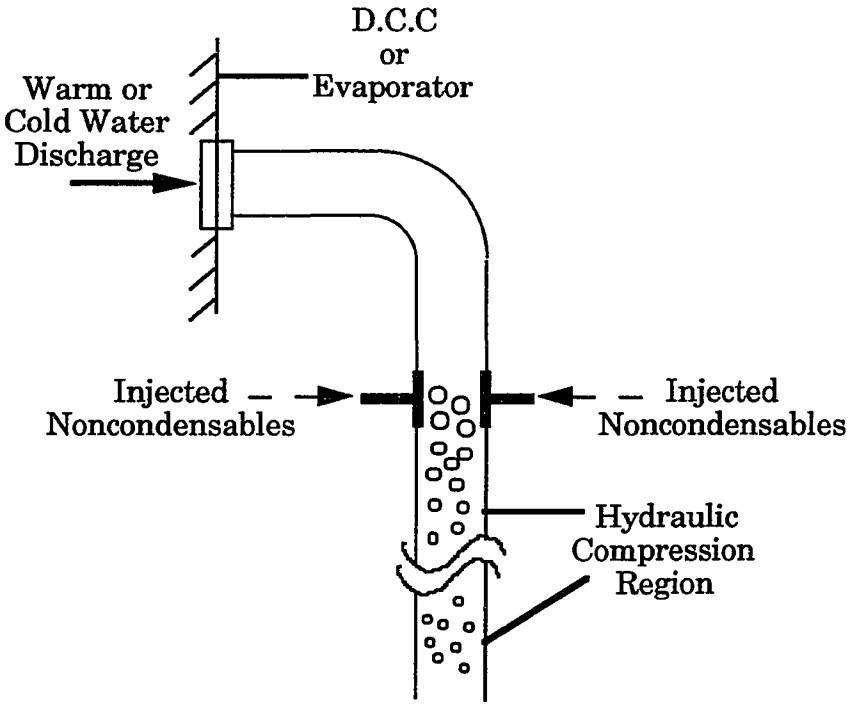

Figure 5.7: Standard Downcomer Pipe - Hydraulic Compressor

The primary concerns for the hydraulic compressor design is to obtain a good approximation of the necessary water head required for the compression portion of the discharge water systems, which can be translated into parasitic pumping power in the flow system analysis. Other important parameters determined in the hydraulic compressor design include the length of compressor required to reduce the gas void fraction below 0.5% (at which point gas volume no longer significantly interferes with liquid flow), the initial diameter for the tapering pipe analysis and the appropriate point of gas injection.

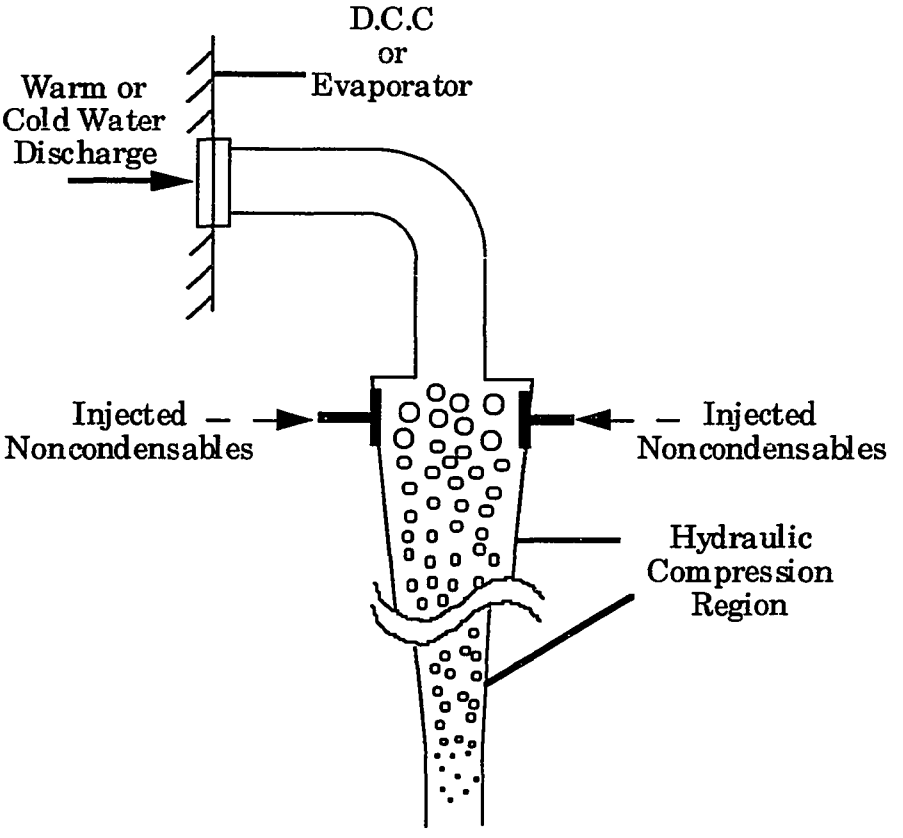

Figure 5.8: Tapering Pipe Downcomer - Hydraulic Compressor

The specific means of gas injection is beyond the scope of this investigation and is neglected in this analysis. In order to optimize the hydraulic compressor efficiency, the most appropriate injection configuration should be investigated experimentally in working OC-OTEC components.

5.8.2.1 HYDRAULIC COMPRESSION USING STANDARD DISCHARGE PIPE

To dispose of the noncondensable gases desorbed in a predeaerator (warm water hydraulic compressor) or from a condenser and predeaerator (cold water hydraulic compressor), the gas pressure at the gas injection point has to be equal to or greater than the local water pressure so that the gas can be discharged into the water stream. Therefore, the desired injection point into the seawater discharge pipe (and this holds for the tapering pipe hydraulic compressor as well) is determined by adding the system pressure at the discharge pipe entrance (2.82 KPa for warm water compressor and 1.73 KPa for the cold water compressor) and the required seawater head to be arbitrarily set at 0.5 KPa less than the respective vent compressor outlet pressures determined in earlier sections of the report (2.26 m for warm water and 2.30 m for cold water) (see Appendix G.3.3.1 and G.4.6.1, respectively, for more details).

With the point of injection determined, the design of the hydraulic compression region of the effluent water downcomer can be initiated. At the injection point the noncondensable gas (molar composition defined in the respective vent compression analyses outlined earlier) assumes the same pressure and temperature as the seawater in the pipe at the point of injection. From this information the volumetric flow of noncondensables in the known seawater flow can be defined. Since the desired length of the hydraulic compression region is unknown, an iterative process is employed to determine the principal compressor length. In essence, the entire discharge

flow system will act as an hydraulic compressor. But, for determining the hydraulic head required to overcome the vapor flow injected into the effluent stream, only an analysis over the section of significant noncondensable void fraction in the flow stream is required. Therefore, for the first iteration, no gas reabsorption is assumed and the hydraulic compressor length is estimated by first determining the change in pressure with hydraulic compressor length (dP/dh) as

$$dP/dh = \rho_{sw} G \qquad (5\text{-}3)$$

where

ρ_{sw} = density of seawater

G = gravitation constant

Upon assuming that at the "end" of the compression region the seawater velocity will resume its original design rate prior to injection (2.00 m/s plus an acceptable level of error), the volume flow of noncondensable gases can be determined as well as the pressure at this point in the system (P_{end}). From those values an initial estimated value of the hydraulic compressor length (h_{comp}) is determined as

$$h_{comp} = (P_{end} - P_{inj}) / (dP/dh). \qquad (5\text{-}4)$$

This hydraulic compressor length is then numerically integrated over its entire length in order to determine the complete water head required to overcome the pressure of the injected gases in the effluent stream. This water head is defined as the change in free water surface at the discharge pipe entrance caused by the change in void fraction within the pipe when the

noncondensables are injected into the water stream. The vertical difference in the free water surface with and without gas injection is the applied water head required to achieve the desired air compression [13]. This applied head is directly related in this analysis to the change in flow velocity over the length of the hydraulic compressor length as

$$H_{loss} = \sum (\Delta x_{sw})^2 / 2\,g \qquad (5\text{-}5)$$

where

H_{loss} = total hydraulic head required

Δx_{sw} = difference in seawater velocity over hydraulic compressor increment from expected velocity of 2.00 m/s without gas injection.

This procedure requires estimating the noncondensable reabsorption rate in the effluent stream at system temperatures and pressures. In order to perform this approximation the data presented in Zapka [51] for deaeration of noncondensables (overall mass transfer coefficients, K_l*a) at various system pressure gradients and noncondensable injection rates is shown in Figure 5.9. This data was developed from the following absorption equation which in Zapka's case [51] was utilized to determine the desorption rates for the noncondensables:

$$\ln \{(C_o - C_s)/(C_L - C_s)\} = K_l{*}a * t \qquad (5\text{-}6)$$

where

C_o = initial concentration of gas in liquid

C_L = liquid concentration of gas

C_s = saturation concentration of gas

K_l*a = overall mass transfer coefficient (1/S)

t = time (S).

Continuing with the assumptions utilized in Zapka's analyses [51] that the K_l*a values obtained using this equation apply to both absorption and desorption of the noncondensables, then it is appropriate to assume that Zapka's determined K_l*a values shown in Figure 5.9 would apply to the reabsorption of the reinjected noncondensables under similar system conditions (ie. temperature, pressure, injection rate etc.).

Thus, upon comparing the ratio of noncondensable molar injection rate versus seawater molar flow for both the warm and cold water hydraulic compressors (1.6×10^{-5} and 1.0×10^{-5}, respectively) to Zapka's ratio of experimental molar injection rates to seawater molar volume (1.8×10^{-5} and 2.5×10^{-5} for the injection rates of 95 and 142.5 cm^3/min, respectively), it was determined that the ratios for both the warm and cold water hydraulic compressors most nearly approximated Zapka's experimental injection rate of 95 cm^3/min (for first approximation). Therefore, the K_l*a values corresponding to this injection rate have been used to develop the overall mass transfer coefficient (K_l*a) versus pressure differential diagram shown in Figure 5.10.

Unfortunately, Zapka's data only possessed two points of differing pressure gradients vs. K_l*a. Therefore, the estimates of gas reabsortion will only be good as a first approximation estimate for this analysis. The two points provided by Zapka [51] and the knowledge that a zero pressure gradient would lead to a K_l*a value of nearly zero (with no pressure gradient

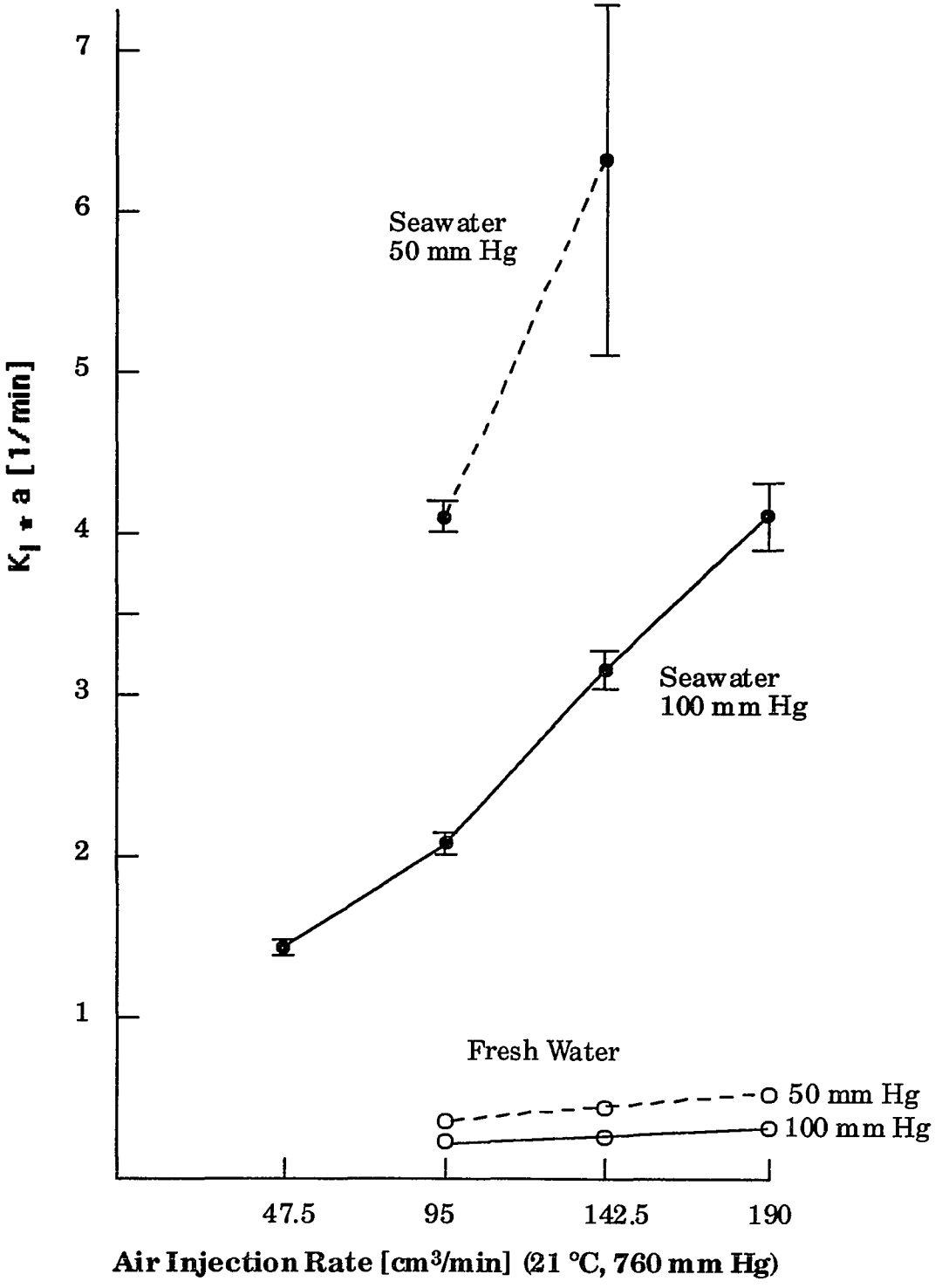

Figure 5.9: Overall Transfer Coefficient K_l* a for Fresh Water and Seawater Deaeration
(Taken from [51])

only molecular diffusion would apply) allows for two separate linear equations to be utilized as a means of approximating a K_l*a value for a given pressure gradient in the hydraulic compressor region (the compressor pressure gradient in this analysis corresponds to the local hydrostatic pressure at the specific hydraulic compressor incremental length versus the discharge pipe entrance pressure). From Figure 5.10 we obtain the following K_l*a approximations:

$$K_l*a = 0.00039\,(\Delta P) \text{ for } P_{local} < 90 \text{ KPa} \qquad (5\text{-}7)$$

$$K_l*a = 0.0053\,(\Delta P) - 0.43 \text{ for } P_{local} \geq 90 \text{ KPa} \qquad (5\text{-}8)$$

where

ΔP = $P_{local} - P_o$

P_o = pipe entrance pressure

P_{local} = local hydrostatic pressure

With the knowledge of gas reabsorption rates available, incremental estimates as to the gas void fraction in liquid flow is attainable and thus the incremental velocity difference (Δx_{sw}) accompanying the reduction in noncondensables can be determined. A new hydraulic compressor is then estimated by choosing the length corresponding to a final seawater velocity of approximately 2.00 m/s. This entire procedure is then repeated until the final liquid velocity calculated corresonds to ± 0.5% of the desired 2.00 m/s value. At this point the design hydraulic compressor length is defined as well as the total hydraulic head required to perform the necessary compression. See Appendix G.4.6.1 for a more detailed procedural explanation.

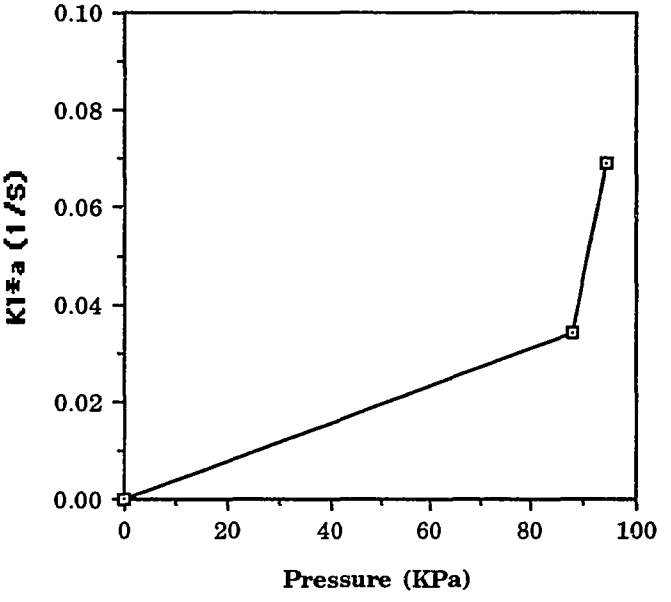

Figure 5.10: Kl*a vs. Pressure Driving Force in Seawater (derived from data presented [51])

5.8.2.2 TAPERING HYDRAULIC COMPRESSOR ANALYSIS

As stated in the previous section, the point of injection for the noncondensables in this design is performed in the same manner as well as the initial estimate of hydraulic compressor length. Likewise, this analysis requires numerical integration along the tapering hydraulic compressor region to determine the total water head requirements as well as the design length.

The purpose of investigating a tapering pipe hydraulic compressor configuration is that it should require less hydrostatic head to perform the

necessary compression since the only losses associated with the analysis are frictional losses associated with the boundaries of the pipe with a constant seawater flow velocity of 2.00 m/s for this design.

At the point of injection, and along the entire converging hydraulic compressor region for that matter, the necessary pipe area to maintain this desired flow velocity is defined as

$$A_{p,i} = A_{p,i-1} + [Q_g / (Q_g + Q_{sw})] A_{p,i-1} \qquad (5\text{-}9)$$

where

$A_{p,i}$ = area of pipe at hydraulic compressor increment

$A_{p,i-1}$ = area of pipe at previous hydraulic compressor increment

Q_g = volumetric flow of gas

Q_{sw} = volumetric flow of seawater.

As in the previous hydraulic compressor analysis, Zapka's $K_l * a$ estimates are utilized to approximate the noncondensable reabsorption rate which directly affects the Q_g value.

The hydraulic compressor length is readjusted to the length corresponding to a final pipe area approximating the initial discharge pipe area associated with no gas injection. This procedure is repeated until the final pipe area is ± 0.5% of the initial discharge pipe area.

The total pressure loss associated with this form of hydraulic compressor is determined according to standard engineering practice with calculated friction factors determined for each incremental pipe length and converted to incremental pressure losses for each section of the compressor.

The total pressure loss corresponds to the summation of these incremental pressure losses. See Appendix G.4.6.2 for a more complete development.

5.9 SEAWATER FLOW SYSTEMS AND SEAWATER PUMPS

The seawater flow system and seawater pump design procedures followed in this section are very similar to the ones outlined and performed in Sections 4.7 and 4.8 in the previous chapter. The only variations included additional analysis and water head requirements necessary to account for the additional expansion losses for both the warm and cold water predeaerators incorporated in this design as well as the necessary water head requirements to overcome the hydraulic compression mechanisms developed in the previous section (Section 5.8). Otherwise, the seawater flow system and seawater pump analysis is the same as that performed for the non-predeaerated system. A complete detailed calculation procedure and design is developed in Appendices G.5 and G.6.

5.10 SYSTEM SUMMARY

The following system summary has been developed to present the important design parameters determined in Appendix G for the predeaerated/reinjected 10 MW_{gross} OC-OTEC system. The sections are broken down into the specific system components described previously in this section. The complete procedural analyses utilized in this investigation to arrive at these values is presented and described in detail in Appendix G.

Turbine System:

Total power produced (including noncondensable flow) = 10.003 MW

Turbine steam inlet temperature = 22.50 °C

Turbine steam outlet temperature = 12.00 °C

Number of turbines necessary for power requirements = 5

Turbine diameter = 6.16 M

Mass of steam flow entering turbine = 150.3 KG/S

Mass of steam flow exiting turbine = 146.9 KG/S

Turbine power density = 67.2 KW/M^2

Turbine Diffuser:

Turbine diffuser steam inlet temperature = 12.00 °C

Turbine diffuser steam outlet temperature = 12.47 °C

Pressure at diffuser exit = 1.44 KPa

Number of diffusers (corresponds to number of turbines) = 5

Inlet diffuser diameter = 6.17 M

Outlet diffuser diameter = 10.37 M

Diffuser length = 24.06 M

Evaporator and Mist Eliminator:

Seawater temperature entering evaporator = 27.00 °C

Seawater temperature exiting evaporator = 23.46 °C

Steam temperature from evaporator = 23.11 °C

Working pressure of evaporator = 2.82 KPa

Mole fraction of steam in evaporator = 0.9998

Number of vertical spouts necessary = 1003

Total evaporator area = 425.6 M^2

Total warm water flow necessary = 25 953 KG/S

Total noncondensable flow from evaporator = 0.051 KG/S

Evaporator Predeaerator:

Predeaerator pressure = 6.67 KPa

Total flow of noncondensables in predeaerator = 0.91 KG/S

Injection rate for bubble seeding = 0.52 KG/S

Water depth of predeaerator = 1.50 M

Residence time of seawater in predeaerator = 25.1 S

Evaporator Predeaerator Vent Compression Train:

Number of compressors = 2

Design compression ratio = 2.00

Design exhaust pressure = 26.06 KPa

Total parasitic power for vent compression = 169 KW

Evaporator Hydraulic Compressor:

Standard Pipe:

Point of injection (from evaporator discharge) = 2.26 M

Hydraulic Compressor length = 12.57 M

Seawater velocity at injection point = 2.11 M/S

Tapering Pipe:

Width of pipe at injection point = 4.12 M

Direct-Contact Condenser:

Seawater temperature entering DCC = 5.00 °C

Seawater temperature exiting DCC = 10.84 °C

Working pressure of DCC = 1.43 KPa

Exit pressure of counter-current section (to vent) = 1.23 KPa

Inlet steam mass flow rate = 146.9 KG/S

Number of contactors necessary = 599

Total DCC area = 254.2 M^2

Total cold water flow necessary = 15 566 KG/S

Total noncondensable flow from DCC = 0.13 KG/S

Condenser Predeaerator:

Predeaerator pressure = 6.67 KPa

Total flow of noncondensables in predeaerator = 0.56 KG/S

Injection rate for bubble seeding = 0.31 KG/S

Water depth of predeaerator = 1.50 M

Residence time of seawater in predeaerator = 25.2 S

Condenser Predeaerator Vent Compression Train:

Number of compressors = 2

Design compression ratio = 1.96

Design exhaust pressure = 25.00 KPa

Total parasitic power for vent compression = 103 KW

Condenser Hydraulic Compressor:

Standard Pipe:

Point of injection (from evaporator discharge) = 2.30 M

Hydraulic Compressor length = 11.30 M

Seawater velocity at injection point = 2.17 M/S

Tapering Pipe:

Width of pipe at injection point = 3.23 M

Condenser Vent Compression Train:

Number of compressors = 4

Design compression ratio = 2.33

Design exhaust pressure = 30.73 KPa

Total parasitic power for vent compression = 133 KW

Seawater Flow System:

Warm Water Side:

Intake pipe diameter = 4.02 M

Number of design intake pipes = 1

Length of intake pipe = 500 M

Discharge pipe diameter = 4.02 M

Number of design discharge pipes = 1

Length of discharge pipe = 650 M

Standard Pipe Hydraulic Compressor:

Total pressure loss through system = 25.69 KPa

Corresponding seawater head loss = 2.56 M

Tapering Pipe Hydraulic Compressor:

Total pressure loss through system = 25.41 KPa

Corresponding seawater head loss = 2.54 M

Cold Water Side:

Intake pipe diameter = 3.11 M

Number of design intake pipes = 1

Length of intake pipe = 2750 M

Discharge pipe diameter = 3.11 M

Number of discharge pipes = 1

Length of discharge pipe = 650 M

Standard Pipe Hydraulic Compressor:

Total pressure loss through system = 46.15 KPa

Corresponding seawater head loss = 4.59 M

Tapering Pipe Hydraulic Compressor:

Total pressure loss through system = 45.54 KPa

Corresponding seawater head loss = 4.53 M

Seawater Pumps:

Warm Water Side (Standard Pipe Hydraulic Compressor):

Number of pumps = 3

Pump diameter = 1.80 M

Volumetric seawater flow per pump = 8.46 M^3/S

Total parasitic power for warm water pumps = 737 KW

Warm Water Side (Tapering Pipe Hydraulic Compressor):

Number of pumps = 3

Pump diameter = 1.81 M

Volumetric seawater flow per pump = 8.46 M^3/S

Total parasitic power for warm water pumps = 729 KW

Cold Water Side (Standard Pipe Hydraulic Compressor):

Number of pumps = 2

Pump diameter = 1.48 M

Volumetric seawater flow per pump = 7.60 M^3/S

Total parasitic power for cold water pumps = 792 KW

Cold Water Side (Tapering Pipe Hydraulic Compressor):

Number of pumps = 2

Pump diameter = 1.48 M

Volumetric seawater flow per pump = 7.60 M^3/S

Total parasitic power for cold water pumps = 781 KW

Standard Pipe Hydraulic Compressor:

Total Parasitic Power to Run Plant = 1922 KW

Tapering Pipe Hydraulic Compressor:

Total Parasitic Power to Run Plant = 1918 KW

CHAPTER 6
CONCLUSIONS AND RECOMMENDATIONS

From the data collected from the HMTSTA in this investigation and the analysis procedure described in the previous sections of this report, the following conclusions have been drawn:

1) Under prototypical non-predeaerated OC-OTEC conditions, the warm water stream can be expected to outgas approximately 72% (0.31 mmol/l) of the available nitrogen, 70% (0.0073 mmol/l) of the available argon, 0.6% (0.011 mmol/l) of the total carbon dioxide (138% of the available "free" carbon dioxide), and 81% (0.183 mmol/l) of the available dissolved oxygen within the evaporator.

2) The cold water stream can be expected to outgas approximately 98% (0.56 mmol/l) of the available dissolved nitrogen, 90% (0.0139 mmol/l) of the available argon, 1.3% (0.030 mmol/l) of the total carbon dioxide (56% of the available "free" carbon dioxide), and 100% (0.055 mmol/l) of the available dissolved oxygen under prototypical non-predeaerated OC-OTEC coaxial direct-contact condenser configurations.

3) The measuring techniques utilized in this investigation were very accurate and precise, as displayed by the relatively tight grouping of the nitrogen and argon data and its consistent predictions of nitrogen and argon compositions in the air injection data. The error experienced in the outgassing rates is primarily attributed to the inherent variability of the ocean water background compositions for each of the gases, which was used in each case as

the basis of comparison for outgassing percentages. This is particularly true of the biologically and chemically active gases (oxygen and carbon dioxide). In addition, some of the observed variability is due to the somewhat less than steady state operating conditions of the HMTSTA. This includes variations in pump rates due to in-ocean pressure changes, changes in leak rates and different residuals from pre-test conditions.

4) The level of carbon dioxide outgassing projects a CO_2 emission rate of approximately 21.7 g CO_2/KWh for warm and cold water feed stream rates estimated by SERI for a prototype 1 MW OC-OTEC power plant. This value is an order of magnitude lower than the average emission rates of conventional fossil fueled power plants. Thus, the implementation of an OC-OTEC power plant could significantly reduce the release of carbon dioxide if it were to replace existing fossil fueled plants, even if these gases were directly vented to the atmosphere.

5) The leak estimates performed in this investigation suggest that as much as 22% of the gas samples analyzed by the RGA were contaminated with atmospheric air leaking in through the mass spectrometer sampling system. This leak should be consistent throughout the experimental data acquisition period since test conditions (ie. working pressures, etc.) were very consistent throughout. Since precise quantification of HMTSTA inleakage rates were not able to be achieved during this investigation, estimates made by SERI and PICHTR investigators on static leaks of the HMTSTA should be considered the best estimates for these values.

6) The fraction of the gases released appears to be independent of the level of feed stream flow rates. At first analysis, this seems to be contrary to

chemical engineering mass-transfer logic, however, this phenomena can be explained.

First of all, as the level of feed stream outgassing approaches 100%, the linearity of the zero flow curves (fraction of gas release independent of liquid flow rates) becomes more appropriate. Therefore, since degassing of the cold water stream is nearly 100% for all the gases, only the warm water data must be questioned. However, a projection of 70-80% outgassing for the warm water would suggest nearly linear flow curves as well. It is also very likely that some artificial bubble injection is occurring in the barometric upcomer of the evaporator creating a surplus of nucleation sites which increases the availability of naturally occurring mass transfer surface areas (these excess bubbles could be the results of leaks into the barometric upcomer or through cavitation at the pumps). This excess of available gas exchange surfaces could provide the necessary surface area for the levels of degassification experienced in the experiment. If in fact 70-80% outgassing of the warm water stream is the maximum level attainable at the working pressures of the evaporator (these levels are not at all contradictory with predeaeration measurements conducted previously by Zapka [51] using bubble seeding of the feed streams) then observing a constant fraction of gas released over a range of flow rates would not be inconsistent with chemical engineering mass transfer logic.

Also, the majority of mass transfer of the noncondensables on the warm water side occurs within the evaporator itself at the point where the continuous phase changes from liquid to gas (that is, during the "explosion" of the water from the spouts into the vacuum space above the liquid continuum). Most of the mass transfer of the noncondensables occurs at this point due to

the explosive nature of the process and the very high surface area created by the change in continuous phase.

If this is indeed the case as far as mass transfer is concerned, then the extent of mass transfer would be dependent on the amount of time the water droplets spent in the gaseous continuum in the evaporator above the liquid reservoir (which would be essentially the same for all flow rates, if not more for the higher feed stream flow rates). Therefore, the data appearing to be independent of the warm and cold water feed stream flow rates is in fact what one could expect under the experimental conditions experienced in this investigation.

7) The level of noncondensable outgassing experienced in this investigation is significantly larger than the levels predicted by earlier experimenters [11] [12] which utilized fresh water as the working fluid. However, these results are not inconsistent with previous research performed by the author [30] and Zapka [51] who utilized both fresh water and natural seawater in their gas exchange experiments. Therefore, a brief explanation incorporating Oney's [30] and Zapka's [51] previous results should help clarify the potential reasons for the differences in fresh water and seawater noncondensable evolution rates.

Molecular diffusion is the primary means of noncondensable mass transfer within the gas exchange regions of the OC-OTEC facility. With this being the case a comparison of fresh water and seawater diffusion coefficients for the noncondensable gases involved in the OC-OTEC process should provide a means of understanding the results obtained when comparing previous experiments with those reported in this investigation. Specifically, the

question of how the diffusion coefficients in seawater of the noncondensables representative of OC-OTEC consideration compare to those in fresh water needs to be addressed.

To answer this question and make a direct comparison of diffusion coefficient values, Oney [30] performed molecular diffusion experiments in both natural seawater and fresh water measuring the diffusion rates of nitrogen and oxygen via gas chromatography. The results showed that molecular diffusion of nitrogen and oxygen in seawater ($D_{sw,N2}$ = 2.68 x 10^{-5} cm^2/sec and $D_{sw,O2}$ = 3.90 x 10^{-5} cm^2/sec) is approximately 10 - 15% more substantial than in fresh water ($D_{fw,N2}$ = 2.49 x 10^{-5} cm^2/sec and $D_{fw,O2}$ = 3.60 x 10^{-5} cm^2/sec). These results substantiate the trend observed in this investigation of higher gas evolution in OC-OTEC components under seawater usage versus the fresh water experiments. However, they only suggest a 10 - 15% increase in noncondensable desorption while this investigation suggests a 70 - 100% increase over the fresh water experiments previously reported [11] [12] which concluded that only 50% of the noncondensables would be expected to be released in an OC-OTEC vacuum system. This result suggests that another factor is contributing to enhancing the noncondensable desorption rate in seawater over fresh water. With molecular diffusion acting as the primary means of mass transfer for the noncondensables from the liquid phase to the vapor phase above the liquid, active surface area for the mass transfer becomes as important a consideration as the actual diffusion coefficients.

Zapka [51] performed noncondensable bubble experiments using both seawater and fresh water on model OC-OTEC components in an attempt to observe the differences in bubble behavior on a macro scale. Zapka's results

[51] show that bubble coalescence in fresh water is much more substantial than that of noncondensable bubbles in natural seawater. He found that, essentially, bubble coalescence in seawater is non-existent. This phenomena suggests that in the absence of bubble coalescence in the upcomers of the OC-OTEC components, the active surface area available for noncondensable diffusion out of the liquid phase should be significantly higher for seawater then fresh water. Thus, Zapka's results [51] further substantiate those of this investigation that noncondensable outgassing from seawater should be significantly higher than those experienced in the earlier experiments utilizing fresh water as the working fluid [11] [12].

In essence, it is probably a combination of these two factors, enhanced molecular diffusion rates and the lack of noncondensable bubble coalescence in seawater, which has contributed to the significant difference in levels of noncondensable outgassing reported in this investigation versus the values predicted by previous research which utilized fresh water as the working fluid.

8) From the thermodynamic analysis performed in Section 4.0 of this investigation, a 10 MW_{gross} non-predeaerated OC-OTEC plant can be expected to provide an additional 27 KW due to the noncondensable flow accompanying the evolved steam through the turbine from the evaporator. Likewise, a non-predeaerated system of this size can be expected to lose approximately 878 KW due to vent compression of noncondensables to the atmosphere and 1439 KW to pumping the warm and cold water resource. These values translate into a total parasitic power loss of approximately 2317 KW; approximately 23.1% of the total power produced is consumed by parasitic losses.

9) From the thermodynamic analysis performed in Section 5.0 of this investigation, a 10 MW_{gross} predeaerated/reinjected OC-OTEC plant can be expected to provide an additional 3 KW due to the noncondensables leaking into the system through the evaporator and accompanying the evolved steam through the turbine configuration. A predeaerated/reinjected system of this size utilizing a standard discharge pipe as the hydraulic compression mechanism can be expected to lose approximately 405 KW due to vent compression of the noncondensables into the system's downcomer and approximately 1529 KW to pumping the warm and cold water resource. These values translate into a total parasitic power loss of approximately 1934 KW; approximately 19.3% of the total power produced is consumed in parasitic losses utilizing a standard discharge pipe as the hydraulic compression mechanism.

A predeaerated/reinjected system of this magnitude utilizing a tapering discharge pipe as the hydraulic compression mechanism can be expected to lose approximately 405 KW due to vent compression of the noncondensables into the system's downcomer and approximately 1510 KW to pumping the warm and cold seawater resource. These values translate into a total parasitic power loss of approximately 1915 KW; approximately 19.2% of the total power produced is consumed in parasitic losses when a tapering pipe system is utilized as the hydraulic compression mechanism.

10) The utilization of predeaeration and reinjection of the noncondensables can translate into a savings of nearly 54% in vent compression parasitic power losses with an increase in total pumping power of approximately 6% for a standard pipe hydraulic compression system and 5%

for a tapering pipe hydraulic compression system. These results translate into a savings of 3.8% and 3.9% of total power production, respectively, for a predeaerated/reinjected 10 MW_{gross} OC-OTEC system.

Considering the results and conclusions presented in the previous text, the following recommendations have been developed:

1) The level of outgassing experienced in both the warm and cold water streams proves significant enough to warrant serious consideration of a predeaeration system being implemented within the OC-OTEC system design. The presence of a predeaeration system could greatly reduce the amount of noncondensable build-up in the direct contact condenser, as well as significantly reduce the pumping requirements of the compressor system presently used in OC-OTEC designs for handling the DCC noncondensables.

2) The level of oxygen and carbon dioxide outgassing predicted by the data presented in this report suggests the need for reinjection of the desorbed noncondensables in order to avoid the discharge of oxygen deficient effluent water back into the ocean environment. This reinjection consideration would also completely eliminate any more need for discussion of carbon dioxide outgassing considerations since there would no longer be the need for venting the desorbed noncondensables directly into the atmosphere as is being proposed under present OC-OTEC designs such as that designed in Section 4.0.

3) Both of the previously mentioned recommendations (predeaeration and reinjection systems) will require a great deal more research before they are ready for implementation in an OC-OTEC design. However, potential cost savings, the potential improvement in condenser performance, the reduction in compression power needs, the potential for reducing the environmental

concerns of the OC-OTEC process exemplified in the design of the predeaerated/reinjected system presented in Section 5.0 should provide the necessary incentives for continuing research along these lines in light of the data presented throughout this investigation. The thermodynamic evaluation accompanying this investigation suggests that the implementation of noncondensable predeaeration and reinjection should be incorporated within future OC-OTEC design considerations.

4) The relative merits and potential cost savings associated with utilizing a tapering pipe hydraulic compressor versus a standard discharge pipe hydraulic compressor design should be further investigated. Although the potential thermodynamic efficiency improvements associated with the tapering pipe design is nominal, any potential efficiency improvements for a system with as low efficiencies as OC-OTEC should be pursued.

5) A more specific design as to the predeaeration mechanism and the reinjection mechanism should be investigated further on an experimental level in order to develop the most efficient and cost effective means of providing an OC-OTEC system with these beneficial system components.

APPENDIX A
MASS SPECTROMETER CALIBRATION

A.1 THE MASS SPECTROMETER

The Quadrex 100 Residual Gas Analyzer (RGA - mass spectrometer) allows or the direct measurement of specific gas partial pressures from a vacuum system. This proved to be an ideal method by which the various noncondensable gases being deaerated within the OC-OTEC system could be measured in the vacuum spaces above the liquid continuum. In order to utilize the mass spectrometer, it was initially necessary to set the calibration factors for each specific gas prior to actual data acquisition. Therefore, a detailed description of the calibration techniques utilized in this experiment is included.

A.1.1 ESTIMATION OF CALIBRATION FACTORS

In order to determine the composition of the gases present at various stages of the OC-OTEC process, it is necessary to know the partial pressures of significant gases or vapors. The Quadrex 100 is capable of providing direct partial pressure values for the sensing chamber which is representative of the relative partial pressures at the desired sample location.

In order for the RGA to read partial pressures directly, it is necessary to determine a calibration factor for converting the electrical signal received from the sensor head into a representative pressure.

The following symbols will be used:

PP = Partial pressure of a given substance "A" in a gas mixture-torr.

I = Current output of the Quadrex sensor, signal amplitude of a mass peak, "B" resulting from substance "A".

FF_{AB} = Fragmentation factor, fraction of total ions from substance "A" having mass "B" see Table A.1.

FF_{N28} = Fragmentation factor for N_2 ions from nitrogen (typically .90 to .95 and often taken as 1.0).

XF = Ionization Probability, relative yield of ions from substance "A" compared to nitrogen at the same partial pressure, (see Table A.2).

TF = Transmission factor, the number of ions of mass "B" that pass through the analyzer, relative to ions of mass 28. TF = (28/M) (nominal).

DF = Detection factor, the relative current per ion at mass "B" compared to nitrogen ions at mass 28. For the Quadrex RGA with Faraday Cup, DF = 1. For the Quadrex RGA with electron multiplier, DF = 1 when voltage is 2,000 volts.

S = Sensitivity for nitrogen, output current (at mass 28) per unit absolute pressure for pure nitrogen-amp/torr. For the Quadrex RGA with Faraday Cup, $S = 2 \times 10^{-4}$ amp/torr (nominal). For the Quadrex RGA with electron multiplier, S varies widely depending on the operating voltage and

condition of the multiplier. For a new sensor S = 1 at a voltage typically in the 1800 - 2000 range.

Then we can say, the partial pressure of substance "A" indicated by the amplitude (I) of signal at mass "B" is

$$PP = (I \times FF_{N28})/(FF_{AB} \times XF \times TF \times DF \times S) \qquad (A\text{-}1)$$

This equation is quite general and holds true for all mass spectrometers [24].

The constants for these equations can be obtained from tables or, for the best accuracy, measured for each instrument (instruments will not be identical).

The Table mode used in these experiments provides a means where the constants for each substance may be factored into the measurements by the Quadrex, permitting direct readout. In this case, determine a multiplying factor "C" as follows:

$$C = 1 / D \qquad (A\text{-}2)$$

where

D = denominator of the previous equation.

The calibration factors calculated using these equations are presented in the following table (Table A.3)

Table A.1: Fragmentation Factors (Factor of Total Ions)

(Taken from [24])

Noncondensable	Mass	FF
Nitrogen (N_2)	28	0.94
	14	0.05
	29	0.01
Oxygen (O_2)	32	0.95
	16	0.05
Argon (Ar)	40	0.88
	20	0.12
Carbon Dioxide (CO_2)	44	0.85
	28	0.05
	16	0.05
	12	0.02

Table A.2: Ionization Probability

(Taken from [24])

Substance	Relative Ionization Gauge Sensitivity (XF)	Substance	Relative Ionization Gauge Sensitivity (XF)
Nitrogen (N_2)	1.0	Argon (Ar)	1.2
Oxygen (O_2)	1.0	Carbon Dioxide (CO_2)	1.4

Table A.3: Estimated Calibration Factors

	H_20	N_2	O_2	CO_2	Ar
Cal. Factor	0.86	1.06	1.20	1.32	1.35

These calibration factors can be used as a first approximation for determining the true calibration factor for each gas. However, each sensor head and mass spectrometer requires individual calibration to ensure correct values are being obtained. Therefore, it is necessary to continually recalibrate the Quadrex using a standard gas of known composition.

A.1.2 AIR CALIBRATION

The Quadrex 100 Residual Gas Analyzer (RGA) was calibrated on site prior to experimental runs on five (5) separate occasions using two different standards. Initially, an attempt was made to calibrate the RGA using atmospheric air leaked into the electron multiplier sensor head vacuum space. This was accomplished by connecting a 1/16" stainless steel sampling capillary to the Quadrex sampling valve and leaving the other end of the tube open to the atmosphere (this size and type of capillary was supplied by Inficon, the Quadrex manufacturer, for sampling gases at atmospheric pressures). After

the capillary had been sufficiently roughed down by the Quadrex roughing pump, the sample was drawn into the sensor chamber by the Quadrex system's turbovacuum pump and the relative atmospheric partial pressures were read by the Quadrex and displayed on the system's monitor. The partial pressures were then converted into relative volumetric percents of composition and compared to actual locally measured values using a psychrometric sling and psychrometric tables to determine relative humidity from which atmospheric humid air concentrations could be determined. The calibration factors for the Quadrex were then adjusted accordingly so that the partial pressures read would indicate actual atmospheric air compositions.

This calibration technique proved satisfactory for gases such as nitrogen, oxygen and water vapor which are the most significant contributors to atmospheric air composition. However, due to the very small amounts of carbon dioxide (CO_2) and Argon (Ar) present in atmospheric air, it was extremely difficult to obtain reliable calibration factors for these gases and the need for a more suitable standard gas with higher concentrations of these gases was realized. Thus, this method of calibration was only utilized further as a means of calibrating water vapor content. With the implementation of the argon tracer method to be discussed in detail later in this report, water vapor concentrations were no longer necessary and this method became obsolete and was only used further as a rough check of the standard gas calibration. Table A.4 shows the calibration data using atmospheric air.

A.1.3 STANDARD GAS CALIBRATION

The second method of calibration, as previously mentioned, utilized a known scientific standard calibration gas from Linde Gases, Inc. Since the maximum pressure the RGA system could sample from was slightly above atmospheric pressure (using the 1/16" s.s. sampling capillaries discussed earlier), it was necessary to develop a separate chamber which could be maintained and monitored at a pressure only slightly above atmospheric pressure into which the standard gas could flow and from which the standard gas could be accurately sampled.

Figure A.1 shows the chamber designed and used for standard gas calibration. The chamber body was constructed of a 12" x 1-1/2" PVC pipe vacuum sealed with a pressure/vacuum gauge to monitor the internal pressure of the chamber and two 1/4" metering valves to control the injection flow rate of the standard gas and the sampling rate to the sensor chamber, respectively. A 1/16" sampling capillary was used as the sampling line between the sample chamber and the sensing chamber.

Initially, the sample chamber was roughed down by the Quadrex roughing pump, then the sample gas was slowly bled into the container until a steady state of slightly higher than atmospheric pressure was reached (this ensured that the pressurized standard gas was indeed flowing through the sampling system). The sample gas was then drawn into the sensor chamber and the relative standard gas partial pressures were read by the Quadrex and displayed on the monitor. The partial pressures were then converted into relative volumetric percents of composition and compared to the actual known

Table A.4: Calibration Data - Atmospheric Air

Data Set	Vapor Composition (%)				
	H_20	N_2	O_2	Ar	CO_2
Actual Air Composition (5/11)	2.59	76.10	20.38	0.90	0.03
Actual Air Composition (5/13)	2.40	76.24	20.42	0.90	0.03
Actual Air Composition (5/19)	2.40	76.24	20.42	0.90	0.03
CALA1 (5/11)	3.00	74.00	21.90	1.00	0.15
CALA2 (5/11)	2.10	75.60	21.20	1.00	0.14
CAL5151	2.90	74.40	21.60	0.90	0.10
CAL5191	2.70	76.20	20.20	0.90	0.10

volumetric composition of the standard gas. The calibration factors for the Quadrex were then adjusted accordingly so that the partial pressures read would indicate the actual standard gas compositions. The calibration data obtained using this method is presented in Table A.5. Table A.6 presents the calibration values actually used during this experiment to obtain the calibration data as well as the actual data to be presented in subsequent sections of this report.

Table A.5: Calibration Data - Standard Gas Calculations

Data Set	Vapor Composition (%)				
	H_20	N_2	O_2	Ar	CO_2
Standard Gas Composition	-	60.00	19.99	10.00	10.01
CAL1 (5/11)	-	60.62	19.83	9.84	9.70
CAL2 (5/11)	-	60.06	20.35	9.85	9.75
CAL3 (5/11)	-	60.00	19.20	10.40	10.40
CAL4 (5/11)	-	59.00	20.40	10.20	10.30
CAL5 (5/11)	-	59.80	20.20	9.90	10.00
CAL 5151	-	59.90	19.90	10.20	10.00
CAL 5171	-	59.10	20.80	10.20	9.90
CAL 5191	-	59.80	20.00	10.10	10.10
CAL 5231	-	60.50	19.60	9.90	10.00
CAL 5232	-	60.50	19.50	9.90	10.10

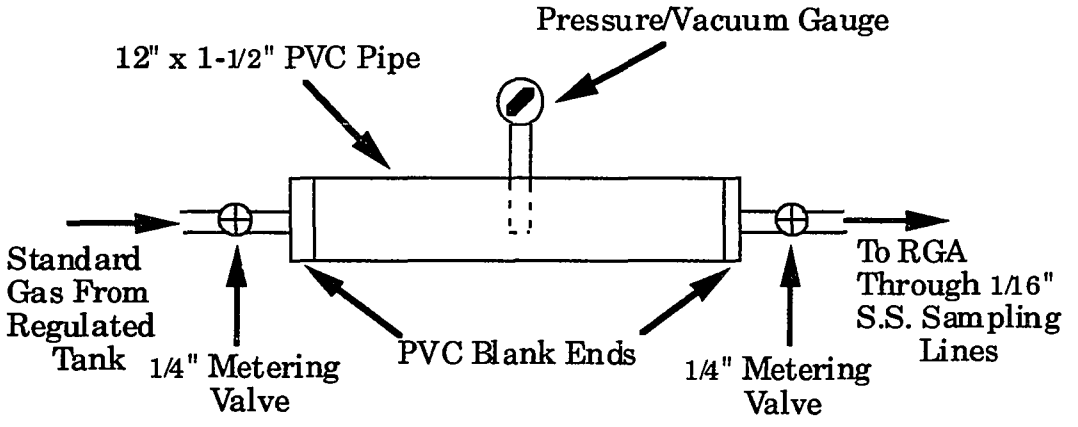

Figure A.1: Standard Gas Calibration Sample Chamber

Table A.6: Actual Calibration Factors for Experimental EM Sensor Head

	H_20	N_2	O_2	Ar	CO_2
Calibration Factor	0.7	0.9	1.1	1.4	1.05

APPENDIX B
EXPERIMENTAL ERROR ANALYSIS

B.1 PARTIAL PRESSURE DATA

The ensuing appendix presents the method upon which the errors presented in the text were based. A natural progression of the error (uncertainty) in the data, from its most basic form of raw partial pressures measured directly from the RGA to the final calculated noncondensable outgassing rates is also presented.

This section presents the raw partial pressure data as read by the Quadrex RGA and its associated error determined from the following equations. For the standard deviation in the data:

$$\sigma_y = [(\sum Y^2 - n \sum \overline{Y}^2 / n]^{1/2} \qquad \text{(B-1)}$$

and for the expected error of a random sample about the sample mean Y:

$$\sigma_{\overline{y}} = \sigma_y / (n)^{1/2} \qquad \text{(B-2)}$$

The following tables have been developed incorporating the partial pressure raw data in conjunction with its associated standard deviation and the expected error of the sample mean according to the equations presented above.

B.1.1 FOR RGA CALIBRATION (STANDARD GAS):

Table B.1: Typical Errors for Standard Gas Calibration (Partial Pressures)

Gas	n	Typical Partial Pressures ($\bar{Y}$) (x 10^8 torr)	Typical σ_y (x 10^8 torr)	$\sigma_{\bar{y}}$ (x 10^8 torr)	% Error About Mean
N_2	3	12.87	± 0.17	± 0.10	± 0.78
O_2	3	4.40	± 0.04	± 0.02	± 0.45
CO_2	3	2.10	± 0.04	± 0.02	± 0.95
Ar	3	2.10	± 0.04	± 0.02	± 0.95

Table B.2: Typical Errors for Standard Gas Calibration (% Composition)

Gas	n	Typical % Composition ($\bar{Y}$)	Typical σ_y (%)	$\sigma_{\bar{y}}$ (%)	% Error About Mean
N_2	10	59.93	± 0.52	± 0.16	± 0.27
O_2	10	19.98	± 0.45	± 0.14	± 0.70
CO_2	10	10.03	± 0.21	± 0.07	± 0.70
Ar	10	10.04	± 0.18	± 0.06	± 0.60

B.1.2 FOR OUTGASSING CALCULATIONS

Table B.3: Typical Partial Pressure Errors for 10/10 (l/s) Flows

Gas	n	Typical Partial Pressures ($\bar{Y}$) (x 10^8 torr)	Typical σ_y (x 10^8 torr)	$\sigma_{\bar{y}}$ (x 10^8 torr)	% Error About Mean
N_2	3	1.317	± 0.012	± 0.007	± 0.53
O_2	3	1.017	± 0.005	± 0.003	± 0.29
CO_2	3	0.1663	± 0.0005	± 0.0003	± 0.18
Ar	3	0.0263	± 0.0009	± 0.0005	± 1.90

Table B.4: Typical Partial Pressure Errors for 25/25 (l/s) Flows

Gas	n	Typical Partial Pressures ($\bar{Y}$) (x 10^8 torr)	Typical σ_y (x 10^8 torr)	$\sigma_{\bar{y}}$ (x 10^8 torr)	% Error About Mean
N_2	3	1.117	± 0.012	± 0.007	± 0.64
O_2	3	0.573	± 0.009	± 0.005	± 0.94
CO_2	3	0.0833	± 0.0012	± 0.0007	± 0.86
Ar	3	0.0177	± 0.0005	± 0.0003	± 1.54

Table B.5: Typical Partial Pressure Errors for 50/50 (l/s) Flows

Gas	n	Typical Partial Pressures ($\bar{Y}$) (x 10^8 torr)	Typical σ_y (x 10^8 torr)	$\sigma_{\bar{y}}$ (x 10^8 torr)	% Error About Mean
N_2	3	1.750	± 0.008	± 0.005	± 0.27
O_2	3	0.733	± 0.005	± 0.003	± 0.39
CO_2	3	0.1162	± 0.0005	± 0.0003	± 0.23
Ar	3	0.0357	± 0.0005	± 0.0003	± 0.76

Table B.6: Typical Partial Pressure Errors for 73/62 (l/s) Flows

Gas	n	Typical Partial Pressures ($\bar{Y}$) (x 10^8 torr)	Typical σ_y (x 10^8 torr)	$\sigma_{\bar{y}}$ (x 10^8 torr)	% Error About Mean
N_2	3	2.300	± 0.041	± 0.0024	± 1.02
O_2	3	0.840	± 0.014	± 0.008	± 0.97
CO_2	3	0.1343	± 0.0005	± 0.0003	± 0.20
Ar	3	0.0510	± 0.0014	± 0.0008	± 1.60

B.1.3 FOR AIR INJECTION

Table B.7: Typical Partial Pressure Errors for 10/10 (l/s) Flows + 100 (scfh) Air Injection

Gas	n	Typical Partial Pressures $(\bar{Y})$ (x 10^8 torr)	Typical σ_y (x 10^8 torr)	$\sigma_{\bar{y}}$ (x 10^8 torr)	% Error About Mean
N_2	3	3.133	± 0.047	± 0.027	± 0.87
O_2	3	0.720	± 0.014	± 0.008	± 1.13
CO_2	3	0.248	± 0.004	± 0.002	± 0.95
Ar	3	0.044	± 0.003	± 0.002	± 3.44

Table B.8: Typical Partial Pressure Errors for 10/10 (l/s) Flows + 120 (scfh) Air Injection

Gas	n	Typical Partial Pressures $(\bar{Y})$ (x 10^8 torr)	Typical σ_y (x 10^8 torr)	$\sigma_{\bar{y}}$ (x 10^8 torr)	% Error About Mean
N_2	3	2.533	± 0.094	± 0.054	± 2.15
O_2	3	0.987	± 0.009	± 0.005	± 0.55
CO_2	3	0.0930	± 0.0004	± 0.0002	± 0.25
Ar	3	0.0323	± 0.0012	± 0.0007	± 2.23

Table B.9: Typical Partial Pressure Errors for 10/10 (l/s) Flows + 300 (scfh) Air Injection

Gas	n	Typical Partial Pressures $(\bar{Y})$ (x 10^8 torr)	Typical σ_y (x 10^8 torr)	$\sigma_{\bar{y}}$ (x 10^8 torr)	% Error About Mean
N_2	3	4.900	± 0.041	± 0.024	± 0.48
O_2	3	1.560	± 0.008	± 0.005	± 0.30
CO_2	3	0.0890	± 0.0014	± 0.0008	± 0.92
Ar	3	0.0590	± 0.0014	± 0.0008	± 1.38

Table B.10: Typical Partial Pressure Errors for 10/25 (l/s) Flows + 100 (scfh) Air Injection

Gas	n	Typical Partial Pressures $(\bar{Y})$ (x 10^8 torr)	Typical σ_y (x 10^8 torr)	$\sigma_{\bar{y}}$ (x 10^8 torr)	% Error About Mean
N_2	3	3.200	± 0.041	± 0.024	± 0.74
O_2	3	0.843	± 0.017	± 0.010	± 1.16
CO_2	3	0.1920	± 0.0014	± 0.0008	± 0.43
Ar	3	0.0527	± 0.0005	± 0.0003	± 0.52

Table B.11: Typical Partial Pressure Errors for 73/50 (l/s) Flows + 100 (scfh) Air Injection

Gas	n	Typical Partial Pressures $(\bar{Y})$ (x 10^8 torr)	Typical σ_y (x 10^8 torr)	$\sigma_{\bar{y}}$ (x 10^8 torr)	% Error About Mean
N_2	3	5.167	± 0.047	± 0.027	± 0.53
O_2	3	1.743	± 0.012	± 0.007	± 0.41
CO_2	3	0.229	± 0.004	± 0.002	± 1.03
Ar	3	0.1023	± 0.0012	± 0.0007	± 0.70

B.2 LINEAR REGRESSION ERROR (OUTGASSING UNCERTAINTY)

When analyzing the predicted error (uncertainty) in the outgassing rates presented in Section 3, it is necessary to account for the error attributable to the data after it has been linearly regressed. To accomplish this, the following equations have been utilized to estimate the standard deviation of the data included in the reported linearly regressed line. The actual estimated error attributable to the data was then calculated as in the previous section using equation B-2.

$$\sigma_y = [\, (n / n - 2)\, (1 - r^2)\, S_{yy}\,]^{1/2} \qquad \text{(B-3)}$$

and

$$S_{yy} = (1 / n) [\sum Y^2 - n (\bar{Y})^2] \qquad \text{(B-4)}$$

The following tables have been prepared to display the values obtained using this method and to display the progression which led to the ultimate outgassing errors presented in the text.

Table B.12: Error in the Linear Regression of the 10 l/s Warm Water Outgassing Line

Gas	n	$\bar{Y}$ (mmols/sec)	r^2	S_{yy}	$\sum Y^2$	σ_y (mmols/sec)	$\sigma_{\bar{y}}$ (mmols/sec)
N_2	9	33.18	0.9688	112.67	10922.2	± 2.13	± 0.71
O_2	9	11.34	0.0203	0.7155	1163.8	± 0.95	± 0.32
CO_2	9	2.86	0.8959	0.3304	76.59	± 0.21	± 0.07
Ar	9	0.73	0.9953	0.0842	5.554	± 0.023	± 0.008

Table B.13: Error in the Linear Regression of the 10 l/s Cold Water Outgassing Line

Gas	n	$\bar{Y}$ (mmols/sec)	r^2	S_{yy}	$\sum Y^2$	σ_y (mmols/sec)	$\sigma_{\bar{y}}$ (mmols/sec)
N_2	6	27.26	0.8669	32.53	4653.8	± 2.55	± 1.04
O_2	6	18.96	0.9090	28.57	2328.3	± 1.97	± 0.80
CO_2	6	2.25	0.7782	0.036	30.59	± 0.109	± 0.04
Ar	6	0.43	0.9298	0.0061	1.146	± 0.025	± 0.01

Table B.14: Error in the Linear Regression of the 25 l/s Warm Water Outgassing Line

Gas	n	$\bar{Y}$ (mmols/sec)	r^2	S_{yy}	$\sum Y^2$	σ_y (mmols/sec)	$\sigma_{\bar{y}}$ (mmols/sec)
N_2	9	43.30	0.9646	155.92	18277.3	± 2.66	± 0.89
O_2	9	18.96	0.0158	8.174	3308.9	± 3.22	± 1.07
CO_2	9	3.17	0.9457	0.372	93.79	± 0.16	± 0.05
Ar	9	0.80	0.9811	0.0948	6.613	± 0.05	± 0.02

Table B.15: Error in the Linear Regression of the 25 l/s Cold Water Outgassing Line

Gas	n	$\bar{Y}$ (mmols/sec)	r^2	S_{yy}	$\sum Y^2$	σ_y (mmols/sec)	$\sigma_{\bar{y}}$ (mmols/sec)
N_2	10	37.39	0.8674	71.35	14693.6	± 3.44	± 1.09
O_2	10	17.61	0.6875	33.54	3436.5	± 3.62	± 1.14
CO_2	10	2.95	0.6258	0.052	87.54	± 0.16	± 0.05
Ar	10	0.77	0.8440	0.041	6.334	± 0.09	± 0.03

Table B.16: Error in the Linear Regression of the 50 l/s Warm Water Outgassing Line

Gas	n	$\overline{Y}$ (mmols/sec)	r^2	S_{yy}	$\sum Y^2$	σ_y (mmols/sec)	$\sigma_{\overline{y}}$ (mmols/sec)
N_2	9	52.17	0.9846	177.25	26090.6	± 1.87	± 0.62
O_2	9	22.83	0.0168	16.32	4837.8	± 4.54	± 1.51
CO_2	9	3.39	0.8518	0.489	107.83	± 0.31	± 0.10
Ar	9	1.06	0.9455	0.099	11.00	± 0.08	± 0.03

Table B.17: Error in the Linear Regression of the 50 l/s Cold Water Outgassing Line

Gas	n	$\overline{Y}$ (mmols/sec)	r^2	S_{yy}	$\sum Y^2$	σ_y (mmols/sec)	$\sigma_{\overline{y}}$ (mmols/sec)
N_2	9	55.99	0.9218	108.8	29192.9	± 3.31	± 1.10
O_2	9	18.93	0.5910	33.20	3523.9	± 4.18	± 1.39
CO_2	9	3.63	0.4863	0.170	120.12	± 0.33	± 0.11
Ar	9	1.20	0.9204	0.060	13.50	± 0.08	± 0.03

Table B.18: Error in the Linear Regression of the 73 l/s Warm Water Outgassing Line

Gas	n	$\overline{Y}$ (mmols/sec)	r^2	S_{yy}	$\sum Y^2$	σ_y (mmols/sec)	$\sigma_{\bar{y}}$ (mmols/sec)
N_2	6	63.46	0.8760	164.10	24847.7	± 4.61	± 1.88
O_2	6	25.39	0.6403	4.148	3892.8	± 1.50	± 0.61
CO_2	6	3.93	0.8909	0.215	93.96	± 0.19	± 0.08
Ar	6	1.40	0.8046	0.068	12.17	± 0.14	± 0.06

Table B.19: Error in the Linear Regression of the 62 l/s Cold Water Outgassing Line

Gas	n	$\overline{Y}$ (mmols/sec)	r^2	S_{yy}	$\sum Y^2$	σ_y (mmols/sec)	$\sigma_{\bar{y}}$ (mmols/sec)
N_2	8	62.15	0.8658	87.08	31597.6	± 3.95	± 1.40
O_2	8	21.29	0.8706	36.05	3914.5	± 2.49	± 0.88
CO_2	8	4.08	0.6997	0.094	133.92	± 0.19	± 0.07
Ar	8	1.33	0.9550	0.026	14.36	± 0.04	± 0.01

Table B.20: Maximum Error in Nitrogen Outgassing Rate for Minimum Feed Stream Flow Rates

Flow Rates (WW/CW) (liters/sec)	Minimum Regressed Outgassing Rate (mmols/sec)	Maximum $\sigma_{\bar{y}}$ (mmols/sec)	Maximum Error (%)
0 / 10	18.1	± 1.0	± 5.5
0 / 25	25.1	± 1.1	± 4.4
0 / 50	38.3	± 1.1	± 2.9
0 / 62	47.9	± 1.4	± 2.9
10 / 0	14.3	± 0.7	± 4.9
25 / 0	19.2	± 0.9	± 4.7
50 / 0	26.5	± 0.6	± 2.3
73 / 0	33.9	± 1.9	± 5.6

Table B.21: Maximum Error in Oxygen Outgassing Rate for Minimum Feed Stream Flow Rates

Flow Rates (WW/CW) (liters/sec)	Minimum Regressed Outgassing Rate (mmols/sec)	Maximum $\sigma_{\bar{y}}$ (mmols/sec)	Maximum Error (%)
0 / 10	10.1	± 0.8	± 7.9
0 / 25	7.5	± 1.1	± 14.7
0 / 50	11.1	± 1.4	± 12.6
0 / 62	12.0	± 0.9	± 7.5
10 / 0	11.2	± 0.3	± 2.7
25 / 0	13.1	± 1.1	± 8.4
50 / 0	23.9	± 1.5	± 6.3
73 / 0	20.7	± 0.6	± 2.9

Table B.22: Maximum Error in Carbon Dioxide Outgassing Rate for Minimum Feed Stream Flow Rates

Flow Rates (WW/CW) (liters/sec)	Minimum Regressed Outgassing Rate (mmols/sec)	Maximum $\sigma_{\bar{y}}$ (mmols/sec)	Maximum Error (%)
0 / 10	1.91	± 0.04	± 2.1
0 / 25	2.06	± 0.05	± 2.4
0 / 50	3.15	± 0.11	± 3.5
0 / 62	3.58	± 0.07	± 2.0
10 / 0	1.86	± 0.07	± 3.8
25 / 0	2.00	± 0.05	± 2.5
50 / 0	2.08	± 0.10	± 4.8
73 / 0	2.59	± 0.08	± 3.1

Table B.23: Maximum Error in Argon Outgassing Rate for Minimum Feed Stream Flow Rates

Flow Rates (WW/CW) (liters/sec)	Minimum Regressed Outgassing Rate (mmols/sec)	Maximum $\sigma_{\bar{y}}$ (mmols/sec)	Maximum Error (%)
0 / 10	0.27	± 0.01	± 3.7
0 / 25	0.53	± 0.03	± 5.7
0 / 50	0.78	± 0.03	± 3.8
0 / 62	1.03	± 0.01	± 1.0
10 / 0	0.21	± 0.01	± 4.8
25 / 0	0.31	± 0.02	± 6.5
50 / 0	0.45	± 0.03	± 6.7
73 / 0	0.68	± 0.06	± 8.8

Table B.24: Error in the Linear Regression of the Zero Flow Curves (% Outgassing) (CW Flow = 0 l/s)

Gas	n	$\bar{Y}$ (mmols/sec)	r^2	S_{yy}	$\sum Y^2$	σ_y (mmols/sec)	$\sigma_{\bar{y}}$ (mmols/sec)
N_2	4	23.48	0.9996	54.84	2424.6	± 0.21	± 0.10
O_2	4	17.23	0.7071	27.83	1296.8	± 4.00	± 2.00
CO_2	4	2.13	0.8705	0.0856	18.49	± 0.15	± 0.07
Ar	4	0.41	0.9821	0.0332	0.805	± 0.03	± 0.02

Table B.25: Error in the Linear Regression of the Zero Flow Curves (% Outgassing) (WW Flow = 0 l/s)

Gas	n	$\overline{Y}$ (mmols/sec)	r^2	S_{yy}	$\sum Y^2$	σ_y (mmols/sec)	$\sigma_{\bar{y}}$ (mmols/sec)
N_2	4	32.35	0.9904	133.2	4718.9	± 1.60	± 0.8
O_2	4	10.18	0.4453	2.743	425.5	± 1.74	± 0.9
CO_2	4	2.68	0.9651	0.4751	30.63	± 0.18	± 0.09
Ar	4	0.65	0.9823	0.0833	2.023	± 0.05	± 0.03

Table B.26: Error in Background (Leak) Estimate (WW = 0 l/s)

Gas	Extrapolated 0 / 0 Flow	$\sigma_{\bar{y}}$	% Error
N_2	11.7	± 0.8	± 6.8
O_2	8.2	± 0.9	± 11.2
CO_2	1.73	± 0.09	± 5.2
Ar	0.15	± 0.03	± 20.0

Table B.27: Error in Background (Leak) Estimate (CW = 0 l/s)

Gas	Extrapolated 0 / 0 Flow	$\sigma_{\bar{y}}$	% Error
N_2	11.3	± 0.1	± 0.9
O_2	9.9	± 2.0	± 20.2
CO_2	1.73	± 0.07	± 4.0
Ar	0.12	± 0.02	± 16.7

For the respective noncondensable backgrounds (leaks), the following corresponding errors are obtained by the previous analysis (Tables B.26 and B.27).

N_2 (background) = (11.5 ± 0.8) mmols/sec (± 7.0% maximum error)

O_2 (background) = (9.0 ± 2.0) mmols/sec (± 22.2% maximum error)

CO_2 (background) = (1.73 ± 0.09) mmols/sec (± 5.2% maximum error)

Ar (background) = (0.14 ± 0.03) mmols/sec (± 21.4% maximum error)

Using the maximum errors presented in Tables B.26 and B.27 to predict the maximum error which could occur in the slopes of the developed zero outgassing lines gives:

For N_2: $Y = (0.56 \pm 0.04)X + (11.7 \pm 0.8)$

CW outgassing (% error = ± 6.8%)

$Y = (0.31 \pm 0.01)X + (11.3 \pm 0.1)$

WW outgassing (% error = ± 0.9%)

For O_2: $Y = (0.055 \pm 0.006)X + (8.2 \pm 0.9)$

CW (% error = ± 11.2%)

$Y = (0.184 \pm 0.037)X + (9.9 \pm 2.0)$

WW (% error = ± 20.2%)

For CO_2: $Y = (0.030 \pm 0.002)X + (1.73 \pm 0.09)$

CW (% error = ± 5.2%)

$Y = (0.011 \pm 0.0004)X + (1.73 \pm 0.07)$

WW (% error = ± 4.0%)

For Ar: $Y = (0.0139 \pm 0.0028)X + (0.15 \pm 0.03)$

CW (% error = ± 20.0%)

$Y = (0.0073 \pm 0.0012)X + (0.12 \pm 0.02)$

WW (% error = ± 16.7%)

The error for the respective slopes used for the 100% outgassing as reported by Krock [21] are:

For N_2: $Y = (0.57 \pm 0.03)X$ CW outgassing (WW = 0)

$Y = (0.43 \pm 0.04)X$ WW outgassing (CW = 0)

For O_2: $Y = (0.047 \pm 0.006)X$ CW outgassing (WW = 0)

$Y = (0.225 \pm 0.003)X$ WW outgassing (CW = 0)

For "Free" CO_2: $Y = (0.054 \pm 0.002)X$ CW outgassing (WW = 0)

$Y = (0.008 \pm 0.0005)X$ WW outgassing (CW = 0)

For Total CO_2: $Y = (2.325 \pm 0.014)X$ CW outgassing (WW = 0)

$Y = (1.933 \pm 0.012)X$ WW outgassing (CW = 0)

For Ar*: $Y = (0.0154 \pm 0.0008)X$ CW outgassing (WW = 0)

$Y = (0.0104 \pm 0.0010)X$ WW outgassing (CW = 0)

* Used nitrogen % error as a means of estimating the argon error since the actual argon error was unavailable in the literature and nitrogen and argon possess similar inert chemical characteristics in seawater.

B.3 UNCERTAINTY IN CALCULATED PARAMETERS

This section summarizes the error analysis for the calculated extent of outgassing percentages. The equations used for these calculations are presented in Section 3 of this report. The values used are those presented in the previous section to maximize the error present in the calculated values. The measurement errors for each parameter were discussed in previous sections of this Appendix. The partial multiplier comes from the following equations.

Assume: $$F = f(X_1, X_2 \ldots X_n) \qquad \text{(B-5)}$$

then $$\frac{\Delta F}{F} = \left[\sum_{i=1}^{n} \left(\frac{1}{F}\frac{\partial F}{\partial X_i}\Delta X_i\right)^2\right]^{1/2} \qquad \text{(B-6)}$$

The error contribution of each parameter is the partial multiplier times the measurement error. The total error in a calculated parameter is the root-mean-square (RMS) of the individual parameter contributions.

This analysis gives the following errors associated with the extent of the respective noncondensable outgassing percentages:

For N_2:	Warm Water Outgassing	(72 ± 7)%
	Cold Water Outgassing	(98 ± 9)%
For O_2:	Warm Water Outgassing	(81 ± 16)%
	Cold Water Outgassing	(100 ± 17)%
For "Free" CO_2:	Warm Water Outgassing	(138 ± 10)%
	Cold Water Outgassing	(56 ± 4)%
For Total CO_2:	Warm Water Outgassing	(0.6 ± 0.1)%
	Cold Water Outgassing	(1.3 ± 0.1)%
For Ar:	Warm Water Outgassing	(70 ±13)%
	Cold Water Outgassing	(90 ± 19)%

It probably would be more appropriate to consider the previously discussed "error" analysis a variability analysis. Essentially, by analyzing the data in such a way we are combining the variability of the noncondensable background in the natural environment with the actual error in measurement technique and instrumentation. When carefully observing Krock's data [21] shown above, we see that the variability in his data is very similar to that experienced in the data presented in this report. Since our data is entirely dependant upon the dissolved noncondensable compositions in the warm and cold water feed streams, we could not expect the data to be any less variable than that of this naturally occurring ocean water. Therefore, the errors presented in this section do not reflect inaccuracies in technique (on the contrary, they suggest errors approaching ± 6% attributable to the measurement process) but natural fluctuations in noncondensable backgrounds.

Another method used to analyze error in data is to account for the errors in all phases of the data acquisition process. In this case it is necessary to account for the errors present in the measurement of the argon flow during injection as well as the measurement of the partial pressures at the mass spectrometer. The errors breakdown as follows in Table B.28.

Using the manufacturers and estimated errors presented in Table B.28 and the root-mean-square analysis discussed earlier, the error associated with the air injection values is ± 10.3% and the error associated with the noncondensable outgassing rates is ± 6.4%. In either case, the error (or variability in the data) is higher and is therefore presented as the "correct" error.

Table B.28: Errors Contributing to Measurement Uncertainty

Instrument	Scale	% Error Full Scale	Typical Reading	Error
Dwyer Visi-Float Flow Meter (#VFB)	0-10 scfh	± 3%	8.0	± 0.3
Wilkerson GRP-49-038	0-160 psig	± 3%	45	± 3*
Dwyer Rate Master Flow Meter (#RMC-104)	40-400 scfh	± 2%	100	± 8
Quadrex	10^{-10}-10^{-8} torr	± 2%	1.8×10^{-8}	$\pm 0.04 \times 10^{-8}$

* Very liberal estimate of error, gauge was calibrated on site to within ± 1% at working pressures.

APPENDIX C

DR. STUART RIDGEWAY'S COMPUTER PROGRAM

C.1 COMPUTER PROGRAM

The following basic computer program (MYPROG.BAS) was written by Dr. Stuart Ridgway to reduce the Quadrex partial pressures into outgassing rates of the specific gases in both standard cubic feet per hour (scfh) and mmoles per second (mmols/sec). The input data for the program consist of:

(1) Run identifiers (date, time, sample port location, booster on/off and the warm and cold water flow rates.

(2) Argon background partial pressure (10^{-10} torr).

(3) The individual gases' partial pressures (10^{-10} torr) (water, nitrogen, oxygen, carbon dioxide and argon, respectively).

(4) Any comments pertinent to the run.

The ensuing text represents the computer program

```
10    REM gas analysis program REPORT
20    LPRINT "GAS ANALYSIS REPORT":LPRINT;LPRINT
30    C$=  "date, time, sample port, booster, w & c flow..":PRINT C$:PRINT
40    LPRINT
50    INPUT B$
60    IF B$="QUIT"THEN STOP
70    LPRINT
80    LPRINT C$:LPRINT B$
90    LPRINT
100   INPUT"ARGON BACKGROUND":ARGB
110   LPRINT
120   LPRINT "ARGON BACKGROUND IS...",ARGB
130   LPRINT
140   LPRINT"input in order steam, nitro, ooh, cotwo, arg"
```

```
150   INPUT"input in order steam, nitro, ooh, cotwo, arg":STEAM,
NITRO,OOH,COTWO, ARG
160   LPRINT STEAM, NITRO,OOH,COTWO,ARG
170   INPUT"argon flow rate cfh,and metering pressure":ARGFH,
PRESSURE
175   LPRINT"argon flow rate cfh,and metering pressure":ARGFH,
PRESSURE
180   DIM MEASURE(6),BACKGROUND(6),FLOW(6),HEADER$(6),
MOL(6)
190   HEADER$(1)="STEAM":HEADER$(2)="NITROGEN":
HEADER$(3)="OXYGEN"
200   HEADER$(4)= "CO TWO"
210   HEADER$(5)= "ARGON"
220   MEASURE(1)=STEAM
230   MEASURE(2)=NITRO
240   MEASURE(3)=OOH:MEASURE(4)=COTWO
250   MEASURE(5)=ARGB
260   FLOWFACT=SQR((PRESSURE+14.7)*29/(14.7*40))
270   FOR INDEX= 1 TO 5
280   FLOW(INDEX)=MEASURE(INDEX)*ARGFH*FLOWFACT /(ARG-
ARGB)
290   MOL(INDEX)=.3322*FLOW(INDEX)
300   PRINT HEADER$(INDEX),FLOW(INDEX); "CUBIC FEET/HOUR
";MOL(INDEX);"MILLIMOLS/SECOND"
310   LPRINT HEADER$(INDEX),FLOW(INDEX); "CUBIC FEET/HOUR
"MOL(INDEX);"MILLIMOLS/SECOND"
320   NEXT INDEX
330   SUM=0
340   FOR J= 2 TO 5
350   SUM = SUM + FLOW(J)
360   NEXT J
370   PRINT
380   LPRINT
390   PRINT " THE TOTAL FLOW IS ....";SUM;" CUBIC FEET/HR "
400   LPRINT " THE TOTAL FLOW IS ....";SUM;" CUBIC FEET/HR";
.3322*SUM"MILLIMOLS/SEC"
410   GOTO 460
420   INPUT"WARMFLOW EQUALS ?..";WARMFLOW
430   FLOW = 32+ 1.7*WARMFLOW
440   PRINT "WARMFLOW GAS = ";FLOW
450   END
460   LPRINT
470   LPRINT "COMMENTS.."
480   PRINT "AVOID COMMAS, AND TYPE QUIT WHEN FINISHED"
490   REM COMMENT SUBROUTINE
500   INPUT A$
510   IF A$="QUIT"THEN RUN
```

```
520  LPRINT A$
530  GOTO 490
540  END
```

APPENDIX D

EXPERIMENTAL RAW DATA

D.1 RAW DATA

The following two tables represent the original data taken by the Quadrex and subsequently converted into noncondensable outgassing rates. Table D.1 presents the original partial pressures (averaged for three discrete samples) read from the Quadrex sensor and recorded by the IBM-PC in the data set corresponding to the data (column 1 gives the data set name). In every case a preliminary run was performed without argon injection, to establish an argon background (argon outgassing rate), and is presented first in each pair of data sets (indicated by the XS in the last two positions of the data set name). The data set which contained the argon injection (indicated by the AS) is the second data set of the pair. The data is presented in chronological order.

Table D.2 presents the corresponding outgassing rates calculated for each data set with argon injection (argon outgassing rate determined from original argon background) using the computer program presented in the previous appendix.

Table D.1: Original Quadrex Partial Pressure Data

Data Set	WW/CW (liters/sec)	Argon Flow (scfh)	Partial Pressures (x 10^8 torr)			
			N_2	O_2	CO_2	Ar
C35173XS	50/50	----	0.315	0.085	0.016	0.007
C35174AS	50/50	12.0	0.300	0.067	0.016	0.028
C35175XS	10/50	----	0.204	0.033	0.013	0.004
C35176AS	10/50	19.0	0.202	0.029	0.012	0.041
C35182XS	10/10	----	1.211	0.673	0.098	0.016
C35183AS	10/10	11.8	1.182	0.613	0.094	0.215
C35185XS	10/10†	----	2.674	0.987	0.093	0.033
C35186AS	10/10	11.8	2.710	0.977	0.095	0.243
C35187XS	10/10#	----	5.172	1.560	0.089	0.059
C35176AS	10/10	11.8	5.141	1.533	0.088	0.263
C36071XS	25/25	----	2.180	1.067	0.228	0.052
C36072AS	25/25	11.8	2.257	0.833	0.214	0.340
C36073XS	10/25	----	1.743	0.893	0.195	0.040
C36074AS	10/25	11.8	1.810	0.707	0.188	0.313
C36075XS	10/50	----	2.667	0.840	0.232	0.062
C36076AS	10/50	11.8	2.700	0.753	0.229	0.333
C36077XS	10/62	----	3.233	0.880	0.242	0.076
C36078AS	10/62	11.8	3.267	0.820	0.242	0.347
C36081XS	10/10	----	1.317	1.017	0.166	0.027
C36082AS	10/10	11.8	1.320	0.927	0.161	0.327
C36083XS	10/25	----	1.817	0.817	0.179	0.040
C36084AS	10/25	11.8	1.803	0.757	0.173	0.313
C36085XS	10/50	----	2.667	0.737	0.199	0.062
C36086AS	10/50	11.8	2.633	0.687	0.200	0.320
C36087XS	10/62	----	3.100	0.870	0.229	0.071
C36088AS	10/62	11.8	3.100	0.807	0.229	0.320

Table D.1 (Continued): Original Quadrex Partial Pressure Data

Data Set	WW/CW (liters/sec)	Argon Flow (scfh)	Partial Pressures (x 10^8 torr)			
			N_2	O_2	CO_2	Ar
C36089XS	50/25	----	2.567	1.387	0.194	0.063
C36080AS	50/25	11.8	2.667	1.330	0.191	0.320
C36091XS	10/10*	----	3.133	0.720	0.248	0.044
C36092AS	10/10	11.8	2.833	0.660	0.220	0.310
C36093XS	10/25*	----	3.200	0.860	0.192	0.053
C36094AS	10/25	11.8	3.233	0.803	0.192	0.290
C36095XS	10/25	----	1.683	0.640	0.179	0.034
C36096AS	10/25	11.8	1.723	0.607	0.175	0.270
C36097XS	73/25	----	3.267	1.467	0.221	0.073
C36098AS	73/25	11.8	3.233	1.390	0.220	0.320
C36099XS	73/50*	----	5.167	1.743	0.229	0.102
C36090AS	73/50	11.8	5.067	1.660	0.224	0.313
C3609!XS	73/50	----	3.600	1.377	0.214	0.083
C3609@AS	73/50	11.8	3.600	1.310	0.213	0.280
C36285XS	73/50	----	1.927	0.803	0.121	0.042
C36286AS	73/50	11.8	1.963	0.690	0.116	0.156
C36287XS	50/50	----	1.777	0.643	0.110	0.035
C36288AS	50/50	11.8	1.760	0.710	0.111	0.152
C36289XS	25/50	----	1.513	0.580	0.107	0.029
C36280AS	25/50	11.8	1.563	0.517	0.104	0.144
C3628!XS	25/25	----	1.150	0.560	0.085	0.019
C3628@AS	25/25	11.8	1.127	0.583	0.084	0.132
C36291XS	50/62	----	2.003	0.773	0.136	0.042
C36292AS	50/62	11.8	2.010	0.690	0.130	0.157
C36293XS	25/62	----	1.813	0.583	0.122	0.036
C36294AS	25/62	11.8	1.807	0.627	0.124	0.154

Table D.1 (Continued): Original Quadrex Partial Pressure Data

Data Set	WW/CW (liters/sec)	Argon Flow (scfh)	Partial Pressures (x 10^8 torr)			
			N_2	O_2	CO_2	Ar
C36295XS	25/10	----	0.997	0.777	0.084	0.014
C36296AS	25/10	11.8	1.003	0.717	0.084	0.155
C36297XS	50/10	----	1.390	1.083	0.104	0.024
C36298AS	50/10	11.8	1.440	1.010	0.105	0.196
C36299XS	50/25	----	1.503	0.763	0.097	0.028
C36290AS	50/25	11.8	1.460	0.787	0.097	0.154
C3629!XS	73/25	----	1.657	0.953	0.114	0.033
C3629@AS	73/25	11.8	1.647	0.887	0.110	0.174
C3629#XS	73/62	----	2.163	0.783	0.134	0.048
C3629$AS	73/62	11.8	2.127	0.827	0.135	0.169
C3629%XS	50/50	----	1.750	0.733	0.116	0.036
C3629^AS	50/50	11.8	1.797	0.690	0.116	0.157
C3629&XS	25/50	----	1.523	0.560	0.101	0.029
C3629JAS	25/50	11.8	1.443	0.570	0.101	0.133
C36301XS	50/62	----	1.773	0.750	0.117	0.035
C36302AS	50/62	11.8	1.790	0.693	0.113	0.135
C36303XS	50/10	----	1.263	0.907	0.092	0.020
C36304AS	50/10	11.8	1.220	0.953	0.091	0.160
C36305XS	25/10	----	0.930	0.700	0.074	0.013
C36306AS	25/10	11.8	0.927	0.657	0.074	0.147
C36307XS	25/25	----	1.117	0.573	0.083	0.018
C36308AS	25/25	11.8	1.103	0.607	0.084	0.133

Table D.1 (Continued): Original Quadrex Partial Pressure Data

Data Set	WW/CW (liters/sec)	Argon Flow (scfh)	Partial Pressures (x 10^8 torr) N_2	O_2	CO_2	Ar
C36309XS	25/62	----	1.767	0.607	0.117	0.036
C36300AS	25/62	11.8	1.813	0.580	0.116	0.161
C3630!XS	73/62	----	2.300	0.840	0.134	0.051
C3630@AS	73/62	11.8	2.300	0.883	0.134	0.175

† 120 cfh air injected into evaporator
# 300 cfh air injected into evaporator
* 100 cfh air injected into evaporator

Table D.2 : Original Noncondensable Outgassing Rate Data

Data Set	WW/CW (liters/sec)	Argon Flow (scfh)	Outgassing Rate (mmols/sec) N_2	O_2	CO_2	Ar
C35174AS	50/50	12.0	57.44	12.83	3.06	1.34
C35176AS	10/50	19.0	34.81	5.00	2.07	0.69
C35183AS	10/10	11.8	23.44	12.16	1.86	0.32
C35184AS	10/10†	11.8	50.92	18.36	1.79	0.62
C35186AS	10/10#	11.8	99.44	29.65	1.70	1.14
C36072AS	25/25	11.8	31.14	11.49	2.95	0.75
C36074AS	10/25	11.8	26.36	10.29	2.74	0.61

Table D.2 (Continued): Original Noncondensable Outgassing Rate Data

Data Set	WW/CW (liters/sec)	Argon Flow (scfh)	Outgassing Rate (mmols/sec)			
			N_2	O_2	CO_2	Ar
C36076AS	10/50	11.8	39.46	11.01	3.35	0.92
C36078AS	10/62	11.8	47.75	11.98	3.54	1.13
C36082AS	10/10	11.8	17.36	12.19	2.12	0.36
C36084AS	10/25	11.8	26.06	10.94	2.50	0.58
C36086AS	10/50	11.8	40.12	10.47	3.05	0.93
C36088AS	10/62	11.8	49.13	12.79	3.63	1.13
C36080AS	50/25	11.8	41.27	20.58	2.96	1.01
C36092AS	10/10*	11.8	41.40	9.65	3.22	0.59
C36094AS	10/25*	11.8	54.06	13.43	3.21	0.90
C36096AS	10/25	11.8	28.93	10.19	2.94	0.59
C36098AS	73/25	11.8	51.44	22.12	3.50	1.15
C36090AS	73/50	11.8	93.87	30.75	4.15	1.85
C3609@AS	73/50	11.8	72.11	26.24	4.27	1.66
C36286AS	73/50	11.8	68.55	24.10	4.05	1.50
C36288AS	50/50	11.8	59.36	23.95	3.74	1.18
C36280AS	25/50	11.8	54.10	17.90	3.60	1.04
C3628@AS	25/25	11.8	39.36	20.36	2.93	0.66
C36292AS	50/62	11.8	68.97	23.68	4.46	1.44
C36294AS	25/62	11.8	60.43	20.97	4.15	1.20

Table D.2 (Continued): Original Noncondensable Outgassing Rate Data

Data Set	WW/CW (liters/sec)	Argon Flow (scfh)	Outgassing Rate (mmols/sec)			
			N_2	O_2	CO_2	Ar
C36296AS	25/10	11.8	28.07	20.07	2.35	0.39
C36298AS	50/10	11.8	33.23	23.31	2.42	0.58
C36290AS	50/25	11.8	45.36	24.45	3.01	0.84
C3629@AS	73/25	11.8	46.09	24.82	3.08	0.92
C3629$AS	73/62	11.8	68.80	26.75	4.37	1.52
C3629^AS	50/50	11.8	59.09	22.69	3.81	1.22
C3629JAS	25/50	11.8	53.72	21.22	3.76	1.01
C36302AS	50/62	11.8	70.63	27.35	4.46	1.38
C36304AS	50/10	11.8	34.14	26.67	2.55	0.53
C36306AS	25/10	11.8	27.30	19.35	2.18	0.38
C36308AS	25/25	11.8	37.85	20.83	2.88	0.62
C36300AS	25/62	11.8	57.69	18.46	3.69	1.18
C3630@AS	73/62	11.8	73.79	28.33	4.30	1.64

† 120 cfh air injected into evaporator
# 300 cfh air injected into evaporator
* 100 cfh air injected into evaporator

APPENDIX E

RGA SAMPLING SYSTEM/MASS BALANCE

E.1 RGA SAMPLING SYSTEM

The basic components of the RGA sampling system (see Figure E.1) are a 50 liter per second turbomolecular pump (#2) backed by a 1.0 cubic foot per minute rotary vane mechanical pump (#4). A 2-3/4" ConFlat tee (#1) acts as the high vacuum chamber for the Quadrex sensor. A normally open vent valve (#3) is attached to the turbomolecular pump to allow automatic venting of the high vacuum chamber whenever there is a power failure, or whenever the vacuum system is shut off. The RGA has a single switch to start the vacuum system. It runs on standard 120VAC and doesn't require water or liquid nitrogen for cooling, an air cooling system is all that is required on the turbomolecular pump under typical Kona weather conditions. These components are all mounted in a box for easy mobility and protection from adverse weather.

The RGA is used with a high pressure multicapillary inlet (#14). This allows sampling from four discrete locations at sampling pressures of between 2 atmospheres to 5 torr using two different sampling capillaries. For this investigation, however, only one location was used and thus only one sampling capillary. The sampling capillary used in this investigation was a 1/4" O.D. pre-cleaned, stainless steel capillary capable of sampling from pressures of 5 - 20 torr.

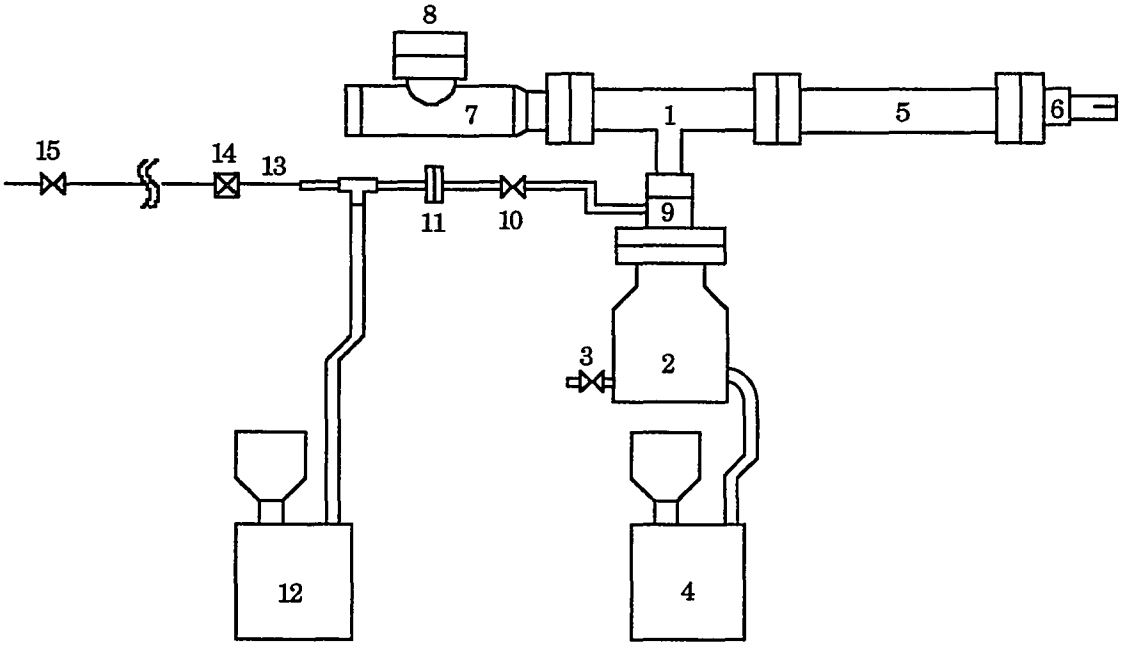

BASIC UNIT
1. 2-3/4" Conflat Tee
2. Turbo Pump
3. Automatic Venting Device
4. Rotary Vane Pump

QUADREX RGA
5. Extension Flange
6. Sensor Head

IPC-2 INLET
7. IPC-2 Pressure Converter
8. 2-3/4" Conflat Blank Flange

SINGLE CAPILLARY INLET
9. Double Sided Conflat Flange
10. Analyzer Valve
11. Orifice
12. Rotary Vane Pump
13. Capillary

MULTI-CAPILLARY INLET
14. Selector Valve
15. NUPRO Valve to Condenser Outlet

Figure E.1: Schematic of RGA Mass Spectrometer Sampling System

The capillary inlet is a dual stage pressure reduction system. The first pressure reduction of the sample is across the capillary (#13). It will be reduced to an intermediate pressure of approximately 5 torr. The sample is pumped by a second 1.0 CFM rotary vane mechanical pump (#12). This two-stage reduction technique will help prevent mass discrimination from occurring. The sample then achieves its second reduction across the orifice (#11).

The sample capillary is attached via stainless steel SWAGELOK fittings to a stainless steel NUPRO needle valve at the condenser outlet (#15) from which the sample is extracted.

E.2 MASS BALANCE

The following represents the calculations performed to attain a rough estimate of the relative contribution that atmospheric leaks have on the sample data. To attain this result, the following mass balance was performed across the sample lines (see Figure E.2) using the reported parameters which were common or expected values obtained during the data acquisition period. Ideal gas behavior is assumed which should be a good approximation under the experimental conditions (pressures) experienced in this investigation. Likewise, common atmospheric temperature is assumed to be the temperature of the gas throughout the length of the tube (302 °K).

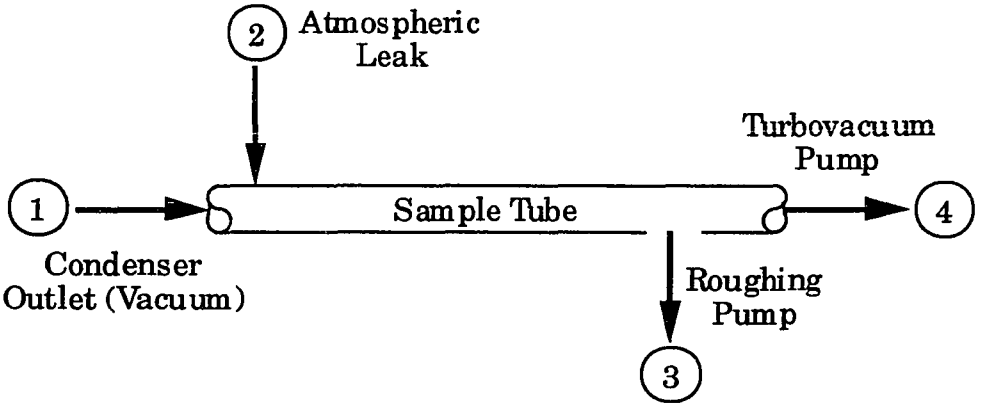

Figure E.2: Mass Balance Reference Points

Point 1: $P_1 = 11$ torr

$V_1 = ?$

$T_1 = 302\ ^{\circ}K$

$n_1 = ?$

Point 2: $P_2 = 1$ atm (760 torr)

$V_2 = ?$

$T_2 = 302\ ^{\circ}K$

$n_2 = ?$

Point 3: $P_{3,B}^{*} = 5$ torr (6.6×10^{-3} atm) CASE A

$P_{3,B} = ?$ CASE B

$\dot{V}_3^{\dagger} = 1.6\ m^3/h$ (0.44 l/s)

$T_3 = 302\ ^{\circ}K$

$n_3 = ?$

Point 4: $P_{4,B}^{\#} = 2.2 \times 10^{-6}$ torr (2.9×10^{-9} atm) CASE A

$P_{4,B} = 1.0 \times 10^{-5}$ torr (1.3×10^{-8} atm) CASE B

$V_4^{\dagger} = 55$ l/s

$T_4 = 302\ ^{\circ}K$

$n_4 = ?$

* Nominal pressure expected (estimate) by Inficon engineers according to manufacturers specifications given in Leybold-Heraeus [23].

† Manufacturers specifications [23].

\# Measured pressure of 3.0×10^{-6} torr adjusted for natural background of 0.8×10^{-6} torr experienced by the RGA.

CASE A: The valve at Point 1 is closed off to the HMTSTA and the only gas measured by the RGA is attributable only to atmospheric leaks into the sampling system.

CASE B: The valve at Point 1 is now open to the HMTSTA so the values obtained by the RGA represent the contribution of gases from the condenser outlet, the leak attributed to the HMTSTA, and the leak into the mass spectrometer sampling system measured in CASE A.

$$n_{4,A} = \{P_{4,A}V_3/RT\}*[MW_{air}]$$

$$= \{(2.9 \times 10^{-9})(55)/(0.082)(302)\}*[29] \qquad \text{(E-1)}$$

$$n_{4,A} = 1.87 \times 10^{-7}\ \text{g/s}$$

$$n_{4,B} = \{P_{4,B}V_3/RT\}*[MW_{air}]$$

$$= \{(1.3 \times 10^{-8})(55)/(0.082)(302)\}*[29] \qquad \text{(E-2)}$$

$$n_{4,B} = 8.3 \times 10^{-7}\ \text{g/s}$$

$$n_{3,A} = \{P_{3,A}V_3/RT\}*[MW_{air}]$$

$$= \{(6.6 \times 10^{-3})(0.44)/(0.082)(302)\}*[29] \quad \text{(E-3)}$$

$$n_{3,A} = 3.40 \times 10^{-3} \text{ g/s}$$

$$n_{4,A}/ n_{4,B} = n_{3,A} / n_{3,B} \text{ ====> } 1.87 / 8.3 = 3.40 / n_{3,B} \quad \text{(E-4)}$$

$$n_{3,B} = 1.51 \times 10^{-2} \text{ g/s}$$

$$P_{3,B} = \{n_{3,B}RT/V_3\} / [MW_{air}]$$

$$= \{(1.51 \times 10^{-2})(0.082)(302)/(0.44)\}/[29] \quad \text{(E-5)}$$

$$P_{3,B} = 2.93 \times 10^{-2} \text{ atm (22.3 torr)}$$

For CASE A: $n_2 = n_{3,A} + n_{4,A}$ (E-6)

$$n_2 = 3.4 \text{ mg/s}$$

For CASE B: $n_1 + n_2 = n_{3,B} + n_{4,B}$ (E-7)

$$n_1 = 11.7 \text{ mg/s}$$

Approximately 22% of the entire gas sampled in this particular, representative sample run is attributable to leaks in the mass spectrometer sample lines.

APPENDIX F

10 MW_{gross} NON-PREDEAERATED/REINJECTED OC-OTEC PLANT COMPONENT DESIGN CALCULATIONS

The following appendix represents the calculations performed to reach the thermodynamic properties presented earlier in this report for the 10 MW_{gross} non-predeaerated OC-OTEC system. Both the equations utilized to perform the calculations as well as the final results are presented. For iterative procedures, the initial value utilized to begin the iteration as well as the final value arrived through the iteration are presented to assist in comprehension of the design calculation procedure. The equations immediately following this discussion are the equations utilized throughout this investigation to determine the respective thermodynamic properties of the noncondensables, steam and seawater. These equations were obtained through various references which accompany each equation with its definition. Any reference to these thermodynamic properties in the remainder of the design calculations in this appendix as well as the following one for the predeaerated/reinjected system are referred to these equations.

Physical and thermodynamic properties of seawater:

$$Cp_{sw}(T) = 3.9937 + 3.82647\times10^{-4}(T) - 5.83008\times10^{-7}(T^2) + 2.14752\times10^{-8}(T^3) \quad [32] \qquad \text{(F-1)}$$

$$\mu_{sw}(T) = 1.88584\times10^{-3} - 5.841997\times10^{-5}(T) + 1.129032\times10^{-6}(T^2) - 1.20807\times10^{-8}(T^3) + 5.188375\times10^{-11}(T^4) \quad [32] \qquad \text{(F-2)}$$

$$\rho_{sw}(T) = 1026.1401 - 0.1828409\,(T) + 7.13456\times10^{-3}\,(T^2) - 3.40164\times10^{-4}\,(T^3) + 4.04591\times10^{-6}\,(T^4) - 1.605344\times10^{-8}\,(T^5) \quad [32] \qquad \text{(F-3)}$$

where

T = seawater temperature in $^{\circ}C$

Cp_{sw} = heat capacity of seawater (KJ/KG-$^{\circ}C$)

μ_{sw} = dynamic viscosity of seawater (KG/M-SEC)

ρ_{sw} = density of seawater (KG/M^3)

Physical and thermodynamic properties of steam:

$$h_{vap}(T) = 2501.389 - 2.37236\,(T) + 7.2288\times10^{-4}\,(T^2) - 1.52482\times10^{-5}\,(T^3) + 8.739\times10^{-9}\,(T^4) \quad [32] \qquad \text{(F-4)}$$

$$S_g(T) = 9.1565 - 2.67472\times10^{-2}\,(T) + 1.225378\times10^{-4}\,(T^2) - 4.3438\times10^{-7}\,(T^3) + 8.21672\times10^{-10}\,(T^4) \quad [32] \qquad \text{(F-5)}$$

$$T_{sat}(P) = -16.6867053 + 35.653865\,(P) - 15.529131\,(P^2) + 3.9159267\,(P^3) - 0.39651699\,(P^4) \quad [32] \qquad \text{(F-6)}$$

$$V_{steam}(T) = 205.925 - 13.1755\,(T) + 0.390727\,(T^2) - 6.13854\times10^{-3}\,(T^3) + 4.85293\times10^{-5}\,(T^4) - 1.598644\times10^{-7}\,(T^5) \quad [32] \qquad \text{(F-7)}$$

where

P = steam pressure KPa

T = steam temperature in $^{\circ}C$

h_{vap} = heat of vaporization of steam (KJ/KG)

S_g = entropy of saturated steam (KJ/KG-$^{\circ}C$)

T_{sat} = saturation temperature of steam ($^{\circ}C$)

V_{steam} = volume of saturated steam (M^3/KG)

Physical and thermodynamic properties of fresh water:

$$h_f(T) = -0.0276 + 4.2143\,(T) - 9.40824\times10^{-4}\,(T^2) + 8.99971\times10^{-6}\,(T^3) - 1.95223\times10^{-8}\,(T^4)\ [32] \quad \text{(F-8)}$$

$$P_{sat}(T) = 0.610802 + 0.0443917\,(T) + 0.14202\times10^{-2}\,(T^2) + 0.273291\times10^{-4}\,(T^3) + 0.262311\times10^{-6}\,(T^4) + 0.289737\times10^{-8}\,(T^5)\ [32] \quad \text{(F-9)}$$

$$S_f(T) = -1.1119\times10^{-4} + 1.54151\times10^{-2}\,(T) - 3.08479\times10^{-5}\,(T^2) + 9.08704\times10^{-8}\,(T^3) - 1.689982\times10^{-10}\,(T^4)\ [32] \quad \text{(F-10)}$$

where

T = temperature of water in $^{\circ}C$

h_f = saturated liquid enthalpy (KJ/KG)

MW_{H2O} = molecular weight of water = 18.02 KG/KGMOL [17]

P_{sat} = saturation pressure of water (KPa)

S_f = saturated liquid entropy of freshwater (KJ/KG-$^{\circ}C$)

Physical and thermodynamic properties of Nitrogen:

$$\ln C_{N2} = -172.4965 + 248.4262\,(100 / T^*) + 143.0738\,\ln(T^* / 100) - 21.7120\,(T^* / 100) + S^{o}/_{oo}\{-0.049781 + 0.025018\,(T^* / 100) - 0.0034861\,(T^* / 100)^2\}\ [47] \quad \text{(F-11)}$$

$$C_{pN2}(T^*) = \{28.90 - 0.1571\times10^{-2}\,(T^*) + 0.8081\times10^{-5}\,(T^{*2}) - 2.873\times10^{-9}\,(T^{*3})\} / MW_{N2}\ [17] \quad \text{(F-12)}$$

where

T^* = gas temperature ($^{\circ}K$)

C_{N2} = solubility of nitrogen in seawater (ml/l)

C_{pN2} = heat capacity of nitrogen (KJ/KG-$^{\circ}K$)

MW_{N2} = molecular weight of nitrogen = 28.02 (KG/KGMOL) [17]

Physical and thermodynamic properties of Oxygen:

$$\ln C_{O2} = -173.4292 + 249.6339\,(100 / T^*) + 143.3483 \ln (T^* / 100) - 21.8492\,(T^* / 100) + S‰ \{-0.033096 + 0.014259\,(T^* / 100) - 0.0017000\,(T^* / 100)^2\} \quad [47] \qquad \text{(F-13)}$$

$$C_{pO2}(T^*) = \{25.48 + 1.520\text{x}10^{-2}\,(T^*) - 0.7155\text{x}10^{-5}\,(T^{*2}) + 1.312\text{x}10^{-9}\,(T^{*3})\} / MW_{O2} \quad [17] \qquad \text{(F-14)}$$

where

T^* = gas temperature ($^\circ$K)

C_{O2} = solubility of oxygen in seawater (ml/l)

C_{pO2} = heat capacity of oxygen (KJ/KG-$^\circ$K)

MW_{O2} = molecular weight of oxygen = 32.00 (KG/KGMOL) [17]

Physical and thermodynamic properties of Argon:

$$\ln C_{Ar} = -173.5146 + 245.4510\,(100 / T^*) + 141.8222 \ln (T^* / 100) - 21.8020\,(T^* / 100) + S‰ \{-0.034474 + 0.014934\,(T^* / 100) - 0.0017729\,(T^* / 100)^2\} \quad [47] \qquad \text{(F-15)}$$

where

C_{Ar} = solubility of argon in seawater (ml/l)

C_{pAr} = heat capacity of argon = 0.5207 (KJ/KG-$^\circ$K) [17]

MW_{Ar} = molecular weight of argon = 39.944 (KG/KGMOL) [17]

Physical and thermodynamic properties of Carbon Dioxide:

$$\ln C_{CO2} = -60.2409 + 93.4517\,(100 / T^*) + 23.3585 \ln (T / 100) + S^{o}/_{oo}\{0.023517 - 0.023656\,(T / 100) + 0.0047036\,(T / 100)^2\}\ [39] \quad \text{(F-16)}$$

$$C_{PCO2}(T^*) = \{22.26 + 5.981\text{x}10^{-2}\,(T^*) - 3.501\text{x}10^{-5}\,(T^{*2}) + 7.469\text{x}10^{-9}\,(T^{*3})\} / MW_{CO2}\ [17] \quad \text{(F-17)}$$

where

T^* = gas temperature (^{o}K)

C_{CO2} = solubility of carbon dioxide in seawater (MOL/KG_{sw}-ATM)

C_{PCO2} = heat capacity of carbon dioxide (KJ/KG- ^{o}K)

MW_{CO2} = molecular weight of CO_2 = 44.01 (KG/KGMOL) [17]

The following component analyses utilize these physical values and thermodynamic properties in conjunction with the presented formulas to model the 10 MW_{gross} non-predeaerated OC- OTEC facility described earlier in this investigation. All numerical subscripts refer to Figure 4.1 to simplify definition of system stream path values.

F.1 TURBINE DESIGN

Initially, the turbine inlet steam temperature and exit steam temperature are set at values suggested by M.I.T. [27] so that the other parameters are set at:

Turbine inlet steam:

$T_{s,5}$	=	22.50 °C	295.65 °K
$P_{sat,5}$	=	2.72 KPa	
$H_{g,5}$	=	2542.7 KJ/KG	
$H_{f,5}$	=	94.4 KJ/KG	
$S_{g,5}$	=	8.612 KJ/KG-°C	
$S_{f,5}$	=	0.332 KJ/KG-°C	
$V_{steam,5}$	=	48.9 M^3/KG	

Turbine outlet steam:

$T_{s,6}$	=	12.00 °C	285.15 °K
$P_{sat,6}$	=	1.40 KPa	
$H_{g,6}$	=	2523.4 KJ/KG	
$H_{f,6}$	=	50.42 KJ/KG	
$S_{g,6}$	=	8.85 KJ/KG-°C	
$S_{f,6}$	=	0.181 KJ/KG-°C	
$V_{steam,6}$	=	94.4 M^3/KG	

Assuming isentropic expansion through the rotor and stator sections of the turbine suggest that the inlet and outlet steam have the same entropy [32] (see Figure 4.3).

$$S_5 = S_{6ss} \tag{F-18}$$

Therefore, the isentropic outlet conditions can be determined as:

x_{6ss} = isentropic outlet steam quality

$$= (S_{g,5} - S_{f,6}) / (S_{g,6} - S_{f,6}) = 0.9723 \tag{F-19}$$

h_{6ss} = isentropic outlet enthalpy

$= H_{f,6} + x_{6ss}(H_{g,6} - H_{f,6}) = 2454.9$ KJ/KG (F-20)

With the inlet and isentropic outlet conditions completely described, an iterative approach is now performed to determine the actual outlet conditions and the inlet and outlet stagnation conditions [32]. Since the turbine dimensions are unknown, the steam inlet velocity (C_5) and the turbine steam exit velocity (C_6) are unknown. For the first iteration assume

$$C_5 = 60.00 \text{ m/s} \quad \text{and} \quad C_6 = 0.00 \text{ m/s}.$$

The final value arrived at for these velocities after completing the iterative process are:

$$C_5 = 59.7 \text{ m/s} \quad \text{and} \quad C_6 = 112.1 \text{ m/s}.$$

The inlet stagnation enthalpy (h_{05}) is the steam enthalpy created by the temperature and the steam inlet kinetic energy [32] as

$$h_{05} = h_5 + C_5^2 / (2 \times 1000) = 2544.5 \text{ KJ/KG}. \quad \text{(F-21)}$$

The factor of 1000 simply converts the kinetic energy factor to units of KJ/KG [32]. The isentropic exit velocity (C_{6ss}) is now determined from the inlet steam velocity (C_5), the isentropic steam exit quality (x_{6ss}) and the ratio of the exit to inlet steam specific volumes ($V_{steam,6}$ and $V_{steam,5}$, respectively) [32] as

$$C_{6ss} = C_5 x_{6ss} (V_{steam,6} / V_{steam,5}) = 112.1 \text{ m/s}. \quad \text{(F-22)}$$

Now the isentropic exit enthalpy (h_{06ss}) is determined

$$h_{06ss} = h_6 + C_{6ss}^2 / (2 \times 1000) = 2461.2 \text{ KJ/KG}. \quad \text{(F-23)}$$

Parsons et al. [32] define two isentropic enthalpy drops across the turbine, the total-to-total ($\Delta h_{t\text{-}t}$) and the total-to-static ($\Delta h_{t\text{-}s}$) as

$$\Delta h_{t\text{-}t} = h_{05} - h_{06ss} = 83.3 \text{ KJ/KG} \quad \text{(F-24)}$$

$$\Delta h_{t\text{-}s} = h_{05} - h_{6ss} = 89.6 \text{ KJ/KG.} \quad \text{(F-25)}$$

With these values now determined, the design steam mass flow rate through the turbine can be determined as

$$m_{steam} = Po_{gross} / (\Delta h_{t\text{-}s}\, \eta_{t\text{-}s}\, \eta_{gen}\, N_{turb}) = 29.4 \text{ KG/S} \quad \text{(F-26)}$$

where

Po_{gross} = gross power of plant = 10,000 KW (design)

$\eta_{t\text{-}s}$ = total-to-static turbine efficiency = 0.80 [32]

η_{gen} = generator efficiency = 0.95 [32]

N_{turb} = number of turbines = 5 (technological limit 2 MW/turbine) [27].

The actual exit stagnation enthalpy (h_{06}) can now be found from the definition of total-to-static efficiency

$$\eta_{t\text{-}s} = (h_{05} - h_{06}) / (h_{05} - h_{06ss}) \Longrightarrow h_{06} = 2472.8 \text{ KJ/KG.} \quad \text{(F-27)}$$

From Figure 4.3 it can be seen that the constant pressure lines are nearly parallel [32]; from which the actual outlet enthalpy (h_6) can be determined if C_6 is known:

for first iteration assume outlet velocity (C_6) is equivalent to the outlet stagnation velolcity (C_{6ss}) :

$$C_6 = C_{6ss} = 112.1 \text{ m/s}$$

final determined value after iterative procedure:

$$C_6 = 112.61 \text{ m/s}$$

$$h_6 = h_{06} - C_6^2 / (2 \times 1000) = 2466.5 \text{ KJ/KG.} \quad \text{(F-28)}$$

This sets the actual outlet steam quality (x_6) at

$$x_6 = (h_6 - H_{f,6}) / (H_{g,6} - H_{f,6}) = 0.9770 \quad \text{(F-29)}$$

Now that the inlet and outlet turbine conditions have been approximated, the turbine design speed and size can be approximated as well. Parsons et al. [32] define the dimensionless specific diameter (d_s) and the maximum specific speed-specific diameter product ($n_s\, d_s$) as

$$d_s = \{\sqrt{8}\, C_o / [\pi\, C_6\, (1-\lambda^2)]\}^{1/2} = 2.01 \qquad \text{(F-30)}$$

$$(n_s\, d_s)_{max} = \sqrt{8}\, U_t / C_o \;\Longrightarrow\; n_s = 1.55 \qquad \text{(F-31)}$$

where

$$C_o = \text{spouting velocity} = (2\ \Delta h_{t\text{-}t}\ 1000)^{1/2} = 408.2\ \text{M/S} \qquad \text{(F-32)}$$

λ = hub-to-tip ratio = 0.44 [32]

U_t = maximum tip speed = 450 M/S [8].

The volumetric flow rate of steam through the turbine is found as

$$V_6 = V_{steam,6}\, m_{steam}\, x_6 = 2710.6\ M^3/S \qquad \text{(F-33)}$$

which combined with the definition of specific speed (n_s) yields the maximum rotational speed (ω_t) as

$$n_s = \omega_t \sqrt{V_{steam,6}} / (C_o^2 / 2)^{3/4} \;\Longrightarrow\; \omega_t = 782 \qquad \text{(F-34)}$$

$$RPM_t = \omega_t\, 60 / (2\,\pi) = 7468 \;\Longrightarrow \qquad \text{(F-35)}$$

RPM_t = 7440 RPM (even multiple of 60 for ease in design).

Now recalculate n_s and ω_t to coincide with the actual RPM_t

$$n_s = 1.54$$

$$\omega_t = 779$$

From the definition of dimensionless diameter (d_s) the actual turbine diameter can be found:

$$D_t = \sqrt{V_{steam,6}}\, d_s / (\Delta h_{t\text{-}t}\, 1000)^{1/4} = 6.16\ \text{M.} \qquad \text{(F-36)}$$

Now the steam flow area and hence the steam inlet and outlet flow velocities can be found as

$$A_t = \pi D_t^2 (1 - \lambda^2) / 4 = 24.1 \text{ M}^2 \quad \text{(F-37)}$$

$$C_5 = V_{steam,5} \, m_{steam} / A_t = 59.7 \text{ M/S} \quad \text{(F-38)}$$

$$C_6 = V_6 / A_t = 112.6 \text{ M/S} \quad \text{(F-39)}$$

From here the iteration is repeated until the outlet steam velocities (C_6) converge to ± 0.1% from beginning to end of iterative procedure.

Finally, the turbine power density is calculated according to the area of each turbine as

$$Po_{density} = Po_{gross} / (N_{turb} \, \pi D_t^2 / 4) = 67.0 \text{ KW/M}^2. \quad \text{(F-40)}$$

Section 4.2.2 of this report gives the general description of the detailed procedures outlined in this section. Some of the values determined in this section will be further utilized in the subsequent sections.

F.2 TURBINE DIFFUSER

The diffuser inlet conditions are set at the turbine exit conditions determined in the previous section with the inlet pressure assumed to be the saturation pressure ($P_6 = P_{sat,6}$) calculated previously. The diffuser inlet conditions are denoted with the subscript 6 and the exit conditions with 7 as prescribed by Figure 4.1. As in the turbine analysis, the subscript s denotes the isentropic end condition at P_7.

From the turbine analysis we can determine the turbine inlet steam flow ($m_{steam,5}$) (with assumed quality $x_5 = 1.0$) and turbine exit steam flow ($m_{steam,6}$) with the following equations:

$$m_{steam,5} = m_{steam} \, N_{turb} / x_6 = 150.3 \text{ KG/S} \quad \text{(F-41)}$$

$$m_{steam,6} = m_{steam} \, N_{turb} = 146.9 \text{ KG/S}. \quad \text{(F-42)}$$

The total turbine area ($A_{t,tot}$) is simply

$$A_{t,tot} = A_t N_{turb} = 120.4 M^2. \quad \text{(F-43)}$$

From this area the diffuser inlet steam velocity (C_{6*}) is determined

$$C_{6*} = m_{steam,6} V_6 / A_{t,tot} = 115.3 M/S. \quad \text{(F-44)}$$

The diffuser steam inlet enthalpy (h_6) is defined as:

$$h_6 = (1.0 - x_6) H_{f,6} + x_6 H_{g,6} = 2466.6 KJ/KG. \quad \text{(F-45)}$$

Parsons et al. [32] suggest setting the diffuser steam exit velocity (C_7) for this type of diffuser design at

$$C_7 = 0.5 C_{6*} = 57.6 M/S. \quad \text{(F-46)}$$

From the definition of diffuser efficiency (η_d) the isentropic steam exit velocity (C_{7s}) can be determined

$$\eta_d = (h_{7s} - h_6) / (h_7 - h_6) = (C_{6*}^2 - C_{7s}^2) / (C_{6*}^2 - C_7^2) ==> \quad \text{(F-47)}$$

$$C_{7s} = 72.9 M/S$$

where

η_d = turbine diffuser efficiency = 0.80 [32].

In order to determine the diffuser outlet conditions, an iterative process is now necessary. For the first iteration the outlet steam specific volume ($V_{steam,7}$) is set equal to the inlet steam specific volume ($V_{steam,6}$).

$$V_{steam,7} = V_{steam,6} = 94.4 M^3/KG$$

Final value after iterative procedure yields

$$V_{steam,7} = 91.6 M^3/KG.$$

Parsons et al. [32] suggest that by assuming that the constant pressure lines in Figure 4.4 do not diverge, the pressure loss through the diffuser (ΔP_d) can be approximated as

$$\Delta P_d = (C_{7s}^2 - C_7^2) / (2 \times 1000 V_7) = 0.011 KPa \quad \text{(F-48)}$$

where the factor 1000 converts the pressure drop from Pa to KPa. From this pressure drop the diffuser outlet pressure (P_7) can now be found as

$$P_7 = P_6 + [C_6^{*2} / (2 \times 1000\ V_6)] - [C_7^2 / (2 \times 1000\ V_7)] - \Delta P_d \qquad \text{(F-49)}$$

$$= 1.44 \text{ KPa.}$$

By assuming saturation conditions at the diffuser outlet condition, the outlet steam temperature (T_7) can now be determined as described at the beginning of this appendix at P_7

$$T_{7,d} = 12.47\ ^{\circ}\text{C} \qquad 285.62\ ^{\circ}\text{K}$$

from which the new specific volume ($V_{7,d}$) is recalculated

$$V_{7,d} = 91.6\ \text{M}^3/\text{S}$$

and the procedure is repeated until the final outlet specific volume coincides to the specific volume utilized to begin the procedure to within ± 0.1%.

With the outlet conditions defined by the outlet steam temperature (T_7), the isentropic steam quality is defined by

$$x_{7s} = (S_{g,7} - S_{f,6}) / (S_{g,6} - S_{f,6}) = 0.9987 \qquad \text{(F-50)}$$

which can be used to find the isentropic outlet enthalpy (h_{7s})

$$h_{7s} = (1 - x_{7s})\, H_{f,7} + x_{7s}\, H_{g,7} = 2521.1 \text{ KJ/KG.} \qquad \text{(F-51)}$$

The isentropic enthalpy, with the knowledge of the diffuser efficiency (η_d), yields the outlet enthalpy (h_7)

$$h_7 = h_6 + [(h_{7s} - h_6) / \eta_d] = 2534.7 \text{ KJ/KG} \qquad \text{(F-52)}$$

and the outlet steam quality (x_7)

$$x_7 = (h_7 - H_{f,7}) / (H_{g,7} - H_{f,7}) = 1.004. \qquad \text{(F-53)}$$

A value of $x_7 > 1.0$ indicates supersaturation of the steam; however, it is assumed that there is enough liquid available at the diffuser exit to avoid this so the exit quality (x_7) is set to 1.0 [32].

The diffuser steam exit mass flow rate ($m_{steam,7}$) is therefore defined by

$$m_{steam,7} = m_{steam,6}\, x_7 = 146.9 \text{ KG/S.} \qquad \text{(F-54)}$$

Balje [2] defines the parameter necessary for defining the size of the diffuser is the pressure recovery factor (Cp) defined as

$$Cp = [C_6{}^{*2} - C_7{}^2 - (2\, \Delta P_d\, V_7)] / C_6{}^{*2} = 0.750. \qquad \text{(F-55)}$$

From Figure 4.5 [2] for the minimum $L_d / D_{d,6}$, $D_{d,7}/ D_{d,6}$ and θ_d from the figure we obtain

$$L_d / D_{d,6} = 3.90$$

$$D_{d,7} / D_{d,6} = 1.68$$

$$\theta d = 5.00^{\circ}$$

where

$D_{d,6}$ = diffuser inlet diameter = D_t = 6.17 M

$D_{d,7}$ = diffuser outlet diameter = 10.37 M

L_d = diffuser length = 24.06 M.

The graphical calculations are checked by determining the diffuser half angle (θ_d) empirically as

$$\theta_d = \tan^{-1} [(D_{d,7} - D_{d,6}) / 2\, L_d] = 4.99^{\circ}. \qquad \text{(F-56)}$$

Parsons et al. [32] suggest that these correlations are valid for a diffuser pressure recovery factor (Cp) within the range 0.40 and 0.85.

F.3 EVAPORATOR AND MIST REMOVAL DEVICE

The mist removal exit conditions (path 5 in Figure 4.1) have been defined previously in the turbine entrance calculations. The warm seawater resource temperature is set arbitrarily at a temperature common to tropical ocean

locations most suitable to OC-OTEC development. This sets the seawater entrance conditions at

$$T_1 = T_2 = 27.00\,^{\circ}C \qquad 300.15\,^{\circ}K$$

$$P_{sat,1} = P_{sat,2} = 3.56\ KPa$$

$$H_{g,1} = H_{g,2} = 2550.9\ KJ/KG$$

$$H_{f,1} = H_{f,2} = 113.2\ KJ/KG$$

$$S_{g,1} = S_{g,2} = 8.52\ KJ/KG\text{-}^{\circ}C$$

$$S_{f,1} = S_{f,2} = 0.395\ KJ/KG\text{-}^{\circ}C$$

$$V_{g,1} = V_{g,2} = 37.83\ M^3/KG.$$

Initially, the spout velocity ($X_{sp,E}$), the spout diameter ($D_{sp,E}$) and the spout height ($h_{sp,E}$) above the seawater drain pool are all assumed according to values suggested by Parsons et al. [32] as

$$X_{sp,E} = 2.00\ M/S$$

$$D_{sp,E} = 0.127\ M$$

$$h_{sp,E} = 0.50\ M.$$

The evaporator effectiveness (ε_E) is assessed from data presented by Bharathan and Penney [4] for a spout evaporator with one enhancement and the assumed spout velocity as

$$\varepsilon_E = 0.91$$

with the evaporator effectiveness defined as

$$\varepsilon_E = (T_2 - T_3) / (T_2 - T_{4,E}). \qquad \text{(F-57)}$$

The mist removal device included in this design introduces an evaporator-turbine pressure drop and thus $T_4 \neq T_5$ ($T_4 > T_5$) and T_4 must be determined. Since only the turbine entrance conditions (5) are known, an

iterative procedure must be employed. For the first iteration the temperature at the inlet of the mist removal device is set at

$$T_{4,mr} = T_5 = 22.50\,^{\circ}C.$$

The final value after the iterative process yields

$$T_{4,mr} = 23.10\,^{\circ}C.$$

Parsons et al. [32] suggest a pressure drop coefficient (K_{mr}) and a mist removal steam velocity (C_{mr}) of

$$K_{mr} = 10.0$$

$$C_{mr} = 30.00\ M/S.$$

With the estimated mist removal inlet steam temperature an estimated pressure drop (ΔP_{mr}) can be determined

$$\Delta P_{mr} = K_{mr}\,\rho_4\,C_{mr}^2/2 = 95.3\ Pa. \qquad \text{(F-58)}$$

Assuming that the steam is at saturation entering the turbine, the pressure at the mist removal exit must be $P_{sat,5}$ which allows an estimate of the mist removal inlet steam pressure (P_4) of

$$P_4 = P_{sat,5} - \Delta P_{mr} = 2.82\ KPa \qquad \text{(F-59)}$$

from which an estimated inlet steam temperature ($T_{4,mr}$) can be determined assuming saturation of steam. This procedure is repeated until the steam density (ρ_4) changes less than ± 0.1% from one iteration to the next [32].

The mass of steam flow from the evaporator ($m_{steam,4}$) is assumed equal to the mass of steam entering the turbine ($m_{steam,5}$). The area required for the mist removal device (A_{mr}) is then determined as

$$A_{mr} = m_{steam,5} / (X_{mr}\,\rho_4) = 236.7\ M^2. \qquad \text{(F-60)}$$

The evaporator steam generation temperature ($T_{4,E}$) is found in a similar manner to the mist removal inlet steam temperature ($T_{4,mr}$) by first

determining the evaporator-turbine passage pressure drop ($\Delta P_{E\text{-}t}$). However, in this case, the steam generation velocity (C_E) is unknown and an iterative procedure is required with the initial steam generation temperature ($T_{4,E}$) assumed to be equal to the mist removal inlet steam temperature ($T_{4,mr}$)

$$T_{4,E} = T_{4,mr} = 23.10\,^{\circ}C.$$

The final value achieved after the iterative process is

$$T_{4,E} = 23.11\,^{\circ}C.$$

An estimated warm water outlet temperature (T_3) and the design warm water flow rate (m_2) can be determined from the evaporator effectiveness (ε_E) and this estimated steam generation temperature ($T_{4,E}$) as

$$T_3 = T_2 - \varepsilon_E (T_2 - T_{4,E}) = 23.46\,^{\circ}C \qquad \text{(F-61)}$$

$$m_2 = (m_{steam,4}\, h_{vap,4,E}) / [Cp_2 (T_2 - T_3)] = 25953\ KG/S \qquad \text{(F-62)}$$

where

$h_{vap,4,E}$ = heat of vaporization at $T_{4,E}$ = 2446.7 KJ/KG

Cp_2 = heat capacity of seawater at T_2 = 4.004 KJ/KG-$^{\circ}$C.

The mass flow of warm water per spout ($m_{sp,E}$) is then determined as

$$m_{sp,E} = \rho_2\, X_{sp,E}\, \pi\, D_{sp,E}^2 / 4 = 25.88\ KG/S \qquad \text{(F-63)}$$

which yields an estimate of the number of spouts ($N_{sp,E}$) necessary as

$$N_{sp,E} = m_2 / m_{sp,E} = 1002.7 \Longrightarrow 1003\ \text{spouts.} \qquad \text{(F-64)}$$

Assuming a hexagonal configuration for the spouts with a center-center spacing of 0.7 M between spouts yields an approximate area of 0.4243 M^2/spout [32] which yields an approximate evaporator area (A_E) of

$$A_E = N_{sp,E}\,(0.4243) = 425.57\ M^2 \qquad \text{(F-65)}$$

From this planform area the evaporator-turbine passage inlet velocity (C_4) can now be found

$$C_4 = m_{steam,4} / (A_E \rho_4) = 16.67 \text{ M/S} \quad \text{(F-66)}$$

which leads to an evaporator-turbine passage pressure drop ($\Delta P_{E\text{-}t}$) of

$$\Delta P_{E\text{-}t} = K_{E\text{-}t} \rho_4 C_4^2 / 2 = 1.47 \text{ Pa} \quad \text{(F-67)}$$

where

ρ_4 = steam density at $T_{4,E}$ = 0.0212 KG/M^3

$K_{E\text{-}t}$ = evaporator-turbine pressure loss coefficient = 0.50 [32].

This pressure drop then determines the evaporator steam generation pressure ($P_{4,E}$)

$$P_{4,E} = P_{4,mr} + \Delta P_{E\text{-}t} = 2.82 \text{ KPa} \quad \text{(F-68)}$$

which is then used to revise the estimated steam generation temperature ($T_{4,E}$) and the procedure from equation F-61 is repeated until the $T_{4,E}$ changes less than ± 0.1 % from one iteration to the next.

With the design warm water flow rate determined (m_2) the noncondensable desorption rate can now be estimated from the desorption rates determined previously in the experimental portion of this report.

Warm water outgassing %:

$x_{N2,E}$ = 0.72

$x_{O2,E}$ = 0.81

$x_{Ar,E}$ = 0.70

$x_{CO2,E}$ = 0.006 (total carbon)

Warm water entrance noncondensable concentrations [21]:

$M_{N2,2}$ = 0.380 MMOL/L

$M_{O2,2}$ = 0.204 MMOL/L

$$M_{Ar,2} = 0.0100 \text{ MMOL/L}$$

$$M_{CO2,2} = 1.93 \text{ MMOL/L (total carbon)}$$

From these values the molar release of each noncondensable is determined as

$$M_{N2,DES} = x_{N2,E} M_{N2,2} = 0.274 \text{ MMOL/L} \quad \text{(F-69)}$$

$$M_{O2,DES} = x_{O2,E} M_{O2,2} = 0.204 \text{ MMOL/L} \quad \text{(F-70)}$$

$$M_{Ar,DES} = x_{Ar,E} M_{Ar,2} = 0.0070 \text{ MMOL/L} \quad \text{(F-71)}$$

$$M_{CO2,DES} = x_{CO2,E} M_{CO2,2} = 0.0110 \text{ MMOL/L} \quad \text{(F-72)}$$

which delivers the mass release of noncondensables as

$$m_{N2,DES} = M_{N2,DES} m_2 MW_{N2} / (1000 \rho_2) = 0.195 \text{ KG/S} \quad \text{(F-73)}$$

$$m_{O2,DES} = M_{O2,DES} m_2 MW_{O2} / (1000 \rho_2) = 0.134 \text{ KG/S} \quad \text{(F-74)}$$

$$m_{Ar,DES} = M_{Ar,DES} m_2 MW_{Ar} / (1000 \rho_2) = 0.0071 \text{ KG/S} \quad \text{(F-75)}$$

$$m_{CO2,DES} = M_{CO2,DES} m_2 MW_{CO2} / (1000 \rho_2) = 0.0123 \text{ KG/S} \quad \text{(F-76)}$$

where the factor 1000 converts G/S to KG/S.

These mass flows of noncondensables are not the only noncondensables attributable to the evaporator system. Any vacuum containment vessel such as the evaporator in this design will contain leaks which permit atmospheric air into the containment vessel. Since the respective atmospheric leakage will be specific for each particular vessel, with proper design and manufacturing care, this source of noncondensables in an OC-OTEC system can be minimized. Parsons et al. [32] suggest a simple conservative formula for estimating atmospheric leakage of air into the evaporator as

$$m_{air,lk,E} = 0.005 Po_{gross} / 1000 = 0.05 \text{ KG/S} \quad \text{(F-77)}$$

which combined with the known mass fraction of each noncondensable in the air determined in Kona earlier in this report as

$$x_{N2,air} = 0.788$$

$$x_{O2,air} = 0.185$$

$$x_{Ar,air} = 0.0065$$

$$x_{CO2,air} = 0.0002$$

$$x_{H2O,air} = 0.0402$$

yields a mass flow of noncondensables attributable to atmospheric leakage

$$m_{N2,lk,E} = x_{N2,air}\, m_{air,lk,E} = 0.0394 \text{ KG/S} \quad \text{(F-78)}$$

$$m_{O2,lk,E} = x_{O2,air}\, m_{air,lk,E} = 0.0092 \text{ KG/S} \quad \text{(F-79)}$$

$$m_{Ar,lk,E} = x_{Ar,air}\, m_{air,lk,E} = 0.0003 \text{ KG/S} \quad \text{(F-80)}$$

$$m_{CO2,lk,E} = x_{CO2,air}\, m_{air,lk,E} = 0.0000 \text{ KG/S} \quad \text{(F-81)}$$

$$m_{H2O,lk,E} = x_{H2O,air}\, m_{air,lk,E} = 0.0020 \text{ KG/S.} \quad \text{(F-82)}$$

The total noncondensable mass flows from the evaporator are defined as

$$m_{N2,E} = m_{N2,lk,E} + m_{N2,DES} = 0.234 \text{ KG/S} \quad \text{(F-83)}$$

$$m_{O2,E} = m_{O2,lk,E} + m_{O2,DES} = 0.144 \text{ KG/S} \quad \text{(F-84)}$$

$$m_{Ar,E} = m_{Ar,lk,E} + m_{Ar,DES} = 0.0074 \text{ KG/S} \quad \text{(F-85)}$$

$$m_{CO2,E} = m_{CO2,lk,E} + m_{CO2,DES} = 0.0123 \text{ KG/S} \quad \text{(F-86)}$$

$$m_{H20,E} = m_{steam,4} + m_{H20,lk,E} = 150.3 \text{ KG/S.} \quad \text{(F-87)}$$

The noncondensable mass flow ($m_{NC,E}$) from the evaporator becomes

$$m_{NC,E} = m_{N2,E} + m_{O2,E} + m_{Ar,E} + m_{CO2,E} = 0.400 \text{ KG/S} \quad \text{(F-88)}$$

The total moles of noncondensables in the evaporator is then determined

$$M_{N2,E} = m_{N2,E} / MW_{N2} = 0.0084 \text{ KG-MOL/S} \quad \text{(F-89)}$$

$$M_{O2,E} = m_{O2,E} / MW_{O2} = 0.0045 \text{ KG-MOL/S} \quad \text{(F-90)}$$

$$M_{Ar,E} = m_{Ar,E} / MW_{Ar} = 0.0002 \text{ KG-MOL/S} \quad \text{(F-91)}$$

$$M_{CO2,E} = m_{CO2,E} / MW_{CO2} = 0.0003 \text{ KG-MOL/S} \quad \text{(F-92)}$$

$$M_{H2O,E} = m_{H2O,E} / MW_{H2O} = 8.3454 \text{ KG-MOL/S} \quad \text{(F-93)}$$

which yields a mole fraction ($y_{steam,E}$) of steam in the evaporator of

$$y_{steam,E} = M_{H2O,E} / (M_{H2O,E} + M_{N2,E} + M_{O2,E} + M_{Ar,E} + M_{CO2,E}) \quad \text{(F-94)}$$

$$= 0.9984.$$

The evaporator working pressure (P_E) can then be determined as

$$P_E = P_{4,E} / y_{steam,E} = 2.83 \text{ KPa.} \quad \text{(F-95)}$$

Originally, in the turbine analysis section, the additional energy available due to the desorbed and leaked noncondensables accompanying the steam through the turbine section was ignored so that the turbine design analysis could be performed since the noncondensable flow was unknown and represents less than 0.3% error. At this point the power available from the existing designed turbine system is calculated as

$$Po_{gross} = m_{tot,gas,E} \Delta h_{t\text{-}s} \eta_{t\text{-}s} \eta_g = 10{,}027 \text{ KW} \quad \text{(F-96)}$$

where

$$m_{tot,gas,E} = \text{total gas flow from evaporator}$$

$$= m_{NC,E} + m_{steam,6} = 147.3 \text{ KG/S.} \quad \text{(F-97)}$$

F.4 DIRECT-CONTACT CONDENSER

The direct-contact condenser analysis begins by determining the inlet steam conditions to the co-current condensing section. Initially, it is necessary to determine the diffuser-condenser pressure drop ($\Delta P_{d\text{-}CO}$) in a similar manner as the evaporator-turbine pressure drop ($\Delta P_{E\text{-}t}$) found in the previous section by first finding the diffuser exit steam velocity from the diffuser exit temperature ($T_{7,d}$), steam specific volume ($V_{7,d}$), steam mass flow rate ($m_{steam,6}$) and the turbine flow area (A_t)

$$C_d = m_{steam,6} V_{7,d} / A_t = 57.6 \text{ M/S.} \quad \text{(F-98)}$$

With the steam velocity known, the pressure drop through the diffuser-condenser passage can be determined

$$\Delta P_{d\text{-}C} = K_{d\text{-}C} \rho_{7,d} C_d^2 / 2 = 0.018 \text{ KPa} \quad \text{(F-99)}$$

where

$K_{d\text{-}C}$ = diffuser-condenser passage loss coefficient = 1.0 [32].

This pressure drop accompanied by the diffuser exit steam pressure ($P_{7,d}$) yield the co-current condenser entrance pressure ($P_{7,CO}$) as

$$P_{7,CO} = P_{7,d} - \Delta P_{d\text{-}C} = 1.43 \text{ KPa} \quad \text{(F-100)}$$

which can be used to determine the co-current condenser entrance temperature ($T_{7,CO}$) using equation F-6 presented at the outset of this appendix

$$T_{7,CO} = 12.31 \text{ °C} \quad 285.46 \text{ °K.}$$

F.4.1 CO-CURRENT DESIGN

For the purposes of simplifying the design procedure, the condenser design has been broken into two distinct sections, the co-current and counter-current section.

With the utilization of a direct-contact condenser configuration chosen for this investigation, noncondensable gas desorption will accompany the cold water flow designed in this analysis. As discussed previously, the presence of these noncondensables and those accompanying the steam from the evaporator will hinder the condensation process and alter the shape of the heat load diagram for the condensing region. Therefore, since the design cold water

flow is unknown, an iterative process is necessary for further development of the direct-contact condenser.

For the first iteration in developing the heat load analysis for the co-current condensing section the noncondensable loading is assumed to be that desorbed only from the evaporator.

Upon completing the iterative process for the co-current condensing region the following noncondensable flows apply and are the values reflected in the following heat load development analysis.

$$M_{N2,CO} = 0.0179 \text{ KG-MOL/S}$$

$$M_{O2,CO} = 0.0055 \text{ KG-MOL/S}$$

$$M_{Ar,CO} = 0.0004 \text{ KG-MOL/S}$$

$$M_{CO2,CO} = 0.0007 \text{ KG-MOL/S}$$

$$M_{H2O,CO} = 8.1534 \text{ KG-MOL/S}$$

These molar flows correspond to the following mass flows

$$m_{N2,CO} = 0.5014 \text{ KG/S}$$

$$m_{O2,CO} = 0.1760 \text{ KG/S}$$

$$m_{Ar,CO} = 0.0160 \text{ KG/S}$$

$$m_{CO2,CO} = 0.0308 \text{ KG/S.}$$

From the molar values the mole fraction of steam in the co-current condenser section ($y_{steam,CO}$) can be determined

$$y_{steam,CO} = M_{H2O,CO} / (M_{H2O,CO} + M_{N2,CO} + M_{O2,CO} + M_{Ar,CO} + M_{CO2,CO})$$

$$= 0.9970. \qquad \text{(F-101)}$$

The total pressure of the co-current condensing section is then found assuming that the steam entering the condenser is saturated at the inlet steam temperature ($T_{7,CO}$) and thus the co-current pressure (P_{CO}) is defined as

$$P_{CO} = P_{7,CO} / y_{steam,CO} = 1.43 \text{ KPa.} \quad \text{(F-102)}$$

Parsons et al. [32] suggest that since the steam and seawater in the co-current section of the condenser are flowing in the same direction that the frictional vapor pressure drop can be assumed zero. Therefore this co-current pressure can be assumed constant throughout the entire co-current condensing region [32].

For the development of the heat load analysis and the co-current condenser design, Figure 4.7 should be referred to assist in clarifying the procedure. This figure, taken from Parsons et al. [32], shows the condenser heat load (HL_{CO}) plotted against the steam outlet temperature ($T_{7*,CO}$). As stated previously, the shape of the curve is dependant upon the steam inlet temperature ($T_{7,CO}$), the condenser pressure (P_{CO}) and the steam ($m_{steam,7}$) and noncondensable ($m_{NC,CO}$) inlet mass flow rates where

$$m_{steam,7} = m_{steam,6} = 146.9 \text{ KG/S.} \quad \text{(F-103)}$$

For a yet undetermined co-current steam exit temperature ($T_{7*,CO}$) the steam exit mass fraction ($x_{7*,CO}$) is

$$x_{7*,CO} = P_{sat,7*,CO} / P_{CO} \quad \text{(F-104)}$$

which yields a steam outlet mass flow ($m_{steam,7*,CO}$) rate of

$$m_{steam,7*,CO} = M_{NC,CO} MW_{H2O} x_{7*,CO} / (1 - x_{7*,CO}) \quad \text{(F-105)}$$

where

$$M_{NC,CO} = M_{N2,CO} + M_{O2,CO} + M_{Ar,CO} + M_{CO2,CO}. \quad \text{(F-106)}$$

Parsons et al. [32] describe the heat load as composed of the latent heat required to condense the difference in inlet ($m_{steam,7}$) and outlet ($m_{steam,7*,CO}$) steam mass flow rates, the sensible load required to cool the condensed steam

and the sensible load required to cool the noncondensables present in the co-current condensing region:

$$HL_{CO} = m_{steam,7}\, H_{g,7,CO} - m_{steam,7*,CO}\, H_{g,7*,CO} - (m_{steam,7} - m_{steam,7*,CO})\, H_{f,7*,CO} - (m_{N2,CO}\, C_{PN2,7,CO} + m_{O2,CO}\, C_{PO2,7,CO} + m_{Ar,CO}\, C_{PAr,7,CO} + m_{CO2,CO}\, C_{PCO2,7,CO})\,(T_{7,CO} - T_{7*,CO}). \quad \text{(F-107)}$$

Initially, the maximum heat load ($HL_{max,CO}$) is determined by setting the steam outlet temperature ($T_{7*,CO}$) equal to the inlet cold water temperature (T_{11})

$$HL_{max,CO} = 365935 \text{ KW}.$$

This represents the "ideal" line from the origin to point A in Figure 4.7. Realistically, it is impossible for the exit steam temperature to ever reach the inlet cold water temperature since this would require an infinite contact time between steam and cooling water. Parsons et al. [32] suggest that the slope of this "ideal flow" water line is directly related to the cold water mass flow ($m_{11,CO}$) times its specific heat (C_{p11}) as

$$m_{11,CO,ideal} = HL_{max,CO} / [C_{p11}\,(T_{7,CO} - T_{11})] = 12534 \text{ KG/S}. \quad \text{(F-108)}$$

The design heat load ($HL_{design,CO}$) for the co-current condenser region is defined by Parsons et al. [32] as the heat load where the "ideal" seawater line intersects the gas heat load curve (see Figure 4.7) and is determined iteratively since the exit steam temperature ($T_{7*,CO}$) is still unknown. An initial guess at the design steam exit temperature is used to obtain an initial design heat load approximation from which a new outlet steam temperature is obtained from

$$T_{7*,CO} = HL_{design,CO} / m_{11,CO,ideal}\, C_{p11} + T_{11} = 11.72\ ^{\circ}C \quad \text{(F-109)}$$

with a corresponding heat load of

$$HL_{design,CO} = 336543 \text{ KW}.$$

This procedure is repeated until the outlet steam temperature ($T_{7*,CO}$) changes less than ± 0.1% from one iteration to the next.

The ideal flow rate determined earlier has been deemed impossible since an infinite residence time in the co-current condenser is unreasonable, common engineering practice dictates a design/ideal scaling factor of 1.2 [32]. Therefore, the design seawater mass flow is

$$m_{11,CO,design} = 1.2\, m_{11,CO,ideal} = 15041 \text{ KG/S.} \qquad \text{(F-110)}$$

A heat balance utilizing this design mass water flow and the design heat load yield an outlet cold water temperature ($T_{9,CO}$) of

$$T_{9,CO} = T_{11} + HL_{design,CO} / m_{11,CO,design}\, C_{p11} = 10.60\ ^{\circ}C. \qquad \text{(F-111)}$$

Now, with an estimate of the design seawater flow rate, the noncondensable loading accompanying this seawater flow is recalculated in the same manner as described earlier in the evaporator analysis. In this case the desorption rates determined in the experimental section of this report for the cold water stream and the inlet cold water molar concentrations predicted by Krock [21] are utilized

$$x_{N2,11} = 0.98$$

$$x_{O2,11} = 1.00$$

$$x_{Ar,11} = 0.90$$

$$x_{CO2,11} = 0.013 \text{ ("total" carbon)}$$

and

$$M_{N2,11} = 0.564 \text{ MMOL/L}$$

$$M_{O2,11} = 0.0474 \text{ MMOL/L}$$

$$M_{Ar,11} = 0.0154 \text{ MMOL/L}$$

$$M_{CO2,11} = 2.33 \text{ MMOL/L ("total" carbon).}$$

Also, it is necessary to predict the atmospheric leakage into the direct-contact condenser and add this noncondensable flow to the combined flow of the co-current desorbed gases with those entering with the steam from the evaporator

$$m_{air,lk,CO} = 0.005\ Po_{gross} / 1000 = 0.0500\ KG/S. \qquad (F\text{-}112)$$

For the purposes of this direct-contact condenser investigation, it is assumed that all atmospheric leakage occurs in the co-current section of the condenser. Parsons et al. [32] suggest that this is a reasonable assumption since the counter-current section will most likely be shrouded to induce counter-current flow of the vapors and water and minimal leakage would be possible.

With the new noncondensable flow now determined the entire procedure from equation F-101 is repeated and a new heat load and flow rate are recomputed. This procedure is repeated until the noncondensable flows do not change more than ± 0.05% from one iteration to the next.

The co-current condenser effectiveness (ε_{CO}) is now determined from its definition

$$\varepsilon_{CO} = (T_9 - T_{11}) / (T_{7*,CO} - T_{11}) = 0.83 \qquad (F\text{-}113)$$

which yields the number of transfer units (NTU_{CO}) and height of the co-current contactor (Ht_{CO}) with height of transfer unit (HTU_{CO} = 0.30 M) predicted by [32]

$$NTU_{CO} = -\ln (1 - \varepsilon_{CO}) = 1.79 \qquad (F\text{-}114)$$

$$Ht_{CO} = NTU_{CO}\ HTU_{CO} = 0.54\ M. \qquad (F\text{-}115)$$

F.4.2 COUNTER-CURRENT CONDENSER DESIGN

The inlet conditions of the counter-current condenser are taken from the exit conditions of the co-current condenser section. The counter-current outlet conditions are specified by an assumed temperature difference ($\Delta T_{8\text{-}11} = 1.00$ °C) [32] between the outlet steam (T_8) and inlet cooling water (T_{11})

$$T_8 = T_{11} + \Delta T_{8\text{-}11} \tag{F-116}$$

and an assumed constant pressure throughout the counter-current section corresponding to the co-current condenser pressure ($P_{7*,CO} = P_{7*,CC}$) with an associated pressure drop ($\Delta P_{7*\text{-}8} = 0.2000$ KPa) [32] through the counter-current section used to determine the outlet pressure (P_8) to be used in the vent compressor analysis in the following section

$$P_8 = P_{7*,CC} - \Delta P_{7*\text{-}8} = 1.23 \text{ KPa.} \tag{F-117}$$

The assumption of constant pressure through the counter-current condensing section is not as accurate as it was for the co-current flow due to the expected pressure drop caused by the counter-flow of the condensing and cooling mediums. However, as will be discovered in the following development, the necessary mass flows of both the steam and especially the seawater are much less than that encountered in the co-current analysis and therefore this assumption will not introduce any significant error [32].

A similar heat load development procedure to that utilized in the co-current section is also employed for the counter-current analysis. For this purpose the noncondensable flows from the co-current section are used as a first approximation of expected flows in the counter-current design for the initial iteration.

The design outlet steam temperature (T_8) calculated above is used with these noncondensable flows to determine the design heat load for the counter-current condenser ($HL_{7*,CC}$) using equation F-107 discussed previously in the co-current design

$$HL_{7*,CC} = 25031 \text{ KW.}$$

From this value the ideal seawater mass flow ($m_{11,CC,ideal}$) can be determined

$$m_{11,CC,ideal} = HL_{7*,CC} / [C_{P11} (T_8 - T_{11})] = 932.24 \text{ KG/S} \qquad \text{(F-118)}$$

which yields a design seawater mass flow ($m_{11,CC,design}$) of

$$m_{11,CC,design} = 1.2 \; m_{11,CC,ideal} = 1118.69 \text{ KG/S.} \qquad \text{(F-119)}$$

Once again, with the design flow approximated, the noncondensables desorbed from this flow are determined as described above and the heat load development is repeated until the noncondensable flows differ less than ± 0.05% from one iteration to the next.

As described in the co-current section, a heat balance is performed to determine the outlet seawater temperature ($T_{9,CC}$)

$$T_{9,CC} = T_{11} + HL_{7*,CC} / (m_{11,CC,design} C_{P11}) = 10.60\,^{\circ}C \qquad \text{(F-120)}$$

which permits the calculation of the counter-current effectiveness (ε_{CC})

$$\varepsilon_{CC} = (T_{9,CC} - T_{11}) / (T_8 - T_{11}) = 0.83. \qquad \text{(F-121)}$$

The number of transfer units for the counter-current condenser (NTU_{CC}) is integrated numerically (100 iterations) utilizing

$$NTU_{CC} = \int_{T_{7*,CO}}^{T_8} dT_{steam} / (T_{steam} - T_{water}) = 2.34 \qquad \text{(F-122)}$$

and equation F-107 to determine the heat load value corresponding to the incremental steam temperature and the following equation to determine the

seawater temperature (T_{water}) corresponding to the incremental steam temperature (T_{steam}) through the counter-current region [32]

$$T_{water} = T_9 + [HL_{Tsteam} (T_{9,CC} - T_{11})] / HL_{7*,CC}. \quad \text{(F-123)}$$

The height of contactor (Ht_{CC}) for the counter-current condenser is thus

$$Ht_{CC} = NTU_{CC}\ HTU_{CC} = 0.70\ M. \quad \text{(F-124)}$$

The area required for each of the condenser sections is determined in two different manners. The first method determines the condenser area based on the liquid loading of each condenser section assuming seawater flow rates (x_{cond}), spout diameters ($d_{cont,cond}$) and a contactor spacing (A_{cont}) of

$$x_{cond} = 2.00\ M/S$$

$$d_{cont,cond} = 0.127\ M$$

$$A_{cont} = 0.4243\ M^2$$

suggested by [32]. The mass flow of seawater per contactor for each condenser section is found as

$$m_{cont,cond} = \rho_{11}\, x_{cond}\, \pi\, d_{cont,cond}^2 / 4 = 26.0\ KG/S \quad \text{(F-125)}$$

which yields a co-current area ($A_{CO,L}$) and counter-current area ($A_{CC,L}$) determined from the number of contactors ($N_{cont,CO}$ and $N_{cont,CC}$, respectively) as

$$N_{cont,CO} = m_{11,CO,design} / m_{cont,cond} = 579.0 \Longrightarrow 579 \quad \text{(F-126)}$$

$$N_{cont,CC} = m_{11,CO,design} / m_{cont,cond} = 43.1 \Longrightarrow 44 \quad \text{(F-127)}$$

$$A_{CO,L} = N_{cont,CO}\, A_{cont} = 245.7\ M^2 \quad \text{(F-128)}$$

$$A_{CC,L} = N_{cont,CC}\, A_{cont} = 18.7\ M^2. \quad \text{(F-129)}$$

The second area calculation is developed from the steam loading of each condenser section. With the steam flow through the co-current condenser

($m_{7,CO}$) and the steam flow through the counter-current section ($m_{7*,CC}$) defined

$$m_{7,CO} = 146.9 \text{ KG/S}$$

$$m_{7*,CC} = 10.9 \text{ KG/S}$$

and the steam velocity ($C_7 = C_{7*} = 57.6$ M/S) the steam flow area is defined as [32]

$$A_{CO,S} = m_{7,CO} V_{steam,7,CO} / C_7 = 236.0 \text{ M}^2 \quad \text{(F-130)}$$

$$A_{CC,S} = m_{7*,CC} V_{steam,7*,CC} / C_{7*} = 18.1 \text{ M}^2. \quad \text{(F-131)}$$

The total cold water ($m_{11,tot}$) necessary for the direct-contact condenser design is

$$m_{11,tot} = m_{11,CO,design} + m_{11,CC,design} = 16159 \text{ KG/S} \quad \text{(F-132)}$$

from which a heat balance can be performed to determine the condenser outlet seawater temperature (T_9) as

$$T_9 = (m_{11,CO,design} T_{9,CO} + m_{11,CC,design} T_{9,CC}) / m_{11,tot} = 10.60 \text{ }^{\circ}\text{C}. \quad \text{(F-133)}$$

F.5 CONDENSER VENT COMPRESSOR

The initial assumptions necessary for the condenser vent compressor analysis are:

1) The compression ratio for each compression stage is equivalent. That is, the following analysis ignores the corresponding condensation of water vapor at the higher system pressures associated with the compression process.

2) The seawater requirements for the compressor intercoolers is insignificant compared to the seawater flow of the direct-contact condenser [32].

3) The inlet vapor temperature to each compressor (after exiting the intercooler) is assumed 2.00 °C greater than the inlet cold water temperature (T_{11} = 5.00 °C) [32].

These assumptions lead to minimizing the necessary parasitic power requirements for the compression mechanism. However, the values obtained will necessarily be conservative values for parasitic power since the analysis ignores the progressive pressure increases which will lead to the subsequent condensation of water vapor along the compression path.

Initially, the design procedure necessitates determining the compression ratio (constant for each stage) from an estimate of the number of compression stages necessary (N_{comp}), an assumed intercooler pressure drop (ΔP_{inter}), an initial compressor pressure ($P_{in,(1)} = P_{CC}$) and an outlet atmospheric pressure (P_{atm}) as

$$N_{comp} = 5$$

$$\Delta P_{inter} = 0.28 \text{ KPa [32]}$$

$$P_{in,(1)} = 1.23 \text{ KPa}$$

$$P_{atm} = 101.33 \text{ KPa.}$$

The compression ratio is determined iteratively by solving

$$R_{comp}^{n} = (P_{atm} + \Delta P_{inter} \sum_{i=1}^{n} R_{comp}^{i}) / P_{in,(1)} = 2.59. \qquad \text{(F-134)}$$

The final iteration is displayed in the following table (Table F.1)

Table F.1: Iteration of Condenser Vent Compression Ratio

Step #	$\sum R_{comp}$	$R_{comp,\,i}$
1	2.59	2.42
2	8.44	2.43
3	22.73	2.44
4	58.47	2.49
5	153.84	2.59

The respective inlet and outlet pressures for each compressor stage is found in the following manner

$$P_{in,(1)} = P_{CC} = 1.23 \text{ KPa}$$

$$P_{out,(1)} = P_{in,(1)} R_{comp} = 3.19 \text{ KPa} \quad \text{(F-135)}$$

$$P_{in,(2)} = P_{out,(1)} - \Delta P_{inter} = 2.91 \text{ KPa} \quad \text{(F-136)}$$

$$P_{out,(2)} = P_{in,(2)} R_{comp} = 7.55 \text{ KPa} \quad \text{(F-137)}$$

$$P_{in,(3)} = P_{out,(2)} - \Delta P_{inter} = 7.28 \text{ KPa} \quad \text{(F-138)}$$

$$P_{out,(3)} = P_{in,(3)} R_{comp} = 18.85 \text{ KPa} \quad \text{(F-139)}$$

$$P_{in,(4)} = P_{out,(3)} - \Delta P_{inter} = 18.58 \text{ KPa} \quad \text{(F-140)}$$

$$P_{out,(4)} = P_{in,(4)} R_{comp} = 48.13 \text{ KPa} \quad \text{(F-141)}$$

$$P_{in,(5)} = P_{out,(4)} - \Delta P_{inter} = 47.85 \text{ KPa} \quad \text{(F-142)}$$

$$P_{out,(5)} = P_{in,(5)} R_{comp} = 123.98 \text{ KPa.} \quad \text{(F-143)}$$

With the inlet vapor temperature for each stage set at 7.00 °C (discussed previously), the water vapor partial pressure entering each compressor stage is simply the saturation pressure at that temperature ($P_{sat,8A}$ = 1.00 KPa). This water vapor pressure combined with the inlet pressures for each compression stage and the noncondensable flows entering from the counter-current condenser yield the inert gas partial pressures for each compressor as

$$PP_{N2,(i)} = (P_{in,(i)} - P_{sat,8A}) / [1+(M_{O2,CC,tot}+ M_{Ar,CC,tot}+ M_{CO2,CC,tot}) / M_{N2,CC,tot}] \quad \text{(F-144)}$$

$$PP_{O2,(i)} = (P_{in,(i)} - P_{sat,8A}) / [1+ (M_{N2,CC,tot}+ M_{Ar,CC,tot}+ M_{CO2,CC,tot}) / M_{O2,CC,tot}] \quad \text{(F-145)}$$

$$PP_{Ar,(i)} = (P_{in,(i)} - P_{sat,8A}) / [1+ (M_{N2,CC,tot}+ M_{O2,CC,tot}+ M_{CO2,CC,tot}) / M_{Ar,CC,tot}] \quad \text{(F-146)}$$

$$PP_{CO2,(i)} = P_{in,(i)} - P_{sat,8A} - PP_{N2,i} - PP_{O2,i} - PP_{Ar,i} \quad \text{(F-147)}$$

where the subscript i denotes the respective compression stages as i = 1 to n with the specific values presented in Table F.2 shown below. The corresponding water vapor flow accompanying this noncondensable flow through each compression stage is determined by

$$m_{wv,(i)} = MW_{H20}\, P_{sat,8A}\, M_{N2,CC,tot} / PP_{N2,(i)}. \quad \text{(F-148)}$$

The total parasitic power consumption for each compression stage is now defined by Parsons et al. [32] as

$$Po(i) = -(r / r-1)\, M_{gas,tot}\, R_g\, T_{8A} [1 - R_{comp}^{\{(r-1)/r\}}] / \eta_m\, \eta_{comp} \quad \text{(F-149)}$$

where

r = ratio of gas specific heats = 1.4 (assumed) [32]

$M_{gas,tot,(i)}$ = molar flow of gas through compressor stage

$$= m_{gas,tot,(i)} / GMWT_{(i)} \quad \text{(F-150)}$$

$$m_{gas,tot,(i)} = m_{wv,(i)} + m_{N2,CC,tot} + m_{O2,CC,tot} + m_{Ar,CC,tot} + m_{CO2,CC,tot} \quad \text{(F-151)}$$

$$GMWT_{(i)} = (PP_{N2,(i)} MW_{N2} + PP_{O2,(i)} MW_{O2} + PP_{Ar,(i)} MW_{Ar} + PP_{CO2,(i)} MW_{CO2} + P_{sat,8A} MW_{H2O}) / P_{in,(i)} \quad \text{(F-152)}$$

R_g = universal gas constant = 8.31 KPa M^3 / KG-MOL ^oK [17]

η_m = compressor motor efficiency = 0.90 [32]

η_{comp} = compressor efficiency = 0.80 [32]

T_{8A} = vapor inlet temperature (intercooler exit temperature)

= 280.15 ^oK.

The volume flow of gas through each compression stage is defined as

$$VOL_{gas,(i)} = M_{gas,tot,(i)} R_g T_{8A} / P_{in,(i)}. \quad \text{(F-153)}$$

The following tables (Table F.2 and F.3) display the calculation procedure for each compression stage and present the parasitic power associated with each stage using the aforementioned equations from which the total parasitic power necessary to maintain proper system vacuum within the designed direct-contact condenser and evaporator systems is derived.

Table F.2: Noncondensable Partial Pressures for Staged Compression from Vent Compressor

Stage #	PP_{N2} (KPa)	PP_{O2} (KPa)	PP_{Ar} (KPa)	PP_{CO2} (KPa)
1	0.1677	0.0515	0.0037	0.0075
2	1.3925	0.4279	0.0311	0.0622
3	4.5660	1.4030	0.1020	0.2041
4	12.7882	3.9293	0.2858	0.5715
5	34.0910	10.4749	0.7618	1.5236

Table F.3: Calculated Values for Staged Compression from Vent Compressor

Stage #	GMWT (KG/KG-MOL)	m_{wv} (KG/S)	$m_{gas,tot}$ (KG/S)	VOL_{gas} (M^3/S)	$Po_{(i)}$ (KW)
1	20.19	1.93	2.65	247.8	464
2	25.63	0.23	0.96	29.9	133
3	28.02	0.071	0.80	9.13	101
4	28.99	0.025	0.75	3.26	92
5	29.38	0.0095	0.74	1.22	88

Total parsitic power for the vent compression train is

$$Po_{comp,tot} = 878 \text{ KW.}$$

F.6 SEAWATER FLOW SYSTEM

The following analysis determines the expected head loss accompanying the OC-OTEC design outlined in this investigation for no predeaeration or reinjection which will be utilized in the subsequent seawater pump design. These head losses are determined utilizing standard engineering practice for estimating frictional losses along the intake and discharge pipes, entrance and exit losses, hydrostatic head losses, density differences between the seawater intake and discharge and minor losses attributable to bends in the piping system. For ease in design and comprehension of procedures, the warm water loop and the cold water loop have been investigated separately in this section.

The following values are utilized for both the warm and cold water flow system designs in the ensuing analysis and are presented here to simplify the calculation descriptions.

G = gravitation constant = 9.81 M/S^2 [46]

K_{bend} = pipe bend head loss coefficient = 0.16 [32]

K_{dis} = discharge loss coefficient = 1.0 [32]

K_{ent} = entrance loss coefficient = 0.78 [32]

ε_{pipe} = pipe roughness = 0.000046 M [32]

$\rho_{\#}$ = seawater density at seawater temperature associated with path #

$\mu_{\#}$ = seawater absolute viscosity at seawater temperature associated with path #

$\nu_{\#}$ = seawater kinematic viscosity = $\mu_{\#} / \rho_{\#}$

$Re_{\#}$ = Reynolds number for flow path # = $X_{\#} D_{\#,pipe} / \nu_{\#}$

The friction factors ($f_{\#}$) for the respective piping systems are determined as prescribed by Parsons et al. [32] by iteratively solving the following equation

$$f_{\#} = \{-2 \log [(\varepsilon_{pipe} / 3.7 D_{\#,pipe}) + 2.51 / (Re_{\#} \sqrt{f_{\#}})]\}^{-2} \qquad \text{(F-154)}$$

developed to approximate the Moody diagram.

F.6.1 WARM WATER FLOW SYSTEM

The following values are exclusive to the warm water flow system and are assumed for usage in the ensuing analysis.

$N_{2,bend}$ = number of bends in warm water intake pipe = 10 [32]

$N_{3,bend}$ = number of bends in warm water discharge pipe = 10 [32]

$L_{2,pipe}$ = warm water intake pipe length = 500 M [32]

$L_{3,pipe}$ = warm water discharge pipe length = 650 M [32]

$D_{spt,E}$ = spout diameter in evaporator = 0.127 M [32]

$L_{spt,E}$ = spout length in evaporator = 2.70 M [32]

$H_{spt,E}$ = spout height above water level in evaporator =0.50 M [32]

The seawater flow velocity ($X_{\#}$) in the piping system has been set throughout this design at

$$X_2 = X_{spt} = X_3 = 2.00 \text{ M/S}$$

which permits the determination of the intake pipe diameter ($D_{2,pipe}$) and the discharge pipe diameter ($D_{3,pipe}$) as

$$D_{2,pipe} = [(4\ m_2) / (\pi\ \rho_2\ X_2\ N_{2,pipes})]^{1/2} = 4.02\ M \qquad \text{(F-155)}$$

$$D_{3,pipe} = [(4\ m_3) / \pi\ \rho_3\ X_3\ N_{3,pipe})]^{1/2} = 4.02\ M \qquad \text{(F-156)}$$

with the knowledge of the design warm water mass flow ($m_2 = m_3$) determined in the evaporator analysis, the inlet and outlet seawater density (ρ_2 and ρ_3, respectively) and the design number of intake and discharge pipes ($N_{2,pipes} = 1 = N_{3,pipes}$).

The warm water flow system is now dissected into three separate analyses which will be summed at the end of this section to describe the total head loss through the warm water flow system. The values utilized for the determination of the head losses are presented and are developed as discussed previously in this report.

Warm Water Intake Pipe Head Losses:

$T_2 = 27.00\ ^{\circ}C$

$\mu_2 = 0.00092$ KG/M-S

$\nu_2 = 9.02 \times 10^{-7}\ M^2/S$

$\rho_2 = 1021.6\ KG/M^3$

$Re_2 = 8918306$

$f_2 = 0.0092$ (friction factor after iteration)

$\Delta P_{2,f}$ = frictional pressure drop of intake pipe

$$= f_2\ (L_{2,pipe} / D_{2,pipe})\ \rho_2\ X_2^2 / 2 = 2331\ Pa \qquad \text{(F-157)}$$

$\Delta P_{2,ent}$ = pressure drop due to entrance losses

$$= K_{ent}\ \rho_2\ X_2^2 / 2 = 1594\ Pa \qquad \text{(F-158)}$$

$\Delta P_{2,bend}$ = pressure drop due to losses at bends

$$= K_{bend}\, N_{2,bend}\, \rho_2\, X_2^2/2 = 3269 \text{ Pa} \quad \text{(F-159)}$$

$\Delta P_{2,tot}$ = total pressure drop in intake pipe

$$= \Delta P_{2,f} + \Delta P_{2,ent} + \Delta P_{2,bend} = 7194 \text{ Pa.} \quad \text{(F-160)}$$

Evaporator Head Losses:

$T_{E,ave}$ = 25.23 °C = average evaporator temperature

μ_E = 0.00096 KG/M-S

ν_E = 9.37×10^{-7} M^2/S

ρ_E = 1022.1 KG/M^3

Re_E = 271104

f_E = 0.0175 (friction factor after iteration)

$\Delta P_{E,f}$ = frictional pressure drop of evaporator spouts

$$= f_E\, (L_{spt,E} / D_{spt,E})\, \rho_E\, X_E^2 / 2 = 762 \text{ Pa} \quad \text{(F-161)}$$

$\Delta P_{E,ent}$ = pressure drop due to entrance losses

$$= K_{ent}\, \rho_E\, X_E^2 / 2 = 1594 \text{ Pa} \quad \text{(F-162)}$$

$\Delta P_{E,dis}$ = pressure drop due to losses at spout discharge

$$= K_{dis}\, \rho_E\, X_E^2/2 = 2044 \text{ Pa} \quad \text{(F-163)}$$

$\Delta P_{E,spt,H}$ = pressure drop due to spout height above water level

$$= H_{spt,E}\, \rho_E\, G = 5012 \text{ Pa} \quad \text{(F-164)}$$

$\Delta P_{E,tot}$ = total pressure drop in evaporator

$$= \Delta P_{E,f} + \Delta P_{E,ent} + \Delta P_{E,dis} + \Delta P_{E,spt,H} = 9413 \text{ Pa.} \quad \text{(F-165)}$$

Warm Water Discharge Pipe:

$$T_3 = 23.46\ ^{\circ}C$$

$$\mu_3 = 0.00100\ KG/M\text{-}S$$

$$\nu_3 = 9.75 \times 10^{-7}\ M^2/S$$

$$\rho_3 = 1022.5\ KG/M^3$$

$$Re_3 = 8249872$$

$$f_3 = 0.0092 \text{ (friction factor after iteration)}$$

$\Delta P_{3,f}$ = frictional pressure drop of discharge pipe

$$= f_3 (L_{3,pipe} / D_{3,pipe}) \rho_3 X_3^2 / 2 = 3053\ Pa \qquad \text{(F-166)}$$

$\Delta P_{3,bend}$ = pressure drop due to losses at bends

$$= K_{bend} N_{3,bend} \rho_3 X_3^2 / 2 = 3272\ Pa \qquad \text{(F-167)}$$

$\Delta P_{3,tot}$ = total pressure drop in discharge pipe

$$= \Delta P_{3,f} + \Delta P_{3,bend} = 6325\ Pa. \qquad \text{(F-168)}$$

The only remaining head loss to be determined is that associated with the density differences between the warm water intake and the warm water discharge. This density difference is going to prove site specific and is impossible to determine exactly without a detailed salinity and temperature profile available for the specific OC-OTEC design location. Since the designation of a particular location for design applications is beyond the scope of this work, the values obtained in the 100 MW OC-OTEC Westinghouse [49] design which determined a 0.05 M head loss for the warm water loop with an intake depth of 30 M and a discharge depth of 100 M will be utilized in this investigation as a good approximation for typical OC-OTEC salinity and temperature profiles. Therefore, the necessary head for overcoming this density difference yields a corresponding pressure loss of

$$HD_{2\text{-}3,density} = 0.05\ M$$

$$\Delta P_{2\text{-}3,density} = HD_{2\text{-}3,density}\ \rho_{2\text{-}3,ave}\ G = 501\ Pa \qquad \text{(F-169)}$$

where

$\rho_{2\text{-}3,ave}$ = average density of seawater from path 2 to path 3.

The total head loss ($HD_{tot,ww}$) for the warm seawater loop is

$$\Delta P_{tot,ww} = \Delta P_{2,tot} + \Delta P_{E,tot} + \Delta P_{3,tot} + \Delta P_{2\text{-}3,density} = 23433\ Pa \qquad \text{(F-170)}$$

$$HD_{tot,ww} = \Delta P_{tot,ww} / (\rho_{2\text{-}3,ave}\ G) = 2.34\ M. \qquad \text{(F-171)}$$

F.6.2 COLD WATER FLOW SYSTEM

The following values are exclusive to the cold water flow system and are assumed for usage in the ensuing analysis.

$N_{11,bend}$ = number of bends in cold water intake pipe = 10 [32]

$N_{9,bend}$ = number of bends in cold water discharge pipe = 10 [32]

$L_{11,pipe}$ = cold water intake pipe length = 2750 M [32]

$L_{9,pipe}$ = cold water discharge pipe length = 650 M [32]

$D_{cont,DCC}$ = contactor diameter in D.C.C. = 0.127 M [32]

$L_{cont,DCC}$ = contactor length in D.C.C. = 1.457 M [32]

$H_{cont,DCC}$ = contactor height above water level in D.C.C. = 0.457 M [32]

The seawater flow velocity ($X_{\#}$) in the piping system has been set throughout this design at

$$X_{11} = X_{cont} = X_9 = 2.00\ M/S$$

which permits the determination of the intake pipe diameter ($D_{11,pipe}$) and the discharge pipe diameter ($D_{9,pipe}$) as

$$D_{11,pipe} = [(4\ m_{11}) / (\pi\ \rho_{11}\ X_{11}\ N_{11,pipes})]^{1/2} = 3.17\ M \qquad \text{(F-172)}$$

$$D_{9,pipe} = [(4\ m_9) / \pi\ \rho_9\ X_9\ N_{9,pipe})]^{1/2} = 3.17\ M \qquad \text{(F-173)}$$

with the knowledge of the design cold water mass flow ($m_{11} = m_9$) determined in the condenser analysis, the inlet and outlet seawater density (ρ_{11} and ρ_9, respectively) and the design number of intake and discharge pipes ($N_{11,pipes} = 1 = N_{9,pipes}$).

The cold water flow system is now dissected into three separate analyses which will be summed at the end of this section to describe the total head loss through the cold water flow system. The values utilized for the determination of the head losses are presented and are developed as discussed previously in this report.

Cold Water Intake Pipe Head Losses:

$T_{11} = 5.00\ ^{\circ}C$

$\mu_{11} = 0.0016$ KG/M-S

$\nu_{11} = 1.58 \times 10^{-6}$ M^2/S

$\rho_{11} = 1025.4$ KG/M^3

$Re_{11} = 4008451$

$f_{11} = 0.0100$ (friction factor after iteration)

$\Delta P_{11,f}$ = frictional pressure drop of intake pipe

$$= f_{11}\ (L_{11,pipe} / D_{11,pipe})\ \rho_{11}\ X_{11}^2 / 2 = 17859\ Pa \qquad \text{(F-174)}$$

$\Delta P_{11,ent}$ = pressure drop due to entrance losses

$$= K_{ent}\ \rho_{11}\ X_{11}^2 / 2 = 1600\ Pa \qquad \text{(F-175)}$$

$\Delta P_{11,bend}$ = pressure drop due to losses at bends

$= K_{bend} N_{11,bend} \rho_{11} X_{11}^2 / 2 = 3281$ Pa (F-176)

$\Delta P_{11,tot}$ = total pressure drop in intake pipe

$= \Delta P_{11,f} + \Delta P_{11,ent} + \Delta P_{11,bend} = 22740$ Pa. (F-177)

Direct-Contact Condenser Head Losses:

$T_{DCC,ave} = 7.80\ ^{\circ}C$ = average condenser temperature

$\mu_{DCC} = 0.0015$ KG/M-S

$\nu_{DCC} = 1.46 \times 10^{-6}$ M^2/S

$\rho_{DCC} = 1025.0$ KG/M^3

$Re_{DCC} = 174344$

$f_{DCC} = 0.0184$ (friction factor after iteration)

$\Delta P_{DCC,f}$ = frictional pressure drop of condenser contactors

$= f_{DCC} (L_{cont,DCC} / D_{cont,DCC}) \rho_{DCC} X_{DCC}^2 / 2 = 432$ Pa (F-178)

$\Delta P_{DCC,ent}$ = pressure drop due to entrance losses

$= K_{ent} \rho_{DCC} X_{DCC}^2 / 2 = 1599$ Pa (F-179)

$\Delta P_{DCC,dis}$ = pressure drop due to losses at contactor discharge

$= K_{dis} \rho_{DCC} X_{DCC}^2 / 2 = 2050$ Pa (F-180)

$\Delta P_{DCC,cont,H}$ = pressure drop due to contactor height above water level

$= H_{cont,DCC} \rho_{DCC} G = 4594$ Pa (F-181)

$\Delta P_{DCC,tot}$ = total pressure drop in direct-contact condenser

$= \Delta P_{DCC,f} + \Delta P_{DCC,ent} + \Delta P_{DCC,dis} + \Delta P_{DCC,cont,H} = 8674$ Pa. (F-182)

Cold Water Discharge Pipe:

$$T_9 = 10.60\,^{\circ}C$$

$$\mu_9 = 0.0014\ KG/M\text{-}S$$

$$\nu_9 = 1.35 \times 10^{-6}\ M^2/S$$

$$\rho_9 = 1024.6\ KG/M^3$$

$$Re_9 = 4706324$$

$$f_9 = 0.0099 \text{ (friction factor after iteration)}$$

$\Delta P_{9,f}$ = frictional pressure drop of discharge pipe

$$= f_9 (L_{9,pipe} / D_{9,pipe}) \rho_9 X_9^2 / 2 = 4151\ Pa \qquad \text{(F-183)}$$

$\Delta P_{9,bend}$ = pressure drop due to losses at bends

$$= K_{bend} N_{9,bend} \rho_9 X_9^2 / 2 = 3279\ Pa \qquad \text{(F-184)}$$

$\Delta P_{9,tot}$ = total pressure drop in discharge pipe

$$= \Delta P_{9,f} + \Delta P_{9,bend} = 7430\ Pa. \qquad \text{(F-185)}$$

The only remaining head loss to be determined is that associated with the density differences between the cold water intake and the cold water discharge. This density difference is going to prove site specific (as discussed previously in the warm water flow system analysis) and is impossible to determine exactly without a detailed salinity and temperature profile available for the specific OC-OTEC design location. Once again the values obtained in the 100 MW OC-OTEC Westinghouse [49] design which determined a 0.45 M head loss for the cold water loop with an intake depth of 940 M and a discharge depth of 100 M will be utilized in this investigation as a good approximation for typical OC-OTEC salinity and temperature profiles. Therefore, the necessary head for overcoming this density difference yields a corresponding pressure loss of

$$HD_{11\text{-}9,density} = 0.45\ M$$

$$\Delta P_{11\text{-}9,density} = HD_{11\text{-}9,density}\ \rho_{11\text{-}9,ave}\ G = 4222\ Pa \qquad (F\text{-}186)$$

where

$\rho_{11\text{-}9,ave}$ = average density of seawater from path 11 to path 9.

The total head loss ($HD_{tot,cw}$) for the cold seawater loop is

$$\Delta P_{tot,cw} = \Delta P_{11,tot} + \Delta P_{DCC,tot} + \Delta P_{9,tot} + \Delta P_{11\text{-}9,density}$$

$$= 43065\ Pa \qquad (F\text{-}187)$$

$$HD_{tot,cw} = \Delta P_{tot,cw} / (\rho_{11\text{-}9,ave}\ G) = 4.28\ M. \qquad (F\text{-}188)$$

F.7 SEAWATER PUMP ANALYSIS

The seawater pump analyses begin by defining the three dimensionless parameters utilized to characterize an axial flow pump at the optimum performance level indicated by Figure 4.11 earlier in this report as

$$C_q = Q_{pump} / (n\ D^3) = 0.0677 \qquad (F\text{-}189)$$

$$C_h = G\ HD / (n^2\ D_3) = 0.017 \qquad (F\text{-}190)$$

$$C_p = Po / (\rho_{\#}\ n^3\ D^5) = 0.0013 \qquad (F\text{-}191)$$

where

n = pump speed (rad / sec)

D = pump impeller diameter (M)

Q_{pump} = volumetric flow rate through pump (M^3/S)

HD = necessary fluid head (M) (from flow system analysis)

$\rho_{\#}$ = seawater density at path #

Po = power required to run pump (W)

G = gravitation constant (acceleration) = 9.81 M/S^2

The efficiency (η_{pump}) of the respective pumps being designed in this analysis is defined as

$$\eta_{pump} = C_h C_q / C_p. \qquad \text{(F-192)}$$

Warm Water Pumps:

Initially it is necessary to determine the warm water volumetric flow through each pump. Since the number of pumps necessary is unknown and dependant upon the maximum diameter commercially available (commercially available pumps approach 1.85 M diameters [32]) the procedure is iterative.

For the first iteration the number of pumps designed is

$$N_{pump,ww} = 1$$

the final iteration yields a value of

$$N_{pump,ww} = 3$$

With an estimate as to the number of pumps to be utilized in the warm water flow loop, the volumetric flow ($Q_{pump,ww}$) for each warm water pump is determined from the warm water mass flow (m_2) and the known seawater density (ρ_2) as

$$Q_{pump,ww} = m_2 / (\rho_2 N_{pump,ww}) = 8.46\ M^3/S \qquad \text{(F-193)}$$

which upon solving the three equations above (F-189 , F-190 and F-191) for the three unknowns ($n_{ww,pump}$, $D_{ww,pump}$ and $Po_{ww,pump}$) yields values of

$$n_{ww,pump} = 19.90 \text{ rad/sec}$$

$$D_{ww,pump} = 1.85\ M$$

$$\eta_{ww,pump} = 0.89$$

$$Po_{ww,pump} = 224\ KW$$

This procedure is repeated until the final pump impeller diameter is less than 1.85 M so that the pumps being designed stay within commercially available limits.

The total parasitic pump power requirements are determined now for each warm water pump utilized as

$$Po_{tot,pump,ww} = N_{pump,ww}\, Po_{ww,pump} = 672 \text{ KW.} \qquad \text{(F-194)}$$

Cold Water Pumps:

As described above for the warm water pumps, it is necessary to determine the cold water volumetric flow through each pump. Once again, since the number of pumps necessary is unknown and dependant upon the maximum diameter commercially available, the procedure is iterative.

For the first iteration the number of pumps designed is

$$N_{pump,cw} = 1$$

the final iteration yields a value of

$$N_{pump,cw} = 2$$

With an estimate as to the number of pumps to be utilized in the cold water flow loop, the volumetric flow ($Q_{pump,cw}$) for each cold water pump is determined from the cold water mass flow (m_{11}) and the known seawater density (ρ_{11}) as

$$Q_{pump,cw} = m_{11} / (\rho_{11}\, N_{pump,cw}) = 8.46 \text{ M}^3\text{/S} \qquad \text{(F-195)}$$

which upon solving the three equations above (F-189 , F-190 and F-191) for the three unknowns ($n_{cw,pump}$, $D_{cw,pump}$ and $Po_{cw,pump}$) yields values of

$$n_{cw,pump} = 32.48 \text{ rad/sec}$$

$$D_{cw,pump} = 1.53 \text{ M}$$

$$\eta_{cw,pump} = 0.89$$

$$Po_{cw,pump} = 383 \text{ KW}$$

This procedure is repeated until the final pump impeller diameter is less than 1.85 M so that the pumps being designed stay within commercially available limits.

The total parasitic pump power requirements are determined now for each cold water pump utilized as

$$Po_{tot,pump,cw} = N_{pump,cw} Po_{cw,pump} = 767 \text{ KW}. \quad \text{(F-196)}$$

Total power necessary for both seawater pump systems is

$$Po_{tot,pumps} = Po_{tot,pump,ww} + Po_{tot,pump,cw} = 1439 \text{ KW}. \quad \text{(F-197)}$$

F.8 TOTAL POWER CONSUMPTION ANALYSIS

The total parasitic power consumption ($Po_{tot,parasitic}$) for the non-predeaerated 10 MW_{gross} OC-OTEC system designed in this report is a function of the total power consumed by the condenser vent compressors ($Po_{comp,tot}$) and the total power utilized by the seawater pumps ($Po_{tot,pumps}$) determined as

$$Po_{tot,parasitic} = Po_{comp,tot} + Po_{tot,pumps} = 2317 \text{ KW}. \quad \text{(F-198)}$$

The total power available from this design (including the flow of noncondensables through the designed turbine as discussed in the evaporator section previously) is

$$Po_{gross} = 10027 \text{ KW}.$$

With the gross power known and the total parasitic power also known, the net power produced from this design is defined as

$$Po_{net} = Po_{gross} - Po_{tot,parasitic} = 7710 \text{ KW.} \quad \text{(F-199)}$$

These values indicate that a non-predearated 10 MW_{gross} OC-OTEC power plant can be expected to lose approximately 23% of its gross power output to parasitic losses.

APPENDIX G

10 MW_{gross} PREDEAERATED/REINJECTED OC-OTEC PLANT COMPONENT DESIGN CALCULATIONS

The following appendix represents the calculations performed to reach the thermodynamic properties presented earlier in this report for the 10 MW_{gross} predeaerated/reinjected OC-OTEC system. Both the equations utilized to perform the calculations as well as the final results are presented. For iterative procedures, the initial value utilized to begin the iteration as well as the final value arrived through the iteration are presented to assist in comprehension of the design calculation procedure. All numerical subscripts refer to Figure 5.1 to simplify definition of system stream path values.

In many cases in the following design description, the procedure is very similar to that described in the previous appendix for the non-predeaerated system. Therefore, some segments of this design will appear redundant but are necessary for the complete design of the predeaerated/reinjected system.

G.1 TURBINE DESIGN

As stated earlier in this investigation, for the purposes of providing an accurate means of comparing a non-predeaerated OC-OTEC facility to a predeaerated/reinjected OC-OTEC facility of nearly equal gross power production, an identical turbine/turbine diffuser design is necessary. Therefore, this portion of the design is identical to that presented earlier in Appendix F.

As described in Section F.1 previously, the turbine inlet steam temperature and exit steam temperature are set at values suggested by M.I.T. [27] so that the other parameters are set at:

Turbine inlet steam:

$T_{s,5}$ = 22.50 °C 295.65 °K

$P_{sat,5}$ = 2.72 KPa

$H_{g,5}$ = 2542.7 KJ/KG

$H_{f,5}$ = 94.42 KJ/KG

$S_{g,5}$ = 8.61 KJ/KG-°C

$S_{f,5}$ = 0.33 KJ/KG-°C

$V_{steam,5}$ = 48.9 M^3/KG

Turbine outlet steam:

$T_{s,6}$ = 12.00 °C 285.15 °K

$P_{sat,6}$ = 1.40 KPa

$H_{g,6}$ = 2523.4 KJ/KG

$H_{f,6}$ = 50.42 KJ/KG

$S_{g,6}$ = 8.85 KJ/KG-°C

$S_{f,6}$ = 0.18 KJ/KG-°C

$V_{steam,6}$ = 94.4 M^3/KG

Assuming isentropic expansion through the rotor and stator sections of the turbine suggest that the inlet and outlet steam have the same entropy [32] (see Figure 4.3).

$$S_5 = S_{6ss} \qquad \text{(G-1)}$$

Therefore, the isentropic outlet conditions can be determined as:

$$x_{6ss} = \text{isentropic outlet steam quality}$$

$$= (S_{g,5} - S_{f,6}) / (S_{g,6} - S_{f,6}) = 0.972 \qquad \text{(G-2)}$$

$$h_{6ss} = \text{isentropic outlet enthalpy}$$

$$= H_{f,6} + x_{6ss} (H_{g,6} - H_{f,6}) = 2454.9 \text{ KJ/KG} \qquad \text{(G-3)}$$

With the inlet and isentropic outlet conditions completely described, an iterative approach is now performed to determine the actual outlet conditions and the inlet and outlet stagnation conditions [32]. Since the turbine dimensions are unknown, the steam inlet velocity (C_5) and the turbine steam exit velocity (C_6) are unknown. For the first iteration assume

$$C_5 = 60.00 \text{ m/s} \quad \text{and} \quad C_6 = 0.00 \text{ m/s.}$$

The final value arrived at for these velocities after completing the iterative process are:

$$C_5 = 59.71 \text{ m/s} \quad \text{and} \quad C_6 = 112.06 \text{ m/s.}$$

The inlet stagnation enthalpy (h_{05}) is the steam enthalpy created by the temperature and the steam inlet kinetic energy [32] as

$$h_{05} = h_5 + C_5^2 / (2 \times 1000) = 2544.5 \text{ KJ/KG.} \qquad \text{(G-4)}$$

The factor of 1000 simply converts the kinetic energy factor to units of KJ/KG [32]. The isentropic exit velocity (C_{6ss}) is now determined from the inlet steam velocity (C_5), the isentropic steam exit quality (x_{6ss}) and the ratio of the exit to inlet steam specific volumes ($V_{steam,6}$ and $V_{steam,5}$, respectively) [32] as

$$C_{6ss} = C_5 x_{6ss} (V_{steam,6} / V_{steam,5}) = 112.06 \text{ m/s.} \qquad \text{(G-5)}$$

Now the isentropic exit enthalpy (h_{06ss}) is determined

$$h_{06ss} = h_6 + C_{6ss}^2 / (2 \times 1000) = 2461.2 \text{ KJ/KG.} \qquad \text{(G-6)}$$

Parsons et al. [32] define two isentropic enthalpy drops across the turbine, the total-to-total ($\Delta h_{t\text{-}t}$) and the total-to-static ($\Delta h_{t\text{-}s}$) as

$$\Delta h_{t\text{-}t} = h_{05} - h_{06ss} = 83.30 \text{ KJ/KG} \qquad \text{(G-7)}$$

$$\Delta h_{t\text{-}s} = h_{05} - h_{6ss} = 89.58 \text{ KJ/KG.} \qquad \text{(G-8)}$$

With these values now determined, the design steam mass flow rate through the turbine can be determined as

$$m_{steam} = Po_{gross} / (\Delta h_{t\text{-}s}\, \eta_{t\text{-}s}\, \eta_{gen}\, N_{turb}) = 29.4 \text{ KG/S} \qquad \text{(G-9)}$$

where

Po_{gross} = gross power of plant = 10,000 KW (design)

$\eta_{t\text{-}s}$ = total-to-static turbine efficiency = 0.80 [32]

η_{gen} = generator efficiency = 0.95 [32]

N_{turb} = number of turbines = 5 (technological limit 2 MW/turbine) [27].

The actual exit stagnation enthalpy (h_{06}) can now be found from the definition of total-to-static efficiency

$$\eta_{t\text{-}s} = (h_{05} - h_{06}) / (h_{05} - h_{06ss}) \Longrightarrow h_{06} = 2472.8 \text{ KJ/KG.} \qquad \text{(G-10)}$$

From Figure 4.3 it can be seen that the constant pressure lines are nearly parallel [32]; from which the actual outlet enthalpy (h_6) can be determined if C_6 is known:

for first iteration assume outlet velocity (C_6) is equivalent to the outlet stagnation velolcity (C_{6ss}) :

$$C_6 = C_{6ss} = 112.06 \text{ m/s}$$

final determined value after iterative procedure:

$$C_6 = 112.61 \text{ m/s}$$

$$h_6 = h_{06} - C_6^2 / (2 \times 1000) = 2466.5 \text{ KJ/KG.} \qquad \text{(G-11)}$$

This sets the actual outlet steam quality (x_6) at

$$x_6 = (h_6 - H_{f,6}) / (H_{g,6} - H_{f,6}) = 0.977 \quad \text{(G-12)}$$

Now that the inlet and outlet turbine conditions have been approximated at this point during the iterative procedure, the turbine design speed and size can be approximated as well. Parsons et al. [32] define the dimensionless specific diameter (d_s) and the maximum specific speed-specific diameter product ($n_s\, d_s$) as

$$d_s = \{\sqrt{8}\, C_o / [\pi\, C_6\, (1 - \lambda^2)]\}^{1/2} = 2.01 \quad \text{(G-13)}$$

$$(n_s\, d_s)_{max} = \sqrt{8}\, U_t / C_o \;\Longrightarrow\; n_s = 1.55 \quad \text{(G-14)}$$

where

C_o = spouting velocity =

$$(2\ \Delta h_{t\text{-}t}\ 1000)^{1/2} = 408.2\ \text{M/S} \quad \text{(G-15)}$$

λ = hub-to-tip ratio = 0.44 [32]

U_t = maximum tip speed = 450 M/S [8].

The volumetric flow rate of steam through the turbine is found as

$$V_6 = V_{steam,6}\, m_{steam}\, x_6 = 2710.6\ M^3/S \quad \text{(G-16)}$$

which combined with the definition of specific speed (n_s) yields the maximum rotational speed (ω_t) as

$$n_s = \omega_t \sqrt{V_{steam,6}} / (C_o^2 / 2)^{3/4} \;\Longrightarrow\; \omega_t = 782.1 \quad \text{(G-17)}$$

$$RPM_t = \omega_t\, 60 / (2\,\pi) = 7468 \;\Longrightarrow \quad \text{(G-18)}$$

RPM_t = 7440 RPM (even multiple of 60 for ease in design).

Now recalculate n_s and ω_t to coincide with the actual RPM_t

$n_s = 1.54$

$\omega_t = 779.1$

From the definition of dimensionless diameter (d_s) the actual turbine diameter can be found:

$$D_t = \sqrt{V_{steam,6}}\, d_s / (\Delta h_{t\text{-}t}\, 1000)^{1/4} = 6.16\ M. \qquad \text{(G-19)}$$

Now the steam flow area and hence the steam inlet and outlet flow velocities can be found as

$$A_t = \pi D_t^2 (1 - \lambda^2) / 4 = 24.0701\ M^2 \qquad \text{(G-20)}$$

$$C_5 = V_{steam,5}\, m_{steam} / A_t = 59.71\ M/S \qquad \text{(G-21)}$$

$$C_6 = V_6 / A_t = 112.61\ M/S \qquad \text{(G-22)}$$

From here the iteration is repeated until the outlet steam velocities (C_6) converge to ± 0.1% from beginning to end of iterative procedure.

Finally, the turbine power density is calculated according to the area of each turbine as

$$Po_{density} = Po_{gross} / (N_{turb}\, \pi D_t^2 / 4) = 67.00\ KW/M^2. \qquad \text{(G-23)}$$

Section 4.2.2 of this report gives the general description of the detailed procedures outlined in this section. Some of the values determined in this section will be further utilized in the subsequent sections.

G.2 TURBINE DIFFUSER

The diffuser inlet conditions are set at the turbine exit conditions determined in the previous section with the inlet pressure assumed to be the saturation pressure ($P_6 = P_{sat,6}$) calculated previously. The diffuser inlet conditions are denoted with the subscript 6 and the exit conditions with 7 as prescribed by Figure 5.1. As in the turbine analysis, the subscript s denotes the isentropic end condition at P_7.

From the turbine analysis we can determine the turbine inlet steam flow ($m_{steam,5}$) (with assumed quality $x_5 = 1.0$) and turbine exit steam flow ($m_{steam,6}$) with the following equations:

$$m_{steam,5} = m_{steam} N_{turb} / x_6 = 150.3 \text{ KG/S} \quad \text{(G-24)}$$

$$m_{steam,6} = m_{steam} N_{turb} = 146.9 \text{ KG/S.} \quad \text{(G-25)}$$

The total turbine area ($A_{t,tot}$) is simply

$$A_{t,tot} = A_t N_{turb} = 120.4 \text{ M}^2. \quad \text{(G-26)}$$

From this area the diffuser inlet steam velocity (C_{6*}) is determined

$$C_{6*} = m_{steam,6} V_6 / A_{t,tot} = 115.3 \text{ M/S.} \quad \text{(G-27)}$$

The diffuser steam inlet enthalpy (h_6) is defined as:

$$h_6 = (1.0 - x_6) H_{f,6} + x_6 H_{g,6} = 2466.6 \text{ KJ/KG.} \quad \text{(G-28)}$$

Parsons et al. [32] suggest setting the diffuser steam exit velocity (C_7) for this type of diffuser design at

$$C_7 = 0.5 C_{6*} = 57.6 \text{ M/S.} \quad \text{(G-29)}$$

From the definition of diffuser efficiency (η_d) the isentropic steam exit velocity (C_{7s}) can be determined

$$\eta_d = (h_{7s} - h_6) / (h_7 - h_6) = (C_{6*}^2 - C_{7s}^2) / (C_{6*}^2 - C_7^2) \Longrightarrow \quad \text{(G-30)}$$

$$C_{7s} = 72.9 \text{ M/S}$$

where

η_d = turbine diffuser efficiency = 0.80 [32].

In order to determine the diffuser outlet conditions, an iterative process is now necessary. For the first iteration the outlet steam specific volume ($V_{steam,7}$) is set equal to the inlet steam specific volume ($V_{steam,6}$).

$$V_{steam,7} = V_{steam,6} = 94.45 \text{ M}^3\text{/KG}$$

Final value after iterative procedure yields

$$V_{steam,7} = 91.61\ M^3/KG.$$

Parsons et al. [32] suggest that by assuming that the constant pressure lines in Figure 4.4 do not diverge, the pressure loss through the diffuser (ΔP_d) can be approximated as

$$\Delta P_d = (C_{7s}^2 - C_7^2) / (2 \times 1000\ V_7) = 0.011\ KPa \qquad (G\text{-}31)$$

where the factor 1000 converts the pressure drop from Pa to KPa. From this pressure drop the diffuser outlet pressure (P_7) can now be found as

$$P_7 = P_6 + [C_6^{*2} / (2 \times 1000\ V_6)] - [C_7^2 / (2 \times 1000\ V_7)] - \Delta P_d \qquad (G\text{-}32)$$

$$= 1.44\ KPa.$$

By assuming saturation conditions at the diffuser outlet condition, the outlet steam temperature (T_7) can now be determined as described at the beginning of this appendix at P_7

$$T_{7,d} = 12.47\ ^\circ C \qquad 285.62\ ^\circ K$$

from which the new specific volume ($V_{7,d}$) is recalculated

$$V_{7,d} = 91.61\ M^3/S$$

and the procedure is repeated until the final outlet specific volume coincides to the specific volume utilized to begin the procedure to within ± 0.1%.

With the outlet conditions defined by the outlet steam temperature (T_7), the isentropic steam quality is defined by

$$x_{7s} = (S_{g,7} - S_{f,6}) / (S_{g,6} - S_{f,6}) = 0.9987 \qquad (G\text{-}33)$$

which can be used to find the isentropic outlet enthalpy (h_{7s})

$$h_{7s} = (1 - x_{7s})\ H_{f,7} + x_{7s}\ H_{g,7} = 2521.1\ KJ/KG. \qquad (G\text{-}34)$$

The isentropic enthalpy, with the knowledge of the diffuser efficiency (η_d), yields the outlet enthalpy (h_7)

$$h_7 = h_6 + [(h_{7s} - h_6) / \eta_d] = 2534.7 \text{ KJ/KG} \quad \text{(G-35)}$$

and the outlet steam quality (x_7)

$$x_7 = (h_7 - H_{f,7}) / (H_{g,7} - H_{f,7}) = 1.0042. \quad \text{(G-36)}$$

A value of $x_7 > 1.0$ indicates supersaturation of the steam; however, it is assumed that there is enough liquid available at the diffuser exit to avoid this so the exit quality (x_7) is set to 1.0 [32].

The diffuser steam exit mass flow rate ($m_{steam,7}$) is therefore defined by

$$m_{steam,7} = m_{steam,6}\, x_7 = 146.9 \text{ KG/S}. \quad \text{(G-37)}$$

Balje [2] defines the parameter necessary for defining the size of the diffuser as the pressure recovery factor (Cp) defined as

$$Cp = [C_6{}^{*2} - C_7{}^2 - (2\, \Delta P_d\, V_7)] / C_6{}^{*2} = 0.75. \quad \text{(G-38)}$$

From Figure 4.5 [2] for the minimum $L_d / D_{d,6}$, $D_{d,7}/ D_{d,6}$ and θ_d from the figure we obtain

$$L_d / D_{d,6} = 3.90$$

$$D_{d,7} / D_{d,6} = 1.68$$

$$\theta d = 5.00^\circ$$

where

$D_{d,6}$ = diffuser inlet diameter = D_t = 6.17 M

$D_{d,7}$ = diffuser outlet diameter = 10.37 M

L_d = diffuser length = 24.06 M.

The graphical calculations are checked by determining the diffuser half angle (θ_d) empirically as

$$\theta_d = \tan^{-1} [(D_7 - D_{d,6}) / 2\, L_d] = 4.99^\circ. \quad \text{(G-39)}$$

Parsons et al. [32] suggest that these correlations are valid for a diffuser pressure recovery factor (Cp) within the range 0.40 and 0.85.

G.3 EVAPORATOR AND MIST REMOVAL DEVICE

The mist removal exit conditions (path 5 in Figure 5.1) have been defined previously in the turbine entrance calculations. The warm seawater resource temperature is set arbitrarily at a temperature common to tropical ocean locations most suitable to OC-OTEC development. This sets the seawater entrance conditions at

$$T_1 = T_2 = 27.00\,^{\circ}C \qquad 300.15\,^{\circ}K$$

$$P_{sat,1} = P_{sat,2} = 3.56\ KPa$$

$$H_{g,1} = H_{g,2} = 2550.9\ KJ/KG$$

$$H_{f,1} = H_{f,2} = 113.2\ KJ/KG$$

$$S_{g,1} = S_{g,2} = 8.52\ KJ/KG\text{-}^{\circ}C$$

$$S_{f,1} = S_{f,2} = 0.40\ KJ/KG\text{-}^{\circ}C$$

$$V_{g,1} = V_{g,2} = 37.8\ M^3/KG$$

which are identical to the values utilized in the previous analysis for the non-predeaerated system.

Initially, the spout velocity ($X_{spt,E}$), the spout diameter ($D_{spt,E}$) and the spout height ($h_{spt,E}$) above the seawater drain pool are all assumed according to values suggested by Parsons et al. [32] as

$$X_{spt,E} = 2.00\ M/S$$

$$D_{spt,E} = 0.127\ M$$

$$h_{spt,E} = 0.50\ M.$$

The evaporator effectiveness (ε_E) is assessed from data presented by Bharathan and Penney [4] for a spout evaporator with one enhancement and the assumed spout velocity as

$$\varepsilon_E = 0.91$$

with the evaporator effectiveness defined as

$$\varepsilon_E = (T_2 - T_3) / (T_2 - T_{4,E}). \qquad \text{(G-40)}$$

The mist removal device included in this design introduces an evaporator-turbine pressure drop and thus $T_4 \neq T_5$ ($T_4 > T_5$) and T_4 must be determined. Since only the turbine entrance conditions (5) are known, an iterative procedure must be employed. For the first iteration the temperature at the inlet of the mist removal device is set at

$$T_{4,mr} = T_5 = 22.50\,^{\circ}C.$$

The final value after the iterative process yields

$$T_{4,mr} = 23.10\,^{\circ}C.$$

Parsons et al. [32] suggest a pressure drop coefficient (K_{mr}) and a mist removal steam velocity (C_{mr}) of

$$K_{mr} = 10.0$$

$$C_{mr} = 30.00\ M/S.$$

With the estimated mist removal inlet steam temperature an estimated pressure drop (ΔP_{mr}) can be determined

$$\Delta P_{mr} = K_{mr}\,\rho_4\,C_{mr}^2 / 2 = 95.29\ Pa. \qquad \text{(G-41)}$$

Assuming that the steam is at saturation entering the turbine, the pressure at the mist removal exit must be $P_{sat,5}$ which allows an estimate of the mist removal inlet steam pressure (P_4) of

$$P_4 = P_{sat,5} - \Delta P_{mr} = 2.82\ KPa \qquad \text{(G-42)}$$

from which an estimated inlet steam temperature ($T_{4,mr}$) can be determined assuming saturation of steam. This procedure is repeated until the steam density (ρ_4) changes less than $\pm$ 0.1% from one iteration to the next [32].

The mass of steam flow from the evaporator ($m_{steam,4}$) is assumed equal to the mass of steam entering the turbine ($m_{steam,5}$). The area required for the mist removal device (A_{mr}) is then determined as

$$A_{mr} = m_{steam,5} / (X_{mr}\ \rho_4) = 236.7\ M^2. \qquad \text{(G-43)}$$

The evaporator steam generation temperature ($T_{4,E}$) is found in a similar manner to the mist removal inlet steam temperature ($T_{4,mr}$) by first determining the evaporator-turbine passage pressure drop ($\Delta P_{E\text{-}t}$). However, in this case, the steam generation velocity (C_E) is unknown and an iterative procedure is required with the initial steam generation temperature ($T_{4,E}$) assumed to be equal to the mist removal inlet steam temperature ($T_{4,mr}$)

$$T_{4,E} = T_{4,mr} = 23.10\ ^\circ C.$$

The final value achieved after the iterative process is

$$T_{4,E} = 23.11\ ^\circ C.$$

An estimated warm water outlet temperature (T_3) and the design warm water flow rate (m_2) can be determined from the evaporator effectiveness (ε_E) and this estimated steam generation temperature ($T_{4,E}$) as

$$T_3 = T_2 - \varepsilon_E\ (T_2 - T_{4,E}) = 23.46\ ^\circ C \qquad \text{(G-44)}$$

$$m_2 = (m_{steam,4}\ h_{vap,4,E}) / [C_{p2}\ (T_2 - T_3)] = 25953\ KG/S \qquad \text{(G-45)}$$

where

$h_{vap,4,E}$ = heat of vaporization at $T_{4,E}$ = 2446.7 KJ/KG

C_{p2} = heat capacity of seawater at T_2 = 4.00 KJ/KG-°C.

The mass flow of warm water per spout ($m_{spt,E}$) is then determined as

$$m_{spt,E} = \rho_2\ X_{spt,E}\ \pi\ D_{spt,E}^2 / 4 = 25.9\ KG/S \qquad \text{(G-46)}$$

which yields an estimate of the number of spouts ($N_{sp,E}$) necessary as

$$N_{spt,E} = m_2 / m_{spt,E} = 1002.7 \text{ ===> } 1003 \text{ spouts.} \qquad \text{(G-47)}$$

Assuming a hexagonal configuration for the spouts with a center-center spacing of 0.7 M between spouts yields an approximate area of 0.424 M^2/spout [32] which yields an approximate evaporator area (A_E) of

$$A_E = N_{spt,E}\,(0.424) = 425.6\ M^2 \qquad \text{(G-48)}$$

From this planform area the evaporator-turbine passage inlet velocity (C_4) can now be found

$$C_4 = m_{steam,4} / (A_E\,\rho_4) = 16.67\ M/S \qquad \text{(G-49)}$$

which leads to an evaporator-turbine passage pressure drop ($\Delta P_{E\text{-}t}$) of

$$\Delta P_{E\text{-}t} = K_{E\text{-}t}\,\rho_4\,C_4^2 / 2 = 1.47\ Pa \qquad \text{(G-50)}$$

where

ρ_4 = steam density at $T_{4,E}$ = 0.021 KG/M^3

$K_{E\text{-}t}$ = evaporator-turbine pressure loss coefficient = 0.50 [32].

This pressure drop then determines the evaporator steam generation pressure ($P_{4,E}$)

$$P_{4,E} = P_{4,mr} + \Delta P_{E\text{-}t} = 2.82\ KPa \qquad \text{(G-51)}$$

which is then used to revise the estimated steam generation temperature ($T_{4,E}$) and the procedure from equation G-44 is repeated until the $T_{4,E}$ changes less than ± 0.1 % from one iteration to the next.

At this point in the design procedure it is necessary to determine the noncondensable flow accompanying this steam production. Since this is a design which calls for predeaeration of the warm water stream prior to introduction into the evaporator vessel and the expected predeaeration level should exceed the desorption percentages obtained previously in the experimental portion of this investigation, only the atmospheric leakage

component of the noncondensable gases is expected to accompany the flow of steam through the turbine. Parsons et al. [32] suggest a simple conservative formula for estimating atmospheric leakage of air into the evaporator as

$$m_{air,lk,E} = 0.005\ Po_{gross} / 1000 = 0.05\ KG/S \quad \text{(G-52)}$$

which combined with the known mass fraction of each noncondensable in the air determined in Kona earlier in this report as

$$x_{N2,air} = 0.788$$

$$x_{O2,air} = 0.185$$

$$x_{Ar,air} = 0.0065$$

$$x_{CO2,air} = 0.0002$$

$$x_{H2O,air} = 0.040$$

yields a mass flow of noncondensables attributable to atmospheric leakage

$$m_{N2,lk,E} = x_{N2,air}\, m_{air,lk,E} = 0.0394\ KG/S \quad \text{(G-53)}$$

$$m_{O2,lk,E} = x_{O2,air}\, m_{air,lk,E} = 0.0092\ KG/S \quad \text{(G-54)}$$

$$m_{Ar,lk,E} = x_{Ar,air}\, m_{air,lk,E} = 0.0003\ KG/S \quad \text{(G-55)}$$

$$m_{CO2,lk,E} = x_{CO2,air}\, m_{air,lk,E} = 0.0000\ KG/S \quad \text{(G-56)}$$

$$m_{H2O,lk,E} = x_{H2O,air}\, m_{air,lk,E} = 0.0020\ KG/S. \quad \text{(G-57)}$$

Therefore, the total noncondensable mass flows from the evaporator are defined as

$$m_{N2,E} = m_{N2,lk,E} = 0.0394\ KG/S \quad \text{(G-58)}$$

$$m_{O2,E} = m_{O2,lk,E} = 0.0092\ KG/S \quad \text{(G-59)}$$

$$m_{Ar,E} = m_{Ar,lk,E} = 0.0003\ KG/S \quad \text{(G-60)}$$

$$m_{CO2,E} = m_{CO2,lk,E} = 0.0000\ KG/S \quad \text{(G-61)}$$

$$m_{H20,E} = m_{steam,4} + m_{H20,lk,E} = 150.3\ KG/S. \quad \text{(G-62)}$$

The noncondensable mass flow ($m_{NC,E}$) from the evaporator becomes

$$m_{NC,E} = m_{N2,E} + m_{O2,E} + m_{Ar,E} + m_{CO2,E} = 0.0510 \text{ KG/S} \quad \text{(G-63)}$$

The total moles of noncondensables in the evaporator is then determined

$$M_{N2,E} = m_{N2,E} / MW_{N2} = 0.0014 \text{ KG-MOL/S} \quad \text{(G-64)}$$

$$M_{O2,E} = m_{O2,E} / MW_{O2} = 0.0003 \text{ KG-MOL/S} \quad \text{(G-65)}$$

$$M_{Ar,E} = m_{Ar,E} / MW_{Ar} = 0.0000 \text{ KG-MOL/S} \quad \text{(G-66)}$$

$$M_{CO2,E} = m_{CO2,E} / MW_{CO2} = 0.0000 \text{ KG-MOL/S} \quad \text{(G-67)}$$

$$M_{H2O,E} = m_{H2O,E} / MW_{H2O} = 8.35 \text{ KG-MOL/S} \quad \text{(G-68)}$$

which yields a mole fraction ($y_{steam,E}$) of steam in the evaporator of

$$y_{steam,E} = M_{H2O,E} / (M_{H2O,E} + M_{N2,E} + M_{O2,E} + M_{Ar,E} + M_{CO2,E}) \quad \text{(G-69)}$$

$$= 0.9998.$$

The evaporator working pressure (P_E) can then be determined as

$$P_E = P_{4,E} / y_{steam,E} = 2.82 \text{ KPa.} \quad \text{(G-70)}$$

Originally, in the turbine analysis section, the additional energy available due to the leaked noncondensables accompanying the steam through the turbine section was ignored so that the turbine design analysis could be performed since the noncondensable flow was unknown and represents less than 0.3% error. At this point the power available from the existing designed turbine system is calculated as

$$Po_{gross} = m_{tot,gas,E} \Delta h_{t\text{-}s} \eta_{t\text{-}s} \eta_g = 10{,}004 \text{ KW} \quad \text{(G-71)}$$

where

$$m_{tot,gas,E} = \text{total gas flow from evaporator}$$

$$= m_{NC,E} + m_{steam,6} = 146.9 \text{ KG/S.} \quad \text{(G-72)}$$

G.3.1 EVAPORATOR PREDEAERATOR DESIGN

The predeaerator design begins by setting the predeaerator pressure ($P_{pre,E}$) at the value utilized in the predeaeration experiments conducted by Zapka [51]

$$P_{pre,E} = 6.67 \text{ KPa.}$$

By setting the predeaerator pressure at this value and utilizing a similar structural design to the experimental predeaeration vessel (Figure 5.2), permits the assumption of predeaeration levels approaching those predicted by Zapka of approximately 85% desorption with bubble seeding within this predeaerator design.

With the design warm water flow rate determined (m_2) the noncondensable desorption rate within the predeaerator can now be estimated from the desorption rates determined by Zapka [51].

Warm water predeaeration % with bubble seeding:

$$x_{N2,E} = 0.85$$

$$x_{O2,E} = 0.85$$

$$x_{Ar,E} = 0.85$$

$$x_{CO2,E} = 0.006 \text{ (total carbon)*}$$

* NOTE: For the purposes of this investigation the desorption rate of carbon dioxide predicted for the predeaerator is assumed the same as that predicted by the experimental portion of this investigation since Zapka's desorption rate of 85% does not readily apply to the concept of "total" carbon and this level of desorption should be conservative and does not introduce any significant error to the predeaeration analysis.

Warm water entrance noncondensable concentrations [21]:

$$M_{N2,2} = 0.3804 \text{ MMOL/L}$$

$$M_{O2,2} = 0.2039 \text{ MMOL/L}$$

$$M_{Ar,2} = 0.0100 \text{ MMOL/L}$$

$$M_{CO2,2} = 1.933 \text{ MMOL/L (total carbon)}$$

From these values the molar release of each noncondensable is determined as

$$M_{N2,DES} = x_{N2,E} M_{N2,2} = 0.323 \text{ MMOL/L} \quad \text{(G-73)}$$

$$M_{O2,DES} = x_{O2,E} M_{O2,2} = 0.173 \text{ MMOL/L} \quad \text{(G-74)}$$

$$M_{Ar,DES} = x_{Ar,E} M_{Ar,2} = 0.0085 \text{ MMOL/L} \quad \text{(G-75)}$$

$$M_{CO2,DES} = x_{CO2,E} M_{CO2,2} = 0.0110 \text{ MMOL/L} \quad \text{(G-76)}$$

which delivers the mass release of noncondensables as

$$m_{N2,DES} = M_{N2,DES} m_2 MW_{N2} / (1000 \rho_2) = 0.230 \text{ KG/S} \quad \text{(G-77)}$$

$$m_{O2,DES} = M_{O2,DES} m_2 MW_{O2} / (1000 \rho_2) = 0.141 \text{ KG/S} \quad \text{(G-78)}$$

$$m_{Ar,DES} = M_{Ar,DES} m_2 MW_{Ar} / (1000 \rho_2) = 0.0086 \text{ KG/S} \quad \text{(G-79)}$$

$$m_{CO2,DES} = M_{CO2,DES} m_2 MW_{CO2} / (1000 \rho_2) = 0.0123 \text{ KG/S} \quad \text{(G-80)}$$

where the factor 1000 converts G/S to KG/S.

These noncondensable flow rates represent the amount of noncondensables expected to be desorbed at the system pressure within the evaporator predeaerator with bubble seeding. However, these are not the only noncondensables present within the predeaeration vessel. The bubble seeding itself introduces a significant level of noncondensables to the predeaeration system. It is therefore necessary to determine the injection rate of noncondensables needed to accomplish the desired level of predeaeration

predicted in the previous equations. This requires the knowledge of noncondensable (air) injection rate performed in Zapka's [51] experiments mentioned previously.

Zapka [51] performed his predeaeration experiments with a ratio of air injection to seawater volume ($R_{air/water}$) of

$R_{air/water}$ = 0.5 L air / 30 L water = 0.0167 M^3air / M^3water

at an approximate seawater temperature and corresponding values of

T_{Zap} = 25.00 °C

ρ_{Zap} = 1022.1 KG/M^3

ρ_{air} = density of air at atmospheric pressure and 21 °C

= 1.20 KG/M^3

MW_{air} = molecular weight of air

= 28.97 KG/KG-MOL [17].

These values suggest a molar fraction of noncondensables to seawater in Zapka's experiments as

$$MF_{NC} = R_{air/water}\ \rho_{air}\ MW_{H20} / (\rho_{Zap}\ MW_{air})$$

$$= 1.22 \times 10^{-5} \text{ KG-MOL air / KG-MOL water.} \qquad \text{(G-81)}$$

With the mass flow of seawater necessary (m_2) determined in the evaporator analysis previously, the volumetric flow of seawater into the predeaerator (Q_2) is determined as

$$Q_2 = m_2 / \rho_2 = 25.40 \text{ } M^3/S \qquad \text{(G-82)}$$

which yields a molar flow of seawater (M_2) as

$$M_2 = m_2 / MW_{H2O} = 1440.61 \text{ KG-MOL/S.} \qquad \text{(G-83)}$$

Thus, the desired noncondensable molar injection rate for the designed evaporator predeaerator is

$$M_{pre,E,inj} = M_2 \, MF_{NC} = 0.0175 \text{ KG-MOL/S} \quad \text{(G-84)}$$

with a corresponding noncondensable mass injection rate of

$$m_{pre,E,inj} = M_{pre,E,inj} \; MW_{NC,DES} = 0.516 \text{ KG/S} \quad \text{(G-85)}$$

where

$MW_{NC,DES}$ = molecular weight of noncondensables predeaerated from the warm water stream since the injection gases are recycled from the evaporator predeaerator vent compressor exhaust gases

$$= (m_{N2,DES} \, MW_{N2} + m_{O2,DES} \, MW_{O2} + m_{Ar,DES} \, MW_{Ar} + m_{CO2,DES} \, MW_{CO2}) / m_{NC,DES,tot}$$

$$= 29.49 \text{ KG/KG-MOL} \quad \text{(G-86)}$$

$$m_{NC,DES,tot} = m_{N2,DES} + m_{O2,DES} + m_{Ar,DES} + m_{CO2,DES} \quad \text{(G-87)}$$

$$= 0.392 \text{ KG/S.}$$

With the corresponding mass fractions assumed for the injected gases, the total flow of noncondensables within the evaporator predeaerator are

$$m_{N2,pre,E,tot} = 0.533 \text{ KG/S}$$

$$m_{O2,pre,E,tot} = 0.326 \text{ KG/S}$$

$$m_{Ar,pre,E,tot} = 0.020 \text{ KG/S}$$

$$m_{CO2,pre,E,tot} = 0.029 \text{ KG/S}$$

with corresponding molar flows of

$$M_{N2,pre,E,tot} = 0.0190 \text{ KG-MOL/S}$$

$$M_{O2,pre,E,tot} = 0.0102 \text{ KG-MOL/S}$$

$$M_{Ar,pre,E,tot} = 0.0005 \text{ KG-MOL/S}$$

$$M_{CO2,pre,E,tot} = 0.0006 \text{ KG-MOL/S.}$$

As discussed previously in this report and represented by Figure 5.2, the evaporator-predeaeration system should be designed as a single component to minimize the initial capital costs for these particular components. Therefore, the design flow area ($A_{pre,E}$) and the predeaerator diameter ($D_{pre,E}$) are the same as the evaporator area (A_E) and diameter (D_E) determined earlier as

$$A_{pre,E} = A_E = 425.6\ M^2$$

$$D_{pre,E} = D_E = 23.28\ M.$$

The design water depth of the predeaerator ($H_{pre,E}$) is then determined iteratively assuming a minimum residence time (RT_{pre} = 25 sec [51]) of the seawater within the predeaerator necessary to achieve the design predeaeration rate of 85% predicted by Zapka [51]. The final values for this design after iteration are

$$H_{pre,E} = 1.50\ M$$

$$VOL_{pre,E} = 638.4\ M^3$$

$$RT_{pre} = VOL_{pre,E} / Q_2 = 25.13\ S. \qquad \text{(G-88)}$$

G.3.2 EVAPORATOR PREDEAERATOR VENT COMPRESSOR DESIGN

The initial assumptions necessary for the evaporator predeaerator vent compressor analysis are the same as those described previously in Appendix F.5 for the condenser vent compression train.

Once again the design procedure necessitates determining the compression ratio (constant for each stage) from an estimate of the number of

compression stages necessary (N_{comp}), an assumed intercooler pressure drop (ΔP_{inter}), an initial compressor pressure ($P_{in,(1)} = P_{pre,E}$) and a design compressor exhaust pressure ($P_{14,design}$) as

$$N_{comp} = 2$$

$$\Delta P_{inter} = 0.276 \text{ KPa [32]}$$

$$P_{in,(1)} = P_{13} = 6.67 \text{ KPa}$$

$$P_{14,design} = 25.00 \text{ KPa.}$$

The design compressor exhaust pressure is not atmospheric as was the case in the condenser vent compressor discussed previously. This predeaerated/reinjected OC-OTEC system permits much lower compression power requirements because of the significantly lower exhaust pressures allowable for noncondensable reinjection versus atmospheric discharges. The minimum exhaust pressure ($P_{14,min}$) is found by determining the minimum injection pressure permitted into the evaporator predeaerator since this compressor exhaust will not only be reinjected into the warm water effluent stream but will also serve as the injection gas for bubble seeding (see Figure 5.1). Therefore, the minimum exhaust pressure ($P_{14,min}$) is found from the predeaerator system pressure ($P_{pre,E}$) and the seawater head as

$$P_{14,min} = P_{pre,E} + H_{pre,E}\, \rho_2\, G / 1000 = 21.69 \text{ KPa.} \qquad \text{(G-89)}$$

From the minimum injection pressure a design compressor exhaust pressure is chosen as

$$P_{14,design} = 25.00 \text{ KPa}$$

to allow enough over pressure to encourage bubble flow through the predeaerator seawater.

With the design parameters set above, the compression ratio is determined iteratively as described previously by solving

$$R_{comp}^{n} = (P_{14,design} + \Delta P_{inter} \sum_{i=1}^{n} R_{comp}^{i}) / P_{in,(1)} = 2.00. \quad \text{(G-90)}$$

The final iteration is displayed in the following table (Table G.1)

Table G.1: Iteration of Condenser Vent Compression Ratio

Step #	$\sum R_{comp}$	$R_{comp,\,i}$
1	2.00	1.96
2	5.83	2.00

The respective inlet and outlet pressures for each compressor stage is found in the following manner

$$P_{in,(1)} = P_{pre,E} = P_{13} = 6.67 \text{ KPa}$$

$$P_{out,(1)} = P_{in,(1)} R_{comp} = 13.32 \text{ KPa} \quad \text{(G-91)}$$

$$P_{in,(2)} = P_{out,(1)} - \Delta P_{inter} = 13.04 \text{ KPa} \quad \text{(G-92)}$$

$$P_{out,(2)} = P_{in,(2)} R_{comp} = P_{14} = 26.06 \text{ KPa} \quad \text{(G-93)}$$

With the inlet vapor temperature for each stage set at 7.00 $^{\circ}$C (discussed previously), the water vapor partial pressure entering each

compressor stage is simply the saturation pressure at that temperature ($P_{sat,13A}$ = 1.00 KPa). This water vapor pressure combined with the inlet pressures for each compression stage and the noncondensable flows entering from the evaporator predeaerator yield the inert gas partial pressures for each compressor stage as

$$PP_{N2,(i)} = (P_{in,(i)} - P_{sat,13A}) / [1+ (M_{O2,pre,E,tot}+ M_{Ar,pre,E,tot}+ M_{CO2,pre,E,tot}) / M_{N2,pre,E,tot}] \quad \text{(G-94)}$$

$$PP_{O2,(i)} = (P_{in,(i)} - P_{sat,13A}) / [1+ (M_{N2,pre,E,tot}+ M_{Ar,pre,E,tot}+ M_{CO2,pre,E,tot}) / M_{O2,pre,E,tot}] \quad \text{(G-95)}$$

$$PP_{Ar,(i)} = (P_{in,(i)} - P_{sat,13A}) / [1+ (M_{N2,pre,E,tot}+ M_{O2,pre,E,tot}+ M_{CO2,pre,E,tot}) / M_{Ar,pre,E,tot}] \quad \text{(G-96)}$$

$$PP_{CO2,(i)} = P_{in,(i)} - P_{sat,13A} - PP_{N2,i} - PP_{O2,i} - PP_{Ar,i} \quad \text{(G-97)}$$

where the subscript i denotes the respective compression stages as i = 1 to n with the specific values presented in Table G.2 shown below. The corresponding water vapor flow accompanying this noncondensable flow through each compression stage is determined by

$$m_{wv,(i)} = MW_{H20}\, P_{sat,13A}\, M_{N2,pre,E,tot} / PP_{N2,(i)}. \quad \text{(G-98)}$$

The total parasitic power consumption for each compression stage is now defined by Parsons et al. [32] as

$$Po(i) = -(r / r\text{-}1)\, M_{gas,tot}\, R_g\, T_{13A} [1 - R_{comp}^{\{(r-1)/r\}}] / \eta_m\, \eta_{comp} \quad \text{(G-99)}$$

where

r = ratio of gas specific heats = 1.4 (assumed) [32]

$M_{gas,tot,(i)}$ = molar flow of gas through compressor stage

$$= m_{gas,tot,(i)} / GMWT_{(i)} \quad \text{(G-100)}$$

$$m_{gas,tot,(i)} = m_{wv,(i)} + m_{N2,pre,E,tot} + m_{O2,pre,E,tot} + m_{Ar,pre,E,tot} + m_{CO2,pre,E,tot} \quad \text{(G-101)}$$

$$GMWT_{(i)} = (PP_{N2,(i)}\, MW_{N2} + PP_{O2,(i)}\, MW_{O2} + PP_{Ar,(i)}\, MW_{Ar} + PP_{CO2,(i)}\, MW_{CO2} + P_{sat,13A}\, MW_{H2O}) / P_{in,(i)} \quad \text{(G-102)}$$

R_g = universal gas constant = 8.31 KPa M^3 / KG-MOL $^{\circ}K$ [17]

η_m = compressor motor efficiency = 0.90 [32]

η_{comp} = compressor efficiency = 0.80 [32]

T_{13A} = vapor inlet temperature (intercooler exit temperature)
= 280.15 $^{\circ}K$.

The volume flow of gas through each compression stage is defined as

$$VOL_{gas,(i)} = M_{gas,tot,(i)}\, R_g\, T_{13A} / P_{in,(i)}. \quad \text{(G-103)}$$

The following tables (Table G.2 and G.3) display the calculation procedure for each compression stage and present the parasitic power associated with each stage using the aforementioned equations from which the total parasitic power necessary to maintain proper system vacuum within the designed evaporator predeaerator is derived.

Table G.2: Noncondensable Partial Pressures for Staged Compression from Evaporator Predeaerator Vent Compressor

Stage #	PP_{N2} (KPa)	PP_{O2} (KPa)	PP_{Ar} (KPa)	PP_{CO2} (KPa)
1	3.5523	1.9070	0.0935	0.1122
2	7.5506	4.0535	0.1987	0.2384
exhaust conditions	15.7121	8.4349	0.4135	0.4962

Table G.3: Calculated Values for Staged Compression from Evaporator Predeaerator Vent Compressor

Stage #	GMWT (KG/KG-MOL)	m_{wv} (KG/S)	$m_{gas,tot}$ (KG/S)	VOL_{gas} (M^3/S)	$Po_{(i)}$ (KW)
1	28.0884	0.0965	1.0015	12.4142	87.9595
2	28.9588	0.2318	0.9504	5.8404	80.9639
exhaust conditions	29.4133	0.0218	0.9268	2.8066	--

Total parsitic power for the evaporator predeaerator vent compression train is

$$Po_{pre,E,VC,tot} = 169 \text{ KW}.$$

G.3.3 EVAPORATOR HYDRAULIC COMPRESSOR DESIGN

The hydraulic compressor design for the evaporator incorporates two varying designs as outlined previously in this report. The first utilizes the existing warm water discharge pipe as the hydraulic compression mechanism while the second utilizes a designed tapering pipe configuration as the compression mechanism. In order to prevent confusion of the two design procedures, the evaporator hydraulic compressor design analysis has been separated into two distinct sections.

G.3.3.1 HYDRAULIC COMPRESSOR - EXISTING PIPE DESIGN

The existing pipe analysis for the hydraulic compression mechanism essentially entails the determination of the portion of the downcomer necessary to perform the majority of the compression of the injected noncondensables to the point where these gases no longer significantly interfere with the warm water discharge flow. This analysis should include a means of estimating the reabsorption rate of the noncondensables and the necessary head required to overcome the seawater velocity change associated with the reduced flow area accompanying the introduction of these noncondensables to the flow stream.

From the warm water flow system analysis of Appendix F.6.1 for the non-predeaerated/reinjected system the design seawater flow velocity (X_3) and the design pipe diameter ($D_{3,pipe}$) and area ($A_{3,pipe}$) were

$$X_3 = 2.00 \text{ M/S}$$

$$D_{3,pipe} = 4.02 \text{ M}$$

$$A_{3,pipe} = 12.7 \text{ M}^2$$

and apply here for the discharge pipe parameters since they are based on design warm water mass flow (m_3) and volumetric flow ($Q_{3,ww}$) which are identical for both the predeaerated/reinjected and the non-predeaerated design

$$m_3 = 25953 \text{ KG/S}$$

$$Q_{3,ww} = 25.4 \text{ M}^3\text{/S}.$$

The design warm water flow velocity (X_3) will not remain this value in this hydraulic compressor design because the void fraction in the discharge pipe

area caused by the presence of the injected noncondensables will increase this velocity at the point of injection and will subsequently decrease as the noncondensable void fraction is reduced with the combined action of hydraulic compression and reabsorption of the injected gases. It will be the estimated effects of the injected noncondensables on the seawater flow velocity which will eventually determine the overall hydraulic losses associated with this type of hydraulic compression device. This will be presented in more detail following.

Initially, it is necessary to ensure that the injected gas bubbles will flow downward along the hydraulic compressor and not rise within the downcomer. To ensure that this is the case, the drag force (F_D) on the injected bubble must be greater than the buoyancy force (F_B) experienced in the seawater medium. The drag force (F_D) for an air bubble within flowing water is defined by Rice [37] as

$$F_D = (\pi / 4)\, C_D\, d_B^2\, \rho_3\, X_3^2 / 2 \approx 7.33 \times 10^{-3}\ N \qquad \text{(G-104)}$$

where

C_D = drag coefficient for spherical air bubbles in water at a Re $\approx 8.9 \times 10^6$ = 2.7 [36]

d_B = bubble diameter $\approx$ 0.0013 M [51]

ρ_3 = seawater density = 1022.5 KG/M^3

X_3 = seawater velocity = 2.00 M/S

The buoyancy force (F_B) for the injected bubbles is defined by Rice [37] as

$$F_B = (\pi / 6)\ d_B^3\, \Delta\rho\, G = 1.15 \times 10^{-5}\ N \qquad \text{(G-105)}$$

where $\Delta\rho$ = density difference between seawater and injected noncondensables

$$= \rho_3 - \rho_{NC,inj} \qquad \text{(G-106)}$$

$$= 1022.2\ KG/M^3$$

$\rho_{NC,inj}$ = density of injected noncondensables from evaporator predeaerator compressor design

$$= m_{gas,tot} / VOL_{gas} = 0.33 \text{ KG/M}^3. \quad \text{(G-107)}$$

Each equation assumes a spherical bubble, which is a poor assumption under the expected Reynolds number and flow conditions. However, as a first approximation, because the difference in drag force is nearly three orders of magnitude larger than the buoyancy force for the largest bubble diameter experienced in Zapka's experiments with seawater [51], this suggests that the injected bubbles will flow downward in the system's downcomer (hydraulic compressor).

In fact, for a bubble to rise in this system under the design flow conditions, it's diameter would have to exceed 0.826 M (determined by setting $F_D = F_B$). This is an unrealistic bubble size (coalescence is minimal in seawater [51]) even considering the low injection pressures experienced in this design. Therefore, due to the large discrepancy between the drag force and buoyancy force estimated here, the injected bubbles in all subsequent hydraulic compressor analyses can be expected to flow downward essentially at the seawater flow velocity (X_3, etc.).

To begin the design procedure for this hydraulic compressor, it is initially necessary to define the pressure change with pipe length (dP/dh) expected as the seawater travels along the downcomer. This value is simply defined as

$$dP/dh = \rho_3 G = 10.03 \text{ KPa/M}. \quad \text{(G-108)}$$

The next step is to determine the desired point of noncondensable injection from which the hydraulic compression analysis can commence. The pressure at the injection point ($P_{inj,ww}$) is then set slightly less than the compressor

exhaust pressure (P_{14}) from the previous evaporator predeaerator compressor analysis and the distance from pipe entrance to the point of reinjection ($h_{inj,E}$) is determined as follows

$$P_{inj,ww} = 25.50 \text{ KPa}$$

$$h_{inj,E} = (P_{inj,ww} - P_E) / (dP/dh) = 2.26 \text{ M.} \quad \text{(G-109)}$$

This is the point where the hydraulic compressor design is initiated.

With the length of the hydraulic compression region necessary to significantly reduce the volumetric flow of the noncondensables unknown, the procedure for determining the hydraulic head requirements is iterative in nature. For the first iteration it is assumed that no reabsorption of the noncondensables occurs and a rough estimate of the necessary length to perform a compression in which the gas volume in the warm water discharge flow approaches 0.5% is determined as

$$Q_{NC,end} = 0.005 \; Q_3 = 0.127 \text{ M}^3\text{/S} \quad \text{(G-110)}$$

which yields an estimated seawater velocity ($X_{3,end}$) at the "end" of the compressor of

$$X_{3,end} = (Q_3 + Q_{NC,end}) / A_{3,pipe} = 2.01 \text{ M/S} \quad \text{(G-111)}$$

and a corresponding local pressure of

$$P_{3,end} = M_{inj,E} R_g T_3^* / Q_{NC,end}) + P_{inj,E,ww} = 296.68 \text{ KPa} \quad \text{(G-112)}$$

where

T_3^* = seawater temperature = 298.61 °K

$M_{inj,E}$ = molar flow of injected gas

$$= m_{inj,E} / MW_{inj,E} = 0.0140 \text{ KG-MOL/S} \quad \text{(G-113)}$$

$m_{inj,E}$ = mass flow of injected gas

$$= m_{NC,pre,E,tot} - m_{pre,inj,E} = 0.411 \text{ KG/S.} \quad \text{(G-114)}$$

This "end" pressure corresponds to a hydraulic compressor length from point of gas injection to compressor "end" of

$$h_{comp} = (P_{3,end} - P_{inj,E,ww}) / (dP/dh) = 27.04\ M \qquad (G\text{-}115)$$

to be used for the first iteration.

The final value after the iterative process accounting for noncondensable reabsorption and gas compression is

$$h_{comp} = 12.57\ M.$$

In order to determine the total head required to overcome the presence of the injected noncondensables, the length of the hydraulic compressor from the point of injection to the "end" of the compression region is iterated (100 iterations) along the total length (h_{comp}). At each segment along the hydraulic compressor (h_i) where

$$h_i = h_{inj,E} + \Delta h_E \qquad (G\text{-}116)$$

for the first segment and h_i is positive downward to the "end" of the design compressor region as

$$h_i = h_{i-1} + \Delta h_E \qquad (G\text{-}117)$$

where

$$\Delta h_E = h_{comp} / 100 = 0.126\ M \qquad (G\text{-}118)$$

the following parameters are determined utilizing the calculated Henry's law constants for the seawater temperature (T_3) and assumed seawater salinity of 35.00 °/oo which yield

$$K_{H,N2} = C_{N2}\, MV_{ideal} / (1000 \times 101.33)$$
$$= 3.96 \times 10^{-6}\ KG\text{-}MOL / M^3\ KPa \qquad (G\text{-}119)$$

$$K_{H,O2} = C_{O2}\, MV_{ideal} / (1000 \times 101.33)$$
$$= 2.14 \times 10^{-6}\ KG\text{-}MOL / M^3\ KPa \qquad (G\text{-}120)$$

$$K_{H,Ar} = C_{Ar} MV_{ideal} / (1000 \times 101.33)$$

$$= 1.05 \times 10^{-7} \text{ KG-MOL} / M^3 \text{ KPa} \quad \text{(G-121)}$$

$$K_{H,CO2} = C_{CO2} \rho_3 / (1000 \times 101.33)$$

$$= 2.98 \times 10^{-4} \text{ KG-MOL} / M^3 \text{ KPa} \quad \text{(G-122)}$$

where

C_{gas} = concentration of specific gas (excluding CO_2) determined from equations presented at outset of Appendix F taken from [47] (ML/L)

C_{CO2} = concentration of CO_2 determined by equation presented at outset of Appendix F taken from [39] (MOL/KG - ATM)

MV_{ideal} = molar volume of an ideal gas

= 22.4 M^3/ KG-MOL ATM [46]

The value of 1000 in the nitrogen, oxygen and argon equations converts milliliters to liters while the 101.33 converts atmospheres to KPa for all equations. For the carbon dioxide equation, the 1000 converts moles to kg-moles.

The development of the hydraulic compressor design continues with the determination of the following values as

P_i = pressure of water column at iteration segment i

$$= h_i \, dP/dh + P_{i-1} \quad \text{(KPa)} \quad \text{(G-123)}$$

$M_{N2,i}$ = molar flow of nitrogen at iteration segment i

$$= M_{N2,i-1} - [(C_{NC,i-1} - C_{NC,i-2}) Q_3 M_{N2,i-1} / (M_{N2,i-1} + M_{O2,i-1} + M_{Ar,i-1} + M_{CO2,i-1})] \quad \text{(G-124)}$$

$M_{O2,i}$ = molar flow of oxygen at iteration segment i

$$= M_{O2,i-1} - [(C_{NC,i-1} - C_{NC,i-2})\, Q_3\, M_{O2,i-1} / (M_{N2,i-1} + M_{O2,i-1} + M_{Ar,i-1} + M_{CO2,i-1})] \quad \text{(G-125)}$$

$M_{Ar,i}$ = molar flow of argon at iteration segment i

$$= M_{Ar,i-1} - [(C_{NC,i-1} - C_{NC,i-2})\, Q_3\, M_{Ar,i-1} / (M_{N2,i-1} + M_{O2,i-1} + M_{Ar,i-1} + M_{CO2,i-1})] \quad \text{(G-126)}$$

$M_{CO2,i}$ = molar flow of CO_2 at iteration segment i

$$= M_{CO2,i-1} - [(C_{NC,i-1} - C_{NC,i-2})\, Q_3\, M_{CO2,i-1} / (M_{N2,i-1} + M_{O2,i-1} + M_{Ar,i-1} + M_{CO2,i-1})] \quad \text{(G-127)}$$

$PP_{N2,i}$ = partial pressure of nitrogen at i

$$= (P_i - P_{sat,3}) / [\, 1 + (M_{O2,i} + M_{Ar,i} + M_{CO2,i}) / M_{N2,i}] \quad \text{(G-128)}$$

$PP_{O2,i}$ = partial pressure of oxygen at i

$$= (P_i - P_{sat,3}) / [\, 1 + (M_{N2,i} + M_{Ar,i} + M_{CO2,i}) / M_{O2,i}] \quad \text{(G-129)}$$

$PP_{Ar,i}$ = partial pressure of argon at i

$$= (P_i - P_{sat,3}) / [\, 1 + (M_{N2,i} + M_{O2,i} + M_{CO2,i}) / M_{Ar,i}] \quad \text{(G-130)}$$

$PP_{CO2,i}$ = partial pressure of carbon dioxide at i

$$= P_i - P_{sat,3} - PP_{N2,i} - PP_{O2,i} - PP_{Ar,i} \quad \text{(G-131)}$$

$C_{sat,i}$ = saturation concentration for all gas species at local pressure and seawater temperature

$$= K_{H,N2}\, PP_{N2,i} + K_{H,O2}\, PP_{O2,i} + K_{H,Ar}\, PP_{Ar,i} + KH_{CO2}\, PP_{CO2,i} \ (\text{KG-MOL/M}^3) \quad \text{(G-132)}$$

$Kl*a_i$ = overall mass transfer coefficient

$$= 0.00039\,(P_{i-1} - P_i) \quad \text{for } P_i < 90 \text{ KPa} \quad \text{(G-133)}$$

$$= 0.0053\,(P_{i-1} - P_i) - 0.428 \quad \text{for } P_i > 90 \text{ KPa} \quad \text{(G-134)}$$

(taken from data in [51]) (1/S)

$t_{RES,i}$ = residence time in iteration segment i

$= \Delta h_i / X_{3,i-1}$ (S) (G-135)

$C_{NC,i}$ = concentration of noncondensables in seawater at i

$= C_{sat,i} - (C_{sat,i} - C_{NC,i-1}) / EXP (Kl*a\ t)$ (KG-MOL/M^3) (G-136)

n_i = number of moles of gas at iteration segment i

$= n_{i-1} - C_{NC,i} Q_3$ (KG-MOL/S) (G-137)

$Q_{NC,i}$ = volumetric flow of gas at iteration segment i

$= n_i R_g T_3^* / P_i$ (M^3/S) (G-138)

$A_{pipe,i}$ = area for liquid flow in discharge pipe at i

$= A_{3,pipe} - [Q_{NC,i} / (Q_{NC,i} + Q_3)] A_{3,pipe}$ (M^2) (G-139)

$X_{3,i}$ = velocity of seawater at iteration segment i

$= Q_3 / A_{pipe,i}$ (M/S) (G-140)

$H_{HC,i}$ = head required to overcome reduced flow area at i

$= (X_3 - X_{3,i})^2 / 2 G$ (M) (G-141)

The initial molar concentrations of the noncondensables and initial partial pressures are passed from the evaporator predeaerator vent compression analysis preceding this section. Likewise, the initial seawater noncondensable concentration was determined from the evaporator predeaerator analysis. The following tables present the data along the entire length of the hydraulic compression region utilizing these initial values to begin the iterative process.

Table G.4 : Hydraulic Compressor Analysis - Standard Discharge Pipe

h_i	P_i	$M_{N2,i}$	$M_{O2,i}$	$M_{Ar,i}$	$M_{CO2,i}$
0.0000	25.5000	8.2135E-03	4.4028E-03	2.1594E-04	2.7944E-04
0.1257	26.7604	8.2124E-03	4.4022E-03	2.1591E-04	2.7940E-04
0.2514	28.0209	8.2112E-03	4.4016E-03	2.1588E-04	2.7936E-04
0.3771	29.2813	8.2098E-03	4.4008E-03	2.1584E-04	2.7931E-04
0.5028	30.5417	8.2082E-03	4.4000E-03	2.1580E-04	2.7926E-04
0.6285	31.8021	8.2064E-03	4.3990E-03	2.1575E-04	2.7919E-04
0.7542	33.0626	8.2044E-03	4.3979E-03	2.1570E-04	2.7913E-04
0.8799	34.3230	8.2021E-03	4.3967E-03	2.1564E-04	2.7905E-04
1.0056	35.5834	8.1997E-03	4.3954E-03	2.1558E-04	2.7897E-04
1.1313	36.8438	8.1970E-03	4.3939E-03	2.1551E-04	2.7887E-04
1.2570	38.1043	8.1940E-03	4.3923E-03	2.1543E-04	2.7877E-04
1.3827	39.3647	8.1907E-03	4.3906E-03	2.1534E-04	2.7866E-04
1.5084	40.6251	8.1872E-03	4.3887E-03	2.1525E-04	2.7854E-04
1.6341	41.8856	8.1834E-03	4.3867E-03	2.1515E-04	2.7841E-04
1.7598	43.1460	8.1792E-03	4.3845E-03	2.1504E-04	2.7827E-04
1.8855	44.4064	8.1748E-03	4.3821E-03	2.1492E-04	2.7812E-04
2.0112	45.6668	8.1700E-03	4.3795E-03	2.1480E-04	2.7796E-04
2.1369	46.9273	8.1649E-03	4.3768E-03	2.1466E-04	2.7778E-04
2.2626	48.1877	8.1595E-03	4.3738E-03	2.1452E-04	2.7760E-04
2.3883	49.4481	8.1536E-03	4.3707E-03	2.1437E-04	2.7740E-04
2.5140	50.7085	8.1474E-03	4.3674E-03	2.1420E-04	2.7719E-04
2.6397	51.9690	8.1409E-03	4.3639E-03	2.1403E-04	2.7697E-04
2.7654	53.2294	8.1339E-03	4.3602E-03	2.1385E-04	2.7673E-04
2.8911	54.4898	8.1265E-03	4.3562E-03	2.1365E-04	2.7648E-04
3.0168	55.7503	8.1188E-03	4.3520E-03	2.1345E-04	2.7621E-04
3.1425	57.0107	8.1105E-03	4.3476E-03	2.1323E-04	2.7593E-04
3.2682	58.2711	8.1019E-03	4.3430E-03	2.1301E-04	2.7564E-04
3.3939	59.5315	8.0928E-03	4.3381E-03	2.1277E-04	2.7533E-04
3.5196	60.7920	8.0832E-03	4.3330E-03	2.1252E-04	2.7501E-04
3.6453	62.0524	8.0732E-03	4.3276E-03	2.1225E-04	2.7466E-04
3.7710	63.3128	8.0627E-03	4.3220E-03	2.1198E-04	2.7431E-04
3.8967	64.5733	8.0517E-03	4.3161E-03	2.1169E-04	2.7393E-04
4.0224	65.8337	8.0402E-03	4.3099E-03	2.1139E-04	2.7354E-04
4.1481	67.0941	8.0282E-03	4.3035E-03	2.1107E-04	2.7313E-04
4.2738	68.3545	8.0157E-03	4.2968E-03	2.1074E-04	2.7271E-04
4.3995	69.6150	8.0027E-03	4.2898E-03	2.1040E-04	2.7226E-04
4.5252	70.8754	7.9891E-03	4.2825E-03	2.1004E-04	2.7180E-04
4.6509	72.1358	7.9749E-03	4.2749E-03	2.0967E-04	2.7132E-04
4.7766	73.3962	7.9602E-03	4.2670E-03	2.0928E-04	2.7082E-04
4.9023	74.6567	7.9449E-03	4.2589E-03	2.0888E-04	2.7030E-04
5.0280	75.9171	7.9291E-03	4.2504E-03	2.0846E-04	2.6976E-04

5.1537	77.1775	7.9126E-03	4.2415E-03	2.0803E-04	2.6920E-04
5.2794	78.4380	7.8956E-03	4.2324E-03	2.0758E-04	2.6862E-04
5.4051	79.6984	7.8779E-03	4.2229E-03	2.0712E-04	2.6802E-04
5.5308	80.9588	7.8596E-03	4.2131E-03	2.0664E-04	2.6740E-04
5.6565	82.2192	7.8407E-03	4.2030E-03	2.0614E-04	2.6675E-04
5.7822	83.4797	7.8212E-03	4.1925E-03	2.0563E-04	2.6609E-04
5.9079	84.7401	7.8010E-03	4.1817E-03	2.0510E-04	2.6540E-04
6.0336	86.0005	7.7801E-03	4.1705E-03	2.0455E-04	2.6469E-04
6.1593	87.2609	7.7586E-03	4.1590E-03	2.0398E-04	2.6396E-04
6.2850	88.5214	7.7364E-03	4.1471E-03	2.0340E-04	2.6321E-04
6.4107	89.7818	7.7135E-03	4.1348E-03	2.0280E-04	2.6243E-04
6.5364	91.0422	7.6899E-03	4.1222E-03	2.0218E-04	2.6162E-04
6.6621	92.3027	7.6649E-03	4.1087E-03	2.0152E-04	2.6077E-04
6.7878	93.5631	7.6347E-03	4.0925E-03	2.0072E-04	2.5974E-04
6.9135	94.8235	7.5992E-03	4.0735E-03	1.9979E-04	2.5854E-04
7.0392	96.0839	7.5584E-03	4.0517E-03	1.9872E-04	2.5715E-04
7.1649	97.3444	7.5122E-03	4.0269E-03	1.9750E-04	2.5558E-04
7.2906	98.6048	7.4603E-03	3.9991E-03	1.9614E-04	2.5381E-04
7.4163	99.8652	7.4028E-03	3.9683E-03	1.9463E-04	2.5186E-04
7.5420	101.1256	7.3396E-03	3.9344E-03	1.9296E-04	2.4971E-04
7.6677	102.3861	7.2705E-03	3.8973E-03	1.9115E-04	2.4736E-04
7.7934	103.6465	7.1955E-03	3.8571E-03	1.8918E-04	2.4480E-04
7.9191	104.9069	7.1146E-03	3.8138E-03	1.8705E-04	2.4205E-04
8.0448	106.1674	7.0277E-03	3.7671E-03	1.8476E-04	2.3909E-04
8.1705	107.4278	6.9346E-03	3.7173E-03	1.8232E-04	2.3593E-04
8.2962	108.6882	6.8445E-03	3.6690E-03	1.7995E-04	2.3286E-04
8.4219	109.9486	6.7391E-03	3.6125E-03	1.7718E-04	2.2928E-04
8.5476	111.2091	6.6276E-03	3.5527E-03	1.7425E-04	2.2548E-04
8.6733	112.4695	6.5099E-03	3.4896E-03	1.7115E-04	2.2148E-04
8.7990	113.7299	6.3860E-03	3.4232E-03	1.6789E-04	2.1726E-04
8.9247	114.9903	6.2559E-03	3.3534E-03	1.6447E-04	2.1284E-04
9.0504	116.2508	6.1196E-03	3.2804E-03	1.6089E-04	2.0820E-04
9.1761	117.5112	5.9771E-03	3.2040E-03	1.5714E-04	2.0335E-04
9.3018	118.7716	5.8284E-03	3.1243E-03	1.5324E-04	1.9829E-04
9.4275	120.0321	5.6736E-03	3.0413E-03	1.4917E-04	1.9303E-04
9.5532	121.2925	5.5128E-03	2.9551E-03	1.4494E-04	1.8755E-04
9.6789	122.5529	5.3458E-03	2.8656E-03	1.4055E-04	1.8187E-04
9.8046	123.8133	5.1729E-03	2.7729E-03	1.3600E-04	1.7599E-04
9.9303	125.0738	4.9939E-03	2.6770E-03	1.3130E-04	1.6990E-04
10.0560	126.3342	4.8091E-03	2.5779E-03	1.2644E-04	1.6361E-04
10.1817	127.5946	4.6185E-03	2.4757E-03	1.2142E-04	1.5713E-04
10.3074	128.8550	4.4221E-03	2.3705E-03	1.1626E-04	1.5045E-04
10.4331	130.1155	4.2201E-03	2.2622E-03	1.1095E-04	1.4357E-04
10.5588	131.3759	4.0125E-03	2.1509E-03	1.0549E-04	1.3651E-04
10.6845	132.6363	3.7994E-03	2.0366E-03	9.9889E-05	1.2926E-04
10.8102	133.8968	3.5809E-03	1.9195E-03	9.4144E-05	1.2183E-04
10.9359	135.1572	3.3571E-03	1.7995E-03	8.8261E-05	1.1421E-04

11.0616	136.4176	3.1281E-03	1.6768E-03	8.2241E-05	1.0642E-04
11.1873	137.6780	2.8941E-03	1.5514E-03	7.6088E-05	9.8462E-05
11.3130	138.9385	2.6551E-03	1.4233E-03	6.9806E-05	9.0332E-05
11.4387	140.1989	2.4113E-03	1.2926E-03	6.3396E-05	8.2037E-05
11.5644	141.4593	2.1628E-03	1.1594E-03	5.6863E-05	7.3583E-05
11.6901	142.7198	1.9098E-03	1.0237E-03	5.0210E-05	6.4974E-05
11.8158	143.9802	1.6523E-03	8.8570E-04	4.3440E-05	5.6213E-05
11.9415	145.2406	1.3905E-03	7.4537E-04	3.6557E-05	4.7307E-05
12.0672	146.5010	1.1245E-03	6.0280E-04	2.9565E-05	3.8258E-05
12.1929	147.7615	8.5456E-04	4.5808E-04	2.2467E-05	2.9073E-05
12.3186	149.0219	5.8070E-04	3.1128E-04	1.5267E-05	1.9757E-05
12.4443	150.2823	3.0312E-04	1.6249E-04	7.9694E-06	1.0313E-05
12.5700	151.5427	2.1960E-05	1.1771E-05	5.7734E-07	7.4711E-07

Table G.4 : Hydraulic Compressor Analysis - Standard Discharge Pipe (Continued)

h_i	$PP_{N2,i}$	$PP_{O2,i}$	$PP_{Ar,i}$	$PP_{CO2,i}$	$C_{sat,i}$
0.0000	14.1655	7.5934	0.3724	0.4819	2.16E-04
0.1257	14.9551	8.0166	0.3932	0.5088	2.28E-04
0.2514	15.7446	8.4398	0.4139	0.5357	2.40E-04
0.3771	16.5342	8.8631	0.4347	0.5625	2.52E-04
0.5028	17.3237	9.2863	0.4555	0.5894	2.64E-04
0.6285	18.1133	9.7096	0.4762	0.6162	2.76E-04
0.7542	18.9029	10.1328	0.4970	0.6431	2.88E-04
0.8799	19.6924	10.5561	0.5177	0.6700	3.00E-04
1.0056	20.4820	10.9793	0.5385	0.6968	3.12E-04
1.1313	21.2716	11.4025	0.5592	0.7237	3.24E-04
1.2570	22.0611	11.8258	0.5800	0.7506	3.36E-04
1.3827	22.8507	12.2490	0.6008	0.7774	3.48E-04
1.5084	23.6403	12.6723	0.6215	0.8043	3.61E-04
1.6341	24.4298	13.0955	0.6423	0.8311	3.73E-04
1.7598	25.2194	13.5188	0.6630	0.8580	3.85E-04
1.8855	26.0089	13.9420	0.6838	0.8849	3.97E-04
2.0112	26.7985	14.3652	0.7046	0.9117	4.09E-04
2.1369	27.5881	14.7885	0.7253	0.9386	4.21E-04
2.2626	28.3776	15.2117	0.7461	0.9655	4.33E-04
2.3883	29.1672	15.6350	0.7668	0.9923	4.45E-04
2.5140	29.9568	16.0582	0.7876	1.0192	4.57E-04
2.6397	30.7463	16.4815	0.8083	1.0460	4.69E-04
2.7654	31.5359	16.9047	0.8291	1.0729	4.81E-04
2.8911	32.3255	17.3279	0.8499	1.0998	4.93E-04

3.0168	33.1150	17.7512	0.8706	1.1266	5.05E-04
3.1425	33.9046	18.1744	0.8914	1.1535	5.17E-04
3.2682	34.6941	18.5977	0.9121	1.1804	5.29E-04
3.3939	35.4837	19.0209	0.9329	1.2072	5.41E-04
3.5196	36.2733	19.4442	0.9537	1.2341	5.53E-04
3.6453	37.0628	19.8674	0.9744	1.2609	5.65E-04
3.7710	37.8524	20.2906	0.9952	1.2878	5.77E-04
3.8967	38.6420	20.7139	1.0159	1.3147	5.89E-04
4.0224	39.4315	21.1371	1.0367	1.3415	6.01E-04
4.1481	40.2211	21.5604	1.0575	1.3684	6.13E-04
4.2738	41.0107	21.9836	1.0782	1.3953	6.25E-04
4.3995	41.8002	22.4069	1.0990	1.4221	6.37E-04
4.5252	42.5898	22.8301	1.1197	1.4490	6.49E-04
4.6509	43.3794	23.2533	1.1405	1.4758	6.62E-04
4.7766	44.1689	23.6766	1.1612	1.5027	6.74E-04
4.9023	44.9585	24.0998	1.1820	1.5296	6.86E-04
5.0280	45.7480	24.5231	1.2028	1.5564	6.98E-04
5.1537	46.5376	24.9463	1.2235	1.5833	7.10E-04
5.2794	47.3272	25.3696	1.2443	1.6101	7.22E-04
5.4051	48.1167	25.7928	1.2650	1.6370	7.34E-04
5.5308	48.9063	26.2160	1.2858	1.6639	7.46E-04
5.6565	49.6959	26.6393	1.3066	1.6907	7.58E-04
5.7822	50.4854	27.0625	1.3273	1.7176	7.70E-04
5.9079	51.2750	27.4858	1.3481	1.7445	7.82E-04
6.0336	52.0646	27.9090	1.3688	1.7713	7.94E-04
6.1593	52.8541	28.3323	1.3896	1.7982	8.06E-04
6.2850	53.6437	28.7555	1.4103	1.8250	8.18E-04
6.4107	54.4332	29.1787	1.4311	1.8519	8.30E-04
6.5364	55.2228	29.6020	1.4519	1.8788	8.42E-04
6.6621	56.0124	30.0252	1.4726	1.9056	8.54E-04
6.7878	56.8019	30.4485	1.4934	1.9325	8.66E-04
6.9135	57.5915	30.8717	1.5141	1.9594	8.78E-04
7.0392	58.3811	31.2950	1.5349	1.9862	8.90E-04
7.1649	59.1706	31.7182	1.5557	2.0131	9.02E-04
7.2906	59.9602	32.1414	1.5764	2.0399	9.14E-04
7.4163	60.7498	32.5647	1.5972	2.0668	9.26E-04
7.5420	61.5393	32.9879	1.6179	2.0937	9.38E-04
7.6677	62.3289	33.4112	1.6387	2.1205	9.50E-04
7.7934	63.1184	33.8344	1.6594	2.1474	9.63E-04
7.9191	63.9080	34.2577	1.6802	2.1743	9.75E-04
8.0448	64.6976	34.6809	1.7010	2.2011	9.87E-04
8.1705	65.4871	35.1041	1.7217	2.2280	9.24E-04
8.2962	66.2767	35.5274	1.7425	2.2548	1.01E-03
8.4219	67.0663	35.9506	1.7632	2.2817	1.02E-03
8.5476	67.8558	36.3739	1.7840	2.3086	1.03E-03
8.6733	68.6454	36.7971	1.8048	2.3354	1.05E-03
8.7990	69.4350	37.2204	1.8255	2.3623	1.06E-03

8.9247	70.2245	37.6436	1.8463	2.3892	1.07E-03
9.0504	71.0141	38.0668	1.8670	2.4160	1.08E-03
9.1761	71.8037	38.4901	1.8878	2.4429	1.09E-03
9.3018	72.5932	38.9133	1.9085	2.4697	1.11E-03
9.4275	73.3828	39.3366	1.9293	2.4966	1.12E-03
9.5532	74.1723	39.7598	1.9501	2.5235	1.13E-03
9.6789	74.9619	40.1831	1.9708	2.5503	1.14E-03
9.8046	75.7515	40.6063	1.9916	2.5772	1.16E-03
9.9303	76.5410	41.0295	2.0123	2.6041	1.17E-03
10.0560	77.3306	41.4528	2.0331	2.6309	1.18E-03
10.1817	78.1202	41.8760	2.0539	2.6578	1.19E-03
10.3074	78.9097	42.2993	2.0746	2.6846	1.20E-03
10.4331	79.6993	42.7225	2.0954	2.7115	1.22E-03
10.5588	80.4889	43.1458	2.1161	2.7384	1.23E-03
10.6845	81.2784	43.5690	2.1369	2.7652	1.24E-03
10.8102	82.0680	43.9922	2.1576	2.7921	1.25E-03
10.9359	82.8575	44.4155	2.1784	2.8190	1.26E-03
11.0616	83.6471	44.8387	2.1992	2.8458	1.28E-03
11.1873	84.4367	45.2620	2.2199	2.8727	1.29E-03
11.3130	85.2262	45.6852	2.2407	2.8995	1.30E-03
11.4387	86.0158	46.1085	2.2614	2.9264	1.31E-03
11.5644	86.8054	46.5317	2.2822	2.9533	1.32E-03
11.6901	87.5949	46.9549	2.3030	2.9801	1.34E-03
11.8158	88.3845	47.3782	2.3237	3.0070	1.35E-03
11.9415	89.1741	47.8014	2.3445	3.0339	1.36E-03
12.0672	89.9636	48.2247	2.3652	3.0607	1.37E-03
12.1929	90.7532	48.6479	2.3860	3.0876	1.38E-03
12.3186	91.5427	49.0712	2.4067	3.1144	1.40E-03
12.4443	92.3323	49.4944	2.4275	3.1413	1.41E-03
12.5700	93.1219	49.9176	2.4483	3.1682	1.42E-03

Table G.4 : Hydraulic Compressor Analysis - Standard Discharge Pipe (Continued)

h_i	$Kl*a_i$	$t_{RES,i}$	$C_{NC,i}$	n_i
0.0000	0.0088	0.0629	8.92E-05	1.3965E-02
0.1257	0.0093	0.0596	8.93E-05	1.3963E-02
0.2514	0.0098	0.0598	8.94E-05	1.3961E-02
0.3771	0.0103	0.0599	8.95E-05	1.3959E-02
0.5028	0.0108	0.0600	8.96E-05	1.3956E-02
0.6285	0.0113	0.0601	8.97E-05	1.3952E-02
0.7542	0.0117	0.0602	8.99E-05	1.3949E-02

0.8799	0.0122	0.0603	9.00E-05	1.3945E-02
1.0056	0.0127	0.0604	9.02E-05	1.3941E-02
1.1313	0.0132	0.0605	9.04E-05	1.3936E-02
1.2570	0.0137	0.0606	9.06E-05	1.3931E-02
1.3827	0.0142	0.0606	9.08E-05	1.3925E-02
1.5084	0.0147	0.0607	9.10E-05	1.3919E-02
1.6341	0.0152	0.0608	9.13E-05	1.3912E-02
1.7598	0.0157	0.0608	9.16E-05	1.3905E-02
1.8855	0.0161	0.0609	9.19E-05	1.3898E-02
2.0112	0.0166	0.0609	9.22E-05	1.3889E-02
2.1369	0.0171	0.0610	9.25E-05	1.3881E-02
2.2626	0.0176	0.0610	9.29E-05	1.3871E-02
2.3883	0.0181	0.0611	9.33E-05	1.3862E-02
2.5140	0.0186	0.0611	9.37E-05	1.3851E-02
2.6397	0.0191	0.0612	9.41E-05	1.3840E-02
2.7654	0.0196	0.0612	9.46E-05	1.3828E-02
2.8911	0.0201	0.0613	9.51E-05	1.3816E-02
3.0168	0.0206	0.0613	9.56E-05	1.3803E-02
3.1425	0.0210	0.0613	9.62E-05	1.3789E-02
3.2682	0.0215	0.0614	9.67E-05	1.3774E-02
3.3939	0.0220	0.0614	9.73E-05	1.3759E-02
3.5196	0.0225	0.0614	9.80E-05	1.3743E-02
3.6453	0.0230	0.0614	9.86E-05	1.3726E-02
3.7710	0.0235	0.0615	9.93E-05	1.3709E-02
3.8967	0.0240	0.0615	1.00E-04	1.3690E-02
4.0224	0.0245	0.0615	1.01E-04	1.3671E-02
4.1481	0.0250	0.0616	1.02E-04	1.3651E-02
4.2738	0.0254	0.0616	1.02E-04	1.3630E-02
4.3995	0.0259	0.0616	1.03E-04	1.3609E-02
4.5252	0.0264	0.0616	1.04E-04	1.3586E-02
4.6509	0.0269	0.0616	1.05E-04	1.3563E-02
4.7766	0.0274	0.0617	1.06E-04	1.3538E-02
4.9023	0.0279	0.0617	1.07E-04	1.3513E-02
5.0280	0.0284	0.0617	1.08E-04	1.3487E-02
5.1537	0.0289	0.0617	1.09E-04	1.3460E-02
5.2794	0.0294	0.0618	1.10E-04	1.3431E-02
5.4051	0.0299	0.0618	1.11E-04	1.3402E-02
5.5308	0.0303	0.0618	1.13E-04	1.3372E-02
5.6565	0.0308	0.0618	1.14E-04	1.3341E-02
5.7822	0.0313	0.0618	1.15E-04	1.3309E-02
5.9079	0.0318	0.0618	1.16E-04	1.3275E-02
6.0336	0.0323	0.0619	1.18E-04	1.3241E-02
6.1593	0.0328	0.0619	1.19E-04	1.3205E-02
6.2850	0.0333	0.0619	1.21E-04	1.3169E-02
6.4107	0.0338	0.0619	1.22E-04	1.3131E-02
6.5364	0.0354	0.0619	1.24E-04	1.3091E-02
6.6621	0.0420	0.0619	1.26E-04	1.3043E-02

6.7878	0.0486	0.0619	1.28E-04	1.2986E-02
6.9135	0.0552	0.0620	1.30E-04	1.2921E-02
7.0392	0.0618	0.0620	1.33E-04	1.2847E-02
7.1649	0.0685	0.0620	1.36E-04	1.2765E-02
7.2906	0.0751	0.0620	1.40E-04	1.2673E-02
7.4163	0.0817	0.0620	1.44E-04	1.2572E-02
7.5420	0.0883	0.0620	1.48E-04	1.2462E-02
7.6677	0.0949	0.0621	1.53E-04	1.2342E-02
7.7934	0.1016	0.0621	1.58E-04	1.2213E-02
7.9191	0.1082	0.0621	1.64E-04	1.2074E-02
8.0448	0.1148	0.0621	1.70E-04	1.1925E-02
8.1705	0.1214	0.0621	1.75E-04	1.1782E-02
8.2962	0.1280	0.0621	1.82E-04	1.1613E-02
8.4219	0.1346	0.0622	1.89E-04	1.1435E-02
8.5476	0.1413	0.0622	1.96E-04	1.1247E-02
8.6733	0.1479	0.0622	2.04E-04	1.1050E-02
8.7990	0.1545	0.0622	2.12E-04	1.0842E-02
8.9247	0.1611	0.0622	2.21E-04	1.0624E-02
9.0504	0.1677	0.0622	2.30E-04	1.0397E-02
9.1761	0.1743	0.0623	2.39E-04	1.0160E-02
9.3018	0.1810	0.0623	2.49E-04	9.9125E-03
9.4275	0.1876	0.0623	2.59E-04	9.6557E-03
9.5532	0.1942	0.0623	2.69E-04	9.3892E-03
9.6789	0.2008	0.0623	2.80E-04	9.1131E-03
9.8046	0.2074	0.0623	2.91E-04	8.8275E-03
9.9303	0.2141	0.0624	3.03E-04	8.5324E-03
10.0560	0.2207	0.0624	3.15E-04	8.2281E-03
10.1817	0.2273	0.0624	3.27E-04	7.9146E-03
10.3074	0.2339	0.0624	3.40E-04	7.5921E-03
10.4331	0.2405	0.0624	3.53E-04	7.2607E-03
10.5588	0.2471	0.0625	3.67E-04	6.9205E-03
10.6845	0.2538	0.0625	3.80E-04	6.5717E-03
10.8102	0.2604	0.0625	3.94E-04	6.2144E-03
10.9359	0.2670	0.0625	4.09E-04	5.8489E-03
11.0616	0.2736	0.0625	4.23E-04	5.4753E-03
11.1873	0.2802	0.0626	4.38E-04	5.0939E-03
11.3130	0.2869	0.0626	4.54E-04	4.7047E-03
11.4387	0.2935	0.0626	4.69E-04	4.3080E-03
11.5644	0.3001	0.0626	4.85E-04	3.9040E-03
11.6901	0.3067	0.0626	5.01E-04	3.4930E-03
11.8158	0.3133	0.0626	5.18E-04	3.0751E-03
11.9415	0.3199	0.0627	5.35E-04	2.6505E-03
12.0672	0.3266	0.0627	5.52E-04	2.2195E-03
12.1929	0.3332	0.0627	5.69E-04	1.7823E-03
12.3186	0.3398	0.0627	5.86E-04	1.3392E-03
12.4443	0.3464	0.0627	6.04E-04	8.9039E-04
12.5700	0.3530	0.0628	6.22E-04	4.3607E-04

Table G.4 : Hydraulic Compressor Analysis - Standard Discharge Pipe (Continued)

h_i	$Q_{NC,i}$	$A_{pipe,i}$	$X_{3,i}$	$H_{HC,i}$
0.0000	1.3506	12.0503	2.1081	5.96E-04
0.1257	1.2868	12.0791	2.1031	5.42E-04
0.2514	1.2287	12.1054	2.0985	4.95E-04
0.3771	1.1756	12.1296	2.0943	4.54E-04
0.5028	1.1269	12.1519	2.0905	4.18E-04
0.6285	1.0820	12.1725	2.0870	3.85E-04
0.7542	1.0404	12.1916	2.0837	3.57E-04
0.8799	1.0020	12.2094	2.0806	3.32E-04
1.0056	0.9662	12.2259	2.0778	3.09E-04
1.1313	0.9328	12.2414	2.0752	2.88E-04
1.2570	0.9016	12.2559	2.0727	2.70E-04
1.3827	0.8724	12.2696	2.0704	2.53E-04
1.5084	0.8449	12.2824	2.0683	2.38E-04
1.6341	0.8191	12.2945	2.0662	2.24E-04
1.7598	0.7948	12.3059	2.0643	2.11E-04
1.8855	0.7718	12.3167	2.0625	1.99E-04
2.0112	0.7501	12.3270	2.0608	1.88E-04
2.1369	0.7295	12.3367	2.0592	1.79E-04
2.2626	0.7099	12.3459	2.0576	1.69E-04
2.3883	0.6913	12.3547	2.0562	1.61E-04
2.5140	0.6736	12.3631	2.0548	1.53E-04
2.6397	0.6568	12.3711	2.0534	1.46E-04
2.7654	0.6407	12.3787	2.0522	1.39E-04
2.8911	0.6253	12.3861	2.0510	1.32E-04
3.0168	0.6106	12.3931	2.0498	1.26E-04
3.1425	0.5965	12.3998	2.0487	1.21E-04
3.2682	0.5830	12.4062	2.0476	1.16E-04
3.3939	0.5700	12.4124	2.0466	1.11E-04
3.5196	0.5575	12.4184	2.0456	1.06E-04
3.6453	0.5455	12.4241	2.0447	1.02E-04
3.7710	0.5340	12.4297	2.0438	9.77E-05
3.8967	0.5229	12.4350	2.0429	9.38E-05
4.0224	0.5121	12.4401	2.0421	9.02E-05

4.1481	0.5018	12.4451	2.0412	8.67E-05
4.2738	0.4918	12.4499	2.0404	8.34E-05
4.3995	0.4821	12.4546	2.0397	8.03E-05
4.5252	0.4727	12.4591	2.0389	7.73E-05
4.6509	0.4637	12.4634	2.0382	7.45E-05
4.7766	0.4549	12.4677	2.0375	7.19E-05
4.9023	0.4464	12.4718	2.0369	6.93E-05
5.0280	0.4381	12.4758	2.0362	6.69E-05
5.1537	0.4301	12.4796	2.0356	6.46E-05
5.2794	0.4223	12.4834	2.0350	6.24E-05
5.4051	0.4147	12.4871	2.0344	6.03E-05
5.5308	0.4073	12.4906	2.0338	5.82E-05
5.6565	0.4002	12.4941	2.0332	5.63E-05
5.7822	0.3932	12.4975	2.0327	5.44E-05
5.9079	0.3863	12.5008	2.0321	5.27E-05
6.0336	0.3797	12.5040	2.0316	5.10E-05
6.1593	0.3732	12.5072	2.0311	4.93E-05
6.2850	0.3669	12.5103	2.0306	4.78E-05
6.4107	0.3607	12.5133	2.0301	4.63E-05
6.5364	0.3546	12.5162	2.0296	4.48E-05
6.6621	0.3485	12.5192	2.0292	4.33E-05
6.7878	0.3423	12.5222	2.0287	4.19E-05
6.9135	0.3361	12.5252	2.0282	4.05E-05
7.0392	0.3297	12.5283	2.0277	3.91E-05
7.1649	0.3234	12.5314	2.0272	3.77E-05
7.2906	0.3170	12.5345	2.0267	3.63E-05
7.4163	0.3105	12.5377	2.0262	3.49E-05
7.5420	0.3039	12.5409	2.0256	3.35E-05
7.6677	0.2973	12.5441	2.0251	3.22E-05
7.7934	0.2906	12.5474	2.0246	3.08E-05
7.9191	0.2838	12.5507	2.0241	2.95E-05
8.0448	0.2770	12.5540	2.0235	2.82E-05
8.1705	0.2705	12.5572	2.0230	2.70E-05
8.2962	0.2635	12.5606	2.0225	2.57E-05
8.4219	0.2565	12.5641	2.0219	2.45E-05
8.5476	0.2494	12.5675	2.0214	2.32E-05
8.6733	0.2423	12.5710	2.0208	2.20E-05
8.7990	0.2351	12.5746	2.0202	2.09E-05
8.9247	0.2279	12.5781	2.0197	1.97E-05
9.0504	0.2206	12.5817	2.0191	1.86E-05
9.1761	0.2132	12.5853	2.0185	1.74E-05
9.3018	0.2058	12.5889	2.0179	1.64E-05
9.4275	0.1984	12.5926	2.0173	1.53E-05
9.5532	0.1909	12.5963	2.0167	1.43E-05
9.6789	0.1834	12.6000	2.0161	1.33E-05
9.8046	0.1758	12.6037	2.0156	1.23E-05
9.9303	0.1682	12.6074	2.0150	1.14E-05

10.0560	0.1606	12.6112	2.0144	1.05E-05
10.1817	0.1530	12.6150	2.0138	9.64E-06
10.3074	0.1453	12.6188	2.0131	8.81E-06
10.4331	0.1376	12.6226	2.0125	8.02E-06
10.5588	0.1299	12.6264	2.0119	7.26E-06
10.6845	0.1222	12.6302	2.0113	6.54E-06
10.8102	0.1145	12.6340	2.0107	5.86E-06
10.9359	0.1067	12.6378	2.0101	5.21E-06
11.0616	0.0990	12.6417	2.0095	4.60E-06
11.1873	0.0912	12.6455	2.0089	4.03E-06
11.3130	0.0835	12.6493	2.0083	3.49E-06
11.4387	0.0758	12.6532	2.0077	3.00E-06
11.5644	0.0681	12.6570	2.0071	2.54E-06
11.6901	0.0604	12.6608	2.0065	2.12E-06
11.8158	0.0527	12.6647	2.0058	1.74E-06
11.9415	0.0450	12.6685	2.0052	1.40E-06
12.0672	0.0374	12.6723	2.0046	1.10E-06
12.1929	0.0297	12.6761	2.0040	8.33E-07
12.3186	0.0222	12.6799	2.0034	6.05E-07
12.4443	0.0146	12.6836	2.0029	4.14E-07
12.5700	0.0071	12.6874	2.0023	2.60E-07

This procedure is repeated until the length of the hydraulic compressor determined yields a final seawater velocity ($X_{3,end}$) at the end of the hydraulic compression region within ± 0.01% of the design seawater flow (X_3).

The total head loss ($H_{HC,tot}$) for this hydraulic compressor design is simply

$$H_{HC,tot} = \sum_{i=1}^{100} H_{HC,i} = 0.0099\ M \qquad \text{(G-142)}$$

which corresponds to a total pressure loss (ΔP_{HC}) of

$$\Delta P_{HC} = H_{HC,tot}\, \rho_3\, G = 98.84\ Pa. \qquad \text{(G-143)}$$

G.3.3.2 HYDRAULIC COMPRESSOR - TAPERING PIPE ANALYSIS

The tapering pipe hydraulic compressor analysis follows a similar procedure as that just described for the standard pipe hydraulic compressor. The principal difference between design procedures is that the tapering pipe is designed assuming a constant seawater velocity (X_3 = 2.00 M/S) with the pipe diameter changing to account for the reduction in volume of the noncondensables being compressed and reabsorbed along the compression region. The associated head loss (pressure drop) associated with the injection of the noncondensables into the tapering downcomer is simply the frictional pressure loss for the downcomer pipe. Although the necessary length of the tapering hydraulic compressor pipe will be the same as that for the standard pipe analysis (compression and reabsorption rates will be the same in both compression systems), it is still necessary for an iterative process to be performed along the compression pipe because the tapering effect will alter the friction factor along the varying diameter of the pipe. Therefore, the analysis entails iterating along the compressor length (100 iterations) and averaging the frictional factor for the corresponding tapering pipe length. The following analytical equations are utilized to obtain the values presented in the ensuing tables (G.5)

ρ_3 = seawater density in compressor = 1022.5 KG/M^3

ν_3 = kinematic viscosity of seawater in compressor

= 9.75×10^{-7} M^2

ε_3 = pipe roughness = 0.000046 (M) [32]

$t_{res,i}$ = residence time in segment i

$$= \Delta h_i / X_3 = 0.063\ S \qquad \text{(G-144)}$$

$A_{i,pipe}$ = average area of pipe for segment i

$$= A_{3,pipe} + [Q_{NC,i} / (Q_{NC,i} + Q_3)]\ A_{3,pipe} \quad (M^2) \qquad \text{(G-145)}$$

$D_{i,pipe}$ = average diameter of pipe for segment i

$$= (4\ A_{i,pipe} / \pi)^{1/2} \quad (M) \qquad \text{(G-146)}$$

Re_i = Reynolds number for segment i

$$= X_3\ D_{i,pipe} / \nu_3 \qquad \text{(G-147)}$$

f_i = friction factor of pipe in segment i (iterative)

$$= \{-2 \log [(\varepsilon_3 / 3.7\ D_{i,pipe}) + 2.51 / (Re_i \sqrt{f_i})]\}^{-2} \qquad \text{(G-148)}$$

ΔP_{fi} = frictional pressure drop along pipe length i

$$= f_i\ (\Delta h_i / D_{i,pipe})\ \rho_3\ X_3^2 / 2 \quad (Pa) \qquad \text{(G-149)}$$

Since the rate of compression and reabsorption along this hydraulic compressor directly corresponds to that of the standard pipe calculations above, many of the values (specifically those related to noncondensable concentrations, molar flows and volumetric flows) are identical and are omitted in the following tables which present the values unique to the tapering hydraulic compressor analysis.

Table G.5 : Hydraulic Compressor Analysis - Tapering Discharge Pipe

h_i	$A_{pipe,i}$	$D_{i,pipe}$	Re_i
0.0000	13.3316	4.1200	8.4556E+06
0.1257	13.3028	4.1155	8.4464E+06
0.2514	13.2765	4.1115	8.4381E+06
0.3771	13.2523	4.1077	8.4304E+06
0.5028	13.2300	4.1043	8.4233E+06

0.6285	13.2094	4.1011	8.4167E+06
0.7542	13.1903	4.0981	8.4106E+06
0.8799	13.1725	4.0953	8.4050E+06
1.0056	13.1559	4.0927	8.3997E+06
1.1313	13.1404	4.0903	8.3947E+06
1.2570	13.1259	4.0881	8.3901E+06
1.3827	13.1123	4.0860	8.3857E+06
1.5084	13.0995	4.0840	8.3816E+06
1.6341	13.0874	4.0821	8.3778E+06
1.7598	13.0759	4.0803	8.3741E+06
1.8855	13.0651	4.0786	8.3706E+06
2.0112	13.0549	4.0770	8.3674E+06
2.1369	13.0452	4.0755	8.3642E+06
2.2626	13.0359	4.0740	8.3613E+06
2.3883	13.0271	4.0727	8.3585E+06
2.5140	13.0188	4.0714	8.3558E+06
2.6397	13.0108	4.0701	8.3532E+06
2.7654	13.0031	4.0689	8.3507E+06
2.8911	12.9958	4.0678	8.3484E+06
3.0168	12.9888	4.0667	8.3461E+06
3.1425	12.9821	4.0656	8.3440E+06
3.2682	12.9756	4.0646	8.3419E+06
3.3939	12.9694	4.0636	8.3399E+06
3.5196	12.9635	4.0627	8.3380E+06
3.6453	12.9577	4.0618	8.3362E+06
3.7710	12.9522	4.0609	8.3344E+06
3.8967	12.9469	4.0601	8.3327E+06
4.0224	12.9417	4.0593	8.3310E+06
4.1481	12.9367	4.0585	8.3294E+06
4.2738	12.9319	4.0578	8.3279E+06
4.3995	12.9273	4.0570	8.3264E+06
4.5252	12.9228	4.0563	8.3249E+06
4.6509	12.9184	4.0556	8.3235E+06
4.7766	12.9142	4.0550	8.3221E+06
4.9023	12.9101	4.0543	8.3208E+06
5.0280	12.9061	4.0537	8.3195E+06
5.1537	12.9022	4.0531	8.3183E+06
5.2794	12.8984	4.0525	8.3171E+06
5.4051	12.8948	4.0519	8.3159E+06
5.5308	12.8912	4.0514	8.3147E+06
5.6565	12.8877	4.0508	8.3136E+06
5.7822	12.8843	4.0503	8.3125E+06
5.9079	12.8810	4.0498	8.3115E+06
6.0336	12.8778	4.0493	8.3104E+06
6.1593	12.8747	4.0488	8.3094E+06
6.2850	12.8716	4.0483	8.3084E+06
6.4107	12.8686	4.0478	8.3074E+06

6.5364	12.8656	4.0473	8.3065E+06
6.6621	12.8627	4.0469	8.3055E+06
6.7878	12.8597	4.0464	8.3046E+06
6.9135	12.8566	4.0459	8.3036E+06
7.0392	12.8536	4.0454	8.3026E+06
7.1649	12.8505	4.0450	8.3016E+06
7.2906	12.8473	4.0445	8.3006E+06
7.4163	12.8442	4.0440	8.2995E+06
7.5420	12.8410	4.0435	8.2985E+06
7.6677	12.8377	4.0430	8.2975E+06
7.7934	12.8345	4.0424	8.2964E+06
7.9191	12.8312	4.0419	8.2953E+06
8.0448	12.8278	4.0414	8.2943E+06
8.1705	12.8246	4.0409	8.2932E+06
8.2962	12.8212	4.0404	8.2921E+06
8.4219	12.8178	4.0398	8.2910E+06
8.5476	12.8143	4.0393	8.2899E+06
8.6733	12.8108	4.0387	8.2888E+06
8.7990	12.8073	4.0382	8.2876E+06
8.9247	12.8037	4.0376	8.2865E+06
9.0504	12.8002	4.0370	8.2853E+06
9.1761	12.7966	4.0365	8.2842E+06
9.3018	12.7929	4.0359	8.2830E+06
9.4275	12.7893	4.0353	8.2818E+06
9.5532	12.7856	4.0347	8.2806E+06
9.6789	12.7819	4.0342	8.2794E+06
9.8046	12.7782	4.0336	8.2782E+06
9.9303	12.7744	4.0330	8.2770E+06
10.0560	12.7707	4.0324	8.2758E+06
10.1817	12.7669	4.0318	8.2745E+06
10.3074	12.7631	4.0312	8.2733E+06
10.4331	12.7593	4.0306	8.2721E+06
10.5588	12.7555	4.0300	8.2709E+06
10.6845	12.7517	4.0294	8.2696E+06
10.8102	12.7479	4.0288	8.2684E+06
10.9359	12.7440	4.0282	8.2671E+06
11.0616	12.7402	4.0276	8.2659E+06
11.1873	12.7364	4.0270	8.2646E+06
11.3130	12.7325	4.0264	8.2634E+06
11.4387	12.7287	4.0257	8.2621E+06
11.5644	12.7248	4.0251	8.2609E+06
11.6901	12.7210	4.0245	8.2597E+06
11.8158	12.7172	4.0239	8.2584E+06
11.9415	12.7134	4.0233	8.2572E+06
12.0672	12.7096	4.0227	8.2559E+06
12.1929	12.7058	4.0221	8.2547E+06
12.3186	12.7020	4.0215	8.2535E+06

12.4443	12.6982	4.0209	8.2523E+06
12.5700	12.6945	4.0203	8.2510E+06

Table G.5 : Hydraulic Compressor Analysis - Tapering Discharge Pipe (Continued)

h_i	$f_{i,guess}$	f_i	ΔP_{fi}
0.0000	0.009197	0.009197	0.5738
0.1257	0.009198	0.009198	0.5745
0.2514	0.009200	0.009200	0.5752
0.3771	0.009201	0.009201	0.5758
0.5028	0.009202	0.009203	0.5764
0.6285	0.009204	0.009204	0.5769
0.7542	0.009205	0.009205	0.5774
0.8799	0.009206	0.009206	0.5778
1.0056	0.009207	0.009207	0.5782
1.1313	0.009207	0.009208	0.5786
1.2570	0.009208	0.009208	0.5790
1.3827	0.009209	0.009209	0.5794
1.5084	0.009210	0.009210	0.5797
1.6341	0.009210	0.009210	0.5800
1.7598	0.009211	0.009211	0.5803
1.8855	0.009212	0.009212	0.5806
2.0112	0.009212	0.009212	0.5808
2.1369	0.009213	0.009213	0.5811
2.2626	0.009213	0.009213	0.5813
2.3883	0.009214	0.009214	0.5816
2.5140	0.009214	0.009214	0.5818
2.6397	0.009215	0.009215	0.5820
2.7654	0.009215	0.009215	0.5822
2.8911	0.009216	0.009216	0.5824
3.0168	0.009216	0.009216	0.5825
3.1425	0.009216	0.009216	0.5827
3.2682	0.009217	0.009217	0.5829
3.3939	0.009217	0.009217	0.5831
3.5196	0.009217	0.009218	0.5832
3.6453	0.009218	0.009218	0.5834
3.7710	0.009218	0.009218	0.5835
3.8967	0.009218	0.009218	0.5836
4.0224	0.009219	0.009219	0.5838
4.1481	0.009219	0.009219	0.5839
4.2738	0.009219	0.009219	0.5840

4.3995	0.009220	0.009220	0.5842
4.5252	0.009220	0.009220	0.5843
4.6509	0.009220	0.009220	0.5844
4.7766	0.009220	0.009220	0.5845
4.9023	0.009221	0.009221	0.5846
5.0280	0.009221	0.009221	0.5847
5.1537	0.009221	0.009221	0.5848
5.2794	0.009221	0.009221	0.5849
5.4051	0.009221	0.009221	0.5850
5.5308	0.009222	0.009222	0.5851
5.6565	0.009222	0.009222	0.5852
5.7822	0.009222	0.009222	0.5853
5.9079	0.009222	0.009222	0.5854
6.0336	0.009222	0.009222	0.5855
6.1593	0.009223	0.009223	0.5855
6.2850	0.009223	0.009223	0.5856
6.4107	0.009223	0.009223	0.5857
6.5364	0.009223	0.009223	0.5858
6.6621	0.009223	0.009223	0.5859
6.7878	0.009223	0.009223	0.5859
6.9135	0.009224	0.009224	0.5860
7.0392	0.009224	0.009224	0.5861
7.1649	0.009224	0.009224	0.5862
7.2906	0.009224	0.009224	0.5863
7.4163	0.009224	0.009224	0.5863
7.5420	0.009224	0.009225	0.5864
7.6677	0.009225	0.009225	0.5865
7.7934	0.009225	0.009225	0.5866
7.9191	0.009225	0.009225	0.5867
8.0448	0.009225	0.009225	0.5868
8.1705	0.009225	0.009225	0.5869
8.2962	0.009226	0.009226	0.5870
8.4219	0.009226	0.009226	0.5870
8.5476	0.009226	0.009226	0.5871
8.6733	0.009226	0.009226	0.5872
8.7990	0.009226	0.009226	0.5873
8.9247	0.009227	0.009227	0.5874
9.0504	0.009227	0.009227	0.5875
9.1761	0.009227	0.009227	0.5876
9.3018	0.009227	0.009227	0.5877
9.4275	0.009227	0.009227	0.5878
9.5532	0.009228	0.009228	0.5879
9.6789	0.009228	0.009228	0.5880
9.8046	0.009228	0.009228	0.5881
9.9303	0.009228	0.009228	0.5882
10.0560	0.009229	0.009229	0.5883
10.1817	0.009229	0.009229	0.5884

10.3074	0.009229	0.009229	0.5885
10.4331	0.009229	0.009229	0.5886
10.5588	0.009229	0.009229	0.5887
10.6845	0.009230	0.009230	0.5888
10.8102	0.009230	0.009230	0.5889
10.9359	0.009230	0.009230	0.5890
11.0616	0.009230	0.009230	0.5891
11.1873	0.009231	0.009231	0.5892
11.3130	0.009231	0.009231	0.5893
11.4387	0.009231	0.009231	0.5894
11.5644	0.009231	0.009231	0.5895
11.6901	0.009231	0.009231	0.5896
11.8158	0.009232	0.009232	0.5897
11.9415	0.009232	0.009232	0.5898
12.0672	0.009232	0.009232	0.5899
12.1929	0.009232	0.009232	0.5900
12.3186	0.009233	0.009233	0.5901
12.4443	0.009233	0.009233	0.5902
12.5700	0.009233	0.009233	0.5903

The total pressure loss (ΔP_{HC}) for this hydraulic compressor design is simply

$$\Delta P_{HC} = \sum_{i=1}^{100} \Delta P_{HC,i} = 59.07 \text{ Pa.} \qquad \text{(G-150)}$$

G.4 DIRECT-CONTACT CONDENSER

As outlined previously, the direct-contact condenser analysis begins by determining the inlet steam conditions to the co-current condensing section. Initially, it is necessary to determine the diffuser-condenser pressure drop ($\Delta P_{d\text{-}CO}$) in a similar manner as the evaporator-turbine pressure drop ($\Delta P_{E\text{-}t}$) found earlier by first finding the diffuser exit steam velocity from the diffuser exit temperature ($T_{7,d}$), steam specific volume ($V_{7,d}$), steam mass flow rate ($m_{steam,6}$) and the turbine flow area (A_t)

$$C_d = m_{steam,6} V_{7,d} / A_t = 57.63 \text{ M/S.} \quad \text{(G-151)}$$

With the steam velocity known, the pressure drop through the diffuser-condenser passage can be determined

$$\Delta P_{d\text{-}C} = K_{d\text{-}C} \rho_{7,d} C_d^2 / 2 = 0.018 \text{ KPa} \quad \text{(G-152)}$$

where

$K_{d\text{-}C}$ = diffuser-condenser passage loss coefficient = 1.0 [32].

This pressure drop accompanied by the diffuser exit steam pressure ($P_{7,d}$) yield the co-current condenser entrance pressure ($P_{7,CO}$) as

$$P_{7,CO} = P_{7,d} - \Delta P_{d\text{-}C} = 1.43 \text{ KPa} \quad \text{(G-153)}$$

which can be used to determine the co-current condenser entrance temperature ($T_{7,CO}$) using equation F-6 presented at the outset of Appendix F

$$T_{7,CO} = 12.31 \text{ °C} \quad 285.46 \text{ °K.}$$

G.4.1 CO-CURRENT DESIGN

Once again, for the purposes of simplifying the design procedure, the condenser design has been broken into two distinct sections, the co-current and counter-current section.

With the utilization of a direct-contact condenser configuration chosen for this investigation, noncondensable gas desorption will accompany the cold water flow designed in this analysis even after the seawater has been predeaerated since the experimental results obtained earlier in this investigation suggest a higher desorption rate from the cold water than is expected from the predeaeration analysis performed by Zapka [51]. As discussed previously, the presence of these noncondensables and those

accompanying the steam from the evaporator leakage will hinder the condensation process and alter the shape of the heat load diagram for the condensing region. Therefore, since the design cold water flow is unknown, an iterative process is necessary for further development of the direct-contact condenser.

For the first iteration in developing the heat load analysis for the co-current condensing section the noncondensable loading is assumed to be that attributable to the evaporator leakage alone.

Upon completing the iterative process for the co-current condensing region the following noncondensable flows apply and are the values reflected in the following heat load development analysis.

$$M_{N2,CO} = 0.0039 \text{ KG-MOL/S}$$

$$M_{O2,CO} = 0.0007 \text{ KG-MOL/S}$$

$$M_{Ar,CO} = 0.0000 \text{ KG-MOL/S}$$

$$M_{CO2,CO} = 0.0000 \text{ KG-MOL/S}$$

$$M_{H2O,CO} = 8.153 \text{ KG-MOL/S}$$

These molar flows correspond to the following mass flows

$$m_{N2,CO} = 0.109 \text{ KG/S}$$

$$m_{O2,CO} = 0.022 \text{ KG/S}$$

$$m_{Ar,CO} = 0.000 \text{ KG/S}$$

$$m_{CO2,CO} = 0.000 \text{ KG/S.}$$

From the molar values the mole fraction of steam in the co-current condenser section ($y_{steam,CO}$) can be determined

$$y_{steam,CO} = M_{H20,CO} / (M_{H20,CO} + M_{N2,CO} + M_{O2,CO} + M_{Ar,CO} + M_{CO2,CO})$$
$$= 0.9996. \quad \text{(G-154)}$$

The total pressure of the co-current condensing section is then found assuming that the steam entering the condenser is saturated at the inlet steam temperature ($T_{7,CO}$) and thus the co-current pressure (P_{CO}) is defined as

$$P_{CO} = P_{7,CO} / y_{steam,CO} = 1.43 \text{ KPa}. \quad \text{(G-155)}$$

Parsons et al. [32] suggest that since the steam and seawater in the co-current section of the condenser are flowing in the same direction that the frictional vapor pressure drop can be assumed zero. Therefore this co-current pressure can be assumed constant throughout the entire co-current condensing region [32].

For the development of the heat load analysis and the co-current condenser design, Figure 4.3 should be referred to assist in clarifying the procedure. This figure, taken from Parsons et al. [32], shows the condenser heat load (HL_{CO}) plotted against the steam outlet temperature ($T_{7*,CO}$). As stated previously, the shape of the curve is dependant upon the steam inlet temperature ($T_{7,CO}$), the condenser pressure (P_{CO}) and the steam ($m_{steam,7}$) and noncondensable ($m_{NC,CO}$) inlet mass flow rates where

$$m_{steam,7} = m_{steam,6} = 146.9 \text{ KG/S}. \quad \text{(G-156)}$$

For a yet undetermined co-current steam exit temperature ($T_{7*,CO}$) the steam exit mass fraction ($x_{7*,CO}$) is

$$x_{7*,CO} = P_{sat,7*,CO} / P_{CO} \quad \text{(G-157)}$$

which yields a steam outlet mass flow ($m_{steam,7*,CO}$) rate of

$$m_{steam,7*,CO} = M_{NC,CO}\, MW_{H2O}\, x_{7*,CO} / (1 - x_{7*,CO}) \quad \text{(G-158)}$$

where

$$M_{NC,CO} = M_{N2,CO} + M_{O2,CO} + M_{Ar,CO} + M_{CO2,CO}. \quad \text{(G-159)}$$

Parsons et al. [32] describe the heat load as composed of the latent heat required to condense the difference in inlet ($m_{steam,7}$) and outlet ($m_{steam,7*,CO}$) steam mass flow rates, the sensible load required to cool the condensed steam and the sensible load required to cool the noncondensables present in the co-current condensing region:

$$HL_{CO} = m_{steam,7} H_{g,7,CO} - m_{steam,7*,CO} H_{g,7*,CO} -$$
$$(m_{steam,7} - m_{steam,7*,CO}) H_{f,7*,CO} - (m_{N2,CO} C_{PN2,7,CO} + m_{O2,CO} C_{PO2,7,CO} +$$
$$m_{Ar,CO} C_{PAr,7,CO} + m_{CO2,CO} C_{PCO2,7,CO}) (T_{7,CO} - T_{7*,CO}). \quad \text{(G-160)}$$

Initially, the maximum heat load ($HL_{max,CO}$) is determined by setting the steam outlet temperature ($T_{7*,CO}$) equal to the inlet cold water temperature (T_{11})

$$HL_{max,CO} = 367329 \text{ KW}.$$

This represents the "ideal" line from the origin to point A in Figure 4.3. Realistically, it is impossible for the exit steam temperature to ever reach the inlet cold water temperature since this would require an infinite contact time between steam and cooling water. Parsons et al. [32] suggest that the slope of this "ideal flow" water line is directly related to the cold water mass flow ($m_{11,CO}$) times its specific heat (C_{p11}) as

$$m_{11,CO,ideal} = HL_{max,CO} / [C_{p11} (T_{7,CO} - T_{11})] = 12582 \text{ KG/S}. \quad \text{(G-161)}$$

The design heat load ($HL_{design,CO}$) for the co-current condenser region is defined by Parsons et al. [32] as the heat load where the "ideal" seawater line intersects the gas heat load curve (see Figure 4.3) and is determined iteratively since the exit steam temperature ($T_{7*,CO}$) is still unknown. An initial guess at

the design steam exit temperature is used to obtain an initial design heat load approximation from which a new outlet steam temperature is obtained from

$$T_{7*,CO} = HL_{design,CO} / m_{11,CO,ideal}\, C_{p11} + T_{11} = 12.01\ ^{\circ}C \qquad \text{(G-162)}$$

with a corresponding heat load of

$$HL_{design,CO} = 352404\ KW.$$

This procedure is repeated until the outlet steam temperature ($T_{7*,CO}$) changes less than ± 0.1% from one iteration to the next.

The ideal flow rate determined earlier has been deemed impossible since an infinite residence time in the co-current condenser is unreasonable, common engineering practice dictates a design/ideal scaling factor of 1.2 [32]. Therefore, the design seawater mass flow is

$$m_{11,CO,design} = 1.2\, m_{11,CO,ideal} = 15098\ KG/S. \qquad \text{(G-163)}$$

A heat balance utilizing this design mass water flow and the design heat load yield an outlet cold water temperature ($T_{9,CO}$) of

$$T_{9,CO} = T_{11} + HL_{design,CO} / m_{11,CO,design}\, C_{p11} = 10.84\ ^{\circ}C. \qquad \text{(G-164)}$$

Now, with an estimate of the design seawater flow rate, the noncondensable loading accompanying this seawater flow is recalculated accounting for the expected noncondensable desorption above the 85% desorption predicted by Zapka for the predeaerator (to be designed in the following section) and the expected atmospheric leakage as outlined in the non-predeaerated co-current condenser analysis. In this case the desorption rates determined in the experimental section of this report for the cold water stream above the rate designed in the subsequent predeaerator analysis and the inlet cold water molar concentrations predicted by Krock [21] are utilized

$$x_{N2,11} = 0.93 - 0.85 = 0.13$$

$$x_{O2,11} = 1.00 - 0.85 = 0.15$$

$$x_{Ar,11} = 0.90 - 0.85 = 0.05$$

$$x_{CO2,11} = 0.013 \text{ ("total" carbon) (not applicable)}$$

and

$$M_{N2,11} = 0.564 \text{ MMOL/L}$$

$$M_{O2,11} = 0.047 \text{ MMOL/L}$$

$$M_{Ar,11} = 0.015 \text{ MMOL/L}$$

$$M_{CO2,11} = 2.33 \text{ MMOL/L ("total" carbon).}$$

Also, it is necessary to predict the atmospheric leakage into the direct-contact condenser and add this noncondensable flow to the combined flow of the co-current desorbed gases with those entering with the steam from the evaporator

$$m_{air,lk,CO} = 0.005 \ Po_{gross} / 1000 = 0.05 \text{ KG/S.} \qquad \text{(G-165)}$$

As outlined in the non-predeaerated analysis, for the purposes of this direct-contact condenser investigation, it is assumed that all atmospheric leakage occurs in the co-current section of the condenser.

With the new noncondensable flow now determined the entire procedure from equation G-154 is repeated and a new heat load and flow rate are recomputed. This procedure is repeated until the noncondensable flows do not change more than ± 0.05% from one iteration to the next.

The co-current condenser effectiveness (ε_{CO}) is determined from its definition

$$\varepsilon_{CO} = (T_9 - T_{11}) / (T_{7*,CO} - T_{11}) = 0.83 \qquad \text{(G-166)}$$

which yields the number of transfer units (NTU_{CO}) and height of the co-current contactor (Ht_{CO}) with height of transfer unit (HTU_{CO} = 0.30 M) predicted by [32]

$$NTU_{CO} = -\ln(1 - \varepsilon_{CO}) = 1.79 \qquad \text{(G-167)}$$

$$Ht_{CO} = NTU_{CO}\ HTU_{CO} = 0.54\ \text{M}. \qquad \text{(G-168)}$$

G.4.2 COUNTER-CURRENT CONDENSER DESIGN

The inlet conditions of the counter-current condenser are taken from the exit conditions of the co-current condenser section. The counter-current outlet conditions are specified by an assumed temperature difference ($\Delta T_{8\text{-}11}$ = 1.00 °C) [32] between the outlet steam (T_8) and inlet cooling water (T_{11})

$$T_8 = T_{11} + \Delta T_{8\text{-}11} \qquad \text{(G-169)}$$

and an assumed constant pressure throughout the counter-current section corresponding to the co-current condenser pressure ($P_{7*,CO} = P_{7*,CC}$) with an associated pressure drop ($\Delta P_{7*\text{-}8}$ = 0.20 KPa) [32] through the counter-current section used to determine the outlet pressure (P_8) to be used in the vent compressor analysis in the following section

$$P_8 = P_{7*,CC} - \Delta P_{7*\text{-}8} = 1.23\ \text{KPa}. \qquad \text{(G-170)}$$

A similar heat load development procedure to that utilized in the co-current section is also employed for the counter-current analysis. For this purpose the noncondensable flows from the co-current section are used as a first approximation of expected flows in the counter-current design for the initial iteration.

The design outlet steam temperature (T_8) calculated above is used with these noncondensable flows to determine the design heat load for the counter-current condenser ($HL_{7*,CC}$) using equation G-160 discussed previously in the co-current design

$$HL_{7*,CC} = 10917 \text{ KW.}$$

From this value the ideal seawater mass flow ($m_{11,CC,ideal}$) can be determined

$$m_{11,CC,ideal} = HL_{7*,CC} / [C_{P11} (T_8 - T_{11})] = 390 \text{ KG/S} \qquad \text{(G-171)}$$

which yields a design seawater mass flow ($m_{11,CC,design}$) of

$$m_{11,CC,design} = 1.2 \; m_{11,CC,ideal} = 468 \text{ KG/S.} \qquad \text{(G-172)}$$

Once again, with the design flow approximated, the noncondensables desorbed from this flow are determined as described above and the heat load development is repeated until the noncondensable flows differ less than ± 0.05% from one iteration to the next.

As described in the co-current section, a heat balance is performed to determine the outlet seawater temperature ($T_{9,CC}$)

$$T_{9,CC} = T_{11} + HL_{7*,CC} / (m_{11,CC,design} C_{P11}) = 10.84\,^{\circ}C \qquad \text{(G-173)}$$

which permits the calculation of the counter-current effectiveness (ε_{CC})

$$\varepsilon_{CC} = (T_{9,CC} - T_{11}) / (T_8 - T_{11}) = 0.83. \qquad \text{(G-174)}$$

The number of transfer units for the counter-current condenser (NTU_{CC}) is integrated numerically (100 iterations) utilizing

$$NTU_{CC} = \int_{T_{7*,CO}}^{T_8} dT_{steam} / (T_{steam} - T_{water}) = 2.21 \qquad \text{(G-175)}$$

and equation G-160 to determine the heat load value corresponding to the incremental steam temperature and the following equation to determine the

seawater temperature (T_{water}) corresponding to the incremental steam temperature (T_{steam}) through the counter-current region [32]

$$T_{water} = T_9 + [HL_{Tsteam} (T_{9,CC} - T_{11})] / HL_{7*,CC}. \quad \text{(G-176)}$$

The height of contactor (Ht_{CC}) for the counter-current condenser is thus

$$Ht_{CC} = NTU_{CC}\ HTU_{CC} = 0.66\ M. \quad \text{(G-177)}$$

The area required for each of the condenser sections is determined in two different manners. The first method determines the condenser area based on the liquid loading of each condenser section assuming seawater flow rates (x_{cond}), spout diameters ($d_{cont,cond}$) and a contactor spacing (A_{cont}) of

$$x_{cond} = 2.00\ M/S$$

$$d_{cont,cond} = 0.127\ M$$

$$A_{cont} = 0.424\ M^2$$

suggested by [32]. The mass flow of seawater per contactor for each condenser section is found as

$$m_{cont,cond} = \rho_{11}\, x_{cond}\, \pi\, d_{cont,cond}^2 / 4 = 26.0\ KG/S \quad \text{(G-178)}$$

which yields a co-current area ($A_{CO,L}$) and counter-current area ($A_{CC,L}$) determined from the number of contactors ($N_{cont,CO}$ and $N_{cont,CC}$, respectively) as

$$N_{cont,CO} = m_{11,CO,design} / m_{cont,cond} = 581.2 \Longrightarrow 582 \quad \text{(G-179)}$$

$$N_{cont,CC} = m_{11,CO,design} / m_{cont,cond} = 18.0 \Longrightarrow 18 \quad \text{(G-180)}$$

$$A_{CO,L} = N_{cont,CO}\, A_{cont} = 246.9\ M^2 \quad \text{(G-181)}$$

$$A_{CC,L} = N_{cont,CC}\, A_{cont} = 7.64\ M^2. \quad \text{(G-182)}$$

The second area calculation is developed from the steam loading of each condenser section. With the steam flow through the co-current condenser

($m_{7,CO}$) and the steam flow through the counter-current section ($m_{7*,CC}$) defined

$$m_{7,CO} = 146.9 \text{ KG/S}$$

$$m_{7*,CC} = 4.53 \text{ KG/S}$$

and the steam velocity ($C_7 = C_{7*} = 57.63$ M/S) the steam flow area is defined as [32]

$$A_{CO,S} = m_{7,CO} V_{steam,7,CO} / C_7 = 236.0 \text{ M}^2 \quad \text{(G-183)}$$

$$A_{CC,S} = m_{7*,CC} V_{steam,7*,CC} / C_{7*} = 7.41 \text{ M}^2. \quad \text{(G-184)}$$

The total cold water ($m_{11,tot}$) necessary for the direct-contact condenser design is

$$m_{11,tot} = m_{11,CO,design} + m_{11,CC,design} = 15566 \text{ KG/S} \quad \text{(G-185)}$$

from which a heat balance can be performed to determine the condenser outlet seawater temperature (T_9) as

$$T_9 = (m_{11,CO,design} T_{9,CO} + m_{11,CC,design} T_{9,CC}) / m_{11,tot} = 10.84 \text{ }^{\circ}\text{C}. \quad \text{(G-186)}$$

G.4.3 CONDENSER PREDEAERATOR DESIGN

The predeaerator design begins by setting the condenser predeaerator pressure ($P_{pre,DCC}$) at the value utilized in the predeaeration experiments conducted by Zapka [51]

$$P_{pre,DCC} = 6.67 \text{ KPa}.$$

By setting the predeaerator pressure at this value and utilizing a similar structural design to the experimental predeaeration vessel (Figure 5.4), permits the assumption of predeaeration levels approaching those predicted by

Zapka of approximately 85% desorption with bubble seeding within this predeaerator design.

With the design cold water flow rate determined (m_{11}) the noncondensable desorption rate within the predeaerator can now be estimated from the desorption rates determined by Zapka [51].

Cold water predeaeration % with bubble seeding:

$$x_{N2,DCC} = 0.85$$

$$x_{O2,DCC} = 0.85$$

$$x_{Ar,DCC} = 0.85$$

$$x_{CO2,DCC} = 0.006 \text{ (total carbon)}^*$$

Cold water entrance noncondensable concentrations [21]:

$$M_{N2,11} = 0.564 \text{ MMOL/L}$$

$$M_{O2,11} = 0.047 \text{ MMOL/L}$$

$$M_{Ar,11} = 0.015 \text{ MMOL/L}$$

$$M_{CO2,11} = 2.33 \text{ MMOL/L (total carbon)}$$

From these values the molar release of each noncondensable is determined as

$$M_{N2,DES} = x_{N2,DCC} M_{N2,11} = 0.480 \text{ MMOL/L} \quad \text{(G-187)}$$

$$M_{O2,DES} = x_{O2,DCC} M_{O2,11} = 0.040 \text{ MMOL/L} \quad \text{(G-188)}$$

$$M_{Ar,DES} = x_{Ar,DCC} M_{Ar,11} = 0.013 \text{ MMOL/L} \quad \text{(G-189)}$$

$$M_{CO2,DES} = x_{CO2,DCC} M_{CO2,11} = 0.030 \text{ MMOL/L} \quad \text{(G-190)}$$

* NOTE: For the purposes of this investigation the desorption rate of carbon dioxide predicted for the predeaerator is assumed the same as that predicted by the experimental portion of this investigation since Zapka's desorption rate of 85% does not readily apply to the concept of "total" carbon.

which delivers the mass release of noncondensables as

$$m_{N2,DES} = M_{N2,DES}\, m_{11}\, MW_{N2} / (1000\, \rho_{11}) = 0.204 \text{ KG/S} \quad \text{(G-191)}$$

$$m_{O2,DES} = M_{O2,DES}\, m_{11}\, MW_{O2} / (1000\, \rho_{11}) = 0.020 \text{ KG/S} \quad \text{(G-192)}$$

$$m_{Ar,DES} = M_{Ar,DES}\, m_{11}\, MW_{Ar} / (1000\, \rho_{11}) = 0.0079 \text{ KG/S} \quad \text{(G-193)}$$

$$m_{CO2,DES} = M_{CO2,DES}\, m_{11}\, MW_{CO2} / (1000\, \rho_{11}) = 0.020 \text{ KG/S} \quad \text{(G-194)}$$

where the factor 1000 converts G/S to KG/S.

These noncondensable flow rates represent the amount of noncondensables expected to be desorbed at the system pressure within the direct-contact condenser predeaerator with bubble seeding. However, these are not the only noncondensables present within the predeaeration vessel. As in the evaporator predeaerator analysis, the bubble seeding itself introduces a significant level of noncondensables to the predeaeration system. It is therefore necessary to determine the injection rate of noncondensables needed to accomplish the desired level of predeaeration predicted in the previous equations. This requires the knowledge of noncondensable (air) injection rate performed in Zapka's [51] experiments mentioned previously.

Zapka [51] performed his predeaeration experiments with a ratio of air injection to seawater volume ($R_{air/water}$) of

$$R_{air/water} = 0.5 \text{ L air} / 30 \text{ L water} = 0.017 \text{ M}^3\text{air} / \text{M}^3\text{water}$$

at an approximate seawater temperature and corresponding values of

$$T_{Zap} = 25.00\ ^{\circ}\text{C}$$

$$\rho_{Zap} = 1022.1 \text{ KG/M}^3$$

ρ_{air} = density of air at atmospheric pressure and 21 °C

$$= 1.20 \text{ KG/M}^3$$

MW_{air} = molecular weight of air

= 28.97 KG/KG-MOL [17].

These values suggest a molar fraction of noncondensables to seawater in Zapka's experiments as

$$MF_{NC} = R_{air/water}\ \rho_{air}\ MW_{H20} / (\rho_{Zap}\ MW_{air})$$

$$= 1.22 \times 10^{-5} \text{ KG-MOL air / KG-MOL water.} \qquad \text{(G-195)}$$

With the mass flow of seawater necessary (m_{11}) determined in the condenser analysis previously, the volumetric flow of seawater into the predeaerator (Q_{11}) is determined as

$$Q_{11} = m_{11} / \rho_{11} = 15.18 \text{ M}^3\text{/S} \qquad \text{(G-196)}$$

which yields a molar flow of seawater (M_{11}) as

$$M_{11} = m_{11} / MW_{H2O} = 864.0 \text{ KG-MOL/S.} \qquad \text{(G-197)}$$

Thus, the desired noncondensable molar injection rate for the designed condenser predeaerator is

$$M_{pre,DCC,inj} = M_{11}\ MF_{NC} = 0.011 \text{ KG-MOL/S} \qquad \text{(G-198)}$$

with a corresponding noncondensable mass injection rate of

$$m_{pre,DCC,inj} = M_{pre,DCC,inj}\ MW_{NC,DES} = 0.31 \text{ KG/S} \qquad \text{(G-199)}$$

where

$MW_{NC,DES}$ = molecular weight of noncondensables predeaerated from the cold water stream since the injection gases are recycled from the condenser predeaerator vent compressor exhaust gases

$$= (m_{N2,DES}\ MW_{N2} + m_{O2,DES}\ MW_{O2} + m_{Ar,DES}\ MW_{Ar} + m_{CO2,DES}\ MW_{CO2}) / m_{NC,DES,tot}$$

$$= 29.44 \text{ KG/KG-MOL} \qquad \text{(G-200)}$$

$$m_{NC,DES,tot} = m_{N2,DES} + m_{O2,DES} + m_{Ar,DES} + m_{CO2,DES}$$
$$= 0.31 \text{ KG/S.} \qquad \text{(G-201)}$$

With the corresponding mass fractions assumed for the injected gases, the total flows of noncondensables within the condenser predeaerator are

$$m_{N2,pre,DCC,tot} = 0.455 \text{ KG/S}$$
$$m_{O2,pre,DCC,tot} = 0.0437 \text{ KG/S}$$
$$m_{Ar,pre,DCC,tot} = 0.0177 \text{ KG/S}$$
$$m_{CO2,pre,DCC,tot} = 0.0450 \text{ KG/S}$$

with corresponding molar flows of

$$M_{N2,pre,DCC,tot} = 0.0162 \text{ KG-MOL/S}$$
$$M_{O2,pre,DCC,tot} = 0.0014 \text{ KG-MOL/S}$$
$$M_{Ar,pre,DCC,tot} = 0.0004 \text{ KG-MOL/S}$$
$$M_{CO2,pre,DCC,tot} = 0.0010 \text{ KG-MOL/S.}$$

As discussed previously in this report and represented by Figure 5.4, the condenser-predeaeration system should be designed as a single component to minimize the initial capital costs for these particular components. Therefore, the design flow area ($A_{pre,DCC}$) and thus predeaerator diameter ($D_{pre,DCC}$) are the same as the direct-contact condenser area (A_{DCC}) and diameter (D_{DCC}) determined earlier as

$$A_{pre,DCC} = A_{DCC} = 254.6 \text{ M}^2$$
$$D_{pre,DCC} = D_{DCC} = 18.00 \text{ M.}$$

The design water depth of the predeaerator ($H_{pre,DCC}$) is then determined iteratively assuming a minimum residence time (RT_{pre} = 25 sec [51]) of the

seawater within the predeaerator necessary to achieve the design predeaeration rate of 85% predicted by Zapka [51]. The final values for this design after iteration are

$$H_{pre,DCC} = 1.50\ M$$

$$VOL_{pre,DCC} = 381.2\ M^3$$

$$RT_{pre} = VOL_{pre,DCC} / Q_{11} = 25.15\ S. \qquad \text{(G-202)}$$

G.4.4 CONDENSER PREDEAERATOR VENT COMPRESSOR DESIGN

The initial assumptions necessary for the condenser predeaerator vent compressor analysis are the same as those described previously in Appendix G.3.2 for the evaporator predeaerator vent compression train.

Once again the design procedure necessitates determining the compression ratio (constant for each stage) from an estimate of the number of compression stages necessary (N_{comp}), an assumed intercooler pressure drop (ΔP_{inter}), an initial compressor pressure ($P_{in,(1)} = P_{pre,DCC}$) and a design compressor exhaust pressure ($P_{17,design}$) as

$$N_{comp} = 2$$

$$\Delta P_{inter} = 0.28\ KPa\ [32]$$

$$P_{in,(1)} = P_{16} = 6.67\ KPa$$

$$P_{17,design} = 25.00\ KPa.$$

As in the evaporator predeaerator design mentioned previously, the design compressor exhaust pressure is not atmospheric. This

predeaerated/reinjected OC-OTEC system permits much lower compression power requirements because of the significantly lower exhaust pressures allowable for noncondensable reinjection versus atmospheric discharges. The minimum exhaust pressure ($P_{17,min}$) is found by determining the minimum injection pressure permitted into the condenser predeaerator since this compressor exhaust will not only be reinjected into the cold water effluent stream but will also serve as the injection gas for bubble seeding (see Figure 5.1). Therefore, the minimum exhaust pressure ($P_{17,min}$) is found from the predeaerator system pressure ($P_{pre,DCC}$) and the seawater head as

$$P_{17,min} = P_{pre,DCC} + H_{pre,DCC}\, \rho_{11}\, G / 1000 = 21.75 \text{ KPa}. \quad \text{(G-203)}$$

From the minimum injection pressure a design compressor exhaust pressure is chosen as

$$P_{17,design} = 25.00 \text{ KPa}$$

to allow enough over pressure to encourage bubble flow through the predeaerator seawater.

With the design parameters set above, the compression ratio is determined iteratively as described previously by solving

$$R_{comp}{}^{n} = (P_{17,design} + \Delta P_{inter} \sum_{i=1}^{n} R_{comp}{}^{i}) / P_{in,(1)} = 1.96. \quad \text{(G-204)}$$

The final iteration is displayed in the following table (Table G.6)

Table G.6: Iteration of Condenser Predeaerator Vent Compression Ratio

Step #	$\sum R_{comp}$	$R_{comp,\,i}$
1	1.96	1.96
2	3.91	1.96

The respective inlet and outlet pressures for each compressor stage is found in the following manner

$$P_{in,(1)} = P_{pre,DCC} = P_{16} = 6.67 \text{ KPa}$$

$$P_{out,(1)} = P_{in,(1)} R_{comp} = 13.05 \text{ KPa} \quad \text{(G-205)}$$

$$P_{in,(2)} = P_{out,(1)} - \Delta P_{inter} = 12.77 \text{ KPa} \quad \text{(G-206)}$$

$$P_{out,(2)} = P_{in,(2)} R_{comp} = P_{17} = 25.00 \text{ KPa} \quad \text{(G-207)}$$

For this analysis the first intercooler to the vent compressor is omitted since the vapor temperature will be that of the incoming cold water (T_{11} = 5.00 °C) and an intercooler would be ineffective. The inlet vapor temperature for the second stage set at 7.00 °C (discussed previously), the water vapor partial pressure entering each compressor stage is simply the saturation pressure at that temperature

$P_{sat,16}$ = 0.87 KPa (first stage water vapor pressure)

$P_{sat,16A}$ = 1.00 KPa (second stage water vapor pressure).

This water vapor pressure combined with the inlet pressures for each compression stage and the noncondensable flows entering from the condenser predeaerator yield the inert gas partial pressures for each compressor stage as

$$PP_{N2,(i)} = (P_{in,(i)} - P_{sat,16A}) / [1+ (M_{O2,pre,DCC,tot}+ M_{Ar,pre,DCC,tot}+ M_{CO2,pre,DCC,tot}) / M_{N2,pre,DCC,tot}] \quad \text{(G-208)}$$

$$PP_{O2,(i)} = (P_{in,(i)} - P_{sat,16A}) / [1+ (M_{N2,pre,DCC,tot}+ M_{Ar,pre,DCC,tot}+ M_{CO2,pre,DCC,tot}) / M_{O2,pre,DCC,tot}] \quad \text{(G-209)}$$

$$PP_{Ar,(i)} = (P_{in,(i)} - P_{sat,16A}) / [1+ (M_{N2,pre,DCC,tot}+ M_{O2,pre,DCC,tot}+ M_{CO2,pre,DCC,tot}) / M_{Ar,pre,DCC,tot}] \quad \text{(G-210)}$$

$$PP_{CO2,(i)} = P_{in,(i)} - P_{sat,16A} - PP_{N2,i} - PP_{O2,i} - PP_{Ar,i} \quad \text{(G-211)}$$

where the subscript i denotes the respective compression stages as i = 1 to n with the specific values presented in Table G.7 shown below. The corresponding water vapor flow accompanying this noncondensable flow through each compression stage is determined by

$$m_{wv,(i)} = MW_{H20} P_{sat,16A} M_{N2,pre,DCC,tot} / PP_{N2,(i)}. \quad \text{(G-212)}$$

The total parasitic power consumption for each compression stage is now defined by Parsons et al. [32] as

$$Po(i) = - (r / r-1) M_{gas,tot} R_g T_{16A} [1 - R_{comp}^{\{(r-1)/r\}}] / \eta_m \eta_{comp} \quad \text{(G-213)}$$

where

r = ratio of gas specific heats = 1.4 (assumed) [32]

$M_{gas,tot,(i)}$ = molar flow of gas through compressor stage

$$= m_{gas,tot,(i)} / GMWT_{(i)} \quad \text{(G-214)}$$

$$m_{gas,tot,(i)} = m_{wv,(i)} + m_{N2,pre,DCC,tot} + m_{O2,pre,DCC,tot} + m_{Ar,pre,DCC,tot} + m_{CO2,pre,DCC,tot} \quad \text{(G-215)}$$

$$GMWT_{(i)} = (PP_{N2,(i)}\,MW_{N2} + PP_{O2,(i)}\,MW_{O2} + PP_{Ar,(i)}\,MW_{Ar} + PP_{CO2,(i)}\,MW_{CO2} + P_{sat,16A}\,MW_{H2O}) / P_{in,(i)} \quad \text{(G-216)}$$

R_g = universal gas constant = 8.31 KPa M^3 / KG-MOL ^oK [17]

η_m = compressor motor efficiency = 0.90 [32]

η_{comp} = compressor efficiency = 0.80 [32]

T_{16A} = vapor inlet temperature (intercooler exit temperature or seawater temperature, depending on compression stage)

= 278.15 ^oK (first stage) 280.15 ^oK (second stage)

The volume flow of gas through each compression stage is defined as

$$VOL_{gas,(i)} = M_{gas,tot,(i)}\,R_g\,T_{16A} / P_{in,(i)}. \quad \text{(G-217)}$$

The following tables (Table G.7 and G.8) display the calculation procedure for each compression stage and present the parasitic power associated with each stage using the aforementioned equations from which the total parasitic power necessary to maintain proper system vacuum within the designed condenser predeaerator is derived.

Table G.7: Noncondensable Partial Pressures for Staged Compression from Condenser Predeaerator Vent Compressor

Stage #	PP_{N2} (KPa)	PP_{O2} (KPa)	PP_{Ar} (KPa)	PP_{CO2} (KPa)
1	4.8301	0.4174	0.1193	0.2982
2	10.0363	0.8673	0.2478	0.6195
exhaust conditions	20.4621	1.7683	0.5052	1.2631

Table G.8: Calculated Values for Staged Compression from Condenser Predeaerator Vent Compressor

Stage #	GMWT (KG/KG-MOL)	m_{wv} (KG/S)	$m_{gas,tot}$ (KG/S)	VOL_{gas} (M^3/S)	$Po_{(i)}$ (KW)
1	27.3408	0.0527	0.6113	7.7845	53.3605
2	28.5078	0.0291	0.5877	3.7464	49.2032
exhaust conditions	28.9443	0.0143	0.5729	1.8375	--

Total parsitic power for the condenser predeaerator vent compression train is

$$Po_{pre,DCC,VC,tot} = 103 \text{ KW}.$$

G.4.5 CONDENSER VENT COMPRESSOR DESIGN

The initial assumptions necessary for the condenser vent compressor analysis are the same as those described previously in Appendix G.3.2 for the evaporator predeaerator vent compression train.

Once again the design procedure necessitates determining the compression ratio (constant for each stage) from an estimate of the number of compression stages necessary (N_{comp}), an assumed intercooler pressure drop (ΔP_{inter}), an initial compressor pressure ($P_{in,(1)} = P_{pre,DCC}$) and a design compressor exhaust pressure ($P_{12,design}$) as

$$N_{comp} = 4$$

$$\Delta P_{inter} = 0.28 \text{ KPa } [32]$$

$$P_{in,(1)} = P_{DCC} = 1.23 \text{ KPa}$$

$$P_{12,design} = 25.00 \text{ KPa.}$$

The design compressor exhaust pressure is not atmospheric as was the case in the evaporator predeaerator and condenser predeaerator vent compressors discussed previously. The minimum exhaust pressure ($P_{12,min}$) is found by determining the minimum injection pressure permitted into the condenser predeaerator since this compressor exhaust will be combined with the condenser predeaerator compressor exhaust to be reinjected into the warm water effluent stream and also serve as the injection gas for bubble seeding (see Figure 5.1). Therefore, the minimum exhaust pressure ($P_{12,min}$) is found from the predeaerator system pressure ($P_{pre,DCC}$) and the seawater head as

$$P_{12,min} = P_{17,min} = P_{pre,DCC} + H_{pre,DCC}\, \rho_{11}\, G / 1000 = 21.75 \text{ KPa.} \quad \text{(G-218)}$$

From the minimum injection pressure a design compressor exhaust pressure is chosen as

$$P_{12,design} = 25.00 \text{ KPa}$$

to allow enough over pressure to encourage bubble flow through the predeaerator seawater.

With the design parameters set above, the compression ratio is determined iteratively as described previously by solving

$$R_{comp}{}^{n} = (P_{12,design} + \Delta P_{inter} \sum_{i=1}^{n} R_{comp}{}^{i}) / P_{in,(1)} = 2.33. \quad \text{(G-219)}$$

The final iteration is displayed in the following table (Table G.9)

Table G.9: Iteration of Condenser Vent Compression Ratio

Step #	$\sum R_{comp}$	$R_{comp,\,i}$
1	2.33	2.14
2	6.90	2.16
3	17.03	2.22
4	41.22	2.33

The respective inlet and outlet pressures for each compressor stage is found in the following manner

$$P_{in,(1)} = P_{DCC} = P_8 = 1.23\ KPa$$

$$P_{out,(1)} = P_{in,(1)}\, R_{comp} = 2.86\ KPa \qquad \text{(G-220)}$$

$$P_{in,(2)} = P_{out,(1)} - \Delta P_{inter} = 2.59\ KPa \qquad \text{(G-221)}$$

$$P_{out,(2)} = P_{in,(2)}\, R_{comp} = 6.04\ KPa \qquad \text{(G-222)}$$

$$P_{in,(3)} = P_{out,(2)} - \Delta P_{inter} = 5.76\ KPa \qquad \text{(G-223)}$$

$$P_{out,(3)} = P_{in,(3)}\, R_{comp} = 13.45\ KPa \qquad \text{(G-224)}$$

$$P_{in,(4)} = P_{out,(3)} - \Delta P_{inter} = 13.17\ KPa \qquad \text{(G-225)}$$

$$P_{out,(4)} = P_{in,(4)}\, R_{comp} = P_{12} = 30.73\ KPa \qquad \text{(G-226)}$$

The inlet vapor temperature for the each stage is set at 7.00 °C (discussed previously), the water vapor partial pressure entering each compressor stage is simply the saturation pressure at that temperature

$$P_{sat,8A} = 1.00 \text{ KPa}.$$

This water vapor pressure combined with the inlet pressures for each compression stage and the noncondensable flows entering from the condenser yield the inert gas partial pressures for each compressor stage as

$$PP_{N2,(i)} = (P_{in,(i)} - P_{sat,8A}) / [1 + (M_{O2,DCC,tot} + M_{Ar,DCC,tot} + M_{CO2,DCC,tot}) / M_{N2,DCC,tot}] \quad \text{(G-227)}$$

$$PP_{O2,(i)} = (P_{in,(i)} - P_{sat,8A}) / [1 + (M_{N2,DCC,tot} + M_{Ar,DCC,tot} + M_{CO2,DCC,tot}) / M_{O2,DCC,tot}] \quad \text{(G-228)}$$

$$PP_{Ar,(i)} = (P_{in,(i)} - P_{sat,8A}) / [1 + (M_{N2,DCC,tot} + M_{O2,DCC,tot} + M_{CO2,DCC,tot}) / M_{Ar,DCC,tot}] \quad \text{(G-229)}$$

$$PP_{CO2,(i)} = P_{in,(i)} - P_{sat,8A} - PP_{N2,i} - PP_{O2,i} - PP_{Ar,i} \quad \text{(G-230)}$$

where the subscript i denotes the respective compression stages as i = 1 to n with the specific values presented in Table G.10 shown below. The corresponding water vapor flow accompanying this noncondensable flow through each compression stage is determined by

$$m_{wv,(i)} = MW_{H20} P_{sat,8A} M_{N2,DCC,tot} / PP_{N2,(i)}. \quad \text{(G-231)}$$

The total parasitic power consumption for each compression stage is now defined by Parsons et al. [32] as

$$Po(i) = -(r / r\text{-}1) M_{gas,tot} R_g T_{8A} [1 - R_{comp}^{\{(r-1)/r\}}] / \eta_m \eta_{comp} \quad \text{(G-232)}$$

where

r = ratio of gas specific heats = 1.4 (assumed) [32]

$M_{gas,tot,(i)}$ = molar flow of gas through compressor stage

$$= m_{gas,tot,(i)} / GMWT_{(i)} \quad \text{(G-233)}$$

$$m_{gas,tot,(i)} = m_{wv,(i)} + m_{N2,DCC,tot} + m_{O2,DCC,tot} + m_{Ar,DCC,tot} + m_{CO2,DCC,tot} \quad \text{(G-234)}$$

$$GMWT_{(i)} = (PP_{N2,(i)} MW_{N2} + PP_{O2,(i)} MW_{O2} + PP_{Ar,(i)} MW_{Ar} + PP_{CO2,(i)} MW_{CO2} + P_{sat,8A} MW_{H2O}) / P_{in,(i)} \quad \text{(G-235)}$$

R_g = universal gas constant = 8.31 KPa M^3 / KG-MOL $^\circ K$ [17]

η_m = compressor motor efficiency = 0.90 [32]

η_{comp} = compressor efficiency = 0.80 [32]

T_{8A} = vapor inlet temperature = 280.15 $^\circ K$

The volume flow of gas through each compression stage is defined as

$$VOL_{gas,(i)} = M_{gas,tot,(i)} R_g T_{8A} / P_{in,(i)}. \quad \text{(G-236)}$$

The following tables (Table G.10 and G.11) display the calculation procedure for each compression stage and present the parasitic power associated with each stage using the aforementioned equations from which the total parasitic power necessary to maintain proper system

Table G.10: Noncondensable Partial Pressures for Staged Compression from Condenser Vent Compressor

Stage #	PP_{N2} (KPa)	PP_{O2} (KPa)	PP_{Ar} (KPa)	PP_{CO2} (KPa)
1	0.1919	0.0344	0.0004	0.0000
2	1.3434	0.2411	0.0026	0.0003
3	4.0301	0.7233	0.0078	0.0010
4	10.2980	1.8484	0.0198	0.0026
exhaust conditions	25.1545	4.5149	0.0484	0.0064

Table G.11: Calculated Values for Staged Compression from Condenser Vent Compressor

Stage #	GMWT (KG/KG-MOL)	m_{wv} (KG/S)	$m_{gas,tot}$ (KG/S)	VOL_{gas} (M^3/S)	$Po_{(i)}$ (KW)
1	19.9772	0.3666	0.4986	47.1787	77.1182
2	24.5318	0.0524	0.1844	6.7618	23.3019
3	26.7957	0.0175	0.1494	2.2541	17.2940
4	27.8338	0.0068	0.1388	2.0157	15.4655
exhaust conditions	28.2954	0.0028	0.1348	1.9252	--

vacuum within the designed condenser and evaporator system is derived. Total parsitic power for the condenser vent compression train is

$$Po_{DCC,VC,tot} = 133 \text{ KW}.$$

G.4.6 CONDENSER HYDRAULIC COMPRESSOR DESIGN

The hydraulic compressor design for the condenser incorporates two varying designs as outlined previously in this report. The first utilizes the existing cold water discharge pipe as the hydraulic compression mechanism while the second utilizes a designed tapering pipe configuration as the compression mechanism. In order to prevent confusion of the two design

procedures, the condenser hydraulic compressor design analysis has been separated into two distinct sections. Unlike the evaporator analysis presented earlier, the condenser hydraulic compressor will reinject the noncondensables from two vent compression locations. The first is the noncondensables desorbed in the cold water predeaerator (from Section G.4.4.4) and the second being the noncondensables accumulating in the direct-contact condenser and removed by the condenser vent compression train (Section G.4.4.5). For the purposes of this investigation, the two vent compressor vent streams (12 and 17 in Figure 5.1) are combined and considered path 18 (see Figure 5.1) with the lowest venting pressure representing path 18 pressure.

G.4.6.1 HYDRAULIC COMPRESSOR - EXISTING PIPE DESIGN

The existing pipe analysis for the hydraulic compression mechanism essentially entails the determination of the portion of the downcomer necessary to perform the majority of the compression of the injected noncondensables to the point where these gases no longer significantly interfere with the cold water discharge flow. This analysis should include a means of estimating the reabsorption rate of the noncondensables and the necessary head required to overcome the seawater velocity change associated with the reduced flow area accompanying the introduction of these noncondensables to the flow stream.

From the cold water flow system analysis following this analysis (Appendix G.5.2) the design seawater flow velocity (X_9) and the design pipe diameter ($D_{9,pipe}$) and area ($A_{9,pipe}$) are

$$X_9 = 2.00 \text{ M/S}$$

$$D_{9,pipe} = 3.11 \text{ M}$$

$$A_{9,pipe} = 7.60 \text{ M}^2$$

and apply here for the discharge pipe parameters since the design calls for the standard downcomer pipe. The design cold water mass flow (m_9) and volumetric flow ($Q_{9,cw}$) are

$$m_9 = 15566 \text{ KG/S}$$

$$Q_{9,cw} = 15.18 \text{ M}^3\text{/S}.$$

The design cold water flow velocity (X_9) will not remain this value in this hydraulic compressor design because the void fraction in the discharge pipe area caused by the presence of the injected noncondensables will increase this velocity at the point of injection and will subsequently decrease as the noncondensable void fraction is reduced with the combined action of hydraulic compression and reabsorption of the injected gases. It will be the estimated effects of the injected noncondensables on the seawater flow velocity which will eventually determine the overall hydraulic losses associated with this type of hydraulic compression device. This will be presented in more detail following.

To begin the design procedure for this hydraulic compressor, it is initially necessary to define the pressure change with pipe length (dP/dh) expected as the seawater travels along the downcomer. This value is simply defined as

$$dP/dh = \rho_9 G = 10.05 \text{ KPa/M}. \qquad \text{(G-237)}$$

The next step is to determine the desired point of noncondensable injection from which the hydraulic compression analysis can commence. The pressure at the injection point ($P_{inj,cw}$) is then set slightly less than the compressor exhaust pressure (P_{18}) from the previous condenser predeaerator compressor

analysis and the distance from pipe entrance to the point of reinjection ($h_{inj,DCC}$) is determined as follows

$$P_{inj,cw} = 24.50 \text{ KPa}$$

$$h_{inj,DCC} = (P_{inj,cw} - P_{DCC}) / (dP/dh) = 2.30 \text{ M.} \quad \text{(G-238)}$$

This is the point where the hydraulic compressor design is initiated.

With the length of the hydraulic compression region necessary to significantly reduce the volumetric flow of the noncondensables unknown, the procedure for determining the hydraulic head requirements is iterative in nature. For the first iteration it is assumed that no reabsorption of the noncondensables occurs and a rough estimate of the necessary length to perform a compression in which the gas volume in the cold water discharge flow approaches 0.5% is determined as

$$Q_{NC,end} = 0.005 \; Q_9 = 0.076 \text{ M}^3\text{/S} \quad \text{(G-239)}$$

which yields an estimated seawater velocity ($X_{9,end}$) at the "end" of the compressor of

$$X_{9,end} = (Q_9 + Q_{NC,end}) / A_{9,pipe} = 2.01 \text{ M/S} \quad \text{(G-240)}$$

and a corresponding local pressure of

$$P_{9,end} = M_{inj,DCC} R_g T_9^* / Q_{NC,end}) + P_{inj,DCC,cw} = 454.05 \text{ KPa} \quad \text{(G-241)}$$

where

T_9^* = seawater temperature = 283.99 °K

$M_{inj,DCC}$ = molar flow of injected gas (from condenser vent compressor and condenser predeaerator vent compressor)

$$= m_{inj,DCC} / MW_{inj,DCC} = 0.0138 \text{ KG-MOL/S} \quad \text{(G-242)}$$

$m_{inj,DCC}$ = mass flow of injected gas

$$= m_{NC,pre + DCC,tot} - m_{pre + DCC,inj} = 0.398 \text{ KG/S.} \quad \text{(G-243)}$$

This "end" pressure corresponds to a hydraulic compressor length from point of gas injection to compressor "end" of

$$h_{comp} = (P_{9,end} - P_{inj,DCC,cw}) / (dP/dh) = 42.75\ M \qquad \text{(G-244)}$$

to be used for the first iteration.

The final value after the iterative process accounting for noncondensable reabsorption and gas compression is

$$h_{comp} = 11.28\ M.$$

In order to determine the total head required to overcome the presence of the injected noncondensables, the length of the hydraulic compressor from the point of injection to the "end" of the compression region is iterated (100 iterations) along the total length (h_{comp}). At each segment along the hydraulic compressor (h_i) where

$$h_i = h_{inj,DCC} + \Delta h_{DCC} \qquad \text{(G-245)}$$

for the first segment and h_i is positive downward to the "end" of the design compressor region as

$$h_i = h_{i-1} + \Delta h_{DCC} \qquad \text{(G-246)}$$

where

$$\Delta h_{DCC} = h_{comp} / 100 = 0.113\ M \qquad \text{(G-247)}$$

the following parameters are determined utilizing the calculated Henry's law constants for the seawater temperature (T_9) and assumed seawater salinity of 35.00 °/oo which yield

$$K_{H,N2} = C_{N2}\, MV_{ideal} / (1000 \times 101.33)$$
$$= 4.94 \times 10^{-6}\ \text{KG-MOL} / M^3\,\text{KPa} \qquad \text{(G-248)}$$

$$K_{H,O2} = C_{O2}\, MV_{ideal} / (1000 \times 101.33)$$
$$= 2.73 \times 10^{-6}\ \text{KG-MOL} / M^3\,\text{KPa} \qquad \text{(G-249)}$$

$$K_{H,Ar} = C_{Ar} MV_{ideal} / (1000 \times 101.33)$$

$$= 1.33 \times 10^{-7} \text{ KG-MOL} / M^3 \text{KPa} \quad \text{(G-250)}$$

$$K_{H,CO2} = C_{CO2} \rho_9 / (1000 \times 101.33)$$

$$= 4.32 \times 10^{-4} \text{ KG-MOL} / M^3 \text{KPa} \quad \text{(G-251)}$$

where

C_{gas} = concentration of specific gas (excluding CO_2) determined from equations presented at outset of Appendix F taken from [47] (ML/L)

C_{CO2} = concentration of CO_2 determined by equation presented at outset of Appendix F taken from [39] (MOL/KG - ATM)

MV_{ideal} = molar volume of an ideal gas

= 22.41 M^3/ KG-MOL ATM [46]

The value of 1000 in the nitrogen, oxygen and argon equations converts milliliters to liters while the 101.33 converts atmospheres to KPa for all equations. For the carbon dioxide equation, the 1000 converts moles to kg-moles.

The development of the hydraulic compressor design continues with the determination of the following values as

P_i = pressure of water column at iteration segment i

$$= h_i \, dP/dh + P_{i-1} \quad \text{(KPa)} \quad \text{(G-252)}$$

$M_{N2,i}$ = molar flow of nitrogen at iteration segment i

$$= M_{N2,i-1} - [(C_{NC,i-1} - C_{NC,i-2}) Q_9 M_{N2,i-1} / (M_{N2,i-1} + M_{O2,i-1} + M_{Ar,i-1} + M_{CO2,i-1})] \quad \text{(G-253)}$$

$M_{O2,i}$ = molar flow of oxygen at iteration segment i

$$= M_{O2,i-1} - [(C_{NC,i-1} - C_{NC,i-2})\, Q_9\, M_{O2,i-1} / (M_{N2,i-1} + M_{O2,i-1} + M_{Ar,i-1} + M_{CO2,i-1})] \quad \text{(G-254)}$$

$M_{Ar,i}$ = molar flow of argon at iteration segment i

$$= M_{Ar,i-1} - [(C_{NC,i-1} - C_{NC,i-2})\, Q_9\, M_{Ar,i-1} / (M_{N2,i-1} + M_{O2,i-1} + M_{Ar,i-1} + M_{CO2,i-1})] \quad \text{(G-255)}$$

$M_{CO2,i}$ = molar flow of CO_2 at iteration segment i

$$= M_{CO2,i-1} - [(C_{NC,i-1} - C_{NC,i-2})\, Q_9\, M_{CO2,i-1} / (M_{N2,i-1} + M_{O2,i-1} + M_{Ar,i-1} + M_{CO2,i-1})] \quad \text{(G-256)}$$

$PP_{N2,i}$ = partial pressure of nitrogen at i

$$= (P_i - P_{sat,9}) / [\,1 + (M_{O2,i} + M_{Ar,i} + M_{CO2,i}) / M_{N2,i}] \quad \text{(G-257)}$$

$PP_{O2,i}$ = partial pressure of oxygen at i

$$= (P_i - P_{sat,9}) / [\,1 + (M_{N2,i} + M_{Ar,i} + M_{CO2,i}) / M_{O2,i}] \quad \text{(G-258)}$$

$PP_{Ar,i}$ = partial pressure of argon at i

$$= (P_i - P_{sat,9}) / [\,1 + (M_{N2,i} + M_{O2,i} + M_{CO2,i}) / M_{Ar,i}] \quad \text{(G-259)}$$

$PP_{CO2,i}$ = partial pressure of carbon dioxide at i

$$= P_i - P_{sat,9} - PP_{N2,i} - PP_{O2,i} - PP_{Ar,i} \quad \text{(G-260)}$$

$C_{sat,i}$ = saturation concentration for all gas species at local pressure and seawater temperature

$$= K_{H,N2}\, PP_{N2,i} + K_{H,O2}\, PP_{O2,i} + K_{H,Ar}\, PP_{Ar,i} + KH_{CO2}\, PP_{CO2,i} \text{ (KG-MOL/M}^3\text{)} \quad \text{(G-261)}$$

$Kl*a_i$ = overall mass transfer coefficient

$$= 0.000388\,(P_{i-1} - P_i) \quad \text{for } P_i < 90 \text{ KPa} \quad \text{(G-262)}$$

$$= 0.00525\,(P_{i-1} - P_i) - 0.428 \quad \text{for } P_i > 90 \text{ KPa} \quad \text{(G-263)}$$

(taken from data in [51]) (1/S)

$t_{RES,i}$ = residence time in iteration segment i

$= \Delta h_i / X_{9,i-1}$ (S) (G-264)

$C_{NC,i}$ = concentration of noncondensables in seawater at i

$= C_{sat,i} - (C_{sat,i} - C_{NC,i-1}) / EXP (K1*a\ t)$ (KG-MOL/M^3) (G-265)

n_i = number of moles of gas at iteration segment i

$= n_{i-1} - C_{NC,i} Q_9$ (KG-MOL/S) (G-266)

$Q_{NC,i}$ = volumetric flow of gas at iteration segment i

$= n_i R_g T_9^* / P_i$ (M^3/S) (G-267)

$A_{pipe,i}$ = area for liquid flow in discharge pipe at i

$= A_{9,pipe} - [Q_{NC,i} / (Q_{NC,i} + Q_9)] A_{9,pipe}$ (M^2) (G-268)

$X_{9,i}$ = velocity of seawater at iteration segment i

$= Q_9 / A_{pipe,i}$ (M/S) (G-269)

$H_{HC,i}$ = head required to overcome reduced flow area at i

$= (X_9 - X_{9,i})^2 / 2G$ (M) (G-270)

The initial molar concentrations of the noncondensables and initial partial pressures are passed from the condenser predeaerator vent compression analysis and condenser vent compressor analysis preceding this section. Likewise, the initial seawater noncondensable concentration was determined from the condenser predeaerator analysis. The following tables present the data along the entire length of the hydraulic compression region utilizing these initial values to begin the iterative process.

Table G.12 : Hydraulic Compressor Analysis - Standard Discharge Pipe

h_i	P_i	$M_{N2,i}$	$M_{O2,i}$	$M_{Ar,i}$	$M_{CO2,i}$
0.0000	24.5000	4.9083E-03	2.6311E-03	1.2904E-04	1.6699E-04
0.1128	25.6329	4.9070E-03	2.6304E-03	1.2901E-04	1.6695E-04
0.2255	26.7658	4.9057E-03	2.6297E-03	1.2898E-04	1.6690E-04
0.3383	27.8988	4.9043E-03	2.6289E-03	1.2894E-04	1.6685E-04
0.4510	29.0317	4.9028E-03	2.6281E-03	1.2890E-04	1.6680E-04
0.5638	30.1646	4.9010E-03	2.6272E-03	1.2885E-04	1.6674E-04
0.6765	31.2975	4.8992E-03	2.6262E-03	1.2880E-04	1.6668E-04
0.7893	32.4304	4.8971E-03	2.6251E-03	1.2875E-04	1.6661E-04
0.9020	33.5633	4.8949E-03	2.6239E-03	1.2869E-04	1.6653E-04
1.0148	34.6963	4.8925E-03	2.6226E-03	1.2863E-04	1.6645E-04
1.1275	35.8292	4.8899E-03	2.6212E-03	1.2856E-04	1.6636E-04
1.2403	36.9621	4.8872E-03	2.6197E-03	1.2849E-04	1.6627E-04
1.3530	38.0950	4.8842E-03	2.6182E-03	1.2841E-04	1.6617E-04
1.4658	39.2279	4.8810E-03	2.6165E-03	1.2833E-04	1.6606E-04
1.5785	40.3609	4.8776E-03	2.6146E-03	1.2824E-04	1.6595E-04
1.6913	41.4938	4.8740E-03	2.6127E-03	1.2814E-04	1.6582E-04
1.8040	42.6267	4.8702E-03	2.6107E-03	1.2804E-04	1.6569E-04
1.9168	43.7596	4.8661E-03	2.6085E-03	1.2794E-04	1.6555E-04
2.0295	44.8925	4.8618E-03	2.6062E-03	1.2782E-04	1.6541E-04
2.1423	46.0254	4.8573E-03	2.6037E-03	1.2770E-04	1.6525E-04
2.2550	47.1584	4.8525E-03	2.6012E-03	1.2758E-04	1.6509E-04
2.3678	48.2913	4.8474E-03	2.5984E-03	1.2744E-04	1.6492E-04
2.4805	49.4242	4.8421E-03	2.5956E-03	1.2730E-04	1.6474E-04
2.5933	50.5571	4.8365E-03	2.5926E-03	1.2716E-04	1.6455E-04
2.7060	51.6900	4.8306E-03	2.5894E-03	1.2700E-04	1.6435E-04
2.8188	52.8230	4.8244E-03	2.5861E-03	1.2684E-04	1.6414E-04
2.9315	53.9559	4.8180E-03	2.5827E-03	1.2667E-04	1.6392E-04
3.0443	55.0888	4.8112E-03	2.5790E-03	1.2649E-04	1.6369E-04
3.1570	56.2217	4.8042E-03	2.5753E-03	1.2631E-04	1.6345E-04
3.2698	57.3546	4.7968E-03	2.5713E-03	1.2611E-04	1.6320E-04
3.3825	58.4875	4.7891E-03	2.5672E-03	1.2591E-04	1.6293E-04
3.4953	59.6205	4.7811E-03	2.5629E-03	1.2570E-04	1.6266E-04
3.6080	60.7534	4.7728E-03	2.5584E-03	1.2548E-04	1.6238E-04
3.7208	61.8863	4.7641E-03	2.5538E-03	1.2525E-04	1.6208E-04
3.8335	63.0192	4.7551E-03	2.5489E-03	1.2502E-04	1.6178E-04
3.9463	64.1521	4.7457E-03	2.5439E-03	1.2477E-04	1.6146E-04
4.0590	65.2851	4.7360E-03	2.5387E-03	1.2451E-04	1.6113E-04
4.1718	66.4180	4.7259E-03	2.5333E-03	1.2425E-04	1.6078E-04
4.2845	67.5509	4.7154E-03	2.5277E-03	1.2397E-04	1.6043E-04
4.3973	68.6838	4.7046E-03	2.5219E-03	1.2369E-04	1.6006E-04
4.5100	69.8167	4.6934E-03	2.5159E-03	1.2339E-04	1.5968E-04

4.6228	70.9496	4.6818E-03	2.5097E-03	1.2309E-04	1.5928E-04
4.7355	72.0826	4.6698E-03	2.5033E-03	1.2277E-04	1.5888E-04
4.8483	73.2155	4.6575E-03	2.4966E-03	1.2245E-04	1.5846E-04
4.9610	74.3484	4.6447E-03	2.4898E-03	1.2211E-04	1.5802E-04
5.0738	75.4813	4.6315E-03	2.4827E-03	1.2177E-04	1.5757E-04
5.1865	76.6142	4.6179E-03	2.4754E-03	1.2141E-04	1.5711E-04
5.2993	77.7472	4.6039E-03	2.4679E-03	1.2104E-04	1.5663E-04
5.4120	78.8801	4.5894E-03	2.4601E-03	1.2066E-04	1.5614E-04
5.5248	80.0130	4.5745E-03	2.4522E-03	1.2027E-04	1.5563E-04
5.6375	81.1459	4.5592E-03	2.4440E-03	1.1987E-04	1.5511E-04
5.7503	82.2788	4.5435E-03	2.4355E-03	1.1945E-04	1.5458E-04
5.8630	83.4117	4.5273E-03	2.4268E-03	1.1903E-04	1.5402E-04
5.9758	84.5447	4.5106E-03	2.4179E-03	1.1859E-04	1.5346E-04
6.0885	85.6776	4.4935E-03	2.4087E-03	1.1814E-04	1.5288E-04
6.2013	86.8105	4.4759E-03	2.3993E-03	1.1767E-04	1.5228E-04
6.3140	87.9434	4.4578E-03	2.3896E-03	1.1720E-04	1.5166E-04
6.4268	89.0763	4.4393E-03	2.3797E-03	1.1671E-04	1.5103E-04
6.5395	90.2093	4.4203E-03	2.3695E-03	1.1621E-04	1.5038E-04
6.6523	91.3422	4.3986E-03	2.3578E-03	1.1564E-04	1.4965E-04
6.7650	92.4751	4.3732E-03	2.3443E-03	1.1498E-04	1.4879E-04
6.8778	93.6080	4.3442E-03	2.3287E-03	1.1421E-04	1.4780E-04
6.9905	94.7409	4.3113E-03	2.3111E-03	1.1335E-04	1.4668E-04
7.1033	95.8738	4.2746E-03	2.2914E-03	1.1238E-04	1.4543E-04
7.2160	97.0068	4.2339E-03	2.2696E-03	1.1131E-04	1.4404E-04
7.3288	98.1397	4.1893E-03	2.2456E-03	1.1014E-04	1.4253E-04
7.4415	99.2726	4.1443E-03	2.2216E-03	1.0896E-04	1.4100E-04
7.5543	100.4055	4.0916E-03	2.1933E-03	1.0757E-04	1.3920E-04
7.6670	101.5384	4.0347E-03	2.1628E-03	1.0608E-04	1.3727E-04
7.7798	102.6714	3.9737E-03	2.1301E-03	1.0447E-04	1.3519E-04
7.8925	103.8043	3.9085E-03	2.0951E-03	1.0276E-04	1.3297E-04
8.0053	104.9372	3.8391E-03	2.0579E-03	1.0093E-04	1.3061E-04
8.1180	106.0701	3.7654E-03	2.0184E-03	9.8995E-05	1.2810E-04
8.2308	107.2030	3.6874E-03	1.9766E-03	9.6946E-05	1.2545E-04
8.3435	108.3359	3.6052E-03	1.9326E-03	9.4784E-05	1.2266E-04
8.4563	109.4689	3.5187E-03	1.8862E-03	9.2510E-05	1.1971E-04
8.5690	110.6018	3.4279E-03	1.8375E-03	9.0122E-05	1.1662E-04
8.6818	111.7347	3.3327E-03	1.7865E-03	8.7621E-05	1.1339E-04
8.7945	112.8676	3.2333E-03	1.7332E-03	8.5006E-05	1.1000E-04
8.9073	114.0005	3.1295E-03	1.6776E-03	8.2279E-05	1.0647E-04
9.0200	115.1335	3.0215E-03	1.6197E-03	7.9438E-05	1.0280E-04
9.1328	116.2664	2.9092E-03	1.5595E-03	7.6485E-05	9.8975E-05
9.2455	117.3993	2.7926E-03	1.4970E-03	7.3420E-05	9.5009E-05
9.3583	118.5322	2.6718E-03	1.4322E-03	7.0243E-05	9.0898E-05
9.4710	119.6651	2.5467E-03	1.3652E-03	6.6956E-05	8.6644E-05
9.5838	120.7980	2.4175E-03	1.2959E-03	6.3558E-05	8.2247E-05
9.6965	121.9310	2.2841E-03	1.2244E-03	6.0051E-05	7.7708E-05
9.8093	123.0639	2.1466E-03	1.1507E-03	5.6435E-05	7.3030E-05

9.9220	124.1968	2.0050E-03	1.0748E-03	5.2712E-05	6.8212E-05
10.0348	125.3297	1.8593E-03	9.9669E-04	4.8884E-05	6.3258E-05
10.1475	126.4626	1.7097E-03	9.1648E-04	4.4950E-05	5.8167E-05
10.2603	127.5956	1.5561E-03	8.3416E-04	4.0912E-05	5.2943E-05
10.3730	128.7285	1.3987E-03	7.4977E-04	3.6773E-05	4.7586E-05
10.4858	129.8614	1.2374E-03	6.6332E-04	3.2533E-05	4.2099E-05
10.5985	130.9943	1.0724E-03	5.7485E-04	2.8194E-05	3.6484E-05
10.7113	132.1272	9.0364E-04	4.8439E-04	2.3758E-05	3.0743E-05
10.8240	133.2601	7.3126E-04	3.9199E-04	1.9226E-05	2.4879E-05
10.9368	134.3931	5.5532E-04	2.9768E-04	1.4600E-05	1.8893E-05
11.0495	135.5260	3.7588E-04	2.0149E-04	9.8822E-06	1.2788E-05
11.1623	136.6589	1.9302E-04	1.0347E-04	5.0746E-06	6.5667E-06
11.2750	137.7918	6.8104E-06	3.6507E-06	1.7905E-07	2.3170E-07

Table G.12 : Hydraulic Compressor Analysis - Standard Discharge Pipe (Continued)

h_i	$PP_{N2,i}$	$PP_{O2,i}$	$PP_{Ar,i}$	$PP_{CO2,i}$	$C_{sat,i}$
0.0000	14.5344	7.7911	0.3821	0.4945	3.07E-04
0.1128	15.2441	8.1715	0.4008	0.5186	3.21E-04
0.2255	15.9538	8.5520	0.4194	0.5428	3.36E-04
0.3383	16.6635	8.9324	0.4381	0.5669	3.51E-04
0.4510	17.3731	9.3128	0.4568	0.5911	3.66E-04
0.5638	18.0828	9.6932	0.4754	0.6152	3.81E-04
0.6765	18.7925	10.0737	0.4941	0.6394	3.96E-04
0.7893	19.5022	10.4541	0.5127	0.6635	4.11E-04
0.9020	20.2119	10.8345	0.5314	0.6876	4.26E-04
1.0148	20.9216	11.2149	0.5500	0.7118	4.41E-04
1.1275	21.6313	11.5954	0.5687	0.7359	4.56E-04
1.2403	22.3410	11.9758	0.5874	0.7601	4.71E-04
1.3530	23.0507	12.3562	0.6060	0.7842	4.86E-04
1.4658	23.7603	12.7366	0.6247	0.8084	5.01E-04
1.5785	24.4700	13.1171	0.6433	0.8325	5.16E-04
1.6913	25.1797	13.4975	0.6620	0.8567	5.31E-04
1.8040	25.8894	13.8779	0.6807	0.8808	5.46E-04
1.9168	26.5991	14.2583	0.6993	0.9049	5.61E-04
2.0295	27.3088	14.6388	0.7180	0.9291	5.76E-04
2.1423	28.0185	15.0192	0.7366	0.9532	5.91E-04
2.2550	28.7282	15.3996	0.7553	0.9774	6.06E-04
2.3678	29.4379	15.7801	0.7739	1.0015	6.21E-04
2.4805	30.1475	16.1605	0.7926	1.0257	6.36E-04
2.5933	30.8572	16.5409	0.8113	1.0498	6.51E-04

2.7060	31.5669	16.9213	0.8299	1.0740	6.66E-04
2.8188	32.2766	17.3018	0.8486	1.0981	6.81E-04
2.9315	32.9863	17.6822	0.8672	1.1222	6.96E-04
3.0443	33.6960	18.0626	0.8859	1.1464	7.11E-04
3.1570	34.4057	18.4430	0.9046	1.1705	7.26E-04
3.2698	35.1154	18.8235	0.9232	1.1947	7.41E-04
3.3825	35.8251	19.2039	0.9419	1.2188	7.56E-04
3.4953	36.5347	19.5843	0.9605	1.2430	7.71E-04
3.6080	37.2444	19.9647	0.9792	1.2671	7.85E-04
3.7208	37.9541	20.3452	0.9978	1.2913	8.00E-04
3.8335	38.6638	20.7256	1.0165	1.3154	8.15E-04
3.9463	39.3735	21.1060	1.0352	1.3396	8.30E-04
4.0590	40.0832	21.4864	1.0538	1.3637	8.45E-04
4.1718	40.7929	21.8669	1.0725	1.3878	8.60E-04
4.2845	41.5026	22.2473	1.0911	1.4120	8.75E-04
4.3973	42.2123	22.6277	1.1098	1.4361	8.90E-04
4.5100	42.9219	23.0082	1.1285	1.4603	9.05E-04
4.6228	43.6316	23.3886	1.1471	1.4844	9.20E-04
4.7355	44.3413	23.7690	1.1658	1.5086	9.35E-04
4.8483	45.0510	24.1494	1.1844	1.5327	9.50E-04
4.9610	45.7607	24.5299	1.2031	1.5569	9.65E-04
5.0738	46.4704	24.9103	1.2217	1.5810	9.80E-04
5.1865	47.1801	25.2907	1.2404	1.6051	9.95E-04
5.2993	47.8898	25.6711	1.2591	1.6293	1.01E-03
5.4120	48.5995	26.0516	1.2777	1.6534	1.02E-03
5.5248	49.3091	26.4320	1.2964	1.6776	1.04E-03
5.6375	50.0188	26.8124	1.3150	1.7017	1.05E-03
5.7503	50.7285	27.1928	1.3337	1.7259	1.07E-03
5.8630	51.4382	27.5733	1.3524	1.7500	1.08E-03
5.9758	52.1479	27.9537	1.3710	1.7742	1.10E-03
6.0885	52.8576	28.3341	1.3897	1.7983	1.11E-03
6.2013	53.5673	28.7145	1.4083	1.8224	1.13E-03
6.3140	54.2770	29.0950	1.4270	1.8466	1.14E-03
6.4268	54.9867	29.4754	1.4457	1.8707	1.16E-03
6.5395	55.6963	29.8558	1.4643	1.8949	1.17E-03
6.6523	56.4060	30.2362	1.4830	1.9190	1.19E-03
6.7650	57.1157	30.6167	1.5016	1.9432	1.20E-03
6.8778	57.8254	30.9971	1.5203	1.9673	1.22E-03
6.9905	58.5351	31.3775	1.5389	1.9915	1.23E-03
7.1033	59.2448	31.7580	1.5576	2.0156	1.25E-03
7.2160	59.9545	32.1384	1.5763	2.0398	1.26E-03
7.3288	60.6642	32.5188	1.5949	2.0639	1.19E-03
7.4415	61.3739	32.8992	1.6136	2.0880	1.29E-03
7.5543	62.0835	33.2797	1.6322	2.1122	1.31E-03
7.6670	62.7932	33.6601	1.6509	2.1363	1.32E-03
7.7798	63.5029	34.0405	1.6696	2.1605	1.34E-03
7.8925	64.2126	34.4209	1.6882	2.1846	1.35E-03

8.0053	64.9223	34.8014	1.7069	2.2088	1.37E-03
8.1180	65.6320	35.1818	1.7255	2.2329	1.38E-03
8.2308	66.3417	35.5622	1.7442	2.2571	1.40E-03
8.3435	67.0514	35.9426	1.7628	2.2812	1.41E-03
8.4563	67.7611	36.3231	1.7815	2.3053	1.43E-03
8.5690	68.4707	36.7035	1.8002	2.3295	1.44E-03
8.6818	69.1804	37.0839	1.8188	2.3536	1.46E-03
8.7945	69.8901	37.4643	1.8375	2.3778	1.47E-03
8.9073	70.5998	37.8448	1.8561	2.4019	1.49E-03
9.0200	71.3095	38.2252	1.8748	2.4261	1.50E-03
9.1328	72.0192	38.6056	1.8935	2.4502	1.52E-03
9.2455	72.7289	38.9860	1.9121	2.4744	1.53E-03
9.3583	73.4386	39.3665	1.9308	2.4985	1.55E-03
9.4710	74.1483	39.7469	1.9494	2.5226	1.56E-03
9.5838	74.8579	40.1273	1.9681	2.5468	1.58E-03
9.6965	75.5676	40.5078	1.9867	2.5709	1.59E-03
9.8093	76.2773	40.8882	2.0054	2.5951	1.61E-03
9.9220	76.9870	41.2686	2.0241	2.6192	1.62E-03
10.0348	77.6967	41.6490	2.0427	2.6434	1.64E-03
10.1475	78.4064	42.0295	2.0614	2.6675	1.65E-03
10.2603	79.1161	42.4099	2.0800	2.6917	1.67E-03
10.3730	79.8258	42.7903	2.0987	2.7158	1.68E-03
10.4858	80.5354	43.1707	2.1174	2.7400	1.70E-03
10.5985	81.2451	43.5512	2.1360	2.7641	1.71E-03
10.7113	81.9548	43.9316	2.1547	2.7882	1.73E-03
10.8240	82.6645	44.3120	2.1733	2.8124	1.74E-03
10.9368	83.3742	44.6924	2.1920	2.8365	1.76E-03
11.0495	84.0839	45.0729	2.2106	2.8607	1.77E-03
11.1623	84.7936	45.4533	2.2293	2.8848	1.79E-03
11.2750	85.5033	45.8337	2.2480	2.9090	1.80E-03

Table G.12 : Hydraulic Compressor Analysis - Standard Discharge Pipe (Continued)

h_i	$K_l * a_i$	$t_{RES,i}$	$C_{NC,i}$	n_i
0.0000	0.0090	0.0564	4.40E-05	1.3806E-02
0.1128	0.0094	0.0519	4.41E-05	1.3804E-02
0.2255	0.0098	0.0521	4.42E-05	1.3802E-02
0.3383	0.0103	0.0522	4.44E-05	1.3799E-02
0.4510	0.0107	0.0524	4.46E-05	1.3797E-02
0.5638	0.0112	0.0525	4.48E-05	1.3794E-02
0.6765	0.0116	0.0527	4.50E-05	1.3790E-02

0.7893	0.0120	0.0528	4.52E-05	1.3787E-02
0.9020	0.0125	0.0529	4.55E-05	1.3783E-02
1.0148	0.0129	0.0530	4.58E-05	1.3779E-02
1.1275	0.0134	0.0531	4.60E-05	1.3774E-02
1.2403	0.0138	0.0532	4.64E-05	1.3770E-02
1.3530	0.0142	0.0533	4.67E-05	1.3765E-02
1.4658	0.0147	0.0534	4.70E-05	1.3759E-02
1.5785	0.0151	0.0535	4.74E-05	1.3753E-02
1.6913	0.0156	0.0536	4.78E-05	1.3747E-02
1.8040	0.0160	0.0537	4.83E-05	1.3741E-02
1.9168	0.0164	0.0537	4.87E-05	1.3734E-02
2.0295	0.0169	0.0538	4.92E-05	1.3727E-02
2.1423	0.0173	0.0539	4.97E-05	1.3719E-02
2.2550	0.0178	0.0539	5.02E-05	1.3711E-02
2.3678	0.0182	0.0540	5.08E-05	1.3703E-02
2.4805	0.0186	0.0540	5.14E-05	1.3694E-02
2.5933	0.0191	0.0541	5.20E-05	1.3684E-02
2.7060	0.0195	0.0541	5.26E-05	1.3674E-02
2.8188	0.0200	0.0542	5.33E-05	1.3664E-02
2.9315	0.0204	0.0542	5.40E-05	1.3653E-02
3.0443	0.0208	0.0543	5.48E-05	1.3642E-02
3.1570	0.0213	0.0543	5.55E-05	1.3630E-02
3.2698	0.0217	0.0544	5.64E-05	1.3618E-02
3.3825	0.0222	0.0544	5.72E-05	1.3605E-02
3.4953	0.0226	0.0544	5.81E-05	1.3592E-02
3.6080	0.0230	0.0545	5.90E-05	1.3578E-02
3.7208	0.0235	0.0545	5.99E-05	1.3564E-02
3.8335	0.0239	0.0546	6.09E-05	1.3549E-02
3.9463	0.0244	0.0546	6.19E-05	1.3533E-02
4.0590	0.0248	0.0546	6.30E-05	1.3517E-02
4.1718	0.0252	0.0547	6.41E-05	1.3500E-02
4.2845	0.0257	0.0547	6.52E-05	1.3483E-02
4.3973	0.0261	0.0547	6.64E-05	1.3465E-02
4.5100	0.0266	0.0547	6.76E-05	1.3447E-02
4.6228	0.0270	0.0548	6.89E-05	1.3428E-02
4.7355	0.0274	0.0548	7.02E-05	1.3408E-02
4.8483	0.0279	0.0548	7.15E-05	1.3387E-02
4.9610	0.0283	0.0549	7.29E-05	1.3366E-02
5.0738	0.0288	0.0549	7.44E-05	1.3345E-02
5.1865	0.0292	0.0549	7.58E-05	1.3322E-02
5.2993	0.0296	0.0549	7.74E-05	1.3299E-02
5.4120	0.0301	0.0550	7.89E-05	1.3275E-02
5.5248	0.0305	0.0550	8.05E-05	1.3251E-02
5.6375	0.0310	0.0550	8.22E-05	1.3226E-02
5.7503	0.0314	0.0550	8.39E-05	1.3200E-02
5.8630	0.0318	0.0550	8.56E-05	1.3173E-02
5.9758	0.0323	0.0551	8.74E-05	1.3146E-02

6.0885	0.0327	0.0551	8.93E-05	1.3118E-02
6.2013	0.0332	0.0551	9.12E-05	1.3089E-02
6.3140	0.0336	0.0551	9.31E-05	1.3059E-02
6.4268	0.0340	0.0551	9.51E-05	1.3029E-02
6.5395	0.0383	0.0552	9.74E-05	1.2995E-02
6.6523	0.0443	0.0552	1.00E-04	1.2954E-02
6.7650	0.0502	0.0552	1.03E-04	1.2908E-02
6.8778	0.0562	0.0552	1.07E-04	1.2855E-02
6.9905	0.0621	0.0552	1.10E-04	1.2797E-02
7.1033	0.0681	0.0553	1.15E-04	1.2732E-02
7.2160	0.0740	0.0553	1.19E-04	1.2660E-02
7.3288	0.0800	0.0553	1.24E-04	1.2589E-02
7.4415	0.0859	0.0553	1.30E-04	1.2504E-02
7.5543	0.0919	0.0553	1.36E-04	1.2414E-02
7.6670	0.0978	0.0554	1.42E-04	1.2316E-02
7.7798	0.1037	0.0554	1.49E-04	1.2212E-02
7.8925	0.1097	0.0554	1.56E-04	1.2101E-02
8.0053	0.1156	0.0554	1.64E-04	1.1984E-02
8.1180	0.1216	0.0554	1.72E-04	1.1859E-02
8.2308	0.1275	0.0555	1.81E-04	1.1728E-02
8.3435	0.1335	0.0555	1.90E-04	1.1590E-02
8.4563	0.1394	0.0555	2.00E-04	1.1445E-02
8.5690	0.1454	0.0555	2.10E-04	1.1293E-02
8.6818	0.1513	0.0555	2.20E-04	1.1134E-02
8.7945	0.1573	0.0556	2.31E-04	1.0969E-02
8.9073	0.1632	0.0556	2.42E-04	1.0796E-02
9.0200	0.1692	0.0556	2.54E-04	1.0617E-02
9.1328	0.1751	0.0556	2.66E-04	1.0431E-02
9.2455	0.1811	0.0556	2.79E-04	1.0238E-02
9.3583	0.1870	0.0557	2.92E-04	1.0038E-02
9.4710	0.1930	0.0557	3.06E-04	9.8320E-03
9.5838	0.1989	0.0557	3.20E-04	9.6190E-03
9.6965	0.2049	0.0557	3.34E-04	9.3995E-03
9.8093	0.2108	0.0557	3.49E-04	9.1734E-03
9.9220	0.2168	0.0558	3.64E-04	8.9410E-03
10.0348	0.2227	0.0558	3.80E-04	8.7021E-03
10.1475	0.2287	0.0558	3.96E-04	8.4570E-03
10.2603	0.2346	0.0558	4.13E-04	8.2056E-03
10.3730	0.2406	0.0559	4.30E-04	7.9482E-03
10.4858	0.2465	0.0559	4.47E-04	7.6847E-03
10.5985	0.2525	0.0559	4.65E-04	7.4153E-03
10.7113	0.2584	0.0559	4.83E-04	7.1402E-03
10.8240	0.2644	0.0559	5.02E-04	6.8593E-03
10.9368	0.2703	0.0560	5.20E-04	6.5728E-03
11.0495	0.2762	0.0560	5.40E-04	6.2809E-03
11.1623	0.2822	0.0560	5.59E-04	5.9837E-03
11.2750	0.2881	0.0560	5.79E-04	5.6812E-03

Table G.12 : Hydraulic Compressor Analysis - Standard Discharge Pipe (Continued)

h_i	$Q_{NC,i}$	$A_{pipe,i}$	$X_{9,i}$	$H_{HC,i}$
0.0000	1.3306	6.9838	2.1737	1.54E-03
0.1128	1.2716	7.0088	2.1659	1.40E-03
0.2255	1.2176	7.0319	2.1588	1.29E-03
0.3383	1.1679	7.0533	2.1523	1.18E-03
0.4510	1.1221	7.0731	2.1463	1.09E-03
0.5638	1.0797	7.0915	2.1407	1.01E-03
0.6765	1.0404	7.1087	2.1355	9.36E-04
0.7893	1.0038	7.1248	2.1307	8.71E-04
0.9020	0.9697	7.1399	2.1262	8.12E-04
1.0148	0.9377	7.1540	2.1220	7.59E-04
1.1275	0.9078	7.1673	2.1180	7.11E-04
1.2403	0.8796	7.1799	2.1143	6.67E-04
1.3530	0.8532	7.1917	2.1109	6.27E-04
1.4658	0.8282	7.2030	2.1076	5.90E-04
1.5785	0.8046	7.2136	2.1045	5.56E-04
1.6913	0.7823	7.2237	2.1015	5.26E-04
1.8040	0.7612	7.2333	2.0987	4.97E-04
1.9168	0.7411	7.2424	2.0961	4.71E-04
2.0295	0.7220	7.2511	2.0936	4.47E-04
2.1423	0.7038	7.2594	2.0912	4.24E-04
2.2550	0.6865	7.2673	2.0889	4.03E-04
2.3678	0.6700	7.2749	2.0867	3.84E-04
2.4805	0.6542	7.2821	2.0847	3.65E-04
2.5933	0.6391	7.2891	2.0827	3.49E-04
2.7060	0.6246	7.2957	2.0808	3.33E-04
2.8188	0.6108	7.3021	2.0790	3.18E-04
2.9315	0.5975	7.3083	2.0772	3.04E-04
3.0443	0.5847	7.3142	2.0755	2.91E-04
3.1570	0.5724	7.3199	2.0739	2.78E-04
3.2698	0.5606	7.3254	2.0723	2.67E-04
3.3825	0.5493	7.3307	2.0709	2.56E-04
3.4953	0.5383	7.3358	2.0694	2.46E-04
3.6080	0.5277	7.3407	2.0680	2.36E-04
3.7208	0.5175	7.3455	2.0667	2.27E-04
3.8335	0.5076	7.3501	2.0654	2.18E-04
3.9463	0.4981	7.3546	2.0641	2.10E-04
4.0590	0.4889	7.3589	2.0629	2.02E-04
4.1718	0.4800	7.3631	2.0617	1.94E-04
4.2845	0.4713	7.3672	2.0606	1.87E-04

4.3973	0.4629	7.3712	2.0595	1.80E-04
4.5100	0.4548	7.3750	2.0584	1.74E-04
4.6228	0.4469	7.3787	2.0574	1.68E-04
4.7355	0.4392	7.3823	2.0564	1.62E-04
4.8483	0.4317	7.3859	2.0554	1.56E-04
4.9610	0.4245	7.3893	2.0544	1.51E-04
5.0738	0.4174	7.3926	2.0535	1.46E-04
5.1865	0.4106	7.3959	2.0526	1.41E-04
5.2993	0.4039	7.3991	2.0517	1.36E-04
5.4120	0.3974	7.4022	2.0509	1.32E-04
5.5248	0.3910	7.4052	2.0500	1.28E-04
5.6375	0.3849	7.4081	2.0492	1.23E-04
5.7503	0.3788	7.4110	2.0484	1.19E-04
5.8630	0.3729	7.4138	2.0476	1.16E-04
5.9758	0.3671	7.4166	2.0469	1.12E-04
6.0885	0.3615	7.4192	2.0461	1.09E-04
6.2013	0.3560	7.4219	2.0454	1.05E-04
6.3140	0.3506	7.4244	2.0447	1.02E-04
6.4268	0.3454	7.4270	2.0440	9.88E-05
6.5395	0.3401	7.4295	2.0433	9.57E-05
6.6523	0.3349	7.4320	2.0426	9.26E-05
6.7650	0.3296	7.4345	2.0419	8.96E-05
6.8778	0.3243	7.4371	2.0412	8.67E-05
6.9905	0.3189	7.4396	2.0405	8.37E-05
7.1033	0.3136	7.4422	2.0398	8.09E-05
7.2160	0.3082	7.4448	2.0391	7.80E-05
7.3288	0.3029	7.4473	2.0384	7.52E-05
7.4415	0.2974	7.4500	2.0377	7.25E-05
7.5543	0.2919	7.4526	2.0370	6.97E-05
7.6670	0.2864	7.4553	2.0362	6.70E-05
7.7798	0.2809	7.4579	2.0355	6.43E-05
7.8925	0.2753	7.4606	2.0348	6.17E-05
8.0053	0.2696	7.4634	2.0340	5.91E-05
8.1180	0.2640	7.4661	2.0333	5.65E-05
8.2308	0.2583	7.4688	2.0325	5.40E-05
8.3435	0.2526	7.4716	2.0318	5.15E-05
8.4563	0.2469	7.4744	2.0310	4.91E-05
8.5690	0.2411	7.4772	2.0303	4.68E-05
8.6818	0.2353	7.4800	2.0295	4.44E-05
8.7945	0.2295	7.4828	2.0288	4.21E-05
8.9073	0.2236	7.4857	2.0280	3.99E-05
9.0200	0.2177	7.4885	2.0272	3.77E-05
9.1328	0.2118	7.4914	2.0264	3.56E-05
9.2455	0.2059	7.4943	2.0256	3.35E-05
9.3583	0.2000	7.4972	2.0249	3.15E-05
9.4710	0.1940	7.5001	2.0241	2.96E-05
9.5838	0.1880	7.5030	2.0233	2.77E-05

9.6965	0.1820	7.5059	2.0225	2.58E-05
9.8093	0.1760	7.5089	2.0217	2.40E-05
9.9220	0.1700	7.5118	2.0209	2.23E-05
10.0348	0.1639	7.5148	2.0201	2.07E-05
10.1475	0.1579	7.5177	2.0193	1.90E-05
10.2603	0.1518	7.5207	2.0185	1.75E-05
10.3730	0.1458	7.5237	2.0177	1.60E-05
10.4858	0.1397	7.5266	2.0169	1.46E-05
10.5985	0.1337	7.5296	2.0161	1.33E-05
10.7113	0.1276	7.5326	2.0153	1.20E-05
10.8240	0.1215	7.5356	2.0145	1.08E-05
10.9368	0.1155	7.5386	2.0137	9.63E-06
11.0495	0.1094	7.5416	2.0129	8.55E-06
11.1623	0.1034	7.5445	2.0122	7.53E-06
11.2750	0.0974	7.5475	2.0114	6.58E-06

This procedure is repeated until the length of the hydraulic compressor determined yields a final seawater velocity ($X_{9,end}$) at the end of the hydraulic compression region within ± 0.01% of the design seawater flow (X_9).

The total head loss ($H_{HC,tot}$) for this hydraulic compressor design is simply

$$H_{HC,tot} = \sum_{i=1}^{100} H_{HC,i} = 0.026\,M \qquad \text{(G-271)}$$

which corresponds to a total pressure loss (ΔP_{HC}) of

$$\Delta P_{HC} = H_{HC,tot}\,\rho_9\,G = 262.40\ Pa. \qquad \text{(G-272)}$$

G.4.6.2 HYDRAULIC COMPRESSOR - TAPERING PIPE ANALYSIS

The tapering pipe hydraulic compressor analysis follows a similar procedure as that just described for the standard pipe hydraulic compressor. The principal difference between design procedures is that the tapering pipe is designed assuming a constant seawater velocity (X_9 = 2.00 M/S) with the pipe diameter changing to account for the reduction in volume of the noncondensables being compressed and reabsorbed along the compression region. The associated head loss (pressure drop) associated with the injection of the noncondensables into the tapering downcomer is simply the frictional pressure loss for the downcomer pipe. Although the necessary length of the tapering hydraulic compressor pipe will be the same as that for the standard pipe analysis (compression and reabsorption rates will be the same in both compression systems), it is still necessary for an iterative process to be performed along the compression pipe because the tapering effect will alter the friction factor along the varying diameter of the pipe. Therefore, the analysis entails iterating along the compressor length (100 iterations) and averaging the frictional factor for the corresponding tapering pipe length. The following analytical equations are utilized to obtain the values presented in the ensuing tables (G.13)

ρ_9 = seawater density in compressor = 1024.6 KG/M^3

ν_9 = kinematic viscosity of seawater in compressor

= 1.34 x 10^{-6} M^2/S

ε_9 = pipe roughness = 0.000046 (M) [32]

$t_{res,i}$ = residence time in segment i

$$= \Delta h_i / X_9 = 0.0564 \ S \qquad \text{(G-273)}$$

$A_{i,pipe}$ = average area of pipe for segment i

$$= A_{9,pipe} + [Q_{NC,i} / (Q_{NC,i} + Q_9)] A_{9,pipe} \quad (M^2) \qquad \text{(G-274)}$$

$D_{i,pipe}$ = average diameter of pipe for segment i

$$= (4 A_{i,pipe} / \pi)^{1/2} \quad (M) \qquad \text{(G-275)}$$

Re_i = Reynolds number for segment i

$$= X_3 D_{i,pipe} / \nu_3 \qquad \text{(G-276)}$$

f_i = friction factor of pipe in segment i (iterative)

$$= \{-2 \log [(\varepsilon_9 / 3.7 D_{i,pipe}) + 2.51 / (Re_i \sqrt{f_i})]\}^{-2} \qquad \text{(G-277)}$$

ΔP_{fi} = frictional pressure drop along pipe length i

$$= f_i (\Delta h_i / D_{i,pipe}) \rho_9 X_9^2 / 2 \quad (Pa) \qquad \text{(G-278)}$$

Since the rate of compression and reabsorption along this hydraulic compressor directly corresponds to that of the standard pipe calculations above, many of the values (specifically those related to noncondensable concentrations, molar flows and volumetric flows) are identical and are omitted in the following tables which present the values unique to the tapering hydraulic compressor analysis.

Table G.13 : Hydraulic Compressor Analysis - Tapering Discharge Pipe

h_i	$A_{pipe,i}$	$D_{i,pipe}$	Re_i
0.0000	8.2081	3.2328	4.8338E+06
0.1128	8.1830	3.2278	4.8264E+06
0.2255	8.1599	3.2233	4.8196E+06
0.3383	8.1386	3.2191	4.8133E+06
0.4510	8.1187	3.2151	4.8074E+06

0.5638	8.1003	3.2115	4.8019E+06
0.6765	8.0831	3.2081	4.7968E+06
0.7893	8.0670	3.2049	4.7921E+06
0.9020	8.0520	3.2019	4.7876E+06
1.0148	8.0378	3.1991	4.7834E+06
1.1275	8.0245	3.1964	4.7794E+06
1.2403	8.0120	3.1939	4.7757E+06
1.3530	8.0001	3.1916	4.7722E+06
1.4658	7.9889	3.1893	4.7688E+06
1.5785	7.9783	3.1872	4.7656E+06
1.6913	7.9682	3.1852	4.7626E+06
1.8040	7.9586	3.1833	4.7598E+06
1.9168	7.9495	3.1814	4.7570E+06
2.0295	7.9408	3.1797	4.7544E+06
2.1423	7.9325	3.1780	4.7519E+06
2.2550	7.9246	3.1765	4.7496E+06
2.3678	7.9170	3.1749	4.7473E+06
2.4805	7.9097	3.1735	4.7451E+06
2.5933	7.9028	3.1721	4.7430E+06
2.7060	7.8961	3.1707	4.7410E+06
2.8188	7.8897	3.1695	4.7391E+06
2.9315	7.8836	3.1682	4.7373E+06
3.0443	7.8776	3.1670	4.7355E+06
3.1570	7.8719	3.1659	4.7338E+06
3.2698	7.8665	3.1648	4.7321E+06
3.3825	7.8612	3.1637	4.7305E+06
3.4953	7.8560	3.1627	4.7290E+06
3.6080	7.8511	3.1617	4.7275E+06
3.7208	7.8463	3.1607	4.7261E+06
3.8335	7.8417	3.1598	4.7247E+06
3.9463	7.8372	3.1589	4.7233E+06
4.0590	7.8329	3.1580	4.7220E+06
4.1718	7.8287	3.1572	4.7208E+06
4.2845	7.8246	3.1564	4.7195E+06
4.3973	7.8207	3.1556	4.7183E+06
4.5100	7.8169	3.1548	4.7172E+06
4.6228	7.8131	3.1540	4.7161E+06
4.7355	7.8095	3.1533	4.7150E+06
4.8483	7.8060	3.1526	4.7139E+06
4.9610	7.8025	3.1519	4.7129E+06
5.0738	7.7992	3.1512	4.7119E+06
5.1865	7.7960	3.1506	4.7109E+06
5.2993	7.7928	3.1499	4.7099E+06
5.4120	7.7897	3.1493	4.7090E+06
5.5248	7.7867	3.1487	4.7081E+06
5.6375	7.7837	3.1481	4.7072E+06
5.7503	7.7809	3.1475	4.7063E+06

5.8630	7.7780	3.1469	4.7055E+06
5.9758	7.7753	3.1464	4.7046E+06
6.0885	7.7726	3.1458	4.7038E+06
6.2013	7.7700	3.1453	4.7030E+06
6.3140	7.7674	3.1448	4.7022E+06
6.4268	7.7649	3.1443	4.7015E+06
6.5395	7.7624	3.1438	4.7007E+06
6.6523	7.7599	3.1433	4.7000E+06
6.7650	7.7573	3.1428	4.6992E+06
6.8778	7.7548	3.1422	4.6984E+06
6.9905	7.7522	3.1417	4.6976E+06
7.1033	7.7496	3.1412	4.6969E+06
7.2160	7.7470	3.1407	4.6961E+06
7.3288	7.7445	3.1402	4.6953E+06
7.4415	7.7419	3.1396	4.6945E+06
7.5543	7.7392	3.1391	4.6937E+06
7.6670	7.7366	3.1385	4.6929E+06
7.7798	7.7339	3.1380	4.6921E+06
7.8925	7.7312	3.1375	4.6913E+06
8.0053	7.7285	3.1369	4.6904E+06
8.1180	7.7258	3.1364	4.6896E+06
8.2308	7.7230	3.1358	4.6888E+06
8.3435	7.7202	3.1352	4.6879E+06
8.4563	7.7175	3.1347	4.6871E+06
8.5690	7.7147	3.1341	4.6862E+06
8.6818	7.7119	3.1335	4.6854E+06
8.7945	7.7090	3.1330	4.6845E+06
8.9073	7.7062	3.1324	4.6837E+06
9.0200	7.7033	3.1318	4.6828E+06
9.1328	7.7005	3.1312	4.6819E+06
9.2455	7.6976	3.1306	4.6811E+06
9.3583	7.6947	3.1300	4.6802E+06
9.4710	7.6918	3.1294	4.6793E+06
9.5838	7.6889	3.1289	4.6784E+06
9.6965	7.6859	3.1283	4.6775E+06
9.8093	7.6830	3.1277	4.6766E+06
9.9220	7.6800	3.1271	4.6757E+06
10.0348	7.6771	3.1265	4.6748E+06
10.1475	7.6741	3.1259	4.6739E+06
10.2603	7.6712	3.1253	4.6730E+06
10.3730	7.6682	3.1246	4.6721E+06
10.4858	7.6652	3.1240	4.6712E+06
10.5985	7.6622	3.1234	4.6703E+06
10.7113	7.6592	3.1228	4.6694E+06
10.8240	7.6563	3.1222	4.6685E+06
10.9368	7.6533	3.1216	4.6676E+06
11.0495	7.6503	3.1210	4.6667E+06

11.1623	7.6473	3.1204	4.6657E+06
11.2750	7.6443	3.1198	4.6648E+06

Table G.13 : Hydraulic Compressor Analysis - Tapering Discharge Pipe (Continued)

h_i	$f_{i,guess}$	f_i	ΔP_{fi}
0.0000	0.009835	0.009835	0.7029
0.1128	0.009837	0.009837	0.7042
0.2255	0.009839	0.009840	0.7053
0.3383	0.009842	0.009842	0.7064
0.4510	0.009844	0.009844	0.7074
0.5638	0.009845	0.009845	0.7083
0.6765	0.009847	0.009847	0.7092
0.7893	0.009849	0.009849	0.7100
0.9020	0.009850	0.009850	0.7108
1.0148	0.009852	0.009852	0.7115
1.1275	0.009853	0.009853	0.7122
1.2403	0.009854	0.009854	0.7129
1.3530	0.009855	0.009856	0.7135
1.4658	0.009857	0.009857	0.7141
1.5785	0.009858	0.009858	0.7146
1.6913	0.009859	0.009859	0.7151
1.8040	0.009860	0.009860	0.7156
1.9168	0.009861	0.009861	0.7161
2.0295	0.009862	0.009862	0.7166
2.1423	0.009862	0.009862	0.7170
2.2550	0.009863	0.009863	0.7174
2.3678	0.009864	0.009864	0.7178
2.4805	0.009865	0.009865	0.7182
2.5933	0.009865	0.009865	0.7186
2.7060	0.009866	0.009866	0.7189
2.8188	0.009867	0.009867	0.7193
2.9315	0.009867	0.009867	0.7196
3.0443	0.009868	0.009868	0.7199
3.1570	0.009869	0.009869	0.7202
3.2698	0.009869	0.009869	0.7205
3.3825	0.009870	0.009870	0.7208
3.4953	0.009870	0.009870	0.7211
3.6080	0.009871	0.009871	0.7213
3.7208	0.009871	0.009871	0.7216
3.8335	0.009872	0.009872	0.7218

3.9463	0.009872	0.009872	0.7221
4.0590	0.009873	0.009873	0.7223
4.1718	0.009873	0.009873	0.7225
4.2845	0.009873	0.009874	0.7228
4.3973	0.009874	0.009874	0.7230
4.5100	0.009874	0.009874	0.7232
4.6228	0.009875	0.009875	0.7234
4.7355	0.009875	0.009875	0.7236
4.8483	0.009875	0.009875	0.7238
4.9610	0.009876	0.009876	0.7239
5.0738	0.009876	0.009876	0.7241
5.1865	0.009876	0.009876	0.7243
5.2993	0.009877	0.009877	0.7245
5.4120	0.009877	0.009877	0.7246
5.5248	0.009877	0.009877	0.7248
5.6375	0.009878	0.009878	0.7250
5.7503	0.009878	0.009878	0.7251
5.8630	0.009878	0.009878	0.7253
5.9758	0.009879	0.009879	0.7254
6.0885	0.009879	0.009879	0.7256
6.2013	0.009879	0.009879	0.7257
6.3140	0.009879	0.009879	0.7259
6.4268	0.009880	0.009880	0.7260
6.5395	0.009880	0.009880	0.7261
6.6523	0.009880	0.009880	0.7263
6.7650	0.009880	0.009881	0.7264
6.8778	0.009881	0.009881	0.7265
6.9905	0.009881	0.009881	0.7267
7.1033	0.009881	0.009881	0.7268
7.2160	0.009882	0.009882	0.7270
7.3288	0.009882	0.009882	0.7271
7.4415	0.009882	0.009882	0.7272
7.5543	0.009882	0.009882	0.7274
7.6670	0.009883	0.009883	0.7275
7.7798	0.009883	0.009883	0.7277
7.8925	0.009883	0.009883	0.7278
8.0053	0.009884	0.009884	0.7280
8.1180	0.009884	0.009884	0.7281
8.2308	0.009884	0.009884	0.7283
8.3435	0.009884	0.009884	0.7284
8.4563	0.009885	0.009885	0.7286
8.5690	0.009885	0.009885	0.7287
8.6818	0.009885	0.009885	0.7289
8.7945	0.009886	0.009886	0.7290
8.9073	0.009886	0.009886	0.7292
9.0200	0.009886	0.009886	0.7294
9.1328	0.009886	0.009887	0.7295

9.2455	0.009887	0.009887	0.7297
9.3583	0.009887	0.009887	0.7298
9.4710	0.009887	0.009887	0.7300
9.5838	0.009888	0.009888	0.7302
9.6965	0.009888	0.009888	0.7303
9.8093	0.009888	0.009888	0.7305
9.9220	0.009889	0.009889	0.7306
10.0348	0.009889	0.009889	0.7308
10.1475	0.009889	0.009889	0.7310
10.2603	0.009890	0.009890	0.7311
10.3730	0.009890	0.009890	0.7313
10.4858	0.009890	0.009890	0.7315
10.5985	0.009891	0.009891	0.7316
10.7113	0.009891	0.009891	0.7318
10.8240	0.009891	0.009891	0.7320
10.9368	0.009891	0.009892	0.7321
11.0495	0.009892	0.009892	0.7323
11.1623	0.009892	0.009892	0.7325
11.2750	0.009892	0.009892	0.7326

The total pressure loss (ΔP_{HC}) for this hydraulic compressor design is simply

$$\Delta P_{HC} = \sum_{i=1}^{100} \Delta P_{HC,i} = 73.04 \text{ Pa.} \qquad \text{(G-279)}$$

G.5 SEAWATER FLOW SYSTEM

The following analysis determines the expected head loss accompanying the OC-OTEC design outlined in this investigation which includes predeaeration and reinjection of the noncondensables. The design head losses will be utilized in the subsequent seawater pump design. These head losses are determined utilizing standard engineering practice for estimating frictional losses along the intake and discharge pipes, entrance and exit losses, hydrostatic head losses, density differences between the seawater intake and

discharge and minor losses attributable to bends in the piping system. For ease in design and comprehension of procedures, the warm water loop and the cold water loop have been investigated separately in this section.

The following values are utilized for both the warm and cold water flow system designs in the ensuing analysis and are presented here to simplify the calculation descriptions.

G = gravitation constant = 9.81 M/S^2 [46]

K_{bend} = pipe bend head loss coefficient = 0.16 [32]

K_{dis} = discharge loss coefficient = 1.0 [32]

K_{ent} = entrance loss coefficient = 0.78 [32]

ε_{pipe} = pipe roughness = 0.000046 M [32]

$\rho_{\#}$ = seawater density at seawater temperature associated with path #

$\mu_{\#}$ = seawater absolute viscosity at seawater temperature associated with path #

$\nu_{\#}$ = seawater kinematic viscosity = $\mu_{\#} / \rho_{\#}$

$Re_{\#}$ = Reynolds number for flow path # = $X_{\#} D_{\#,pipe} / \nu_{\#}$

The friction factors ($f_{\#}$) for the respective piping systems are determined as prescribed by Parsons et al. [32] by iteratively solving the following equation

$$f_{\#} = \{-2 \log [(\varepsilon_{pipe} / 3.7 D_{\#,pipe}) + 2.51 / (Re_{\#} \sqrt{f_{\#}})]\}^{-2} \qquad \text{(G-280)}$$

developed to approximate the Moody diagram.

G.5.1 WARM WATER FLOW SYSTEM

The following values are exclusive to the warm water flow system and are assumed for usage in the ensuing analysis.

$N_{2,bend}$ = number of bends in warm water intake pipe = 10 [32]

$N_{3,bend}$ = number of bends in warm water discharge pipe = 10 [32]

$L_{2,pipe}$ = warm water intake pipe length = 500 M [32]

$L_{3,pipe}$ = warm water discharge pipe length = 650 M [32]

$D_{spt,E}$ = spout diameter in evaporator = 0.127 M [32]

$L_{spt,E}$ = spout length in evaporator = 2.70 M [32]

$H_{spt,E}$ = spout height above water level in evaporator = 0.50 M [32]

The seawater flow velocity ($X_{\#}$) in the piping system has been set throughout this design at

$$X_2 = X_{spt} = X_3 = 2.00 \text{ M/S}$$

which permits the determination of the intake pipe diameter ($D_{2,pipe}$) and the discharge pipe diameter ($D_{3,pipe}$) as

$$D_{2,pipe} = [(4\ m_2) / (\pi\ \rho_2\ X_2\ N_{2,pipes})]^{1/2} = 4.02 \text{ M} \qquad \text{(G-281)}$$

$$D_{3,pipe} = [(4\ m_3) / \pi\ \rho_3\ X_3\ N_{3,pipe})]^{1/2} = 4.02 \text{ M} \qquad \text{(G-282)}$$

with the knowledge of the design warm water mass flow ($m_2 = m_3$) determined in the evaporator analysis, the inlet and outlet seawater density (ρ_2 and ρ_3, respectively) and the design number of intake and discharge pipes ($N_{2,pipes} = 1 = N_{3,pipes}$).

The warm water flow system is now dissected into three separate analyses which will be summed at the end of this section to describe the total

head loss through the warm water flow system. The values utilized for the determination of the head losses are presented and are developed as discussed previously in this report.

Warm Water Intake Pipe Head Losses:

$T_2 = 27.00\ ^{\circ}C$

$\mu_2 = 0.00092$ KG/M-S

$\nu_2 = 9.018 \times 10^{-7}$ M^2/S

$\rho_2 = 1021.6$ KG/M^3

$Re_2 = 8918306$

$f_2 = 0.00918$ (friction factor after iteration)

$\Delta P_{2,f}$ = frictional pressure drop of intake pipe

$= f_2 (L_{2,pipe} / D_{2,pipe}) \rho_2 X_2^2 / 2 = 2331.1$ Pa (G-283)

$\Delta P_{2,ent}$ = pressure drop due to entrance losses

$= K_{ent} \rho_2 X_2^2 / 2 = 1593.7$ Pa (G-284)

$\Delta P_{2,bend}$ = pressure drop due to losses at bends

$= K_{bend} N_{2,bend} \rho_2 X_2^2 / 2 = 3269.2$ Pa (G-285)

$\Delta P_{pre,exp}$ = pressure drop due to flow expansion into predeaerator

$= (X_2^2 / 2G) (1 - D_{2,pipe}^2 / D_{pre,E}^2) (\rho_2 G) = 1982.3$ Pa [14] (G-286)

$\Delta P_{2,tot}$ = total pressure drop in intake pipe

$= \Delta P_{2,f} + \Delta P_{2,ent} + \Delta P_{2,bend} + \Delta P_{pre,exp} = 9176.3$ Pa. (G-287)

Evaporator Head Losses:

$T_{E,ave} = 25.23\ ^{\circ}C$ = average evaporator temperature

$\mu_E = 0.00096$ KG/M-S

$\nu_E = 9.37 \times 10^{-7}$ M^2/S

ρ_E = 1022.1 KG/M^3

Re_E = 271104

f_E = 0.0175 (friction factor after iteration)

$\Delta P_{E,f}$ = frictional pressure drop of evaporator spouts

$$= f_E (L_{spt,E} / D_{spt,E}) \rho_E X_E^2 / 2 = 762.3 \text{ Pa} \quad \text{(G-288)}$$

$\Delta P_{E,ent}$ = pressure drop due to entrance losses

$$= K_{ent} \rho_E X_E^2 / 2 = 1594.4 \text{ Pa} \quad \text{(G-289)}$$

$\Delta P_{E,dis}$ = pressure drop due to losses at spout discharge

$$= K_{dis} \rho_E X_E^2 / 2 = 2044.2 \text{ Pa} \quad \text{(G-290)}$$

$\Delta P_{E,spt,H}$ = pressure drop due to spout height above water level

$$= H_{spt,E} \rho_E G = 5011.6 \text{ Pa} \quad \text{(G-291)}$$

$\Delta P_{E,tot}$ = total pressure drop in evaporator

$$= \Delta P_{E,f} + \Delta P_{E,ent} + \Delta P_{E,dis} + \Delta P_{E,spt,H} = 9412.5 \text{ Pa.} \quad \text{(G-292)}$$

Warm Water Discharge Pipe - Hydraulic Compressor:

T_3 = 23.46 °C

μ_3 = 0.00100 KG/M-S

ν_3 = 9.75 x 10^{-7} M^2/S

ρ_3 = 1022.5 KG/M^3

Re_3 = 8249872

f_3 = 0.00923 (friction factor after iteration)

Standard Pipe Analysis:

$X_{3,ave}$ = average seawater velocity along hydraulic compression region

$$= \sum X_{3,i} / 100 = 2.06 \text{ M/S} \quad \text{(G-293)}$$

$\Delta P_{3,f}$ = frictional pressure drop of discharge pipe

$= f_3 (L_{3,pipe}) / D_{3,pipe}) \rho_3 X_{3,ave}^2 / 2 = 3226.7 Pa$ (G-294)

$\Delta P_{3,bend}$ = pressure drop due to losses at bends

$= K_{bend} N_{3,bend} \rho_3 X_3^2 /2 = 3272.0$ Pa (G-295)

$\Delta P_{HC} = 98.8$ Pa

$\Delta P_{3,tot}$ = total pressure drop in discharge pipe

$= \Delta P_{3,f} + \Delta P_{3,bend} + \Delta P_{HC} = 6597.5$ Pa. (G-296)

Tapering Pipe Analysis:

$\Delta P_{3,f}$ = frictional pressure drop of discharge pipe

(excluding hydraulic compression region)

$= f_3 (L_{3,pipe} - h_{HC}) / D_{3,pipe}) \rho_3 X_3^2 / 2 = 2993.1$ Pa (G-297)

$\Delta P_{3,bend}$ = pressure drop due to losses at bends

$= K_{bend} N_{3,bend} \rho_3 X_3^2 /2 = 3272.0$ Pa (G-298)

$\Delta P_{HC} = 59.1$ Pa

$\Delta P_{3,tot}$ = total pressure drop in discharge pipe

$= \Delta P_{3,f} + \Delta P_{3,bend} + \Delta P_{HC} = 6324.2$ Pa. (G-299)

The only remaining head loss to be determined is that associated with the density differences between the warm water intake and the warm water discharge. This density difference is going to prove site specific and is impossible to determine exactly without a detailed salinity and temperature profile available for the specific OC-OTEC design location. Since the designation of a particular location for design applications is beyond the scope of this work, the values obtained in the 100 MW OC-OTEC Westinghouse [49]

design which determined a 0.05 M head loss for the warm water loop with an intake depth of 30 M and a discharge depth of 100 M will be utilized in this investigation as a good approximation for typical OC-OTEC salinity and temperature profiles. Therefore, the necessary head for overcoming this density difference yields a corresponding pressure loss of

$$HD_{2\text{-}3,density} = 0.05 \text{ M}$$

$$\Delta P_{2\text{-}3,density} = HD_{2\text{-}3,density}\, \rho_{2\text{-}3,ave}\, G = 501.2 \text{ Pa} \qquad \text{(G-300)}$$

where

$\rho_{2\text{-}3,ave}$ = average density of seawater from path 2 to path 3.

The total head loss ($HD_{tot,ww}$) for the warm seawater loop with a standard downcomer is

$$\Delta P_{tot,ww} = \Delta P_{2,tot} + \Delta P_{E,tot} + \Delta P_{3,tot} + \Delta P_{2\text{-}3,density} = 25687.5 \text{ Pa} \qquad \text{(G-301)}$$

$$HD_{tot,ww} = \Delta P_{tot,ww} / (\rho_{2\text{-}3,ave}\, G) = 2.56 \text{ M.} \qquad \text{(G-302)}$$

The total head loss ($HD_{tot,ww,TP}$) for the warm seawater loop with a tapering pipe downcomer is

$$\Delta P_{tot,ww,TP} = \Delta P_{2,tot} + \Delta P_{E,tot} + \Delta P_{3,tot} + \Delta P_{2\text{-}3,density} = 25414.1 \text{ Pa} \qquad \text{(G-303)}$$

$$HD_{tot,ww,TP} = \Delta P_{tot,ww,TP} / (\rho_{2\text{-}3,ave}\, G) = 2.54 \text{ M.} \qquad \text{(G-304)}$$

G.5.2 COLD WATER FLOW SYSTEM

The following values are exclusive to the cold water flow system and are assumed for usage in the ensuing analysis.

$N_{11,bend}$ = number of bends in cold water intake pipe = 10 [32]

$N_{9,bend}$ = number of bends in cold water discharge pipe = 10 [32]

$L_{11,pipe}$ = cold water intake pipe length = 2750 M [32]

$L_{9,pipe}$ = cold water discharge pipe length = 650 M [32]

$D_{cont,DCC}$ = contactor diameter in D.C.C. = 0.127 M [32]

$L_{cont,DCC}$ = contactor length in D.C.C. = 1.457 M [32]

$H_{cont,DCC}$ = contactor height above water level in D.C.C. = 0.457 M [32]

The seawater flow velocity ($X_{\#}$) in the piping system has been set throughout this design at

$$X_{11} = X_{cont} = X_9 = 2.00 \text{ M/S}$$

which permits the determination of the intake pipe diameter ($D_{11,pipe}$) and the discharge pipe diameter ($D_{9,pipe}$) as

$$D_{11,pipe} = [(4\, m_{11}) / (\pi\, \rho_{11}\, X_{11}\, N_{11,pipes})]^{1/2} = 3.11 \text{ M} \qquad \text{(G-305)}$$

$$D_{9,pipe} = [(4\, m_9) / \pi\, \rho_9\, X_9\, N_{9,pipe})]^{1/2} = 3.11 \text{ M} \qquad \text{(G-306)}$$

with the knowledge of the design cold water mass flow ($m_{11} = m_9$) determined in the condenser analysis, the inlet and outlet seawater density (ρ_{11} and ρ_9, respectively) and the design number of intake and discharge pipes ($N_{11,pipes} = 1 = N_{9,pipes}$).

The cold water flow system is now dissected into three separate analyses which will be summed at the end of this section to describe the total head loss through the cold water flow system. The values utilized for the determination of the head losses are presented and are developed as discussed previously in this report.

Cold Water Intake Pipe Head Losses:

$$T_{11} = 5.00\ ^{\circ}\text{C}$$

$$\mu_{11} = 0.00162 \text{ KG/M-S}$$

$$\nu_{11} = 1.58 \times 10^{-6} \text{ M}^2\text{/S}$$

ρ_{11} = 1025.4 KG/M^3

Re_{11} = 4008451

f_{11} = 0.0101 (friction factor after iteration)

$\Delta P_{11,f}$ = frictional pressure drop of intake pipe

= f_{11} ($L_{11,pipe}$ / $D_{11,pipe}$) ρ_{11} X_{11}^2 / 2 = 18252.5 Pa (G-307)

$\Delta P_{11,ent}$ = pressure drop due to entrance losses

= K_{ent} ρ_{11} X_{11}^2 / 2 = 1599.6 Pa (G-308)

$\Delta P_{11,bend}$ = pressure drop due to losses at bends

= K_{bend} $N_{11,bend}$ ρ_{11} X_{11}^2 /2 = 3281.2 Pa (G-309)

$\Delta P_{pre,exp}$ = pressure drop due to flow expansion into predeaerator

= (X_{11}^2/ 2G) (1 - $D_{11,pipe}^2$/ $D_{pre,DCC}^2$) (ρ_{11} G) = 1989.5 Pa [14] (G-310)

$\Delta P_{11,tot}$ = total pressure drop in intake pipe

= $\Delta P_{11,f}$ + $\Delta P_{11,ent}$ + $\Delta P_{11,bend}$ + $\Delta P_{pre,exp}$ = 25122.7 Pa. (G-311)

Direct-Contact Condenser Head Losses:

$T_{DCC,ave}$ = 7.92 °C = average condenser temperature

μ_{DCC} = 0.00149 KG/M-S

ν_{DCC} = 1.45 x 10^{-6} M^2/S

ρ_{DCC} = 1025.0 KG/M^3

Re_{DCC} = 174947

f_{DCC} = 0.0184 (friction factor after iteration)

$\Delta P_{DCC,f}$ = frictional pressure drop of condenser contactors

= f_{DCC} ($L_{cont,DCC}$ / $D_{cont,DCC}$) ρ_{DCC} X_{DCC}^2 / 2 = 431.6 Pa (G-312)

$\Delta P_{DCC,ent}$ = pressure drop due to entrance losses

$$= K_{ent}\,\rho_{DCC}\,X_{DCC}^2/2 = 1599.0 \text{ Pa} \quad \text{(G-313)}$$

$\Delta P_{DCC,dis}$ = pressure drop due to losses at contactor discharge

$$= K_{dis}\,\rho_{DCC}\,X_{DCC}^2/2 = 2045.0 \text{ Pa} \quad \text{(G-314)}$$

$\Delta P_{DCC,cont,H}$ = pressure drop due to contactor height above water level

$$= H_{cont,DCC}\,\rho_{DCC}\,G = 4593.6 \text{ Pa} \quad \text{(G-315)}$$

$\Delta P_{DCC,tot}$ = total pressure drop in direct-contact condenser

$$= \Delta P_{DCC,f} + \Delta P_{DCC,ent} + \Delta P_{DCC,dis} + \Delta P_{DCC,cont,H} = 8674.2 \text{ Pa.} \quad \text{(G-316)}$$

Cold Water Discharge Pipe:

$T_9 = 10.84\ ^{\circ}C$

$\mu_9 = 0.0014$ KG/M-S

$\nu_9 = 1.34 \times 10^{-6}$ M^2/S

$\rho_9 = 1024.6$ KG/M^3

$Re_9 = 4650043$

$f_9 = 0.0099$ (friction factor after iteration)

Standard Pipe Analysis:

$X_{9,ave}$ = average seawater velocity along hydraulic compression region

$$= \sum X_{9,i}/100 = 2.08 \text{ M/S} \quad \text{(G-317)}$$

$\Delta P_{9,f}$ = frictional pressure drop of discharge pipe

$$= f_9\,(L_{9,pipe})/D_{3,pipe})\,\rho_9\,X_{9,ave}^2/2 = 4588.5 \text{ Pa} \quad \text{(G-318)}$$

$\Delta P_{9,bend}$ = pressure drop due to losses at bends

$$= K_{bend}\,N_{9,bend}\,\rho_9\,X_9^2/2 = 3278.8 \text{ Pa} \quad \text{(G-319)}$$

$\Delta P_{HC} = 262.4$ Pa

$\Delta P_{9,tot}$ = total pressure drop in discharge pipe

$$= \Delta P_{9,f} + \Delta P_{9,bend} + \Delta P_{HC} = 8129.7 \text{ Pa.} \quad \text{(G-320)}$$

Tapering Pipe Analysis:

$\Delta P_{9,f}$ = frictional pressure drop of discharge pipe

(excluding hydraulic compression region)

$$= f_9 (L_{9,pipe} - h_{HC}) / D_{9,pipe}) \rho_9 X_9^2 / 2 = 4166.7 \text{ Pa} \quad \text{(G-321)}$$

$\Delta P_{9,bend}$ = pressure drop due to losses at bends

$$= K_{bend} N_{9,bend} \rho_9 X_9^2 / 2 = 3278.8 \text{ Pa} \quad \text{(G-322)}$$

ΔP_{HC} = 73.0 Pa

$\Delta P_{9,tot}$ = total pressure drop in discharge pipe

$$= \Delta P_{9,f} + \Delta P_{9,bend} + \Delta P_{HC} = 7518.5 \text{ Pa.} \quad \text{(G-323)}$$

The only remaining head loss to be determined is that associated with the density differences between the cold water intake and the cold water discharge. This density difference is going to prove site specific (as discussed previously in the warm water flow system analysis) and is impossible to determine exactly without a detailed salinity and temperature profile available for the specific OC-OTEC design location. Once again the values obtained in the 100 MW OC-OTEC Westinghouse [49] design which determined a 0.45 M head loss for the cold water loop with an intake depth of 940 M and a discharge depth of 100 M will be utilized in this investigation as a good approximation for typical OC-OTEC salinity and temperature profiles. Therefore, the necessary head for overcoming this density difference yields a corresponding pressure loss of

$$HD_{11\text{-}9,density} = 0.45 \text{ M}$$

$$\Delta P_{11\text{-}9,density} = HD_{11\text{-}9,density}\,\rho_{11\text{-}9,ave}\,G = 4221.7\ Pa \quad (G\text{-}324)$$

where

$\rho_{11\text{-}9,ave}$ = average density of seawater from path 11 to path 9.

The total head loss ($HD_{tot,cw}$) for the cold seawater loop with a standard downcomer is

$$\Delta P_{tot,cw} = \Delta P_{11,tot} + \Delta P_{DCC,tot} + \Delta P_{9,tot} + \Delta P_{11\text{-}9,density}$$

$$= 46148.2\ Pa \quad (G\text{-}325)$$

$$HD_{tot,cw} = \Delta P_{tot,cw} / (\rho_{11\text{-}9,ave}\,G) = 4.59\ M. \quad (G\text{-}326)$$

The total head loss ($HD_{tot,ww,TP}$) for the cold seawater loop with a tapering pipe downcomer is

$$\Delta P_{tot,cw,TP} = \Delta P_{11,tot} + \Delta P_{DCC,tot} + \Delta P_{9,tot} + \Delta P_{11\text{-}9,density}$$

$$= 45537.1\ Pa \quad (G\text{-}327)$$

$$HD_{tot,cw,TP} = \Delta P_{tot,cw,TP} / (\rho_{11\text{-}9,ave}\,G) = 4.53\ M. \quad (G\text{-}328)$$

G.7 SEAWATER PUMP ANALYSIS

The seawater pump analyses begin by defining the three dimensionless parameters utilized to characterize an axial flow pump at the optimum performance level indicated by Figure 4.11 earlier in this report as

$$C_q = Q_{pump} / (n\,D^3) = 0.068 \quad (G\text{-}329)$$

$$C_h = G\,HD / (n^2\,D_3) = 0.017 \quad (G\text{-}330)$$

$$C_p = Po / (\rho_{\#}\,n^3\,D^5) = 0.0013 \quad (G\text{-}331)$$

where

n = pump speed (rad / sec)

D = pump impeller diameter (M)

Q_{pump} = volumetric flow rate through pump (M^3/S)

HD = necessary fluid head (M) (from flow system analysis)

$\rho_{\#}$ = seawater density at path #

Po = power required to run pump (W)

G = gravitation constant (acceleration) = 9.81 M/S^2

The efficiency (η_{pump}) of the respective pumps being designed in this analysis is defined as

$$\eta_{pump} = C_h C_q / C_p. \qquad \text{(G-332)}$$

Warm Water Pumps:

Initially it is necessary to determine the warm water volumetric flow through each pump. Since the number of pumps necessary is unknown and dependant upon the maximum diameter commercially available (commercially available pumps approach 1.85 M diameters [32]) the procedure is iterative.

For the first iteration the number of pumps designed is

$$N_{pump,ww} = 1$$

the final iteration yields a value of

$$N_{pump,ww} = 3$$

With an estimate as to the number of pumps to be utilized in the warm water flow loop, the volumetric flow ($Q_{pump,ww}$) for each warm water pump is

determined from the warm water mass flow (m_2) and the known seawater density (ρ_2) as

$$Q_{pump,ww} = m_2 / (\rho_2 N_{pump,ww}) = 8.46\ M^3/S \qquad (G\text{-}333)$$

which upon solving the three equations above (G-329 , G-330 and G-331) for the three unknowns ($n_{ww,pump}$, $D_{ww,pump}$ and $Po_{ww,pump}$) yields values of

$$n_{ww,pump} = 21.3 \text{ rad/sec}$$

$$D_{ww,pump} = 1.80\ M$$

$$\eta_{ww,pump} = 0.89$$

$$Po_{ww,pump} = 246\ KW$$

for the standard discharge pipe configuration and

$$n_{ww,pump,TP} = 21.2 \text{ rad/sec}$$

$$D_{ww,pump,TP} = 1.81\ M$$

$$\eta_{ww,pump,TP} = 0.89$$

$$Po_{ww,pump,TP} = 243\ KW$$

for the tapering pipe configuration.

This procedure is repeated until the final pump impeller diameter is less than 1.85 M so that the pumps being designed stay within commercially available limits.

The total parasitic pump power requirements for the standard downcomer design are determined now for each warm water pump utilized as

$$Po_{tot,pump,ww} = N_{pump,ww}\, Po_{ww,pump} = 737\ KW. \qquad (G\text{-}334)$$

The total parasitic pump power requirements for the tapered pipe downcomer design are

$$Po_{tot,pump,ww,TP} = N_{pump,ww}\, Po_{ww,pump,TP} = 729\ KW. \qquad (G\text{-}335)$$

Cold Water Pumps:

As described above for the warm water pumps, it is necessary to determine the cold water volumetric flow through each pump. Once again, since the number of pumps necessary is unknown and dependant upon the maximum diameter commercially available, the procedure is iterative.

For the first iteration the number of pumps designed is

$$N_{pump,cw} = 1$$

the final iteration yields a value of

$$N_{pump,cw} = 2$$

With an estimate as to the number of pumps to be utilized in the cold water flow loop, the volumetric flow ($Q_{pump,cw}$) for each cold water pump is determined from the cold water mass flow (m_{11}) and the known seawater density (ρ_{11}) as

$$Q_{pump,cw} = m_{11} / (\rho_{11} N_{pump,cw}) = 7.59\ M^3/S \qquad (G\text{-}336)$$

which upon solving the three equations above (G-329 , G-330 and G-331) for the three unknowns ($n_{cw,pump}$, $D_{cw,pump}$ and $Po_{cw,pump}$) yields values of

$$n_{cw,pump} = 34.9 \text{ rad/sec}$$

$$D_{cw,pump} = 1.48\ M$$

$$\eta_{cw,pump} = 0.89$$

$$Po_{cw,pump} = 396 \text{ KW}$$

for the standard discharge pipe configuration and

$$n_{cw,pump,TP} = 34.5 \text{ rad/sec}$$

$$D_{cw,pump,TP} = 1.48\ M$$

$$\eta_{cw,pump,TP} = 0.89$$

$$Po_{cw,pump,TP} = 391 \text{ KW}$$

for the tapering pipe configuration.

This procedure is repeated until the final pump impeller diameter is less than 1.85 M so that the pumps being designed stay within commercially available limits.

The total parasitic pump power requirements are determined now for each cold water pump utilized as

$$Po_{tot,pump,cw} = N_{pump,cw}\, Po_{cw,pump} = 792\ KW. \qquad (G\text{-}337)$$

The total parasitic pump power requirements for the tapered pipe downcomer design are

$$Po_{tot,pump,cw,TP} = N_{pump,cw}\, Po_{cw,pump,TP} = 781\ KW. \qquad (G\text{-}338)$$

Total power necessary for both seawater pump systems utilizing the standard discharge piping systems is

$$Po_{tot,pumps} = Po_{tot,pump,ww} + Po_{tot,pump,cw} = 1528\ KW. \qquad (G\text{-}339)$$

And the total power necessary for both seawater pump systems utilizing the tapering discharge piping systems is

$$Po_{tot,pumps,TP} = Po_{tot,pump,ww,TP} + Po_{tot,pump,cw,TP} = 1510\ KW. \qquad (G\text{-}340)$$

G.7 TOTAL POWER CONSUMPTION ANALYSIS

The total parasitic power consumption ($Po_{tot,parasitic}$) for the predeaerated/reinjected 10 MW_{gross} OC-OTEC system designed in this report is a function of the total power consumed by the evaporator predeaerator vent compressors ($Po_{pre,E,VC,tot}$), the condenser predeaerator vent compressor ($Po_{pre,DCC,VC,tot}$), the condenser vent compressor ($Po_{DCC,VC,tot}$) and the total power utilized by the seawater pumps ($Po_{tot,pumps}$) determined as

$$Po_{tot,parasitic} = Po_{pre,E,VC,tot} + Po_{pre,DCC,VC,tot} + Po_{DCC,VC,tot} + Po_{tot,pumps}$$
$$= 1933 \text{ KW} \quad \text{(G-341)}$$

for the standard downcomer systems and

$$Po_{tot,parasitic,TP} = Po_{pre,E,VC,tot} + Po_{pre,DCC,VC,tot} + Po_{DCC,VC,tot} + Po_{tot,pumps,TP}$$
$$= 1915 \text{ KW} \quad \text{(G-342)}$$

for the tapering discharge piping systems.

The total power available from this design (including the flow of noncondensables through the designed turbine as discussed in the evaporator section previously) is

$$Po_{gross} = 10004 \text{ KW}.$$

With the gross power known and the total parasitic power also known, the net power produced from this design is defined as

$$Po_{net} = Po_{gross} - Po_{tot,parasitic} = 8070 \text{ KW} \quad \text{(G-343)}$$

for the standard pipe hydraulic compression system and

$$Po_{net,TP} = Po_{gross} - Po_{tot,parasitic,TP} = 8089 \text{ KW} \quad \text{(G-344)}$$

for the tapering pipe hydraulic compression system.

These values indicate that a predearated/reinjected 10 MW_{gross} OC-OTEC power plant can be expected to lose approximately 19.3% of its gross power output to parasitic losses with the standard hydraulic compressor design and approximately 19.1% of its gross power output.

REFERENCES

[1] d'Arsonval, A., "Utilization des forces naturelles. Avenir de l'electricite," *Revue Scientifique*, Vol. 17, 1881.

[2] Balje, O.E., Turbomachines: A Guide to Design, Selection, and Theory, John Wiley & Sons, New York, 1981.

[3] Bharathan, D., Parsons, B.K., and Althof, J.A., "Direct-Contact Condensers for Open-Cycle OTEC Applications," Solar Energy Research Institute, SERI/TR-252-3108,October, 1988.

[4] Bharathan, D., and T. Penney, "Flash Evaporation from Falling Turbulent Jets," Proceedings of the ASME/JSME Thermal Engineering Joint Conference, Y. Mori and W.J. Wang, Ed., Vol. 2, pp 341-353, 1983.

[5] Bharathan, D., and T. Penney, "Mist Eliminators for Freshwater Production from Open-Cycle OTEC Systems," Solar Energy Research Institute, SERI/TR-252-1991, Golden, CO, December, 1983.

[6] Block, D.L. and Valenzuela, J.A., "Thermoeconomic Optimization of OC-OTEC Electricity and Water Production Plants," Solar Energy Research Institute, SERI/STR-251-2603,May, 1985.

[7] Claude, G., "Power from the Tropical Seas," *Mechanical Engineering*, Vol. 52, No. 12, pp. 1039 - 1044, 1930.

[8] Dixon, S.L., Fluid Mechanics, Thermodynamics of Turbomachinery, Pergamon Press, New York, 3rd Edition, 1978.

[9] Dugger, G.L., F.E. Naef and J.E. Snyder, "Ocean Thermal Energy Conversion," Solar Energy Handbook, McGraw-Hill, New York, pp. 19-1-53, 1981.

[10] Electric Power Research Institute, "Technical Assessment Guide, Electricity Supply - 1986," P-4463-SR, Volume 1, December, 1986.

[11] Golshani, A. and Chen, F.C., "Ocean Thermal Energy Conversion Gas Desorption Studies, Vol. 1, Design of Experiments," Oak Ridge Natural Laboratory, ORNL/TM-7438, Vol. 1, 1980.

[12] Golshani, A. and Chen, F.C., "Ocean Thermal Energy Conversion Gas Desorption Studies, Vol. 2, Deaeration in a Packed Column and a Barometric Intake System," Oak Ridge Natural Laboratory, ORNL/TM-7438, Vol. 2, 1981.

[13] Golshani, A., and Chen, F.C., "A Study of Hydraulic Air Compression for Ocean Thermal Energy Conversion Open-Cycle Applications," Oak Ridge Natural Laboratory, ORNL/TM-8384,January, 1983.

[14] Holland, F.A., and Chapman, F.S., Pumping Liquids, Reinhold Publishing Corporation, New York, 1966.

[15] Horne, R.A., Marine Chemistry, John Wiley & Sons, New York, 1969.

[16] Horne, R.A., The Chemistry of Our Environment, John Wiley & Sons, New York, 1978.

[17] Howell, J.R., and Buckius, R.O., Fundamentals of Engineering Thermodynamics, English/SI Version, McGraw-Hill Company, New York, 1987.

[18] Inficon Leybold-Heraeus, Inc., "PC-QPAK Operation Manual," September, 1986.

[19] Kester, D.R., "Dissolved Gases Other than CO_2," Chemical Oceanography, Vol. 1, 2nd Edition, pp. 497-517, 1975.

[20] King, C.J., Separation Processes, McGraw-Hill, New York, 1980.

[21] Krock, H.J., "Gas Analyses of Water Samples for OTEC Program," University of Hawaii, Look Laboratory, TR-51, December, 1981.

[22] Krock, H.J. and Zapka, M.J., "Gas Evolution in Open-Cycle OTEC," Proceedings, 5th OMAE Conference, Vol. 2, pp. 613-617, ASME, 1986.

[23] Leybold-Heraeus Vacuum Products, Inc., "TMP/NT-50 Turbomolecular Pump and Frequency Converter Manual," 1987.

[24] Leybold-Inficon, Inc., "Quadrex 100 Residual Gas Analyzer Manual," December, 1987.

[25] Lindenmuth, W., Liu, H., and Poquette, G., "Seawater Deaeration in OC-OTEC Risers," Hydronautics, Inc., Draft Report 8031-1, 1982.

[26] Link, H. and B. Parsons, "Potential of Proposed Open-Cycle OTEC: Experiments to Achieve Net Power," Marine Technology Society/IEEE Oceans ' 86 Conference Record, Washington, D.C., September 23 - 25, 1986.

[27] Massachusetts Institute of Technology, Texas A&M University, University of Pennsylvania, "Innovative Turbine Concepts for Open-Cycle OTEC," Solar Energy Research Institute, SERI/TR-253-3549, December, 1989.

[28] Massart, G.L., "The Tribulations of Trying to Harness Thermal Power," *Marine Technology Society Journal*, Vol. 8, No. 9, Oct/Nov 1974.

[29] O'Neill, P., Environmental Chemistry, George Allen & Unwin, London, pp. 70-73, 1985.

[30] Oney, S.K., "Molecular Diffusion of Oxygen and Nitrogen in Seawater," Master's Thesis, Department of Ocean Engineering, University of Hawaii, 1988.

[31] Owens, W.L. and L.C. Trimble, "Mini-OTEC Operational Results," *ASME Journal of Solar Energy Engineering*, Vol. 103, pp. 233 - 240, 1981.

[32] Parsons, B.K., Bharathan, D., and Althof, J.A., "Thermodynamic Systems Analysis of Open-Cycle Ocean Thermal Energy Conversion (OTEC)," Solar Energy Research Institute, SERI/TR-252-2234, September, 1985.

[33] Parsons, B.K. et al., "Test Plan for the Heat and Mass- Transfer Scoping Test Apparatus: Phase I and Phase II Tests," Solar Energy Research Institute, SERI/SP-253-3385, Draft, October, 1988.

[34] Penney, T., D. Bharathan, J. Althof and B. Parsons, An Assessment of Technology for a Small-Scale, Shore-Based, Open-Cycle Ocean Thermal Energy Conversion System-- Design Case Study for an Integrated Research Facility, Solar Energy Research Institute, SERI-TR-252-2184, Golden, CO: May 1984.

[35] Perry, R.H., Chemical Engineer's Handbook, 3rd Edition, McGraw-Hill, New York, 1950

[36] Perry, R.H., and Green, D., Perry's Chemical Engineer's Handbook, 6th Edition, McGraw-Hill, New York, 1984.

[37] Rice, W., "Performance of Hydraulic Gas Compressors," ASME, *Journal of Fluids Engineering*, **98**, pp. 645-653, December, 1976.

[38] Ridgway, S., Personal conversation, September, 1989.

[39] Riley, J.P., and Skirrow, G, Chemical Oceanography, Vol. 2, 2nd Edition, Academic Press, New York, 1975.

[40] Shelpuk, B., "A 165 - kW Open-Cycle OTEC Experiment," SERI/TP-251-2725, Golden, CO, 1985.

[41] Skirrow, G., "The Dissolved Gases- Carbon Dioxide," Chemical Oceanography, Vol. 2, 2nd Edition, pp. 1 - 41, 1985.

[42] Solar Energy Research Institute (SERI), Interim Data Report on Direct-Contact Counter-Current Condenser Tests Conducted at SERI during Fiscal Year 1983, Golden, CO: September 1983.

[43] Solar Energy Research Institute (SERI), "Ocean Thermal Energy Conversion -- An Overview," SERI/SP-220-3024, November 1989.

[44] Titsui, T., F. Ito, Y. Seya, and Y. Nakamoto, "Outline of the 100 MW OTEC Plant in the Republic of Nauru," *IEEE Transactions on Power Apparatus and Systems*, Vol. PAS-102, No. 9, September, 1983.

[45] Valenzuela, J.A., Jasinski, T., Dodd Stacey, W., Patel, B.R., Dolan, F.Y., "Design and Cost Study of Critical OC-OTEC Plant Components," Solar Energy Research Institute, SERI/TP-252-3246, Final Subcontract Report, June, 1988.

[46] Weast, R.C., and Astle, M.J., CRC Handbook of Chemistry and Physics, 62nd Edition, CRC Press, Inc., Boca Raton, Florida, 1981.

[47] Weiss, R.F., *Deep Sea Research*, **17**, pp. 721-735, 1970.

[48] Weiss, R.F., *Deep Sea Research*, **18**, pp. 225, 1971.

[49] Westinghouse Electric Corporation, *100-MW_e OTEC Alternate Power Systems*, final report to U.S. Department of Energy under contract EG-77-C-05-1473, Vol. 1, 1979.

[50] Zangrando, F., Bharathan, D., Green, H.J., Link, H.F., Parsons, B.K., Pesaran, A.A., and Panchal, C.B., "Results of Scoping Tests for Open-Cycle OTEC Components Operating with Seawater," Solar Energy Research Institute, SERI/TP-253-3561, September, 1990.

[51] Zapka, M.J., "Gas Exchange in Seawater with Special Emphasis on Open-Cycle Ocean Thermal Energy Conversion," Ph.D. Dissertation, Department of Ocean Engineering, University of Hawaii, 1988.

[52] Zapka, M.J., and Krock, H.J., "Seawater Pre-Deaerator for Open-Cycle Ocean Thermal Energy Conversion Applications," United States Patent No. 5,096,544, Research Corporation of the University of Hawaii, March 17, 1992.